AD NUMBER

AD485616

NEW LIMITATION CHANGE

TO

Approved for public release, distribution unlimited

FROM

Distribution authorized to U.S. Gov't. agencies and their contractors; Administrative/Operational Use; APR 1966. Other requests shall be referred to Air Force Fligth Dynamics Laboratory, Attn: Fligth Control Division/ FDC, Wright-Patterson AFB, OH 45433.

AUTHORITY

AFFDL ltr, 25 Apr 1972

AFFDL-TR-66-3

RE-ENTRY VEHICLE CONTROL SYSTEM DESIGN AND MECHANIZATION

D. K. SCHARMACK
M. D. WARD

HONEYWELL, INC.

TECHNICAL REPORT AFFDL-TR-66-3

APRIL 1966

AIR FORCE FLIGHT DYNAMICS LABORATORY
RESEARCH AND TECHNOLOGY DIVISION
AIR FORCE SYSTEMS COMMAND
WRIGHT-PATTERSON AIR FORCE BASE, OHIO 45433

NOTICES

When Government drawings, specifications, or other data are used for any purpose other than in connection with a definitely related Government procurement operation, the United States Government thereby incurs no responsibility nor any obligation whatsoever; and the fact that the Government may have formulated, furnished, or in any way supplied the said drawings, specifications, or other data, is not to be regarded by implication or otherwise as in any manner licensing the holder or any other person or corporation, or conveying any rights or permission to manufacture, use, or sell any patented invention that may in any way be related thereto.

Copies of this report should not be returned to the Research and Technology Division unless return is required by security considerations, contractual obligations, or notice on a specific document.

500 - June 1966 - 773-47-1024

RE-ENTRY VEHICLE CONTROL SYSTEM DESIGN AND MECHANIZATION

D. K. SCHARMACK
M. D. WARD

FOREWORD

This document is the final report on a study of an optimal re-entry control mechanization. The research was sponsored by the Flight Dynamics Laboratory, RTD, under Task No. 822501 of Project No. 8225 and Contract No. AF33(615)-1858 with Honeywell Inc., Minneapolis, Minnesota. Mr. R. Haas was the RTD project monitor for this program. Work at Honeywell was performed under the supervision of Drs. W. H. Ito and E. R. Rang. Project personnel were: D. K. Scharmack, principal investigator, and M. D. Ward, W. C. Marshall, H. R. Purtell, A. F. Konar, and E. R. Rang.

A large portion of the digital computation was performed at the RTD computation center.

The work was administered under the direction of the Air Force Flight Dynamics Laboratory, Mr. R. L. Haas, project engineer. This report covers work conducted from June 1, 1964,to August 1, 1965.

The manuscript was released by the authors October 1, 1965 for publication as an RTD Technical Report.

This technical report has been reviewed and is approved.

H. W. BASHAM
Chief, Control Elements Branch
Flight Control Division
AF Flight Dynamics Laboratory

ABSTRACT

A nonlinear optimal feedback control scheme for controlling a vehicle re-entering the earth's atmosphere from lunar return initial conditions is reported.

The optimal feedback control law used in the scheme is obtained from a multi-dimensional surface fit of the control function for several optimal trajectories. Partials of the control with respect to the state vector are included in the fitting procedure. The functional minimized by the trajectories is the total (convective plus radiative) stagnation point heat.

The feedback control scheme is developed, and several re-entry trajectories are simulated. Modest increases in total heat from optimal values are observed, and large (although tolerable) terminal point errors occur. It is believed that the terminal errors can be greatly reduced, if necessary.

A powerful predictor scheme is developed which allows optimal trajectories to be changed as a function of a parameter. This is used to extend the range of an optimal trajectory, to perform an "absolute minimum" test, and to map the optimal re-entry corridor.

Sufficiency tests for a relative minimum are mechanized, and it is shown that the trajectories considered are minimizing paths. The optimization method is extended to include the bounded state-coordinate problem.

CONTENTS

		Page
SECTION I	INTRODUCTION	1
SECTION II	OPTIMAL TRAJECTORY COMPUTATIONS	5
	A. The Re-entry Trajectory Optimization Problem	5
	1. Statement of the Problem	5
	2. The Unconstrained Subarc	8
	3. The Constrained Subarc $u = \pm u_1$	10
	4. The Optimization Scheme and Computer Results	11
	B. Re-entry Corridor Mapping Computations	23
	1. Range Extension	24
	2. Corridor Mapping Program	33
	C. The Data Generating Program	39
	1. Statement of the Problem	39
	2. The Partial Derivatives	55
	3. Computer Results	59
	D. Sufficiency Conditions	61
	1. Sufficiency Conditions for a Relative Minimum	61
	2. An Absolute Minimum Test	67
	E. The Constraint $a_D = B$ and Experiences with Various Optimization Schemes	70
	1. Constrained Subarc Equations	70
	2. Experiences with Various Optimization Schemes	73
	3. Constraint Equation Modification	76
	F. Extension to the Bounded State Coordinate Problem	77
	1. Statement of the Problem	77
	2. Necessary Conditions	78
	3. Basis for Computational Scheme	81
	4. The Bounded Brachistochrone Problem	82
SECTION III	THE CONTROL FUNCTION	97
	A. Justification of the Form of the Control Function	97
	1. Theory	97
	2. Example	98

CONTENTS

		Page
	B. Methods for Determining the Control	102
	C. Development of the Control Function	104
	1. Lagrange Fits	107
	2. Least Squares Fits	110
	3. Chebyscheff Fits	112
SECTION IV	MECHANIZATION AND SIMULATION OF THE NON-LINEAR OPTIMAL FEEDBACK CONTROL SCHEME	143
	A. Simulation Description	143
	1. Re-entry Vehicle and Sensors	143
	2. Navigator	144
	3. Predictor and Control Generator	144
	4. Hold Circuit	146
	B. Simulation Results	146
SECTION V	CONCLUSIONS AND RECOMMENDATIONS	157
	A. Accomplishments	157
	B. Recommendations	158
	Materials Section (Table LXXV)	160
APPENDIX A	A PREDICTOR SCHEME	161
APPENDIX B	THREE OPTIMIZATION TECHNIQUES	165
APPENDIX C	THE TRANSFORMED OPTIMIZATION PROBLEM	171
APPENDIX D	A NON-HOMOGENEOUS RICATTI EQUATION FOR FIELD PARTIAL DERIVATIVES	179
APPENDIX E	RELATIONSHIPS FOR SUFFICIENCY CONDITIONS	181
APPENDIX F	THE LEAST SINGULAR SQUARE MATRIX OF AN nxq MATRIX	189
APPENDIX G	PROOF THAT DISCONTINUITIES IN THE MULTIPLIERS CAN BE DETERMINED AT EITHER END OF A CONSTRAINED SUBARC	193
REFERENCES		197

LIST OF ILLUSTRATIONS

Figure		Page
1-1	Nonlinear Optimal Feedback Control Scheme Mechanization	2
2-1	Altitude versus Range for Several Optimal Trajectories, Parameter u_1	15
2-2	Sensed Acceleration versus Range for Several Optimal Trajectories, Parameter u_1	16
2-3	Range versus Time for Several Optimal Trajectories, Parameter u_1	17
2-4	Velocity versus Range for Several Optimal Trajectories, Parameter u_1	18
2-5	Flight Path Angle versus Range for Several Optimal Trajectories, Parameter u_1	19
2-6	Convective and Radiative Heating Rates versus Range for Several Optimal Trajectories, Parameter u_1	20
2-7	Total Heating Rate versus Range for Several Optimal Trajectories, Parameter u_1	21
2-8	Control Function u versus Range for Several Optimal Trajectories, Parameter u_1	22
2-9	Altitude versus Range for Unconstrained Optimal Trajectories, Parameter $\zeta(T)$	26
2-10	Control Function u versus Range for Unconstrained Optimal Trajectories, Parameter $\zeta(T)$	27
2-11	Velocity versus Range for Unconstrained Optimal Trajectories, Parameter $\zeta(T)$	28
2-12	Sensed Acceleration versus Range for Unconstrained Optimal Trajectories, Parameter $\zeta(T)$	29
2-13	Flight Path Angle versus Range for Unconstrained Optimal Trajectories, Parameter $\zeta(T)$	30
2-14	Total Heat versus Terminal Range for Unconstrained Optimal Trajectories	31

LIST OF ILLUSTRATIONS

Figure		Page
2-15	Terminal Time versus Terminal Range for Unconstrained Optimal Trajectories	32
2-16	Velocity versus Range for Optimal Trajectories 1, 2, and 3	40
2-17	Flight Path Angle versus Range for Optimal Trajectories 1, 2 and 3	41
2-18	Altitude versus Range for Optimal Trajectories 1, 2 and 3	42
2-19	Sensed Acceleration versus Range for Optimal Trajectories 1, 2 and 3	43
2-20	Velocity versus Range for Optimal Trajectories 1, 4 and 5	44
2-21	Flight Path Angle versus Range for Optimal Trajectories 1, 4 and 5	45
2-22	Altitude versus Range for Optimal Trajectories 1, 4 and 5	46
2-23	Sensed Acceleration versus Range for Optimal Trajectories 1, 4 and 5	47
2-24	Velocity versus Range for Optimal Trajectories 1, 6 and 7	48
2-25	Flight Path Angle versus Range for Optimal Trajectories 1, 6 and 7	49
2-26	Altitude versus Range for Optimal Trajectories 1, 6 and 7	50
2-27	Sensed Acceleration versus Range for Optimal Trajectories 1, 6 and 7	51
2-28	Optimal Control Function u versus Range for 27 Optimal Trajectories	52
2-29	Partial Derivatives of the Control With Respect to V, γ and h as Functions of Range for Trajectory 1	60
2-30	Multiplier P_1 for Several Optimal Trajectories	62
2-31	Multiplier P_2 for Several Optimal Trajectories	63

LIST OF ILLUSTRATIONS

Figure		Page
2-32	Absolute Minimum Test Results - Total Heat J versus Terminal Flight Path Angle Γ	69
2-33	State Coordinate Geometry in the Vicinity of the Constrained Subarc Initial Point	80
2-34	Bounded Brachistochrone Problem Geometry	83
2-35	Bounded Brachistochrone Optimal Solution	84
3-1	Optimal Control u and Error of Fit for Trajectory 1	113
3-2	Optimal Control u and Error of Fit for Trajectory 2	114
3-3	Optimal Control u and Error of Fit for Trajectory 3	115
3-4	Optimal Control u and Error of Fit for Trajectory 4	116
3-5	Optimal Control u and Error of Fit for Trajectory 5	117
3-6	Optimal Control u and Error of Fit for Trajectory 6	118
3-7	Optimal Control u and Error of Fit for Trajectory 7	119
3-8	Optimal Control u and Error of Fit for Trajectory 8	120
3-9	Optimal Control u and Error of Fit for Trajectory 9	121
3-10	Optimal Control u and Error of Fit for Trajectory 10	122
3-11	Optimal Control u and Error of Fit for Trajectory 11	123
3-12	Optimal Control u and Error of Fit for Trajectory 12	124
3-13	Optimal Control u and Error of Fit for Trajectory 13	125
3-14	Optimal Control u and Error of Fit for Trajectory 14	126
3-15	Optimal Control u and Error of Fit for Trajectory 15	127
3-16	Optimal Control u and Error of Fit for Trajectory 16	128
3-17	Optimal Control u and Error of Fit for Trajectory 17	129
3-18	Optimal Control u and Error of Fit for Trajectory 18	130

LIST OF ILLUSTRATIONS

Figure		Page
3-19	Optimal Control u and Error of Fit for Trajectory 19	131
3-20	Optimal Control u and Error of Fit for Trajectory 20	132
3-21	Optimal Control u and Error of Fit for Trajectory 21	133
3-22	Optimal Control u and Error of Fit for Trajectory 22	134
3-23	Optimal Control u and Error of Fit for Trajectory 23	135
3-24	Optimal Control u and Error of Fit for Trajectory 24	136
3-25	Optimal Control u and Error of Fit for Trajectory 25	137
3-26	Optimal Control u and Error of Fit for Trajectory 26	138
3-27	Optimal Control u and Error of Fit for Trajectory 27	139
3-28	Coefficient a_{000} as a Function of Range	140
4-1	Nonlinear Optimal Feedback Control Scheme Mechanization for the Re-entry Application	143
4-2	Simulation Results for Trajectory 1 - Altitude versus Range	151
4-3	Simulation Results for Trajectory 1 - Velocity versus Range	152
4-4	Simulation Results for Trajectory 1 - Flight Path Angle versus Range	153
4-5	Simulation Results for Trajectory 1 - Control versus Range	154

LIST OF TABLES

Table		Page
2-1	Control Constraint u_1 and Optimal Criterion J	23
2-2	Initial Conditions and Total Heat for 27 Optimal Trajectories Obtained During the Corridor Mapping Process	36
2-3	Weighting Factors for the Optimal Newton-Raphson Method Used for the Mapping Variables	38
2-4	Comparison of Computed and Exact Optimal Paths	96
3-1	Order of Best Fits Near Terminal Point	112
4-1	Simulation Results for the 27 Optimal Trajectories of Table 2-2	147
4-2	Additional Simulation Results	148
4-3	Initial Conditions for Trajectories 28-31	149
4-4	Effects of Initial Velocity Change on Δ	149

SECTION I
INTRODUCTION

Many schemes have appeared, over the past few years, for the control of vehicles re-entering the earth's atmosphere. They range over a wide spectrum of missions, from the attainment of a given landing site to rather complex in-flight maneuvers, and, in operation, may be completely automatic or may require a pilot in the loop. The schemes have been developed for a variety of vehicles, onboard sensors, and onboard computing capabilities and, additionally, cover a wide range of initial re-entry conditions. A good survey is given by Wingrove in Reference 15.

Under the heading of optimal control, re-entry schemes become sparse. The only seemingly applicable approach published to date is the "neighboring optimum control scheme" of Reference 8. This is a linear control scheme based on small perturbations from a nominal optimal trajectory. Previous studies (Reference 1) indicate that such a method may not be applicable for re-entry control, although for other applications it may be perfectly suitable. The objective of this report is to describe a nonlinear optimal feedback control scheme, developed and simulated during the contract period.

Figure 1-1 illustrates the approach. The vehicle is the plant to be controlled through application of the control vector u(t), and sensors measure parameters of the motion a. The navigator box supplies the state vector and its time derivative at discrete and equally spaced instants of time. (The time increment may be made variable if necessary.) A predictor equation estimates conditions at the next sample point, on the basis of present conditions and past state-vector derivitives, to introduce lead into the control system. The control generator is a known (vector) function of the state and independent variable (usually time). Its evaluation gives the optimal control for the predicted point. The hold circuit supplies the optimal control over the next time interval.

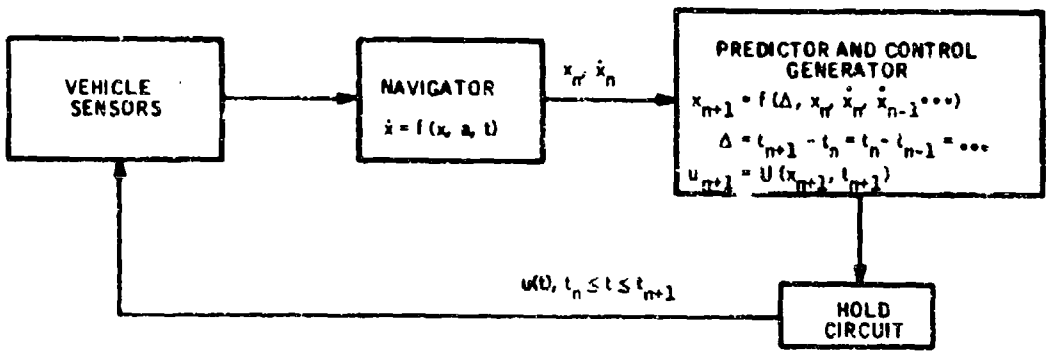

Figure 1-1. Nonlinear Optimal Feedback Control Scheme Mechanization

Development of the control generator equation comprises the bulk of this report. Section II considers a two-dimensional re-entry trajectory optimization problem, in which total stagnation point heat (convective and radiative) is the function minimized. Terminal values of velocity, altitude and range are specified, leaving terminal flight path angle and time unspecified. After this problem is solved, the terminal range is extended, to obtain a design trajectory, and the optimal re-entry corridor is "mapped" through the use of a very powerful predictor scheme. The control function for the mapped trajectories is used for development of the control generator equation. A data generating program is described which supplies partials of the control with respect to the state vector as well as the control itself. This data is punched on cards at equally spaced values of range, since range is used as the independent variable in the program. It is also shown in Section II that the mapped trajectories are minimizing trajectories over a large region of solution space.

In Section III, the control data is fitted as a multidimensional polynomial, and the fit is evaluated, so far as errors are concerned.

Mechanization and simulation of the control equation in the scheme of Figure 1-1 is considered in Section IV. It is found that the scheme produces reasonable re-entry trajectories with modest increases in total heat from the optimal values for most of the trajectories simulated. A few trajectories fail because of control inaccuracies in the area of the first dip into the atmosphere, so the region of initial conditions for application of the scheme must be suitably limited. The region of application is still very large. The terminal condition errors for the successful trajectories are found to be large (although tolerable) and are usually biased in sign and magnitude. It is believed that these errors can be greatly reduced, although no effort was expended in this direction.

Some additional topics are considered in Section II. An inequality constraint on the sensed acceleration is included in the re-entry trajectory optimization problem. Several optimization methods are used in an unsuccessful attempt to obtain a 10-g optimal trajectory. The most powerful method is the predictor scheme, and this fails because of a singular point on the constrained subarc. A means of isolating this singular point was devised, but time limitations prevented exploitation of the idea on the computer. The optimization methods are also extended to the bounded state coordinate problem, and the bounded brachistochrone problem is solved on the computer.

Conclusions and recommendations are presented in Section V.

SECTION II
OPTIMAL TRAJECTORY COMPUTATIONS

A. THE RE-ENTRY TRAJECTORY OPTIMIZATION PROBLEM

1. Statement of the Problem

A re-entry path which minimizes the total stagnation-point heating

$$J = \int_0^T \dot{q}\, d\tau \tag{2.1}$$

of a blunt-nose re-entry vehicle is to be found. The heating rate $\dot{q}$ is the sum of convective and radiative components

$$\dot{q} = \dot{q}_c + \dot{q}_r , \tag{2.2}$$

where

$$\dot{q}_c = cv^3 \sqrt{\frac{\rho}{N}} \tag{2.3}$$

$$\dot{q}_r = 7.5N \left(\frac{\rho}{\rho_o}\right)^{3/2} \left(\frac{v}{10,000}\right)^{12.5} . \tag{2.4}$$

The state vector components are the velocity v, flight path angle γ, dimensionless altitude $\xi = \frac{h}{R}$, and great circle range ζ. The density ρ is given by

$$\rho = \rho_o e^{-\beta R \xi} \tag{2.5}$$

and values for the constants are vehicle nose radius $N = 4$ feet, $c = 2 \times 10^{-8}$, earth radius $R = 20,903,520$ feet, exponential constant $\beta = 1/23,500$ ft.$^{-1}$, and sea level density $\rho_o = 0.0023769$ slugs/ft.^{3}.

The equations of motion are

$$\frac{dv}{dt} = \frac{-S}{2m}\rho v^2 C_D(u) - \frac{g_o \sin\gamma}{(1+\xi)^2}$$

$$\frac{d\gamma}{dt} = \frac{S}{2m}\rho v\, C_L(u) + \frac{v\cos\gamma}{R(1+\xi)} - \frac{g_o \cos\gamma}{v(1+\xi)^2} \qquad (2.6)$$

$$\frac{d\xi}{dt} = \frac{v}{R}\sin\gamma$$

$$\frac{d\zeta}{dt} = \frac{v}{(1+\xi)}\cos\gamma\,.$$

The vehicle frontal area to mass ratio is $\frac{S}{m} = 0.5 \text{ ft.}^2 - \text{slug}^{-1}$, and the lift and drag coefficients are given in terms of the control function u as

$$C_D = C_{DO} + C_{DL}\cos u \qquad (2.7)$$

$$C_L = C_{LO}\sin u\,, \qquad (2.8)$$

where

$$C_{DO} = 0.88$$

$$C_{DL} = 0.52$$

$$C_{LO} = -0.505\,.$$

Inequality constraints include a bound on the control function

$$u_1^2 - u^2 \geq 0, \qquad (2.9)$$

with u_1 a constant, and a pilot's acceleration constraint

$$B - a_p \geq 0. \qquad (2.10)$$

In Equation (2.10), B is a specified constant, and the pilot's acceleration is given by

$$a_p = \frac{S\rho v^2}{2mg_o}\sqrt{C_L^2 + C_D^2}, \tag{2.11}$$

where g_o is sea-level gravity which normalizes the units of a_p to g's. Equation (2.9) was found necessary to produce initial trajectories which neither skipped out of the atmosphere nor dived in too deeply. It is sequentially relaxed during the optimization process.

Initial conditions are taken as v_o = 35,000 ft/sec, γ_o = -5.75 degrees, initial altitude h_o = 400,000 ft, and ζ_o = zero; the terminal surface equations are

$$\begin{aligned} v(T) - X_1 &= 0 \\ h(T) - X_2 &= 0 \\ \zeta(T) - X_3 &= 0 \end{aligned} \tag{2.12}$$

with the constants X_1 = 1650 ft/sec, X_2 = 75,530 ft, and X_3 = 979 statute miles. Note that the final flight path angle and terminal time are left unspecified.

A fairly detailed examination of this problem is contained in Reference 1; consequently, only a brief summary of the results is presented here.

The Hamiltonian may be written

$$H_1 = \dot{q} + p'f + \mu_1\left(u_1^2 - u^2\right) + \mu_2(B - a_p) \tag{2.13}$$

where p is the four-dimensional multiplier vector and f represents the right-hand side of the system (2.6). The Euler-Lagrange equations, where zero terms have been omitted, then read

$$-\dot{p}_1 = \frac{\partial \dot{q}}{\partial v} + p_1 \frac{\partial f_1}{\partial v} + p_2 \frac{\partial f_2}{\partial v} + p_3 \frac{\partial f_3}{\partial v} + p_4 \frac{\partial f_4}{\partial v} - \mu_2 \frac{\partial a_p}{\partial v}$$

$$-\dot{p}_2 = p_1 \frac{\partial f_1}{\partial \gamma} + p_2 \frac{\partial f_2}{\partial \gamma} + p_3 \frac{\partial f_3}{\partial \gamma} + p_4 \frac{\partial f_4}{\partial \gamma} \qquad (2.14)$$

$$-\dot{p}_3 = \frac{\partial \dot{q}}{\partial \xi} + p_1 \frac{\partial f_1}{\partial \xi} + p_2 \frac{\partial f_2}{\partial \xi} + p_4 \frac{\partial f_4}{\partial \xi} - \mu_2 \frac{\partial a_p}{\partial \xi}$$

$$\dot{p}_4 = 0, \left(p_4 = p_{4_o}\right)$$

$$0 = p_1 \frac{\partial f_1}{\partial u} + p_2 \frac{\partial f_2}{\partial u} - 2\mu_1 u - \mu_2 \frac{\partial a_p}{\partial u} . \qquad (2.15)$$

2. The Unconstrained Subarc

Both the multipliers μ_1 and μ_2 are zero here, so Equation (2.15) is used to determine the control function. After the substitutions have been made, the resulting formula is

$$\tan u = \frac{-C_{LO} p_2}{C_{DL} p_1 v} , \qquad (2.16)$$

and u is centered about zero by the constraint (2.9); i.e.,

$$-u_1 \leq u \leq u_1 . \qquad (2.17)$$

The minimum-principle equation is

$$-p_1 v C_{DL} \cos u + p_2 C_{LO} \sin u \leq -p_1 v C_{DL} \cos U + p_2 C_{LO} \sin U , \qquad (2.18)$$

in which U is any admissible value in the range (2.17). The left-hand side of (2.18) may be considered as a dot product, and the choice of a unit vector (cos u, sin u) which has minimum dot product with the vector $(-p_1 v C_{DL}, p_2 C_{LO})$ is

$$\sin u = \frac{-C_{LO} p_2}{\sqrt{\left(C_{LO} p_2\right)^2 + \left(C_{DL} p_1 v\right)^2}}$$

$$\cos u = \frac{C_{DL} p_1 v}{\sqrt{\left(C_{LO} p_2\right)^2 + \left(C_{DL} p_1 v\right)^2}} \qquad (2.19)$$

This is parallel but in the opposite direction. Then, from the signs of p_1 and p_2, assuming C_{LO} negative, it follows that:

If $p_2 = 0$ and $p_1 > 0$, then $u = 0$

$p_2 > 0$	$p_1 > 0$	$0 < u < \frac{\pi}{2}$
$p_2 > 0$	$p_1 = 0$	$u = \frac{\pi}{2}$
$p_2 > 0$	$p_1 < 0$	$\frac{\pi}{2} < u < \pi$
$p_2 = 0$	$p_1 < 0$	$u = \pm \pi$ (bang condition if $u_1 = \pi$)
$p_2 < 0$	$p_1 > 0$	$-\frac{\pi}{2} < u < 0$
$p_2 < 0$	$p_1 = 0$	$u = -\frac{\pi}{2}$
$p_2 < 0$	$p_1 < 0$	$-\pi < u < -\frac{\pi}{2}$.

(2.20)

There are no singular points if p_1 and p_2 are never simultaneously zero. The subarc ends either when (2.10) or (2.9) becomes zero, or when the stopping condition, the first of (2.12), is satisfied.

3. The Constrained Subarc $u = \pm u_1$

Let ϕ be the angle defined by Equation (2.16) and the sign conventions given by (2.20). Then substitution into the minimum principle equation, (2.18), gives

$$\cos(\phi - u) \geq \cos(\phi - U), \tag{2.21}$$

which is satisfied if u and $\phi < \pm \pi$, have the same sign. The condition $\phi = \pi$ indicates a bang. Furthermore, substitution into (2.15) (with $\mu_2 = 0$), and some rearrangement, gives

$$\mu_1 = -\frac{S\rho v}{2m}\sqrt{\left|C_{LO}p_2\right|^2 + \left|C_{DL}p_1 v\right|^2}\ \frac{\sin(\phi-u)}{u}. \tag{2.22}$$

Since u and $\sin(\phi-u)$ have the same sign, $\mu_1 \leq 0$, as required.

There are no singular points, and the control function is continuous at the junction between constrained and unconstrained subarcs. Thus μ_1, from (2.22), must start and end with value zero, since at such points $u = \phi$. Then the terminal surface is either $\mu_1 = 0$, provided $\dot{\mu}_1 \neq 0$, or the stopping condition.

The constrained subarc, over which $a_p = B$, is considered in a separate subsection.

4. The Optimization Scheme and Computer Results

It is shown in Reference 1 that the solution of systems of equations such as (2.6) and (2.14), in which u satisfies (2.16) and (2.20) (with $\mu_1 = 0$), or in which u and μ_1 satisfy (2.21) and (2.22), may be written in the form

$$\begin{aligned} x &= x(t, x_o, p_o) \\ p &= p(t, x_o, p_o), \end{aligned} \tag{2.23}$$

where x_o and p_o are the initial values of the state and multiplier vectors respectively. It is also shown in Reference 1 that the necessary conditions which augment the terminal equations (2.12) are

$$\begin{aligned} p_2(T) &= 0 \\ H &= 0, \end{aligned} \tag{2.24}$$

where H is the Hamiltonian (2.13) with the inequality constraint terms removed. When the functional forms of the solutions (2.23) are taken into consideration (and noting that x_o is fixed for the optimization problem), the set (2.12) and (2.24) become

$$\begin{aligned} v(T, p_o) - X_1 &= 0 \\ \xi(T, p_o) - X_2 \frac{1}{R} &= 0 \\ \zeta(T, p_o) - X_3 &= 0 \\ p_2(T, p_o) &= 0 \\ H(p_o) &= 0 . \end{aligned} \tag{2.25}$$

These five equations in the five unknown quantities (T, p_o) may be solved via the Newton-Raphson method if partial derivatives can be found. The partials with respect to T are the time derivatives (2.6) and (2.14) evaluated at t= T. The other partials are found by integrating the system of equations

$$\frac{d}{dt}\left(\frac{\partial x}{\partial a}\right) = \frac{\partial^2 H_1}{\partial p \partial x}\left(\frac{\partial x}{\partial a}\right) + \frac{\partial^2 H_1}{\partial p^2}\left(\frac{\partial p}{\partial a}\right)$$

$$\frac{d}{dt}\left(\frac{\partial p}{\partial a}\right) = -\frac{\partial^2 H_1}{\partial x^2}\left(\frac{\partial x}{\partial a}\right) - \frac{\partial^2 H_1}{\partial x \partial p}\left(\frac{\partial p}{\partial a}\right) \qquad (2.26)$$

in which "a" represents a particular initial condition. The partial derivatives of the Hamiltonian $H_1(x, p)$ may change from subarc to subarc, and for each subarc it is known that

$$\frac{\partial^2 H_1}{\partial x^2}, \quad \frac{\partial^2 H_1}{\partial p^2}$$

are symmetric matrices and that

$$\frac{\partial^2 H_1}{\partial p \partial x} = \left(\frac{\partial^2 H_1}{\partial x \partial p}\right)'$$

Since (2.26) is a set of 2n linear first-order, homogeneous differential equations, there is a maximal set of 2n independent (column) vector solutions. When initial conditions are taken as the (2n x 2n) identity matrix, the first n (column) vector solutions represent partial derivatives with respect to the vector x_o, and the last n solutions are partials with respect to p_o. The solutions are continuous in time, except possibly at corner points, where the discontinuities are well defined.

In the present case, discontinuities occur at points t_1, where the angle ϕ becomes $\pm \pi$, or equivantly, where $p_2 = 0$ with $p_1 < 0$. Let $\eta_{ij}(t)$ and $\zeta_{ij}(t)$, i, j= 1, . . . , 4, be the elements of the

$$\frac{\partial x(t)}{\partial p_o} \text{ and } \frac{\partial p(t)}{\partial p_o}$$

solution matrices respectively. At $t = t_1$, only the second of Equations (2.6) is discontinuous when u changes signs, and all of Equations (2.14) are continuous (since $p_2(t_1) = 0$). According to Reference 1, this means that only the second row of $\frac{\partial x}{\partial p_o}$ is discontinuous at $t = t_1$, with

$$\eta_{2j}^{+}(t_1) = \eta_{2j}^{-}(t_1) - \frac{2\dot{\gamma}^{-}(t_1)}{\dot{p}_2(t_1)} \zeta_{2j}(t_1), \; j= 1, \ldots, 4, \tag{2.27}$$

and (-), (+) signifies values from the left and from the right, respectively.

Now assume that a path and partial derivative solutions have been found. Then the modified Newton-Raphson equations for the system (2.25) are

$$\begin{bmatrix} dT \\ dp_{1_o} \\ dp_{2_o} \\ dp_{3_o} \\ dp_{4_o} \end{bmatrix} = -C \begin{bmatrix} \dot{v}(T) & \eta_{11}(T) & \eta_{12}(T) & \eta_{13}(T) & \eta_{14}(T) \\ \dot{\xi}(T) & \eta_{31}(T) & \eta_{32}(T) & \eta_{33}(T) & \eta_{34}(T) \\ \dot{\zeta}(T) & \eta_{41}(T) & \eta_{42}(T) & \eta_{43}(T) & \eta_{44}(T) \\ \dot{p}_2(T) & \zeta_{21}(T) & \zeta_{22}(T) & \zeta_{23}(T) & \zeta_{24}(T) \\ 0 & f_1(0) & f_2(0) & f_3(0) & f_4(0) \end{bmatrix}^{-1} \begin{bmatrix} 0 \\ \xi(T)-X_2/R \\ \zeta(T)-X_3 \\ p_2(T) \\ H \end{bmatrix}, 0<C\leq 1. \tag{2.28}$$

The zero in the right-hand vector corresponds to the stopping condition, the first of Equations (2.13), which is satisfied by every trajectory. The Hamiltonian is a constant for each path, so the last row of the matrix contains its partials evaluated at $t = 0$.

An optimal trajectory for u_1 = 16 degrees was obtained and is displayed in Reference 1. It appears here as the first of a family of optimal trajectories in Figures 2-1 through 2-8. The second member, for u_1 = 20 degrees (not shown), was generated by using the modified Newton-Raphson method with the 16-degree optimal values for (T, p_o) as starting conditions. All other members of the family, obtained in a similar fashion, are displayed in Figures 2-1 through 2-8, and values for the optimal criteria are given in Table 2-1.

Figure 2-1 shows that the trajectories dive deeper into the atmosphere and skip higher as the constraint is removed. All these curves end at the same point, as required by the terminal surface equations (2.12). The first dive produces higher pilot's acceleration peaks (Figure 2-2) but reduces the secondary peak. The unconstrained maximum value is 20.5 g's. The flight time increases (Figure 2-3) which is a consequence of the lengthening skip. This is apparent in the velocity curves (Figure 2-4) which tend to level out over the skipping portions of the trajectories. The flight path angles (Figure 2-5) also show the deeper dive and higher skip. All these curves apparently pass through a common point, corresponding roughly with the bottom of the first dip (see Figure 2-1). The convective and radiative heating rates are displayed in Figure 2-6. They peak higher, and fall off faster, as the constraint is relaxed. The total heating rates of Figure 2-7 have the same characteristics, and show that even though the peaks are higher, the enclosed area becomes smaller.

The optimal control functions are displayed in Figure 2-8. When the 16-degree trajectory (which seems to be in a category of its own) is excluded, the control curves tend nicely to the unconstrained trajectory curve. They all have a "bang" which goes towards the endpoint as the constraint is relaxed and, in the limit, produces the -180-degree value of the control function (the angle ϕ goes to -180 degrees at the bang). The first portions of these curves show that the trajectories are forced into the atmosphere, since positive control

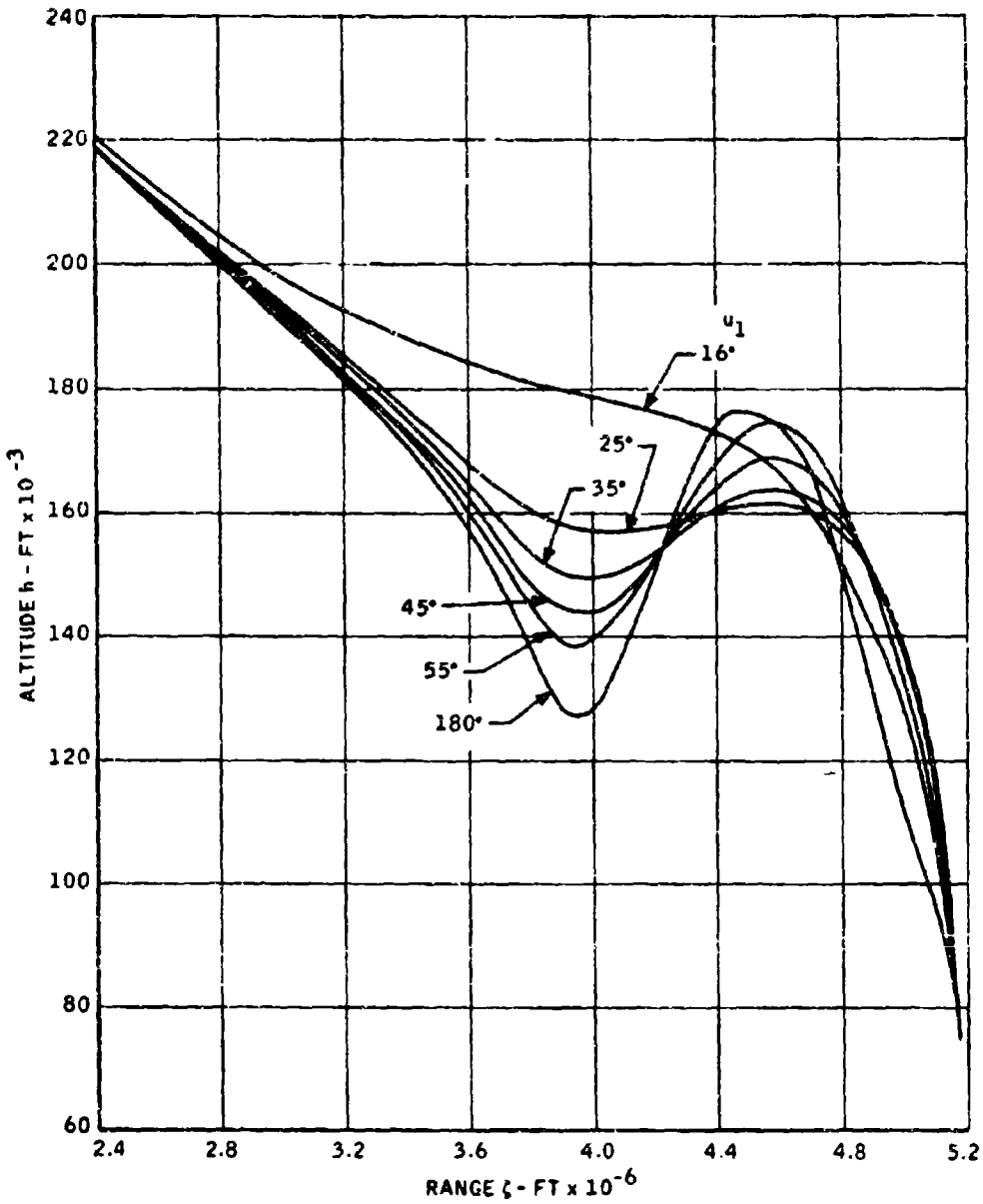

Figure 2-1. Altitude Versus Range for Several Optimal Trajectories, Parameter u_1

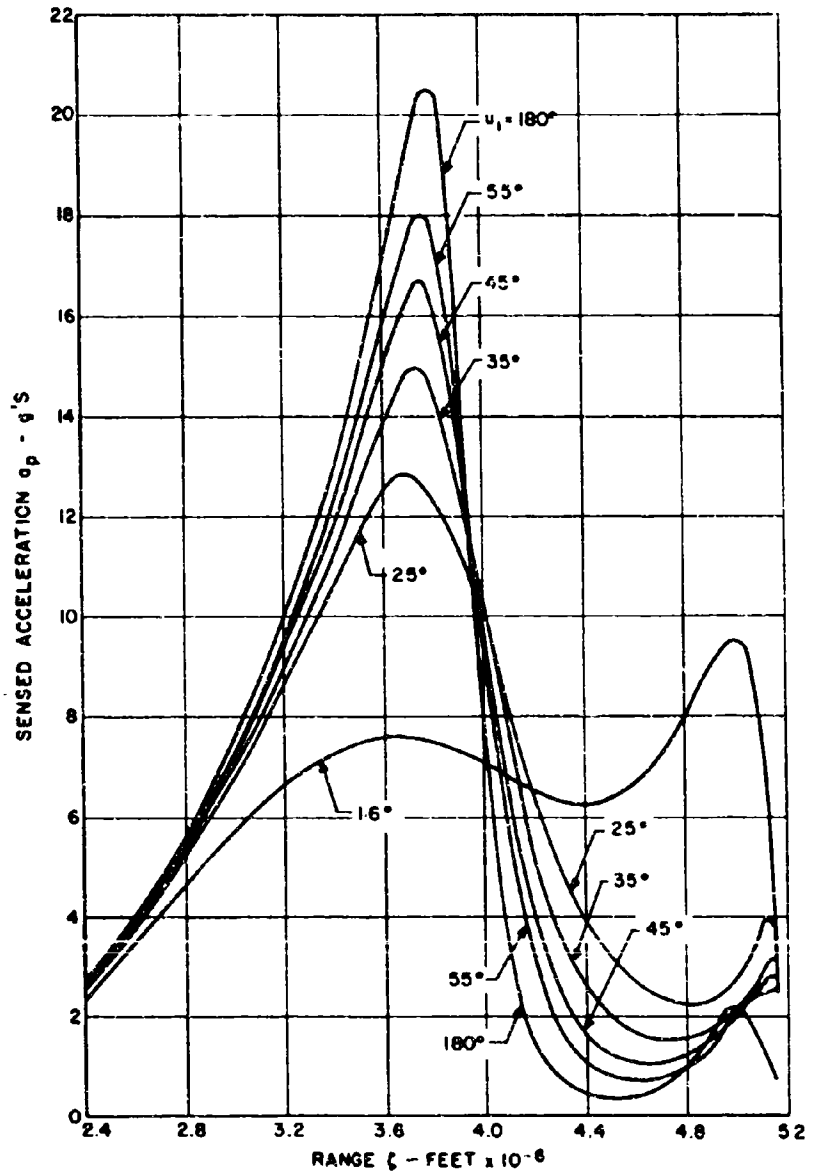

Figure 2-2. Sensed Acceleration Versus Range for Several Optimal Trajectories, Parameter u_1

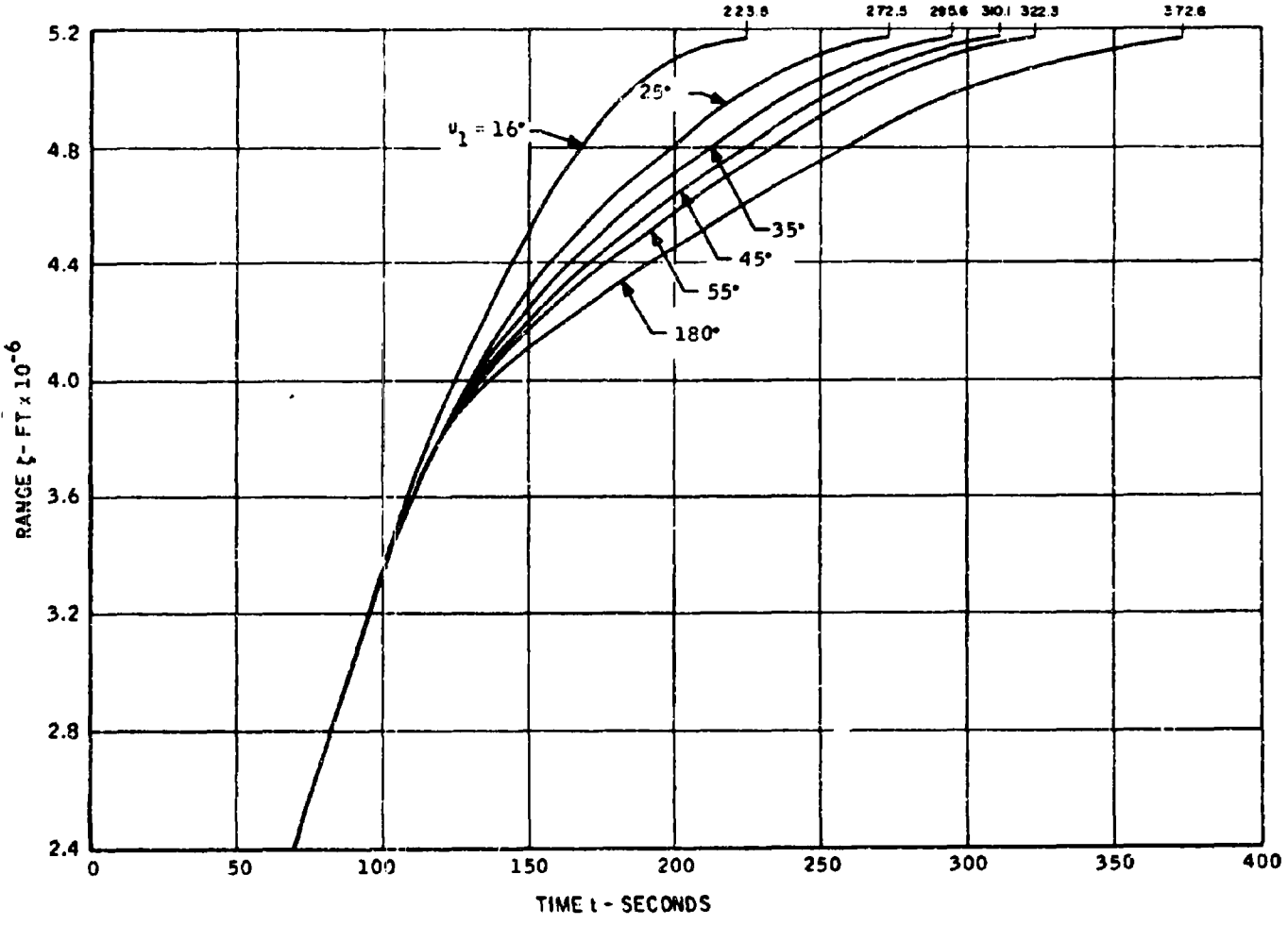

Figure 2-3. Range Versus Time for Several Optimal Trajectories, Parameter u_1

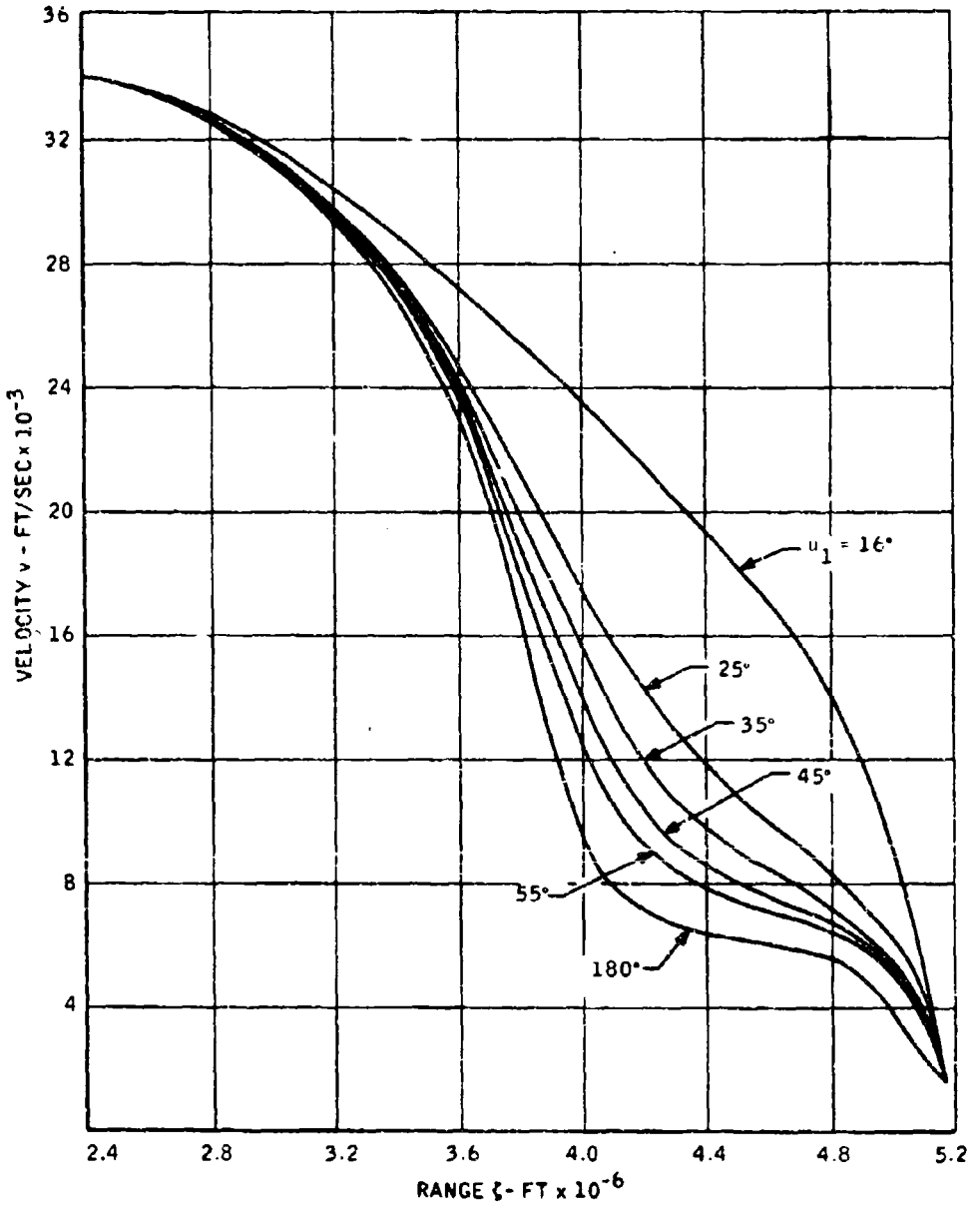

Figure 2-4. Velocity Versus Range for Several Optimal Trajectories, Parameter u_1

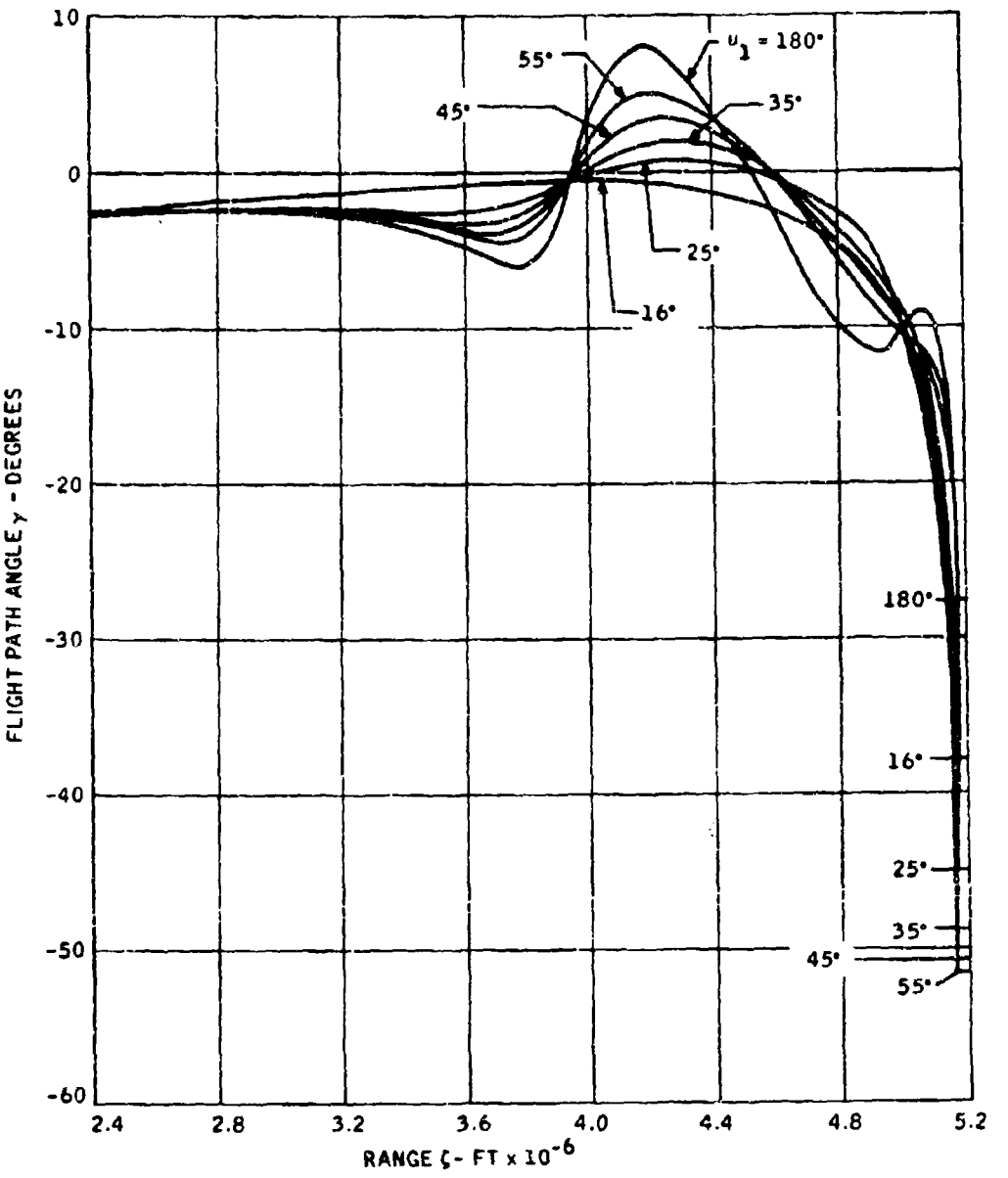

Figure 2-5. Flight Path Angle Versus Range for Several Optimal Trajectories, Parameter u_1

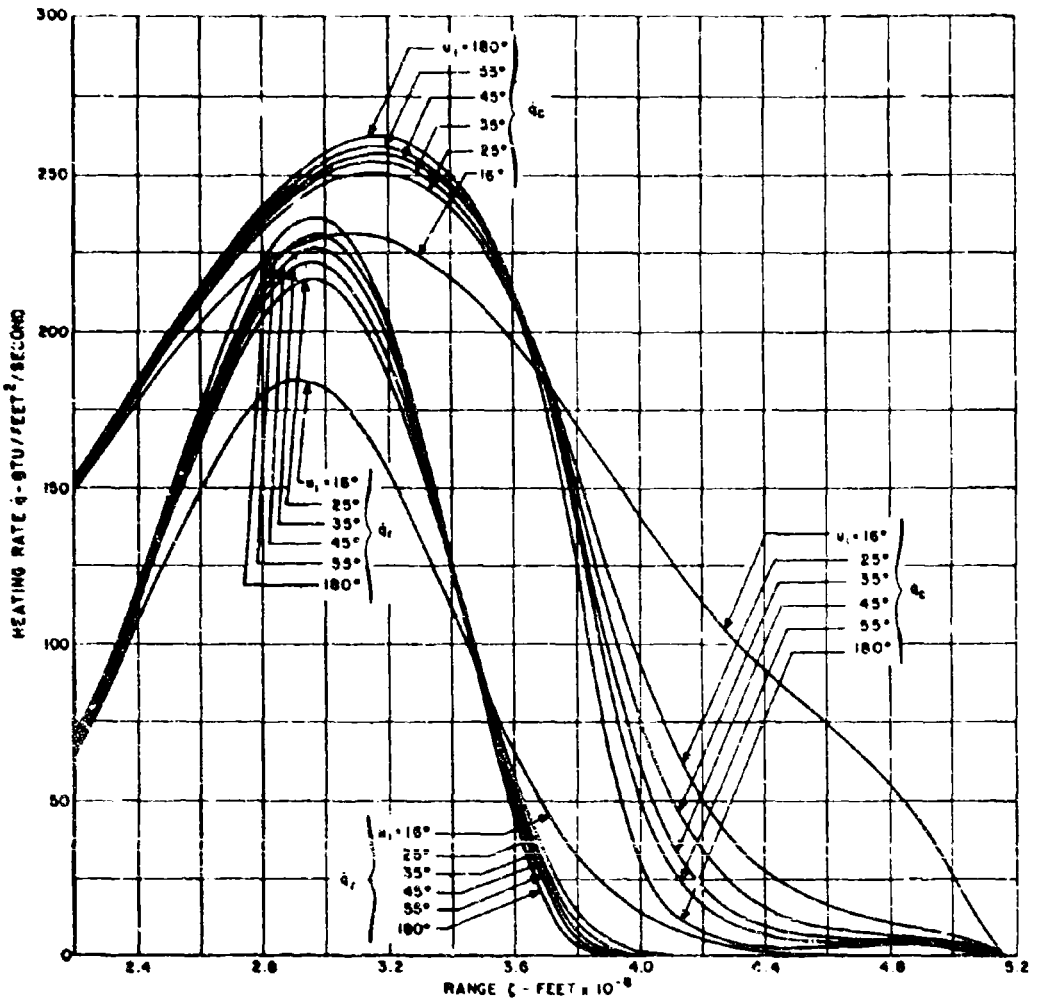

Figure 2-6. Convective and Radiative Heating Rates Versus Range for Several Optimal Trajectories, Parameter u_1

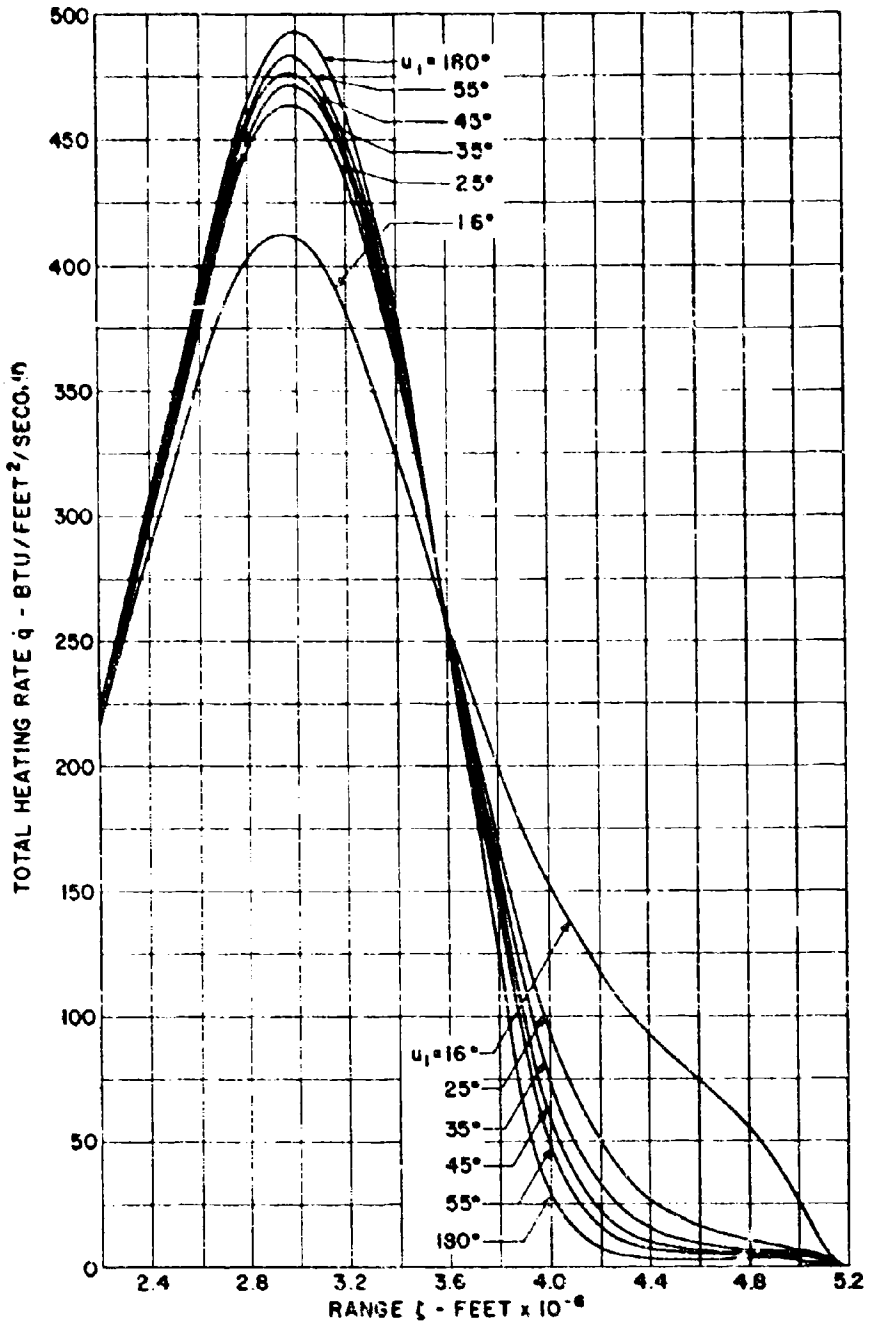

Figure 2-7. Total Heating Rate Versus Range for Several Optimal Trajectories, Parameter u_1

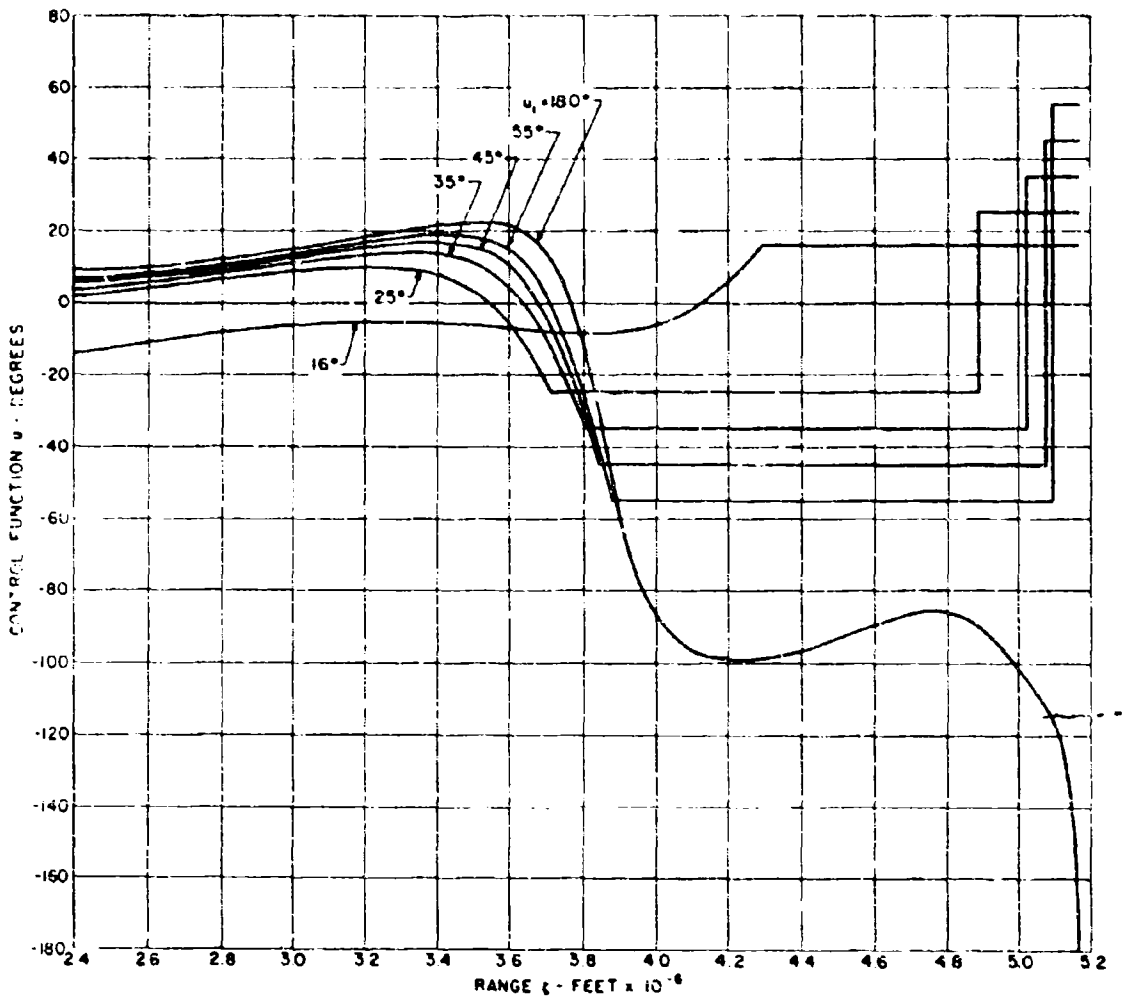

Figure 2-8. Control Function u Versus Range for Several Optimal Trajectories, Parameter u_1

Table 2-1. Control Constraint u_1 and Optimal Criterion J

u_1 (degrees)	J (BTU/ft^2)
16	27,334
25	26,524
35	26,246
45	26,071
55	25,951
180	25,736

corresponds to negative lift. Small values of the control also correspond to maximum drag, so maximum energy is dissipated. Before the bottom of the dive, the control functions all pass through zero and then on to the maximum lift condition (-90 degrees for the 180-degree optimal). The positive lift is required for ranging purposes and is maintained for the remainder of the re-entry process.

B. RE-ENTRY CORRIDOR MAPPING COMPUTATIONS

It was originally planned that optimal trajectories having maximum sensed acceleration loads of 10 g's would be used for the nonlinear optimal feedback control scheme of Section IV. However, a singular point caused computational difficulties. (The details of the problem and the method devised to circumvent the difficulty are presented in another subsection.) It was accordingly decided to proceed using unconstrained trajectories as a basis for demonstrating feasibility for the nonlinear optimal feedback control scheme.

The first step in the corridor mapping process was to round out the terminal conditions following Equations (2.12) to X_2 = 75,000 feet and X_3 = 1000 miles. The original values (75,530 feet and 979 miles, respectively) were made necessary by the initial conditions and the almost ballistic constraint u_1 = 16 degrees. The resulting trajectory is displayed in Figure 2-9 as the first member of a family of optimal trajectories for which the terminal range is the parameter.

1. Range Extension

It was decided to explore the ranging possibilities of the vehicle as the next step in the optimal re-entry corridor mapping process. The predictor scheme presented in Appendix A greatly facilitated the computations.

The differential equations are (2.6) and (2.14) (with μ_1 and μ_2 zero), and the control u satisfies (2.16) and (2.20). The boundary conditions are given by (2.25) where terminal range X_3 is the mapping parameter. Differential equations (2.26) were integrated to obtain the partial derivative solutions for the modified Newton-Raphson equations (2.28). The stopping condition for the integrations was the attainment of a desired terminal time T (updated after each iteration), so the zero element of the last vector in (2.28) was replaced by the term $(v(T) - X_1)$. The change in the stopping condition was made because it is somewhat easier and faster to stop at a given value of T than it is to interpolate for $v(T) = X_1$. The stopping condition for iterations was that the maximum ratio of variable-change to variable be less than a specified constant.

Starting trajectory initial conditions are v_o = 35,000 ft/sec, γ_o = -5.75 degrees, h_o = 400,000 ft, ζ_o = 0, and terminal conditions are X_1 = 1650 ft/sec, X_2 = 75,000 ft, and X_3 = 1000 miles. The next three trajectories were obtained using the optimal Newton-Raphson method, described in Appendix B, with terminal range increments of 10 miles. Succeeding members of the family were obtained using the Adams-Moulton predictor equation

$$x_{m+1} = x_m + \frac{h}{24}\left(55x'_m - 59x'_{m-1} + 37x'_{m-2} - 9x'_{m-3}\right) \qquad (2.29)$$

in which x is the vector (T, p_o), x' is the derivative of (T, p_o) with respect to terminal range, and h is the range increment. It is shown in Appendix A that x' is the third column vector of the inverse Newton-Raphson matrix in Equation (2.28), when (T, p_o) satisfies Equations (2.25).

The range was extended to 2020 miles by this process. Most of the intermediate predicted values of (T, p_o) produced optimal trajectories, which shows the power of the predictor scheme. As the upper limit on range was approached, prediction gradually worsened, and it is doubtful that range could be extended much further for the vehicle and initial conditions considered.

Five of the family of trajectories are plotted in Figures 2-9 through 2-15. Figure 2-9 shows that the first dive into the atmosphere becomes shallower, as range is extended, and that the skip which follows becomes higher and longer. This behavior is caused by the control function (Figure 2-10) which leaves the negative lift region ($u > 0$), and goes to the maximum lift condition ($u = -90$ degrees) earlier in the flight as range is extended. Less energy is lost on the first dive, as can be seen in the velocity curves of Figure 2-11, and the decrease in the first acceleration peak of Figure 2-12. The flight-path angle excursions, Figure 2-13, also become smaller. Toward the end of the skip, the control approaches the negative lift condition, and, for the longer ranges, produces negative lift to more quickly terminate the skip. The secondary acceleration peak rises with increasing range in order to dissipate the increased remaining energy. There is a minor sashay in the paths near the endpoints, due to the control passing through maximum lift and (L/D) on its way to -180 degrees.

Figure 2-14 shows that total heat increases with terminal range, as might be expected. However, it is somewhat surprising that the total flight time of Figure 2-15 first increases with range, and then decreases for longer terminal ranges.

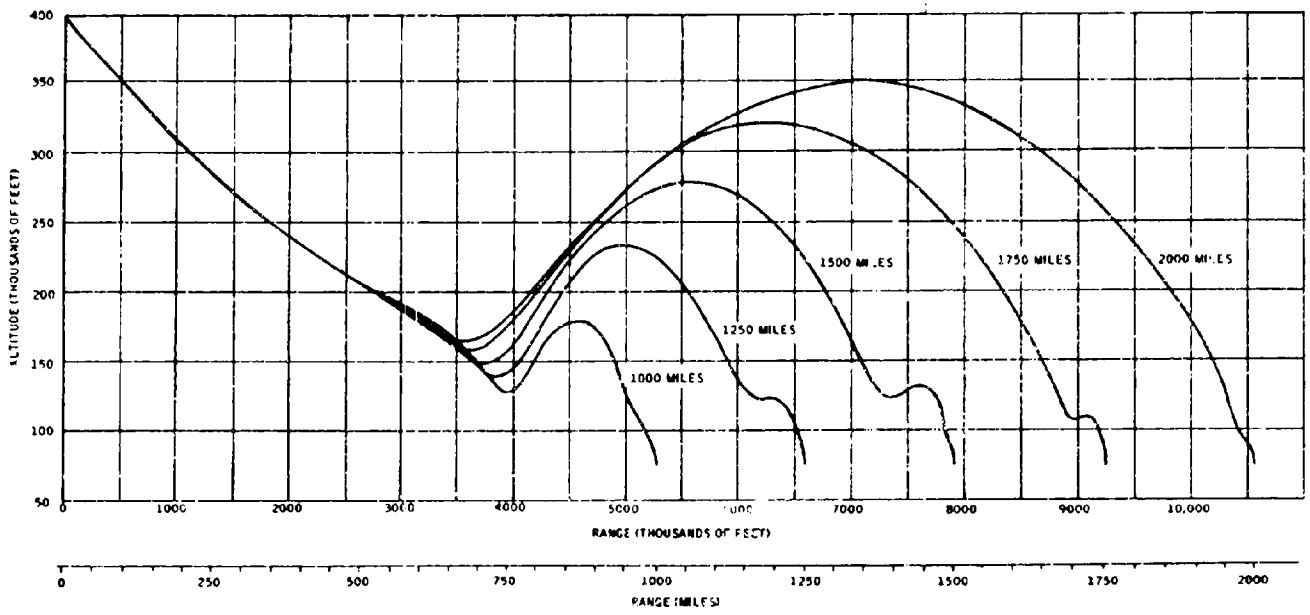

Figure 2-9. Altitude Versus Range for Unconstrained Optimal Trajectories, Parameter ζ (T)

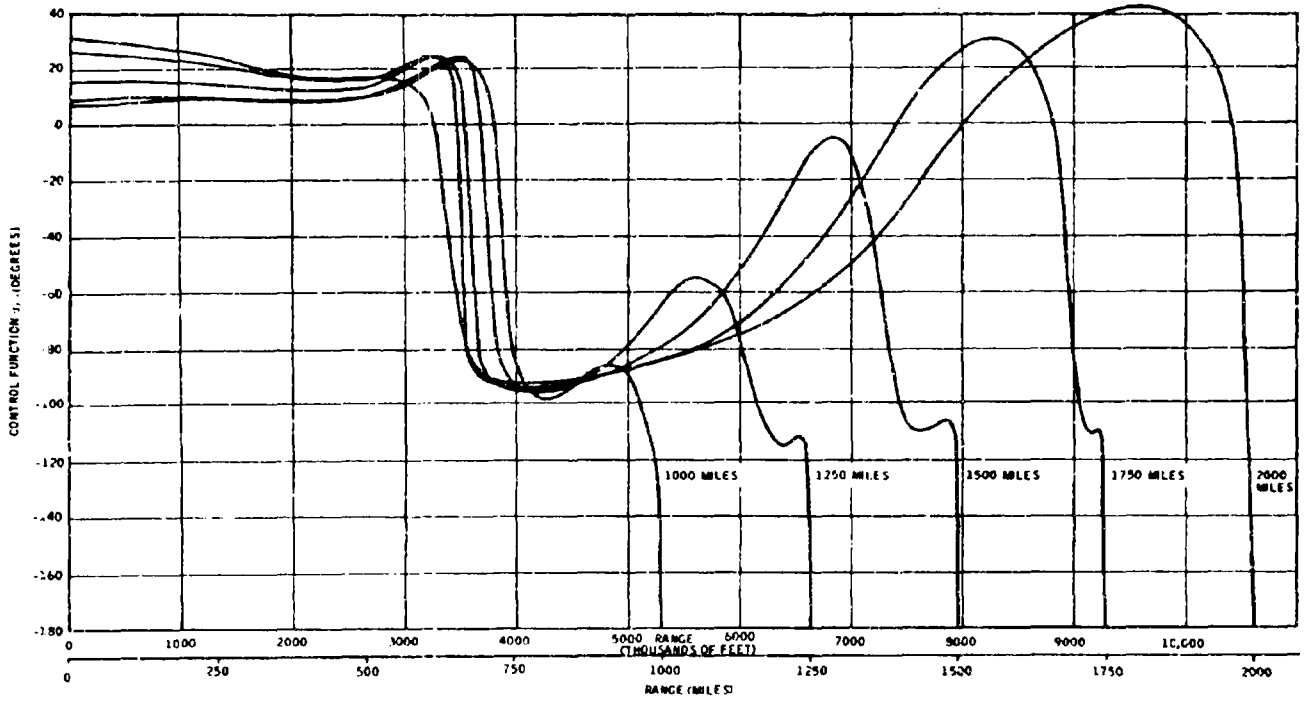

Figure 2-10. Control Function u Versus Range for Unconstrained Optimal Trajectories, Parameter ζ (T)

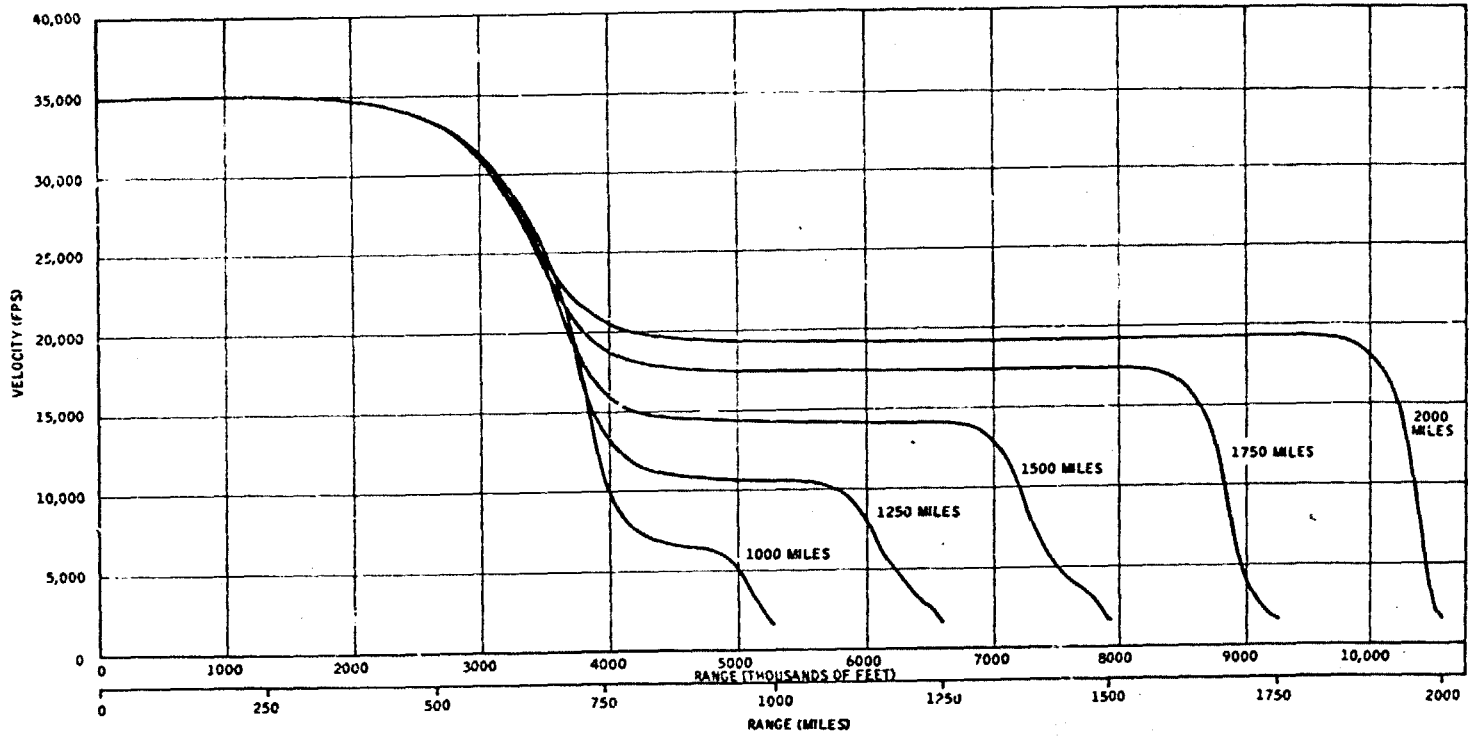

Figure 2-11. Velocity Versus Range for Unconstrained Optimal Trajectories, Parameter ζ (T)

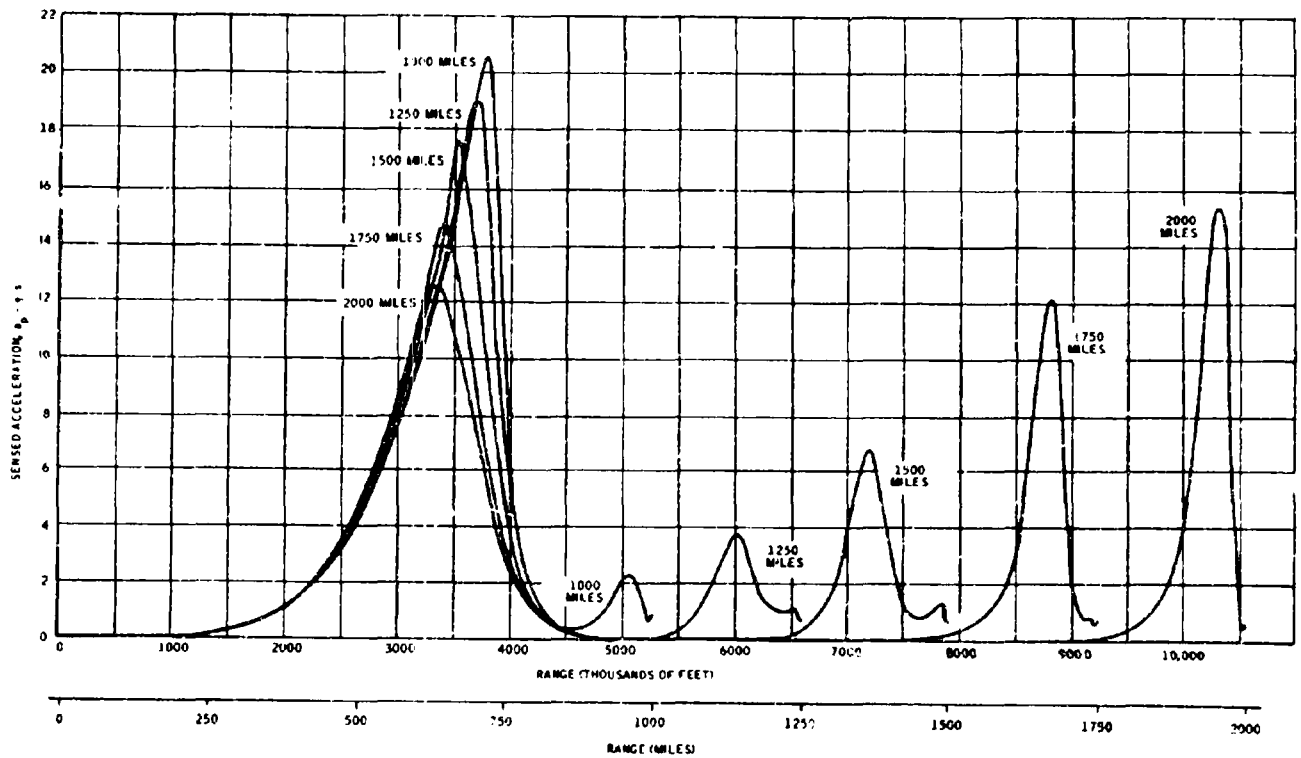

Figure 2-12. Sensed Acceleration Versus Range for Unconstrained Optimal Trajectories, Parameter ζ (T)

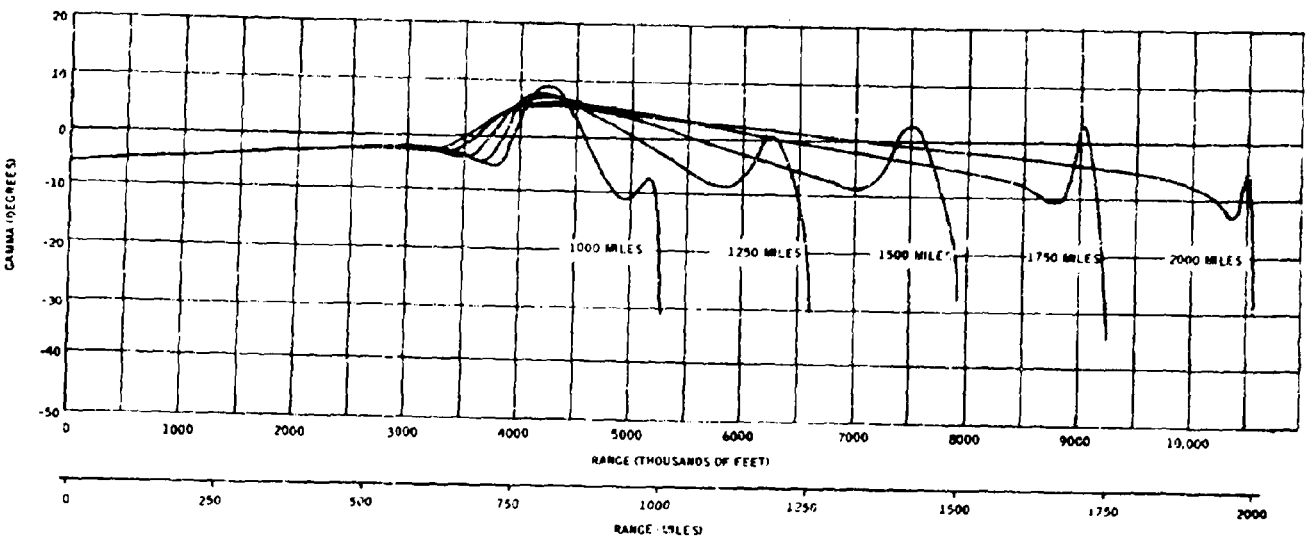

Figure 2-13. Flight Path Angle Versus Range for Unconstrained Optimal Trajectories, Parameter ζ (T)

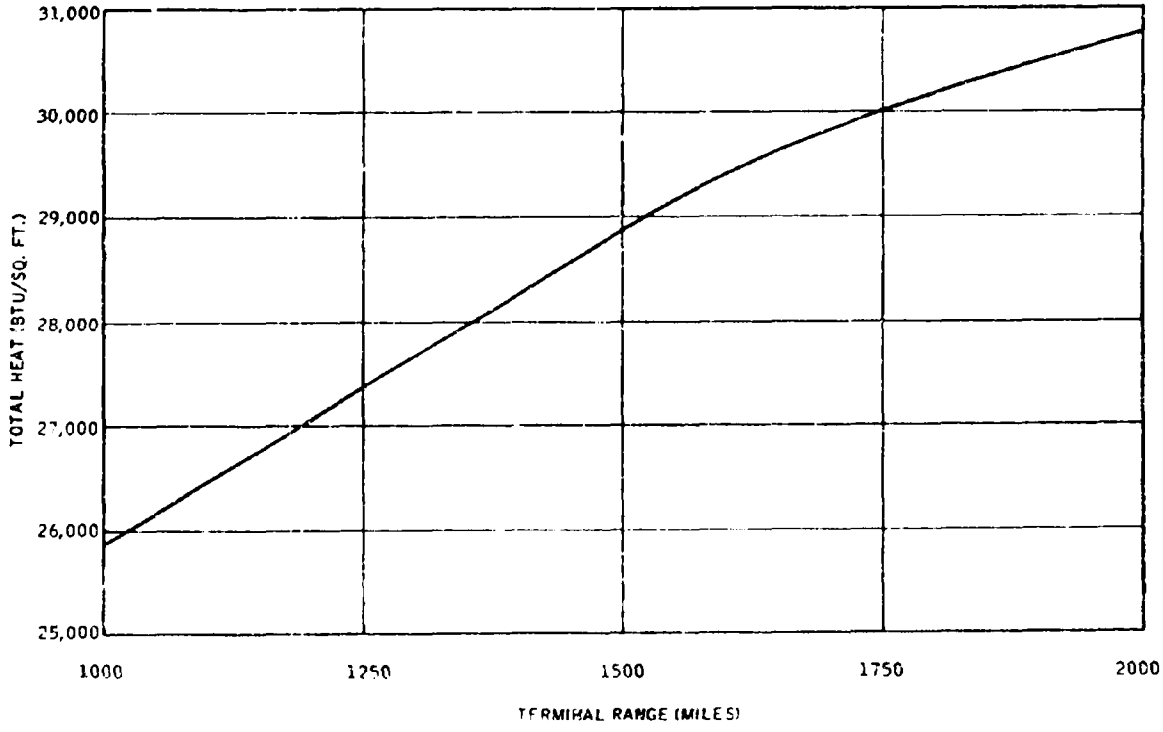

Figure 2-14. Total Heat Versus Terminal Range for Unconstrained Optimal Trajectories

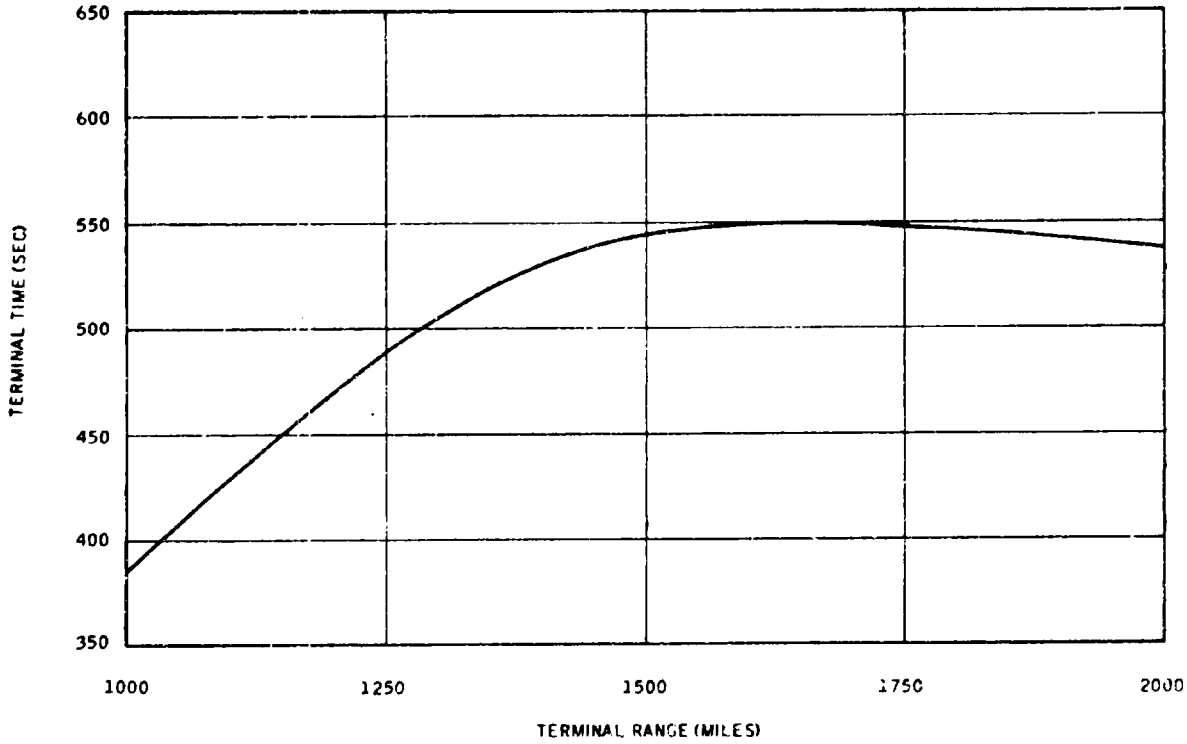

Figure 2-15. Terminal Time Versus Terminal Range for Unconstrained Optimal Trajectories

On the basis of these results, it was decided that the 1500-mile trajectory would be used as the "nominal" trajectory for development of the nonlinear optimal feedback control scheme. This trajectory represents a reasonable compromise between total heat, peak acceleration and total length of skip.

2. Corridor Mapping Program

The corridor mapping problem considered is that of sweeping out a reasonable region of initial conditions about the "nominal" trajectory, and thereby obtaining a set of optimal trajectories covering the expected re-entry corridor. The terminal values of velocity, altitude and range are the same for all these trajectories, as is the terminal value of multiplier p_2 and the Hamiltonian (both zero), so that the trajectories all belong to the same field of extremals (see Section IIIA).

It is shown in subsection C that time is unimportant, so far as this problem is concerned, and furthermore, that all re-entry trajectories may be started at a point where initial range is zero. Hence, the only initial conditions which need be varied are v_o, γ_o and ξ_o.

It is convenient, for the mapping process, to integrate the system of differential equations from the terminal point to the initial point. The predictor scheme may then be used to move the initial conditions over their range of variation. Accordingly, define "back time" by

$$s = T-t \ , \tag{2.30}$$

and note that

$$\frac{dx}{ds} = \frac{dx}{dt}\frac{dt}{ds} = -\frac{dx}{dt} \ , \tag{2.31}$$

so that the change of independent variable changes only the sign of the right-hand sides of the differential equations. The system of equations to be integrated thus includes (2.6), (2.14) -- with $\mu_1 = \mu_2 = 0$ -- and (2.26), with opposite signs for the right-hand sides, and the control u satisfies (2.16) and (2.20). The "initial" conditions for the transformed equations (2.6) and (2.14) are $s = 0$ and

$$\begin{aligned} v_T - X_1 &= 0 \\ \xi_T - X_2/R &= 0 \\ \zeta_T - X_3 &= 0 \\ p_{2_T} &= 0, \end{aligned} \tag{2.32}$$

with $X_1 = 1650$ ft/sec, $X_2 = 75,000$ ft, and $X_3 = 1500$ miles. At $s = T$, the functional dependence of the solutions on the missing initial conditions may be written

$$\begin{aligned} x &= x\left(T, p_{1_T}, \gamma_T, p_{3_T}, p_{4_T}\right) \\ p &= p\left(T, p_{1_T}, \gamma_T, p_{3_T}, p_{4_T}\right), \end{aligned} \tag{2.33}$$

so the set of boundary conditions to be satisfied by each optimal trajectory is

$$\begin{aligned} v\left(T, p_{1_T}, \gamma_T, p_{3_T}, p_{4_T}\right) - X_{10} &= 0 \\ \gamma\left(T, p_{1_T}, \gamma_T, p_{3_T}, p_{4_T}\right) - X_{20} &= 0 \\ \xi\left(T, p_{1_T}, \gamma_T, p_{3_T}, p_{4_T}\right) - X_{30}/R &= 0 \\ \zeta\left(T, p_{1_T}, \gamma_T, p_{3_T}, p_{4_T}\right) &= 0 \\ H\left(p_{1_T}, \gamma_T, p_{3_T}, p_{4_T}\right) &= 0 . \end{aligned} \tag{2.34}$$

X_{10}, X_{20} and X_{30} are, of course, the initial conditions at t= 0 (or terminal conditions at s= T) to be varied in the mapping process.

Let $\eta_{ij}(s)$ and $\zeta_{ij}(s)$, i, j= 1, ..., 4, be the solutions of the transformed system of Equations (2.26) with initial conditions

$$\left[\eta_{ij}(0)\right] = \begin{bmatrix} 0 & 0 & 0 & 0 \\ 0 & 1 & 0 & 0 \\ 0 & 0 & 0 & 0 \\ 0 & 0 & 0 & 0 \end{bmatrix} \qquad \left[\zeta_{ij}(0)\right] = \begin{bmatrix} 1 & 0 & 0 & 0 \\ 0 & 0 & 0 & 0 \\ 0 & 0 & 1 & 0 \\ 0 & 0 & 0 & 1 \end{bmatrix} \tag{2.35}$$

Then the Newton-Raphson equations for system (2.34) are

$$\begin{bmatrix} dT \\ dp_{1_T} \\ d\gamma_T \\ dp_{3_T} \\ dp_{4_T} \end{bmatrix} = - \begin{bmatrix} \dot{v}(T) & \eta_{11}(T) & \eta_{12}(T) & \eta_{13}(T) & \eta_{14}(T) \\ \dot{\gamma}(T) & \eta_{21}(T) & \eta_{22}(T) & \eta_{23}(T) & \eta_{24}(T) \\ \dot{\xi}(T) & \eta_{31}(T) & \eta_{32}(T) & \eta_{33}(T) & \eta_{34}(T) \\ \dot{\zeta}(T) & \eta_{41}(T) & \eta_{42}(T) & \eta_{43}(T) & \eta_{44}(T) \\ 0 & f_1(0) & -\dot{p}_2(0) & f_3(0) & f_4(0) \end{bmatrix}^{-1} \begin{bmatrix} v(T)-X_{10} \\ \gamma(T)-X_{20} \\ \xi(T)-X_{30}/R \\ \zeta(T) \\ H \end{bmatrix} \tag{2.36}$$

The first three columns of the inverse matrix may be identified as the derivatives of (T, p_{1_T}, γ_T, p_{3_T}, p_{4_T}) with respect to X_{10}, X_{20}, and X_{30}/R, respectively, for the predictor equation (2.29).

Twenty-six trajectories spanning the re-entry corridor were generated using the optimal Newton-Raphson method and the predictor scheme. The initial conditions and total heat for these and the "nominal" trajectory (at t= 0) are summarized in Table 2-2. Trajectory 2 was obtained first. The first three trajectories were determined by the optimal Newton-Raphson method, using ΔX_{10} = +50 ft/sec as the increment. The predictor scheme then generated the remaining trajectories. The predictor scheme was used exclusively to obtain trajectory 3, since back derivatives were available from the trajectories leading up to trajectory 2.

Table 2-2. Initial Conditions and Total Heat for 27 Optimal Trajectories Obtained During the Corridor Mapping Process

Trajectory Number	Initial Velocity (ft/sec)	Initial Flight Path Angle (degrees)	Initial Altitude (ft)	Sign of Change From Trajectory 1			Total Heat
				ΔX_{10}	ΔX_{20}	ΔX_{30}	
1	35000	-5.75	400,000	0	0	0	28,872
2	35750	-5.75	400,000	+	0	0	31,888
3	34250	-5.75	400,000	-	0	0	26,252
4	35000	-5.30	400,000	0	+	0	29,278
5	35000	-7.65	400,000	0	-	0	28,666
6	35000	-5.75	440,000	0	0	+	29,032
7	35000	-5.75	360,000	0	0	-	28,757
8	35750	-5.30	400,000	+	+	0	32,280
9	35750	-7.65	400,000	+	-	0	32,116
10	34250	-5.30	400,000	-	+	0	26,657
11	34250	-7.65	400,000	-	-	0	25,792
12	35750	-5.75	440,000	+	0	+	32,135
13	35750	-5.75	360,000	+	0	-	31,944
14	34250	-5.75	440,000	-	0	+	26,362
15	34250	-5.75	360,000	-	0	-	26,128
16	35000	-5.30	427,500	0	+	+	29,963
17	35000	-5.30	360,000	0	+	-	29,017
18	35000	-7.65	440,000	0	-	+	28,510
19	35000	-7.65	360,000	0	-	-	28,817
20	35600	-5.40	430,000	+	+	+	32,444
21	35600	-5.40	370,000	+	+	-	31,374
22	35600	-7.35	430,000	+	-	+	31,110
23	35600	-7.35	370,000	+	-	-	31,375
24	34400	-5.40	430,000	-	+	+	27,326
25	34400	-5.40	370,000	-	+	-	26,891
26	34400	-7.35	430,000	-	-	+	26,216
27	34400	-7.35	370,000	-	-	-	26,368

Trajectories 4 and 5 were generated in a similar fashion, using $\Delta X_{20} = 0.025$ degree. It was found, however, that as the flight path angle became steeper (going toward trajectory 5), the increment could be increased to $\Delta X_{20} = 0.1$ degree with very little degradation in the performance of the predictor scheme.

Trajectories 6 and 7 were obtained similarly, and it was determined that $\Delta X_{30} = 2500$ ft was a satisfactory increment for the altitude mapping process.

From convergence characteristics of the optimal Newton-Raphson process, it was found that velocity changes were easiest to obtain, and that flight path angle changes were hardest to satisfy. Consequently, trajectories 8 through 19 were generated using the most easily changed single parameter. For example, the trajectory for which $X_{20} = -5.30$ degrees was the starting path for the generation of trajectories 8 and 10, and the mapping process took place over X_{10}.

Trajectories 20 through 27 were generated in a similar fashion, except that intermediate maps over X_{30} were performed first, followed by maps over X_{10}. Thus for example, the trajectory for which $X_{20} = -5.40$ degrees was the starting trajectory to generate paths for which $X_{30} = 370,000$ feet and 430,000 feet respectively. The X_{10} map for these paths produced trajectories 21, 25, 20 and 24.

The ease of attainment of the various paths varied considerably as a function of parameter values. As pointed out above, the step size for the X_{20}-map could be increased to $\Delta X_{20} = 0.1$ degree as the flight path angle became steeper. When going in the opposite direction, however, the smaller step size was required. Trajectory 17 was generated with some difficulty, although the process became easier as initial altitude decreased. In trying to increase altitude to 440,000 feet for trajectory 16, the predictor scheme failed to go beyond $X_{30} = 427,500$ feet.

In most cases, the velocity-map was easily accomplished. Optimal Newton-Raphson many times converged in one step, and the predictor scheme (once started) almost always predicted optimal trajectories. Some difficulties were experienced in trying to obtain trajectories 20 and 24 (the worst cases were always shallow initial flight path angle and increased altitude, as might be expected). A trajectory for X_{10} = 34,950 feet was obtained after several optimal Newton-Raphson iterations, and further such steps would have been wasteful of computer time. A two point predictor formula from Reference 2 was used to predict trajectories above and below the two members of the velocity-map family of paths. With these improved estimates, the optimal Newton-Raphson scheme converged rapidly, and, thereafter, the predictor scheme predicted optimal trajectories at each step. This again shows the power of the predictor scheme and indicates that lower-ordered predictor formulas might well be of value during the mapping process.

In all cases, the optimal Newton-Raphson scheme was quite sensitive to the weighting factors used to multiply Equations (2.34) (see Appendix B). It was found, however, that a single set of weights could be used when mapping over a given variable. The numbers used are given in Table 2-3.

Table 2-3. Weighting Factors for the Optimal Newton-Raphson Method Used for the Mapping Variables.

Weights	Variable X_{10}	X_{20}	X_{30}
w_1	10	1×10^{-2}	1
w_2	1×10^{4}	1×10^{4}	1×10^{4}
w_3	1×10^{-2}	1×10^{-2}	10
w_4	1×10^{-3}	1×10^{-3}	1×10^{-3}
w_5	1	1	1

Trajectories 2 through 7 are compared with the "nominal" 1500-mile trajectory in Figures 2-16 through 2-27. It is seen that trajectories 2 and 3 are quite symmetric about the nominal path, except for areas where the curves cross each other. Larger differences from nominal values are observed for trajectories 4 and 5 (Figures 2-20 - 2-23), and particularly for trajectory 5. Note that the steeper initial flight path angle produces a large skip and high acceleration peaks. Somewhat similar results are observed for trajectories 6 and 7 (Figures 2-24 - 2-27). Here however, a lower initial altitude produces a longer skip and higher acceleration peaks. The control functions for all 27 optimal trajectories are plotted in Figure 2-28. Note that the characteristics are similar to those of Figure 2-10. The control functions for those trajectories displaying large skips assume their minimum values earlier, and then rise higher than those for the better behaved paths. A good coverage of the control region of interest was obtained during the mapping process.

C. THE DATA GENERATING PROGRAM

The data to be fit consists of the control function u for the 27 optimal trajectories, and two multipliers like p_1 and p_2. The multipliers are included in hopes that an arctangent relationship such as (2.16) will produce an overall reduction in the size of the control function fit. Additional data includes the partial derivatives of u and the two multipliers with respect to the state vector.

1. Statement of the Problem

The problem is transformed to an equivalent, although somewhat reduced and more convenient, form through a series of transformations. These transformations are carried out in Appendix C and the results are presented here. The new set of differential equations corresponding to (2.2) and system (2.6) are:

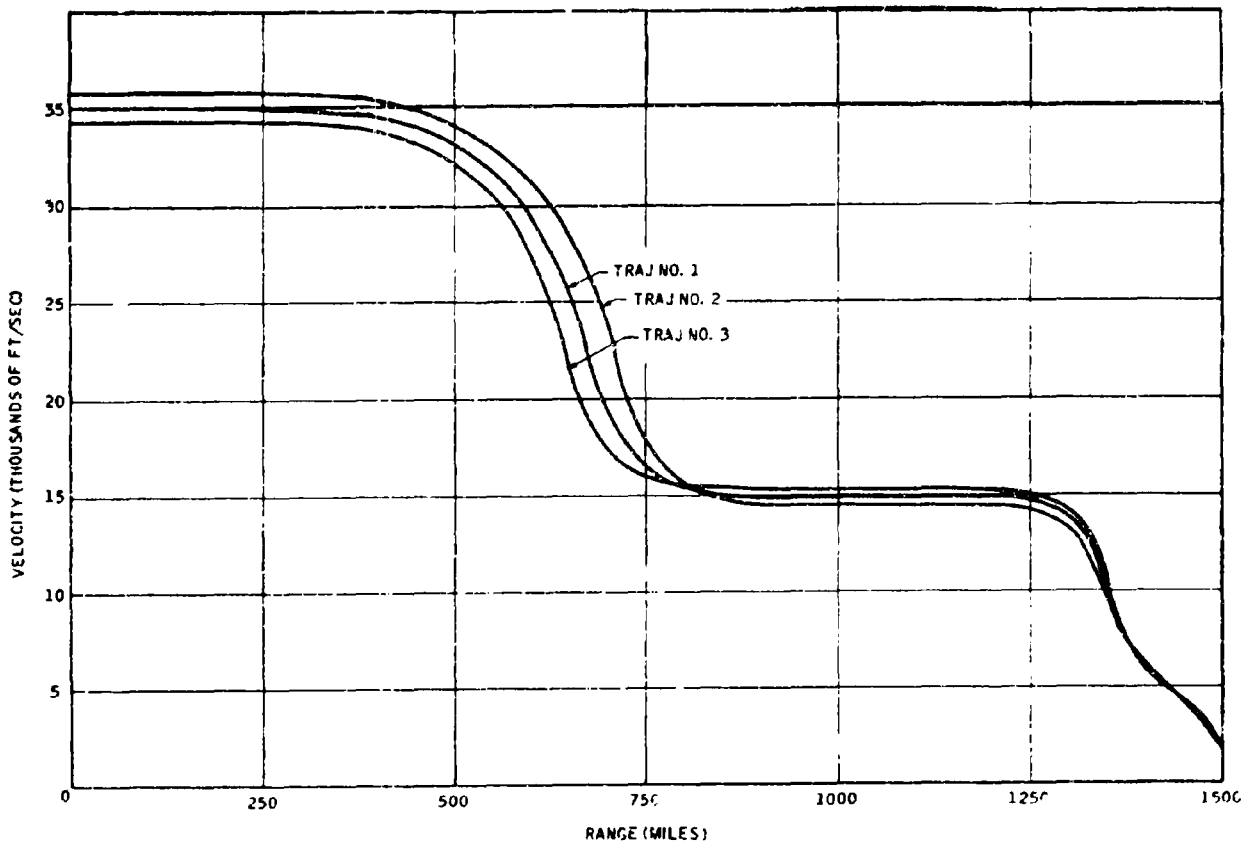

Figure 2-16. Velocity Versus Range for Optimal Trajectories 1, 2, and 3

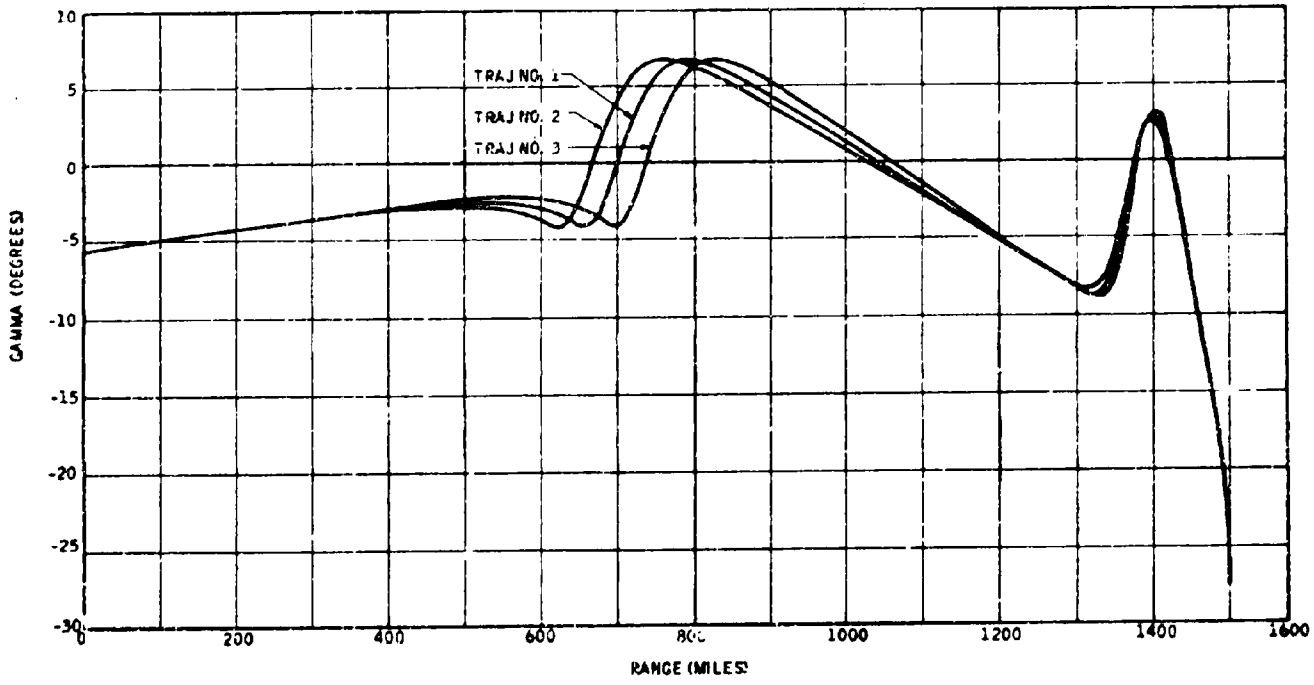

Figure 2-17. Flight Path Angle Versus Range for Optimal Trajectories 1, 2 and 3

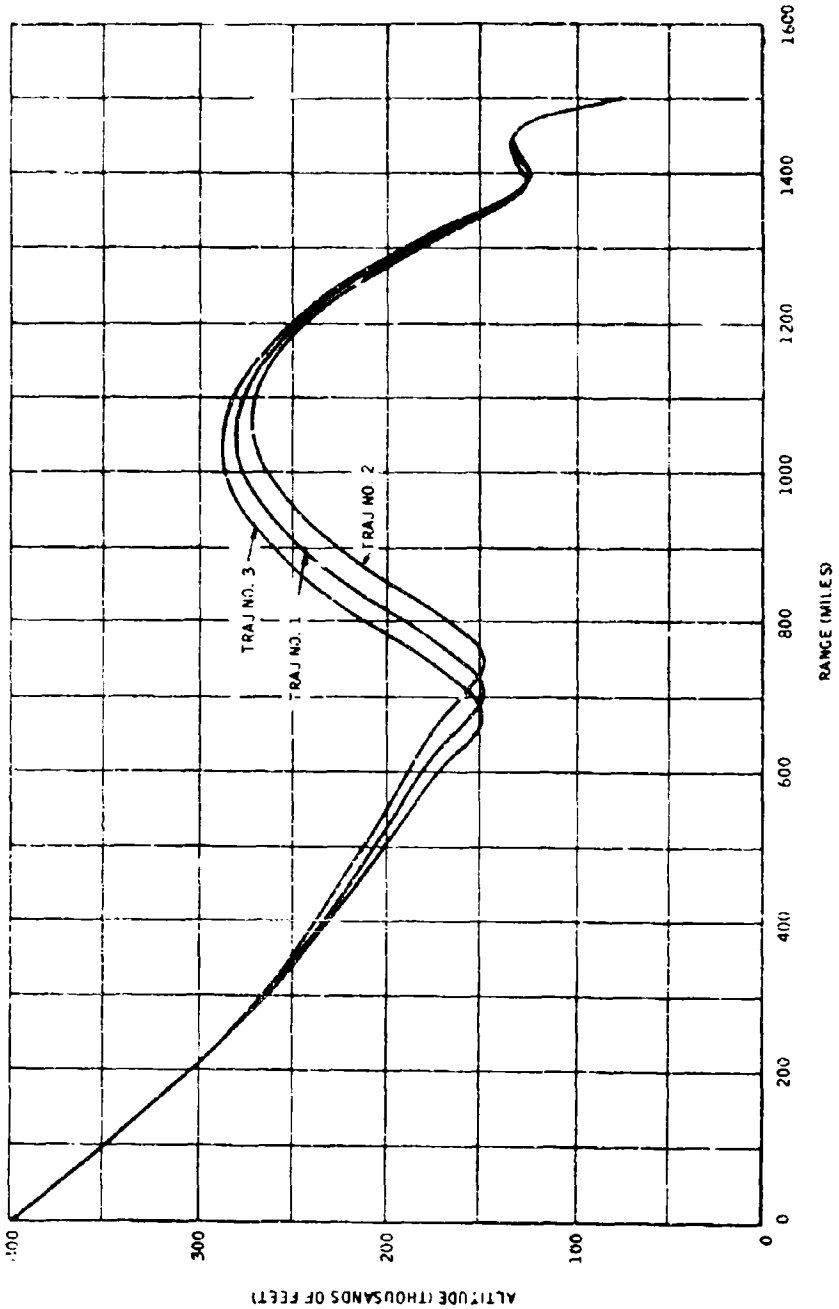

Figure 2-18. Altitude Versus Range for Optimal Trajectories 1, 2 and 3

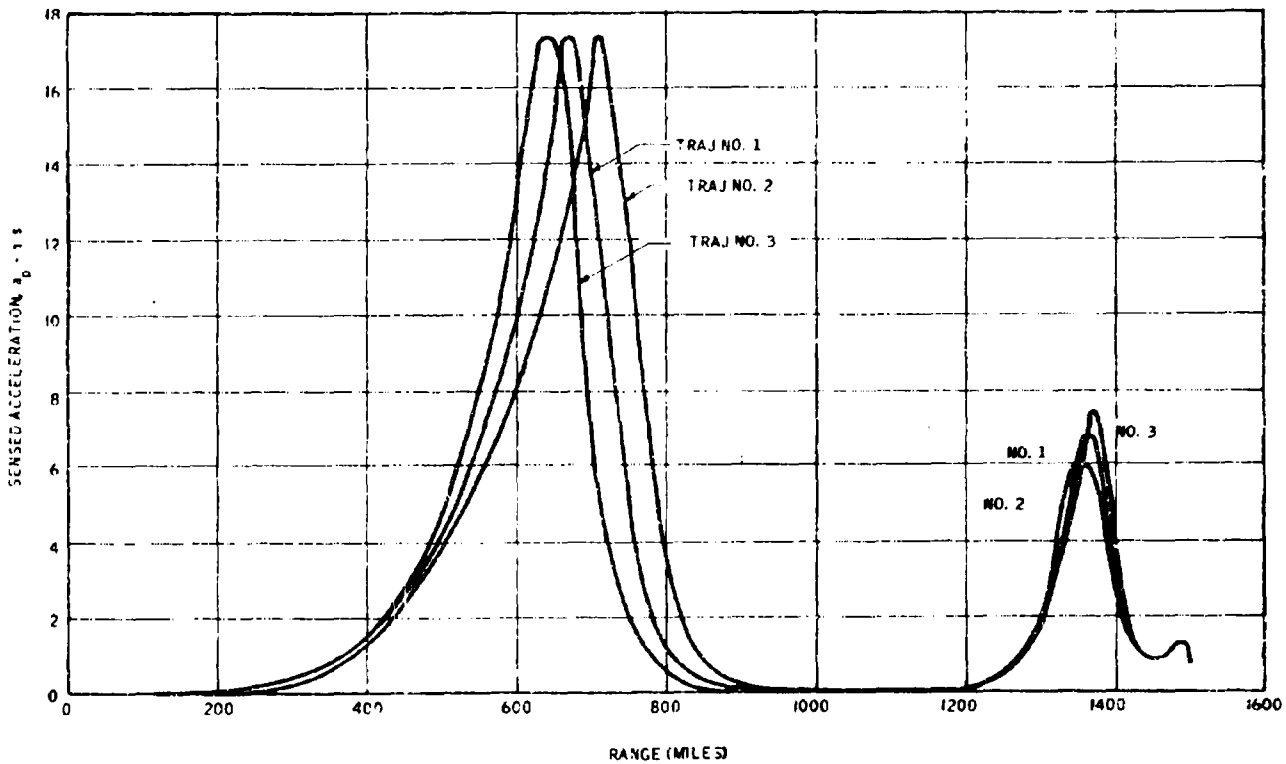

Figure 2-19. Sensed Acceleration Versus Range for Optimal Trajectories 1, 2 and 3

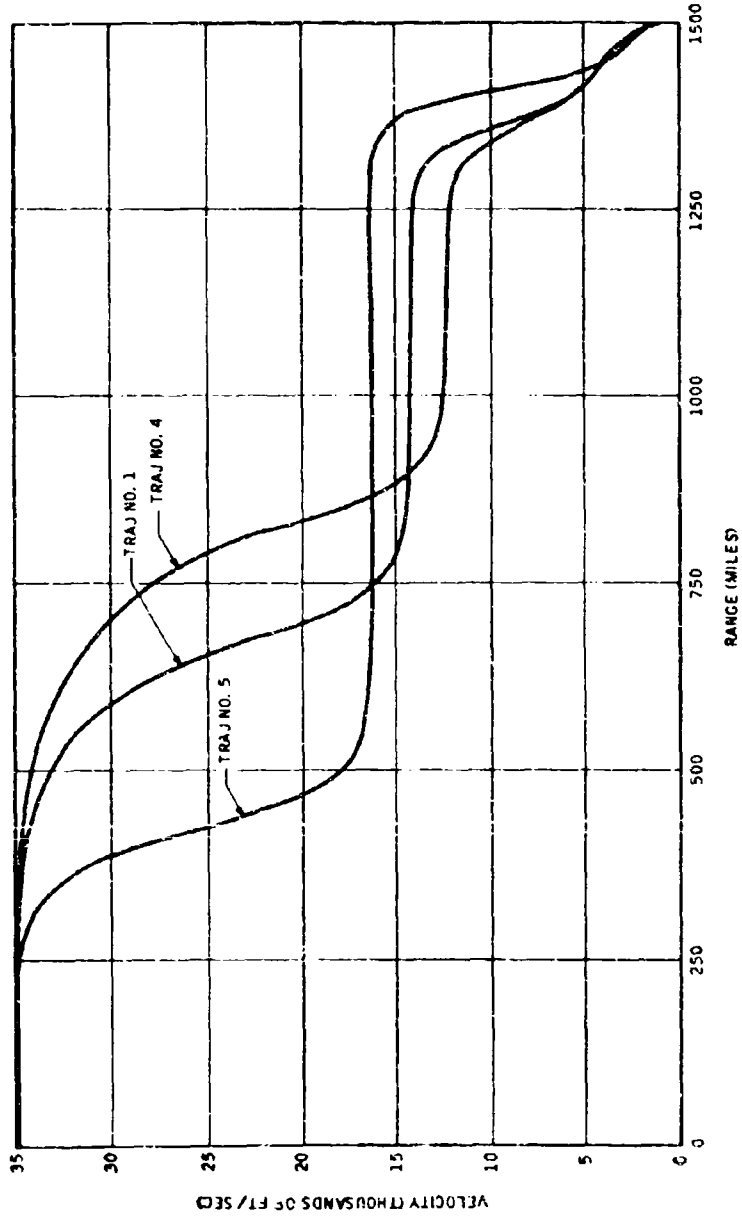

Figure 2-20. Velocity Versus Range for Optimal Trajectories 1, 4 and 5

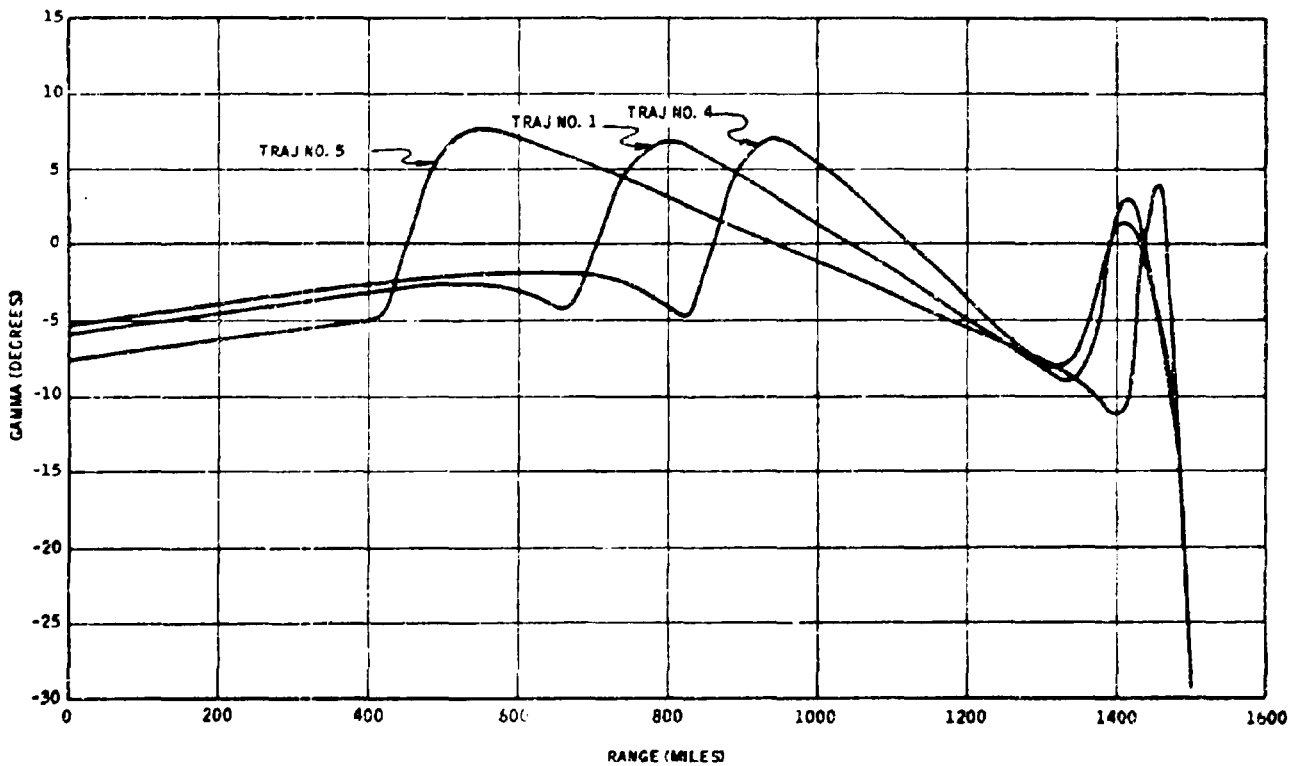

Figure 2-21. Flight Path Angle Versus Range for Optimal Trajectories 1, 4 and 5

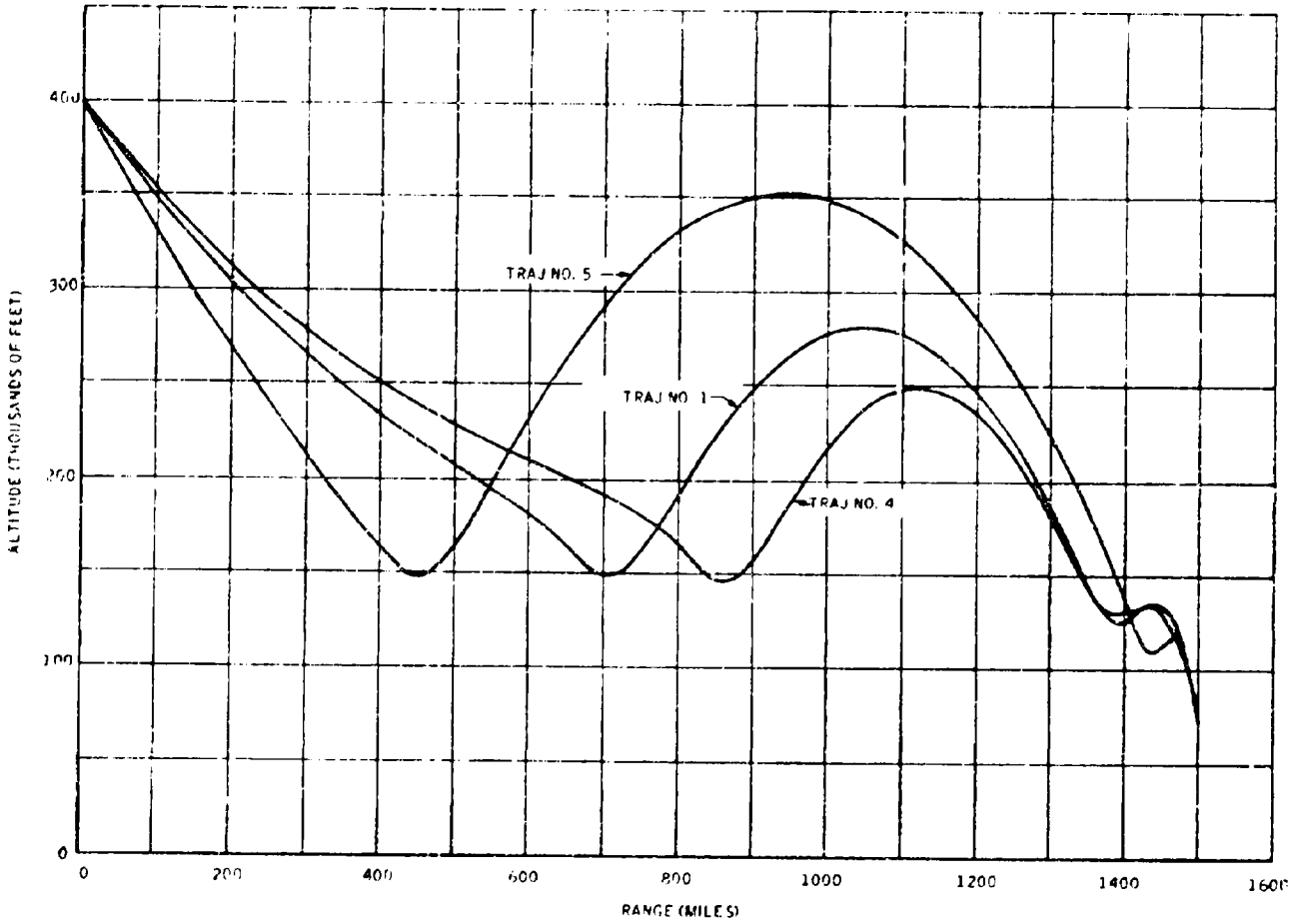

Figure 2-22. Altitude Versus Range for Optimal Trajectories 1, 4 and 5

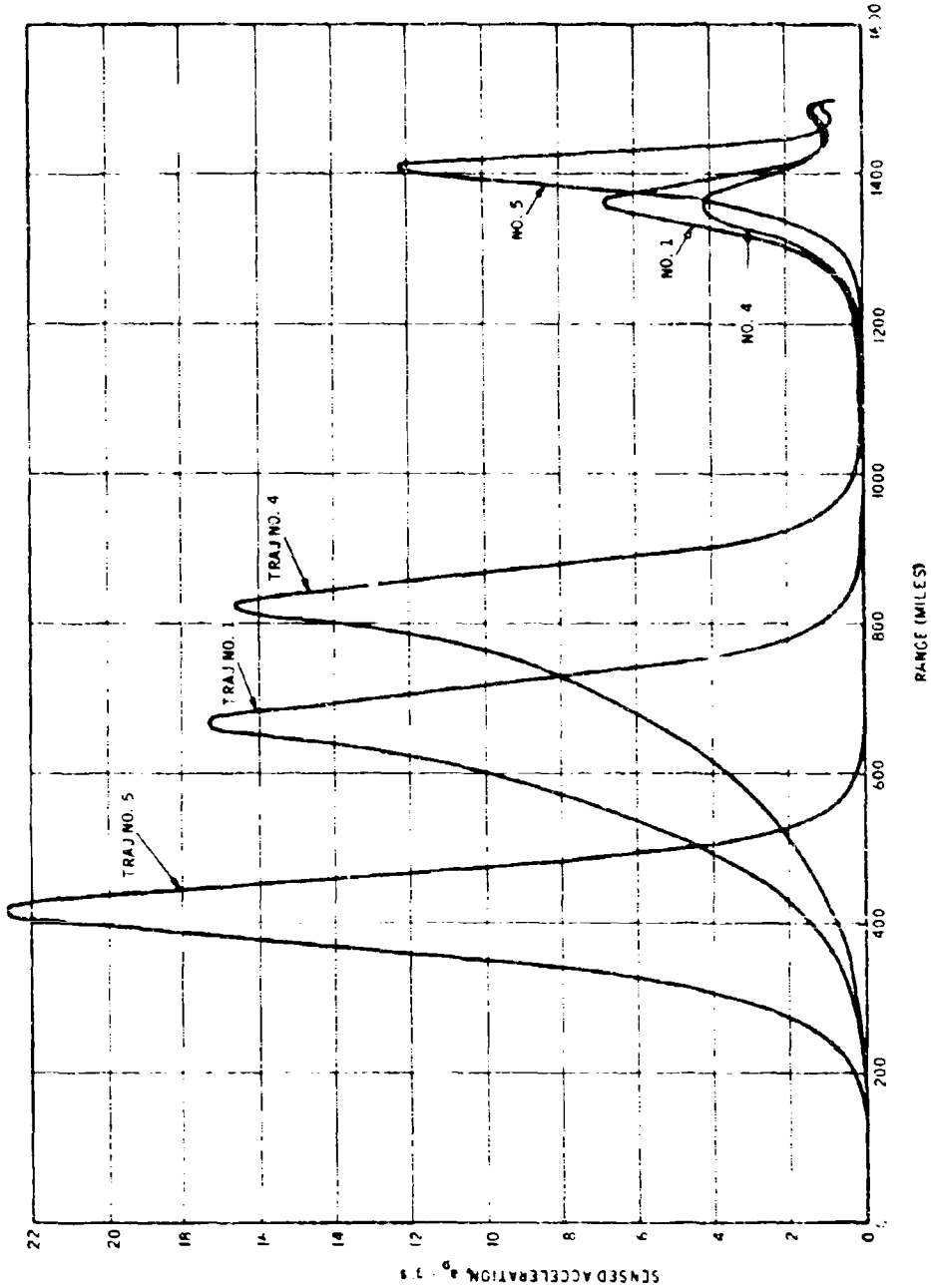

Figure 2-23. Sensed Acceleration Versus Range for Optimal Trajectories 1, 4 and 5

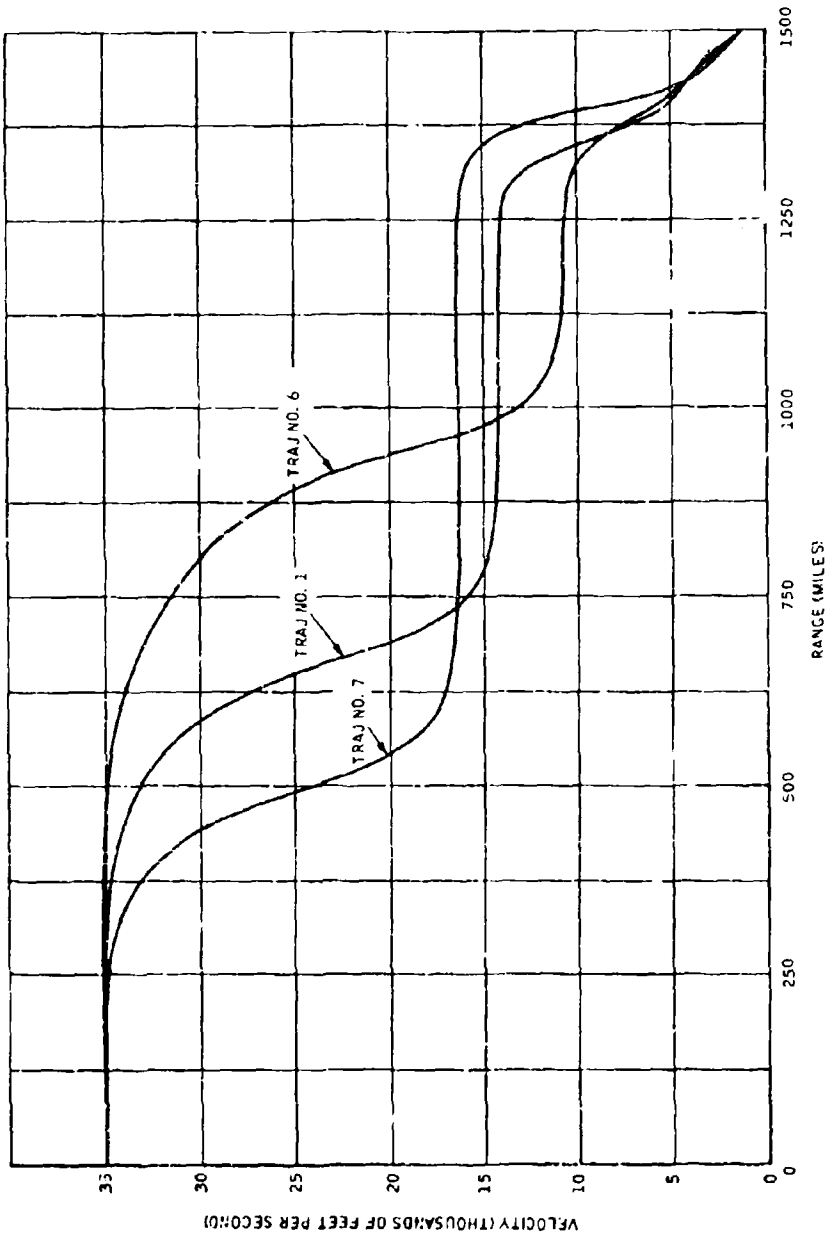

Figure 2-24. Velocity Versus Range for Optimal Trajectories 1, 6 and 7

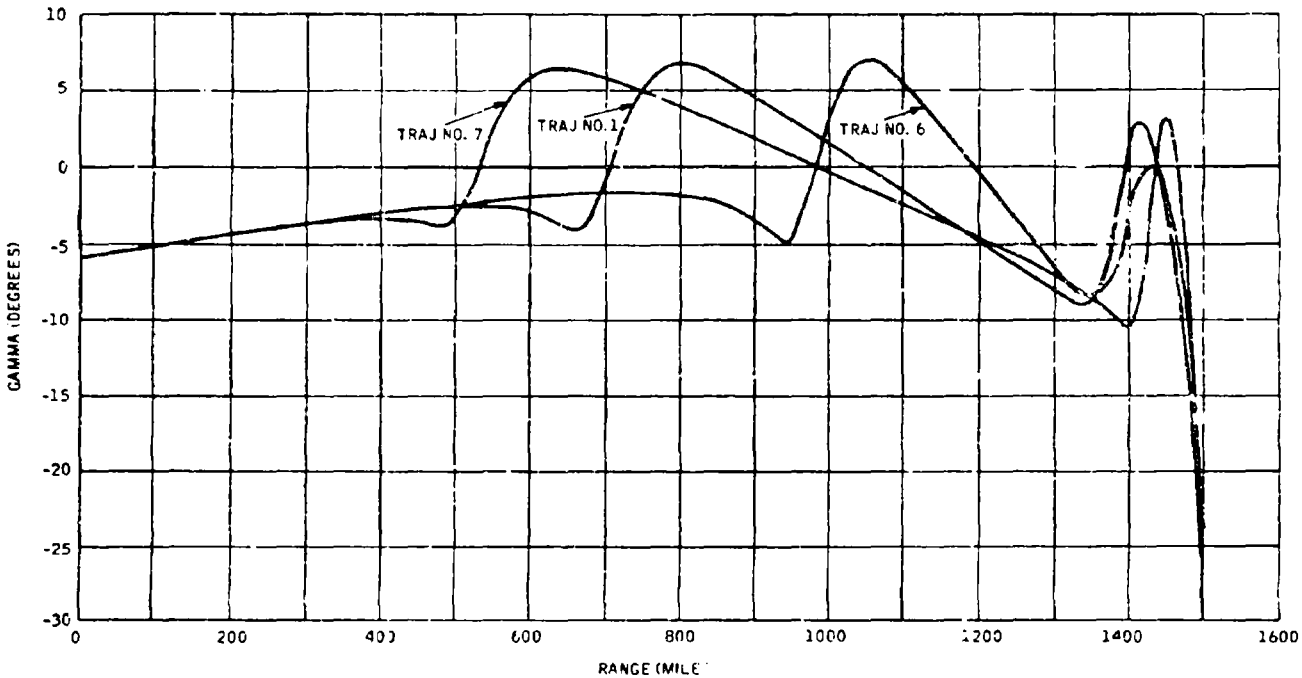

Figure 2-25. Flight Path Angle Versus Range for Optimal Trajectories 1, 6 and 7

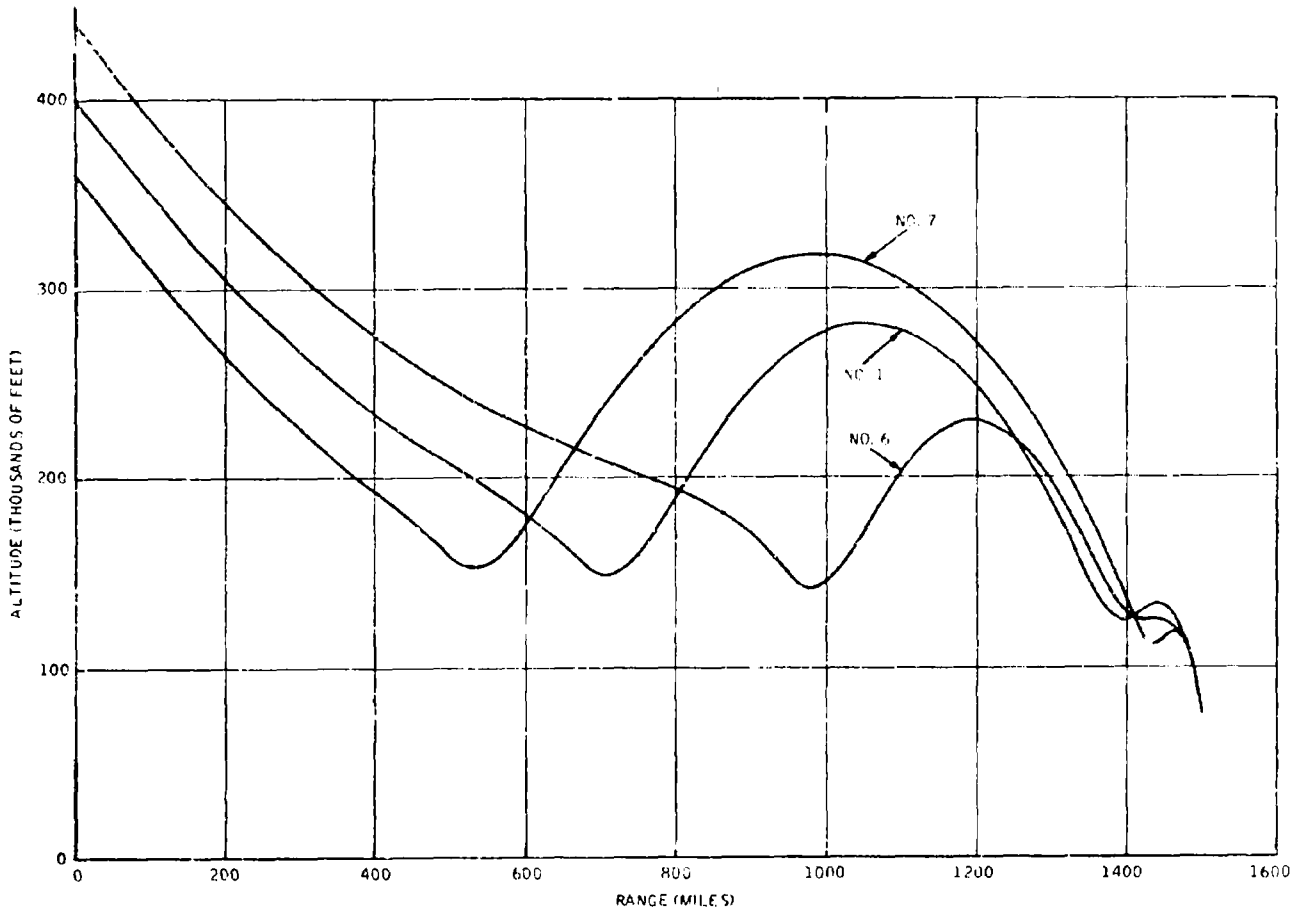

Figure 2-26. Altitude Versus Range for Optimal Trajectories 1, 6 and 7

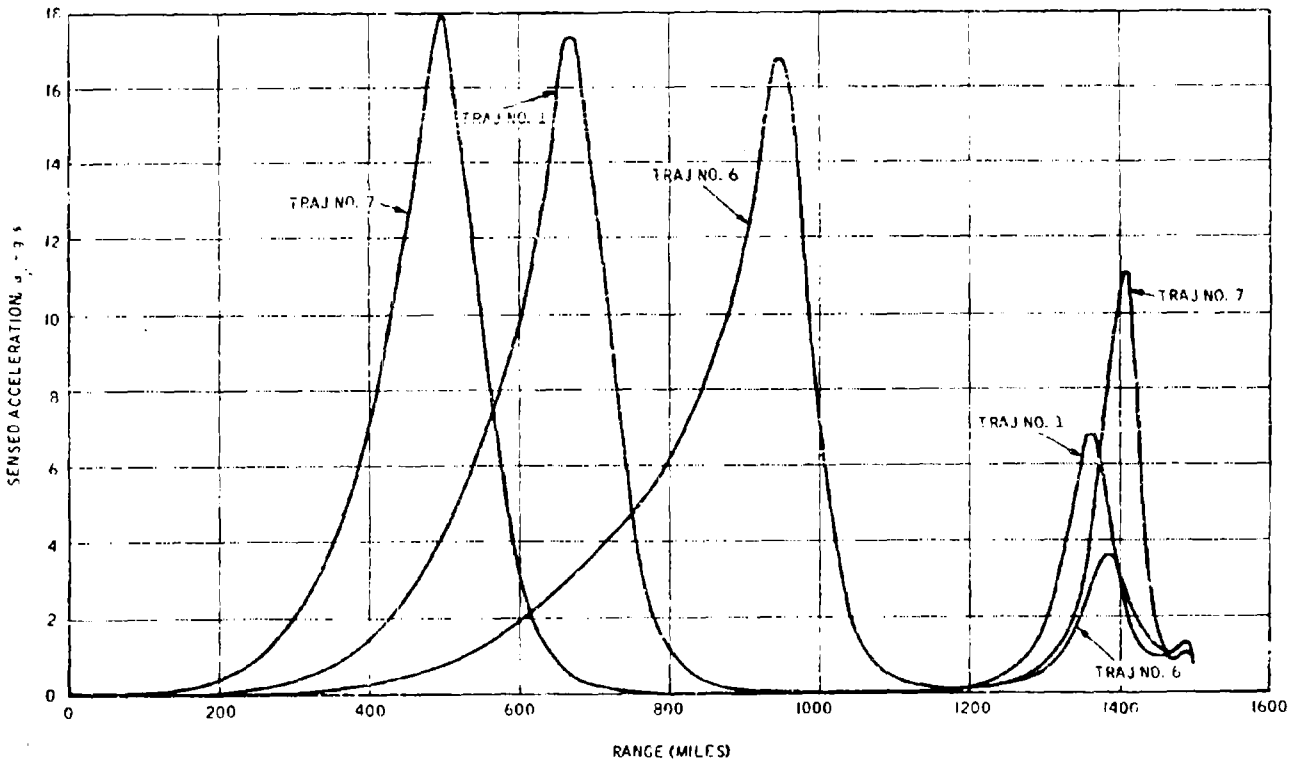

Figure 2-27. Sensed Acceleration Versus Range for Optimal Trajectories 1, 6 and 7

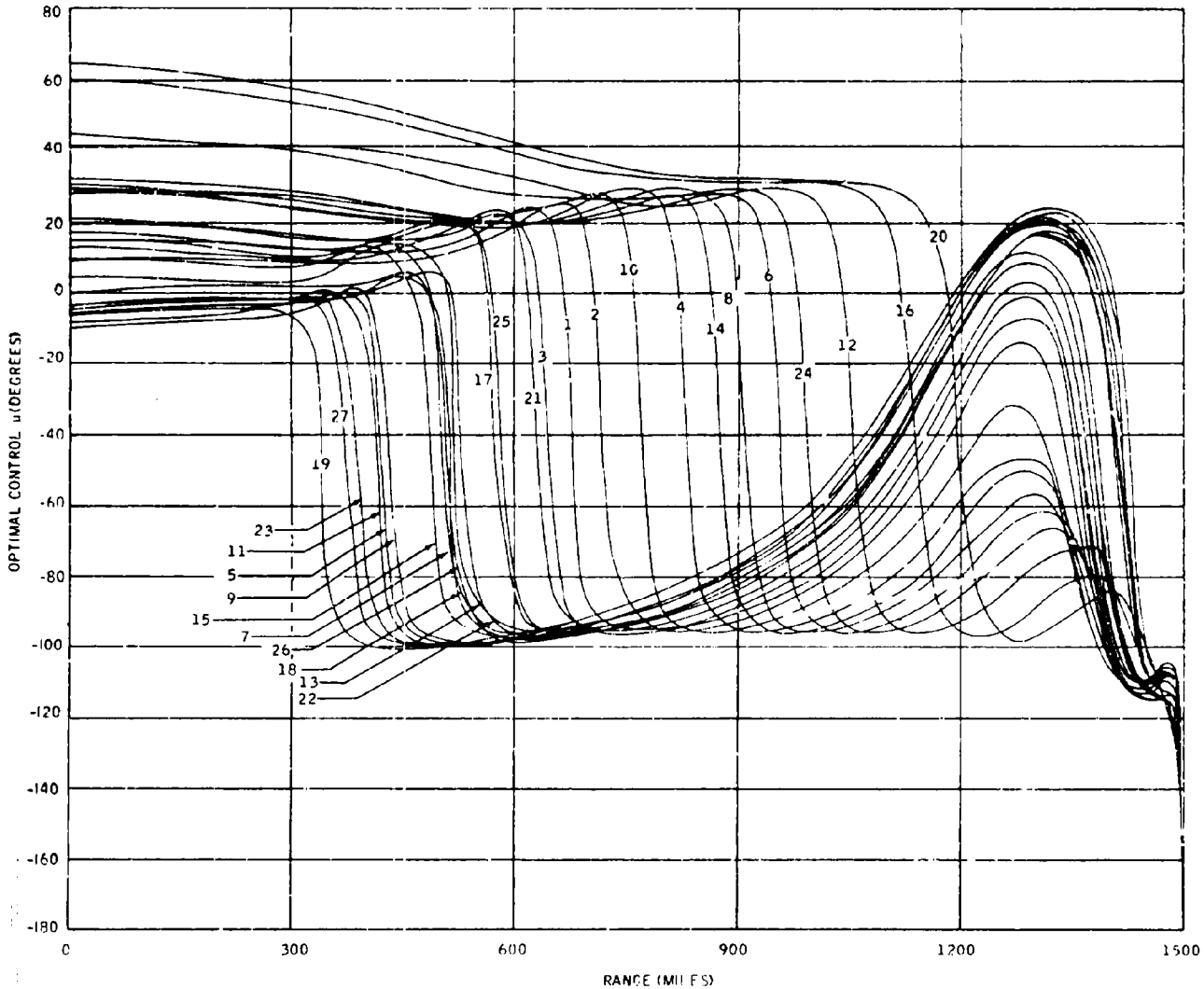

Figure 2-28. Optimal Control Function u Versus Range for 27 Optimal Trajectories

$$\frac{dq}{dz} = \frac{a_1 (R+h)\ \rho^{1/2} V}{\cos\gamma} + \frac{a_2 (R+h)}{\cos\gamma}\left(\frac{\rho}{\rho_o}\right)^{3/2}\left(\frac{V}{10^8}\right)^{\frac{23}{4}}$$

$$\frac{dV}{dz} = \frac{a_3\ \rho V(R+h)}{\cos\gamma}\ C_D(u) + \frac{a_4 \tan\gamma}{(R+h)}$$

$$\frac{d\gamma}{dz} = a_5 + \frac{a_6\ \rho(R+h)}{\cos\gamma}\ C_L(u) + \frac{a_7}{V(R+h)} \qquad (2.37)$$

$$\frac{dh}{dz} = a_5 (R+h) \tan\gamma$$

$$\frac{dt}{dz} = \frac{a_5 (R+h)}{V^{1/2} \cos\gamma}$$

with constants defined by

$$a_1 = \frac{c}{\sqrt{N}} a_5$$

$$a_2 = 7.5 \times 10^{-4} N\ a_5$$

$$a_3 = -\frac{c_3 S}{mR}$$

$$a_4 = 2a_7 \qquad (2.38)$$

$$a_5 = \frac{c_3}{R}$$

$$a_6 = -\frac{a_3}{2}$$

$$a_7 = -c_3 g_o R.$$

The new independent variable is range measured in miles, which is related to ζ through

$$z = \frac{\zeta}{c_3}, \qquad c_3 = 5,280 \tag{2.39}$$

and the new velocity and altitude are given by

$$\begin{aligned} V &= v^2 \\ h &= R\zeta \quad . \end{aligned} \tag{2.40}$$

The terminal conditions corresponding to (2.12) are

$$\begin{aligned} V(z_T) - X_1^2 &= 0 \\ h(z_T) - X_2 &= 0 \\ z_T - X_3/c_3 &= 0. \end{aligned} \tag{2.41}$$

The new Hamiltonian is

$$H_2 = g_o + P'g, \tag{2.42}$$

where g_o is the right-hand side of the first of (2.37), g is a four-dimensional vector denoting the remaining right-hand sides, and P is the new multiplier vector. The Euler-Lagrange equations are

$$\begin{aligned} -\frac{dP_1}{dz} &= \frac{\partial g_o}{\partial V} + P_1\frac{\partial g_1}{\partial V} + P_2\frac{\partial g_2}{\partial V} + P_4\frac{\partial g_4}{\partial V} \\ -\frac{dP_2}{dz} &= \frac{\partial g_o}{\partial \gamma} + P_1\frac{\partial g_1}{\partial \gamma} + P_2\frac{\partial g_2}{\partial \gamma} + P_3\frac{\partial g_3}{\partial \gamma} + P_4\frac{\partial g_4}{\partial \gamma} \\ -\frac{dP_3}{dz} &= \frac{\partial g_o}{\partial h} + P_1\frac{\partial g_1}{\partial h} + P_2\frac{\partial g_2}{\partial h} + P_3\frac{\partial g_3}{\partial h} + P_4\frac{\partial g_4}{\partial h} \\ \frac{dP_4}{dz} &= 0. \end{aligned} \tag{2.43}$$

The control function satisfies

$$\alpha = \tan^{-1} \left(-\frac{C_{LO} P_2}{2 C_{DL} P_1 V} \right) \tag{2.44}$$

with the sign conventions (2.20). Since P_4 is a constant and terminal time is an unspecified quantity, the transversality conditions require

$$P_4 = 0. \tag{2.45}$$

Thus, the time equation, the last of (2.37), is unimportant in the problem, and the set of dependent variables is reduced to (V, γ, h).

Other boundary conditions could be derived. However, this problem is equivalent to the problem of subsection A (when $\mu_1 = \mu_2 = 0$) with equivalence relationships (2.39), (2.40), and, as shown in Appendix C,

$$\begin{aligned} P_1 &= \frac{p_1}{2v} \\ P_2 &= p_2 \\ P_3 &= \frac{p_3}{R} \\ P_4 &= -H = 0 \\ H_2 &= -c_3 P_4. \end{aligned} \tag{2.46}$$

2. The Partial Derivatives

The system of variational equations like (2.26) for the new system of differential equations may be written

$$\frac{d}{dz}\begin{bmatrix}\eta_1\\ \eta_2\\ \eta_3\\ \zeta_1\\ \zeta_2\\ \zeta_3\end{bmatrix} = \begin{bmatrix} \frac{\partial g_1}{\partial V} & \frac{\partial g_1}{\partial \gamma} & \frac{\partial g_1}{\partial h} & \frac{\partial g_1}{\partial P_1} & \frac{\partial g_1}{\partial P_2} & 0 \\ \frac{\partial g_2}{\partial V} & \frac{\partial g_2}{\partial \gamma} & \frac{\partial g_2}{\partial h} & \frac{\partial g_2}{\partial P_1} & \frac{\partial g_2}{\partial P_2} & 0 \\ 0 & \frac{\partial g_3}{\partial \gamma} & \frac{\partial g_3}{\partial h} & 0 & 0 & 0 \\ -\frac{\partial^2 H_2}{\partial V^2} & -\frac{\partial^2 H_2}{\partial V \partial \gamma} & -\frac{\partial^2 H_2}{\partial V \partial h} & -\frac{\partial g_1}{\partial V} & -\frac{\partial g_2}{\partial V} & 0 \\ -\frac{\partial^2 H_2}{\partial V \partial \gamma} & -\frac{\partial^2 H_2}{\partial \gamma^2} & -\frac{\partial^2 H_2}{\partial h \partial \gamma} & -\frac{\partial g_1}{\partial \gamma} & -\frac{\partial g_2}{\partial \gamma} & -\frac{\partial g_3}{\partial \gamma} \\ -\frac{\partial^2 H_2}{\partial V \partial h} & -\frac{\partial^2 H_2}{\partial h \partial \gamma} & -\frac{\partial^2 H_2}{\partial h^2} & -\frac{\partial g_1}{\partial h} & -\frac{\partial g_2}{\partial h} & -\frac{\partial g_3}{\partial h} \end{bmatrix} \begin{bmatrix}\eta_1\\ \eta_2\\ \eta_3\\ \zeta_1\\ \zeta_2\\ \zeta_3\end{bmatrix}, \tag{2.47}$$

Let the fundamental system of solutions to (2.47) be

$$\pi(z) = \begin{bmatrix} \frac{\partial x(z)}{\partial x_o} & \frac{\partial x(z)}{\partial P_o} \\ \frac{\partial P(z)}{\partial x_o} & \frac{\partial P(z)}{\partial P_o} \end{bmatrix}, \qquad \pi(0) = I, \tag{2.48}$$

and furthermore, let the elements of the submatrices be denoted by

$$\begin{aligned} \frac{\partial x(z)}{\partial x_o} &= \left[\eta_{ij}(z)\right], \ i,j = 1,2,3; \quad \frac{\partial x(z)}{\partial P_o} = \left[\eta_{ij}(z)\right], \ i = 1,2,3, \ j = 4,5,6 \\ \frac{\partial P(z)}{\partial x_o} &= \left[\zeta_{ij}(z)\right], \ i,j = 1,2,3; \quad \frac{\partial P(z)}{\partial P_o} = \left[\zeta_{ij}(z)\right], \ i = 1,2,3, \ j = 4,5,6 . \end{aligned} \tag{2.49}$$

An optimal trajectory in the neighborhood of an optimal trajectory will satisfy the perturbed equations

$$\delta x(z) = \frac{\partial x(z)}{\partial x_o}\,\delta x_o + \frac{\partial x(z)}{\partial P_o}\,\delta P_o$$
$$\delta P(z) = \frac{\partial P(z)}{\partial x_o}\,\delta x_o + \frac{\partial P(z)}{\partial P_o}\,\delta P_o \qquad (2.50)$$

at arbitrary values of range, and linearized versions of the boundary conditions (2.41), (2.45) and

$$P_2(z_T) = 0 \qquad (2.51)$$

at the terminal point. These may be written

$$\begin{bmatrix} \delta V(z_T) \\ \delta h(z_T) \\ \delta P_2(z_T) \end{bmatrix} = \begin{bmatrix} 0 \\ 0 \\ 0 \end{bmatrix} = \begin{bmatrix} \eta_{11}(z_T) & \eta_{12}(z_T) & \eta_{13}(z_T) \\ \eta_{31}(z_T) & \eta_{32}(z_T) & \eta_{33}(z_T) \\ \zeta_{21}(z_T) & \zeta_{22}(z_T) & \zeta_{23}(z_T) \end{bmatrix} \begin{bmatrix} \delta V_o \\ \delta\gamma_o \\ \delta h_o \end{bmatrix} + \begin{bmatrix} \eta_{14}(z_T) & \eta_{15}(z_T) & \eta_{16}(z_T) \\ \eta_{34}(z_T) & \eta_{35}(z_T) & \eta_{36}(z_T) \\ \zeta_{24}(z_T) & \zeta_{25}(z_T) & \zeta_{26}(z_T) \end{bmatrix} \begin{bmatrix} \delta P_{10} \\ \delta P_{20} \\ \delta P_{30} \end{bmatrix} \qquad (2.52)$$

since equation (2.45) and the last of (2.41) are always satisfied in the reduced system. Let (2.52) be represented by

$$A\,\delta x_o + B\,\delta P_o = 0, \qquad (2.53)$$

so that

$$\delta P_o = -B^{-1} A\,\delta x_o = K\,\delta x_o. \qquad (2.54)$$

Note that B is the Newton-Raphson matrix in the reduced system, which must be nonsingular. It is shown in Appendix E that if B is nonsingular, the path is normal according to the definition of normality in Reference 7.

When (2.54) is substituted into (2.50) the result is

$$\delta x(z) = \left[\frac{\partial x(z)}{\partial x_o} + \frac{\partial x(z)}{\partial P_o} K\right] \delta x_o$$
$$\delta P(z) = \left[\frac{\partial P(z)}{\partial x_o} + \frac{\partial P(z)}{\partial P_o} K\right] \delta x_o . \qquad (2.55)$$

Under the assumption that the first matrix of (2.55) is nonsingular, it follows that the partial derivatives of the multipliers with respect to the state are

$$\frac{\partial P(z)}{\partial x} = \left[\frac{\partial P(z)}{\partial x_o} + \frac{\partial P(z)}{\partial P_o} K\right]\left[\frac{\partial x(z)}{\partial x_o} + \frac{\partial x(z)}{\partial P_o} K\right]^{-1} . \qquad (2.56)$$

The partial derivatives of the control are derived from Equations (2.44) and (2.50) with the result being

$$\left(\frac{\partial u}{\partial x}\right)' = \left[\frac{\partial u}{\partial V}, \ 0, \ 0\right] + \left[\frac{\partial u}{\partial P_1}, \ \frac{\partial u}{\partial P_2}, \ 0\right] \frac{\partial P}{\partial x} . \qquad (2.57)$$

Several comments should be made. The process described above constructs a particular field of extremals in the neighborhood of an extremal trajectory if the inverse matrix in (2.56) exists at each point along the path (see Reference 7, pp 237-240 and Section IIIA following). By construction, however, the matrix is singular at the endpoint. In spite of this singular point, it can be shown that the results do constitute a field when the endpoint is excluded, so long as the inverse matrix in (2.56) exists at all other points along the extremal path. The 27 optimal trajectories extend this field over a finite region of space. The partial derivatives (2.57) may be used to construct a "neighboring optimal" linear feedback control scheme, as in Reference 8, about any one of the optimal trajectories.

3. Computer Results

The system of differential equations in the computer program includes (2.37) and (2.43), in which the last equation of each set is omitted, and the control function satisfies (2.44) and (2.20). The equivalence relationships (2.40) and (2.46) establish initial conditions from the results of the mapping program. System (2.47) is also integrated to obtain the solutions (2.48). Since the initial conditions for the multipliers may be somewhat in error, Newton-Raphson equations are included to adjust them to their proper values. When the process has converged, the K-matrix of Equation (2.54) is computed, and the initial conditions for system (2.47) are changed to

$$\pi(0) = \begin{bmatrix} I & I \\ K & -I \end{bmatrix} \tag{2.58}$$

for the last pass. The first three column solutions are then the matrices of Equations (2.55), and the last three solutions are used for an auxilliary sufficiency condition computation (see subsection D). On the last pass the control u, multipliers P_1 and P_2, and the partial derivatives [from (2.56) and (2.57)] are punched on cards at specified values of range. In the present case 101 sets of data are obtained spaced at range increments of 15 miles. At the last point (z = 1500 miles) the partials are omitted.

In computing the partials at the output points, the inverse matrix of Equation (2.56) is obtained by inverting the solution in (2.55). This does not increase computing time excessively, since the matrix is small (3 x 3). In larger systems, however, one may wish to solve the nonhomogeneous Ricatti equation derived in Appendix D. and thereby obtain the solutions (2.56) directly.

The partial derivatives of the control function for the nominal trajectory are plotted in Figure 2-29. The $\frac{\partial u}{\partial V}$ curve appears to be rather uninteresting over most of the trajectory, until it is remembered that V is a very large quantity over this region. The hump in the $\frac{\partial u}{\partial h}$ curve corresponds approximately to the

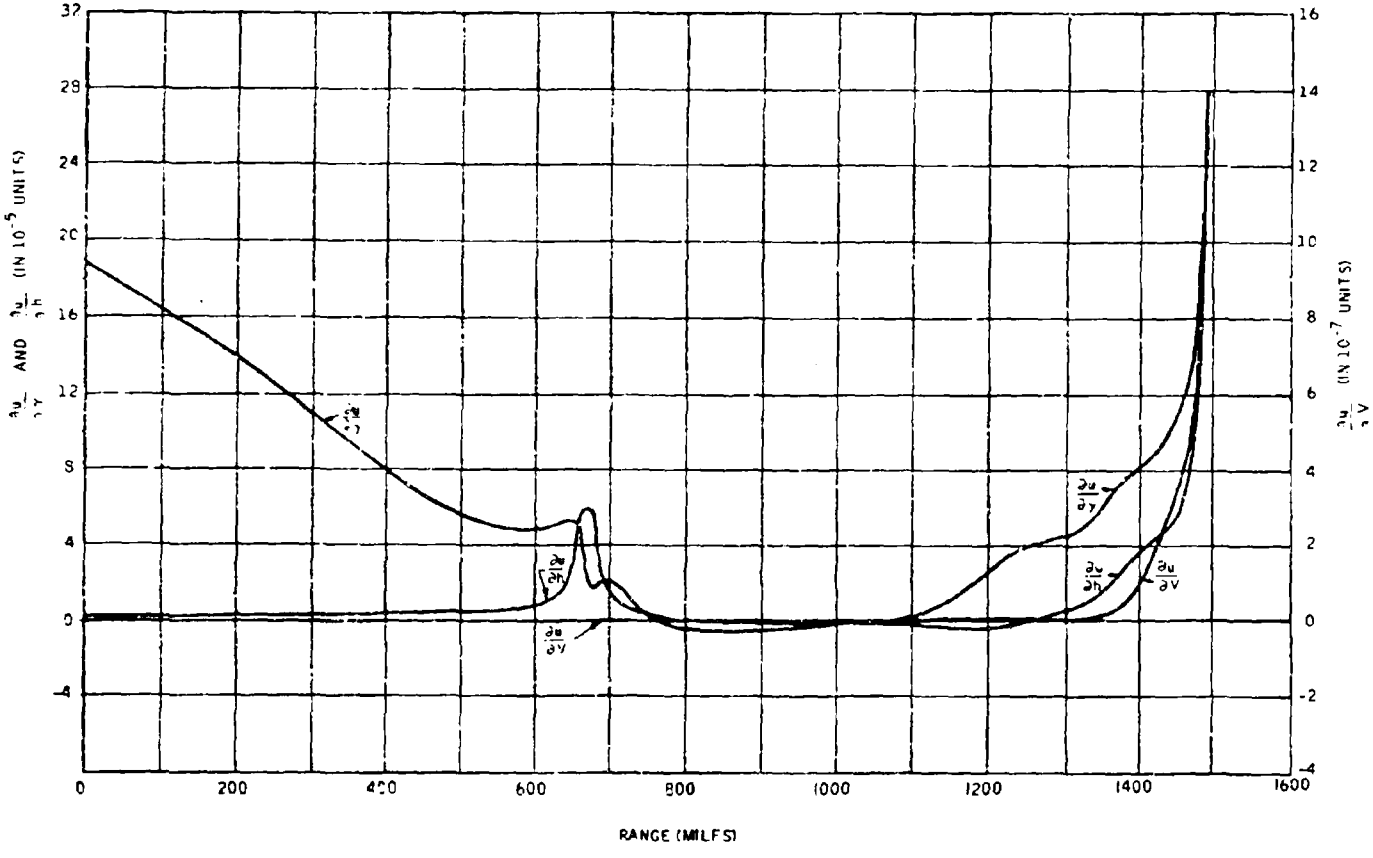

Figure 2-29. Partial Derivatives of the Control With Respect to V, γ and h as Functions of Range for Trajectory 1

bottom of the first dive (see Figures 2-16 through 2-19), where control changes drasticelly influence the remainder of the path. Beyond this point, the partials are small, corresponding to the skip in the trajectory. The partials all head toward $+\infty$ at the end of the trajectory (by construction). Since the partials can be used as time varying gains in a linear feedback control scheme (as in References 1 and 8) one might wonder why they are not negative, to correspond to negative feedback. The reason for this is that positive control produces negative lift. One can intuitively justify that the partials, acting as feedback gains, produce the proper trajectory changes, at least toward the end of the path.

Figures 2-30 and 2-31 are plots of the multipliers P_1 and P_2 for trajectories 1 through 7. They are included to show the nature of the variations over the optimal re-entry corridor.

D. SUFFICIENCY CONDITIONS

The sufficiency tests described in this subsection are tailored to problems like the re-entry problem stated above in which the Lagrange form of the optimization problem is considered and the terminal equations are quite simple. The tests can, of course, be extended to other cases, such as problems with more complex endpoint equations, the addition of a function of the endpoints to the function to be minimized, and the inclusion of inequality constraints in the problem statement.

1. Sufficiency Conditions for a Relative Minimum

Bliss' theorem 85.1 (Reference 7, page 241) forms the basis for the relative minimum sufficiency test. This theorem requires

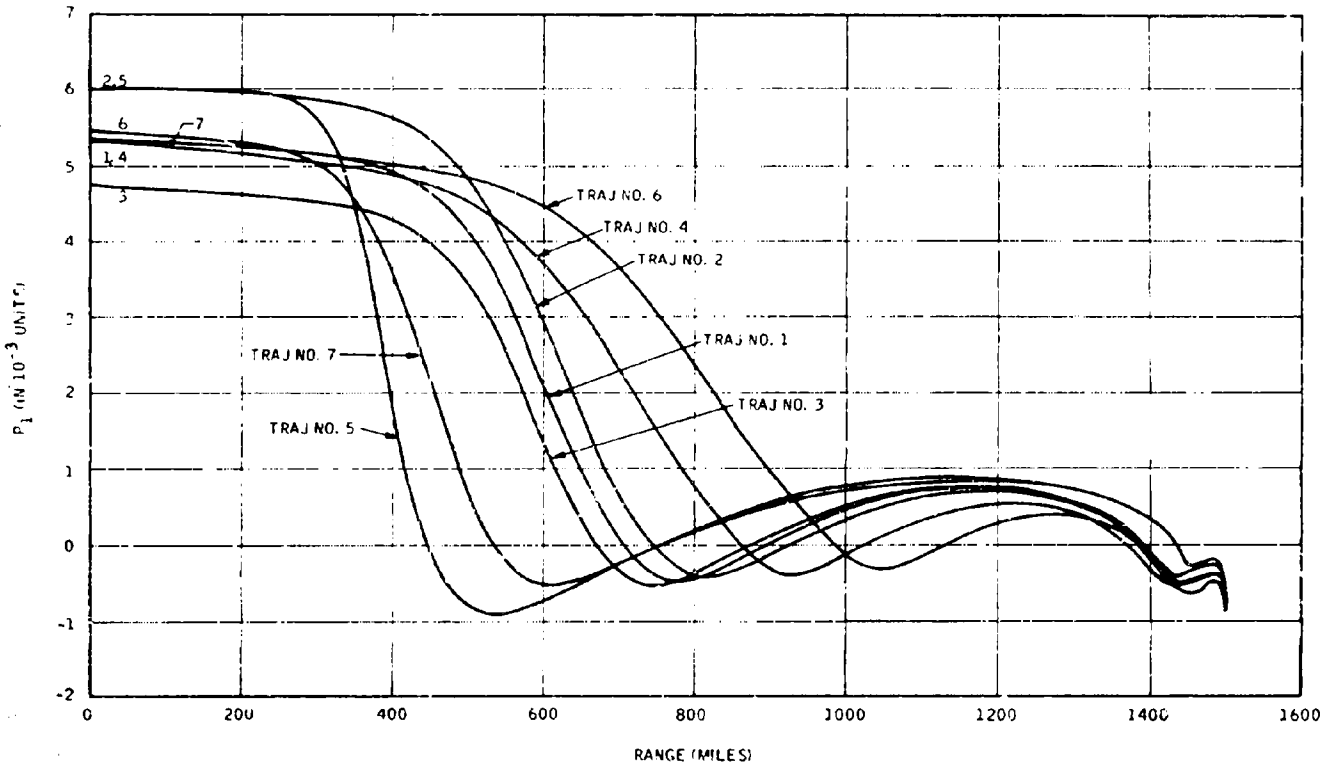

Figure 2-30. Multiplier P_1 for Several Optimal Trajectories

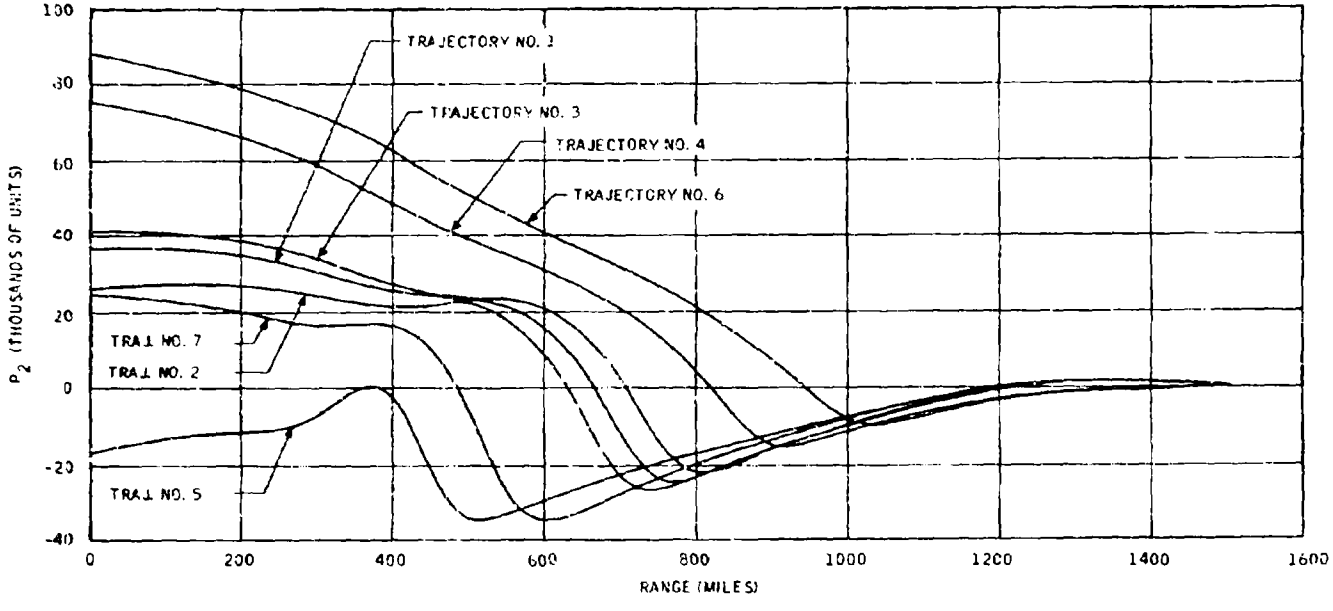

Figure 2-31. Multiplier P_2 for Several Optimal Trajectories

(1) A field in which the extremal is imbedded

(2) The strengthened version of the Weierstrass condition

$$H(u) < H(U) \tag{2.59}$$

(3) The second variation, evaluated with field elements, to have a proper minimum at the ends of the extremal.

If these three conditions are satisfied (for a normal extremal without corners) then the path is a strong relative minimizing path in the sense of Bliss' Theorem 82.1 (Reference 7, page 235).

For application to the re-entry problem, consider the formulation of subsection C. Condition (2) is satisfied since the control (2.44) using sign conventions (2.20) establishes the absolute minimum of the Hamiltonian (with respect to u) and no other control U gives the same value. The problem is normal since the Newton-Raphson matrix B of Equation (2.53) is nonsingular. It is shown in Appendix E that B nonsingular implies normality in the sense of Reference 7.

A field is constructed through the use of lemma 84.2 of Reference 7 (pp 238-240). This requires that the path first be nonsingular. Lemma 87.1 of Reference 7 (page 247) shows that the path is nonsingular if the strengthened Clebsch condition (Theorem 78.2 of Reference 7) holds. With a single control function this requires

$$\frac{\partial^2 H}{\partial u^2} > 0 \tag{2.60}$$

over the path, which is true for the problem under consideration. Then a field is constructed if a conjugate system of solutions U, V (both nxn matrices) to the accessory equations (2.47) can be found, with U nonsingular everwhere along the extremal. By definition, a conjugate system of equations satisfies

$$U'V = V'U. \tag{2.61}$$

A suitable choice for U and V is

$$U = \frac{\partial x}{\partial x_o} - \frac{\partial x}{\partial P_o} = \pi_{11}(z) + \pi_{12}(z) \quad [K-I]$$

$$-V = \frac{\partial P}{\partial x_o} - \frac{\partial P}{\partial P_o} = \pi_{21}(z) + \pi_{22}(z) \quad [K-I] \tag{2.62}$$

which accounts for the second half of the initial conditions (2.58) for Equations (2.47)*. The π notation, adopted here, splits the fundamental solution matrix (2.48) into the four submatrices indicated in (2.62). One can show that the choice (2.62) forms a conjugate system because of the easily proved relationships

$$\pi_{11}'\pi_{21} = \pi_{21}'\pi_{11}$$

$$\pi_{12}'\pi_{22} = \pi_{22}'\pi_{12} \tag{2.63}$$

$$\pi_{22}'\pi_{11} = \pi_{12}'\pi_{21} + I.$$

Then a field is constructed if U of (2.62) is nonsingular at each point along the extremal.

Several comments should be made. Although the results (2.62) and (2.63) are presented for the problem of subsection C, they hold in general. The minus sign in (2.62) arises because of the use of the minimum principle instead of the maximum principle, as explained in Appendix E. Since the original problem included u as the derivative of an additional state coordinate, one might wonder whether the field should be constructed in (n+2) dimensions rather than in (n+1) dimensions. It is shown in Appendix E that the additional dimension need not be considered. The sufficiency proof is complete at this point for fixed endpoint problems.

*Matrix K, from Equation (2.54) is taken as zero in (2.58). It is only necessary to show that there is a conjugate system U, V with det $U \neq 0$.

In the computer program, the determinant of U was computed at each output point ($z = 0$ to 1500 miles with increments $\Delta z = 15$ miles). The determinant started at unity ($z = 0$), and rose to very large values as z increased (about 10^{29} maximum) for each of the 27 trajectories considered. Because of the smoothness of the problem solutions, it was concluded that the determinant did not vanish or become negative between output points, and hence, that fields were indeed constructed for each trajectory.

Condition (3), above, is based upon lemma (87.2) of Reference 7 (page 247). This gives generalized expressions for the second variation test for problems with separated end conditions. There is no contribution to the second variation at the initial point, since conditions at this point are all fixed. Hence, for the type of problem considered, it is required that

$$- \begin{bmatrix} a_o, & a' \end{bmatrix} \begin{bmatrix} \dot{p}(z_T)\,\dot{x}(z_T) & \dot{p}'(z_T)\,U(z_T) \\ U'(z_T)\,\dot{p}(z_T) & U'(z_T)\,V(z_T) \end{bmatrix} \begin{bmatrix} a_o \\ a \end{bmatrix} > 0 \qquad (2.64)$$

for all (a_o, a) satisfying

$$\dot{x}_i(z_T)a_o + U_i(z_T)a = 0, \quad i = 1, \ldots, r. \qquad (2.65)$$

Expression (2.64) is the second variation (as derived in Reference 1) evaluated at the terminal point with field elements, and (2.65) represents the linearized terminal conditions with subscript i on U representing the ith row vector of U.

In the re-entry problem the terminal value of range is also specified, which implies $a_o = 0$, and accordingly reduces the size of expression (2.64). The remainder of the terminal conditions (2.41) may be written in the linearized form

$$U(z_T)\,a = \begin{bmatrix} 0 \\ \Delta \\ 0 \end{bmatrix}, \qquad (2.66)$$

where the middle row of U is included for the unspecified variable γ, and Δ is an arbitrary scalar. When (2.66) is inserted in (2.64) (with $a_0 = 0$) there results

$$- \begin{bmatrix} 0 & \Delta & 0 \end{bmatrix} \quad V(z_T) U^{-1}(z_T) \begin{bmatrix} 0 \\ \Delta \\ 0 \end{bmatrix} > 0. \tag{2.67}$$

Thus, the center element of the product matrix in (2.67) must be negative to satisfy condition (3). It is negative for each of the 27 trajectories considered. Hence, the sufficiency conditions are all satisfied, and each of the 27 trajectories is a stong relative minimizing trajectory.

2. An Absolute Minimum Test

The test given here does not establish global sufficiency. It does, however, allow a large region of solution space to be examined for other solutions to the optimization problem. The method is not applicable to fixed end-point problems. The idea is simple: replace one of the transversality conditions by a new terminal equation in which a parameter is included. Obtain a set of soultions to this problem, as functions of the parameter, and examine the set for satisfaction of the omitted transversality condition.

To illustrate the method, consider the problem statement of subsection A, and in particular, the set of necessary condtions (2.25). The fourth of these is replaced by the equation

$$\gamma(T, p_3) \quad \Gamma = 0 \tag{2.68}$$

in which Γ is the parameter, and solutions as functions of Γ are to be examined for satisfaction of $p_2(T) = 0$. The Newton-Raphson equations for the new system of equations may be written

$$\begin{bmatrix} dT \\ dp_{10} \\ dp_{20} \\ dp_{30} \\ dp_{40} \end{bmatrix} = - \begin{bmatrix} \dot{v}(T) & \eta_{11}(T) & \eta_{12}(T) & \eta_{13}(T) & \eta_{14}(T) \\ \dot{\gamma}(T) & \eta_{21}(T) & \eta_{22}(T) & \eta_{23}(T) & \eta_{24}(T) \\ \dot{\xi}(T) & \eta_{31}(T) & \eta_{32}(T) & \eta_{33}(T) & \eta_{34}(T) \\ \dot{\zeta}(T) & \eta_{41}(T) & \eta_{42}(T) & \eta_{43}(T) & \eta_{44}(T) \\ 0 & f_1(0) & f_2(0) & f_3(0) & f_4(0) \end{bmatrix}^{-1} \begin{bmatrix} v(T)-X_1 \\ \gamma(T)-\Gamma \\ \xi(T)-X_2/R \\ \zeta(T)-X_3 \\ H \end{bmatrix} \quad (2.69)$$

According to Appendix A, the derivatives of the initial conditions with respect to the parameter Γ are in the second column of the inverse matrix. These are used with the predictor equation (2.29) to establish the family of solutions.

An unconstrained optimal trajectory with terminal range of 1450 miles was used for the test. The results certainly hold for the 1500 mile trajectory. During computer runs it was found that an increment $\Delta\Gamma$ = 1/2 degree initially produced a member of the family of solutions at each step. Prediction gradually worsened, however, as the extremes of Γ were approached, and it is unlikely that further extension of Γ can be accomplished.

The total heat J for the family of trajectories is plotted in Figure 2-32. There is only one minimum for the range of Γ given, and it is noted that the minimum is quite insensitive to large variations in terminal flight path angle.

From Hamilton-Jacobi theory, it is known that $-p_2(T)$ is the slope of Figure 2-32. The slope is zero for the optimal trajectory, and becomes very large (in absolute value) at the extremes of the curve, so $-p_2(T)$ is never again zero over the range of Γ. It is concluded that the original optimal trajectory is the absolute minimizing trajectory, at least over the obtainable range of the parameter Γ.

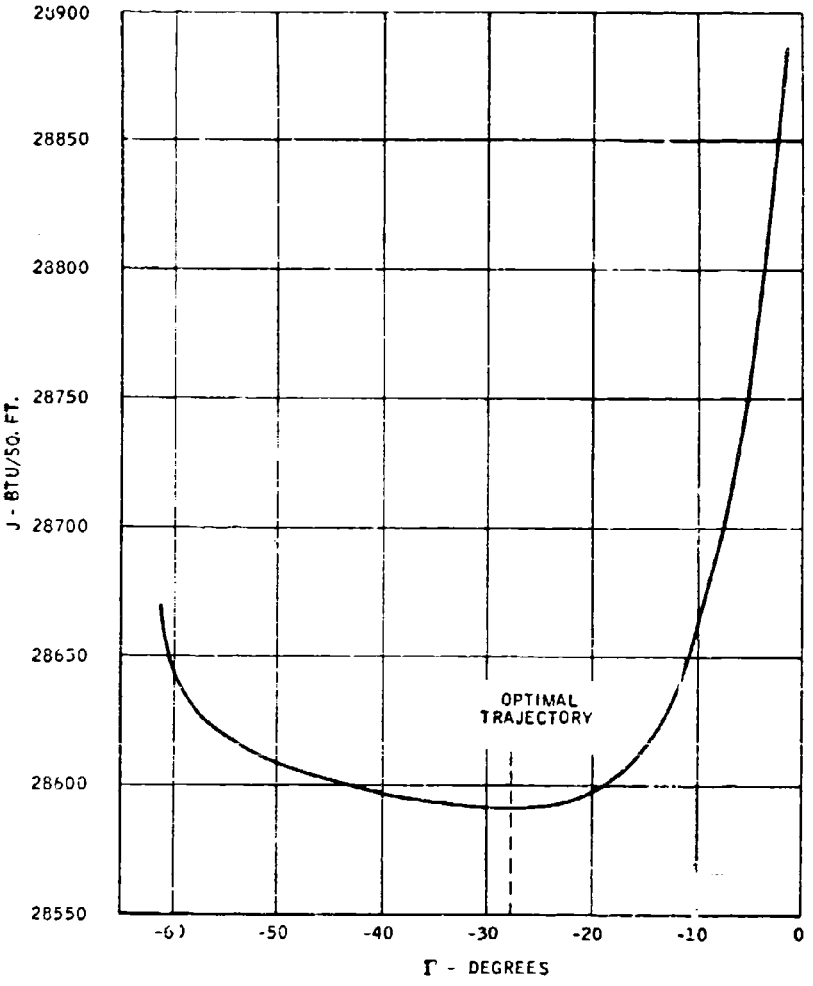

Figure 2-32. Absolute Minimum Test Results - Total Heat J Versus Terminal Flight Path Angle Γ

E. THE CONSTRAINT $a_p = B$ AND EXPERIENCES WITH VARIOUS OPTIMIZATION SCHEMES

1. Constrained Subarc Equations

Consider the problem of subsection A, and include the constraint equation (2.10) in the problem formulation. When equality holds in (2.10), the resulting equation is used to determine the control u. This is squared and rearranged to obtain

$$a \cos^2 u + 2b \cos u + c = 0 \tag{2.70}$$

where

$$\begin{aligned} a &= C_{DL}^2 - C_{LO}^2 \\ b &= C_{DO} C_{DL} \\ c &= C_{DO}^2 + C_{LO}^2 - \left(\frac{2mg_o B}{S\rho v^2}\right)^2 \end{aligned} \tag{2.71}$$

Upper and lower limits for application are found by substituting $u = 0, \pm\pi$ into (2.70) and expanding in the vicinity of these points. It is found that the inquality

$$(C_{DO} + C_{DL}) \geq \frac{2mg_o B}{S\rho v^2} \geq (C_{DO} - C_{DL}) > 0 \tag{2.72}$$

must hold. The expression for $\frac{\partial a_p}{\partial u}$ is proportional to sin u, which is zero at $u = 0, \pm\pi$. These points are thus singular points, so equality must be excluded in (2.72). Assuming this, Equation (2.70) may be solved to obtain

$$\cos u = \frac{b}{a}\left[-1 + \sqrt{1 - \frac{ac}{b^2}}\right], \tag{2.73}$$

where the omitted root falls outside the range $|\cos u| \leq 1$. It is easily shown

that the term in the square root is positive by substituting the upper limit of (2.72) into the expression and evaluating.

The minimum principle again takes the form (2.21), except that this time

$$-|u| < \phi < |u|. \qquad (2.74)$$

Otherwise, ϕ and u would be identical. Then, once again, $\phi \neq 0$ and u must have the same sign, and $\phi = 0$ is the bang condition.

The multiplier μ_2 is determined from Equation (2.15) (with $\mu_1 \neq 0$). When all the substitutions are made, it turns out that

$$\mu_2 = -\frac{g_o}{v}\sqrt{\frac{\left[C_L^2 + C_D^2\right]\left\{\left|C_{LO}p_2\right|^2 + \left|C_{DL}p_1 v\right|^2\right]}{b^2 - ac}}\;\frac{\sin(u-\phi)}{\sin u} \qquad (2.75)$$

Since sin $(u-\phi)$ and sin u have the same signs, $\mu_2 > 0$ as required. Again, u is continuous at junction points, so μ_2 must start and end at zero; and $\mu_2 = 0$ with $\dot{\mu}_2 \neq 0$, describes the subarc terminal surface, unless the stopping condition is satisfied first.

It is convenient to include B as an additional parameter in the problem, and to introduce the new terminal equation

$$B - B_o = 0. \qquad (2.76)$$

B_o is the final maximum g-level (usually taken as 10 g's) in the constraint equation (2.10), and the solutions now depend upon B as well as the set (T, p_o). This allows the computation of extremals for various g-levels.

The accessory equations are system (2.26), modified for the constrained subarc, and the discontinuities (2.27) are included for corner points. An additional column solution is obtained, for partials with respect to B, by integrating the nonhomogeneous accessory equations

$$\frac{d}{dt}\left(\frac{\partial x}{\partial B}\right) = \frac{\partial^2 H_1}{\partial p \partial x}\left(\frac{\partial x}{\partial B}\right) + \frac{\partial^2 H_1}{\partial p^2}\left(\frac{\partial p}{\partial B}\right) + \frac{\partial^2 H_1}{\partial p \partial B}$$

$$\frac{d}{dt}\left(\frac{\partial p}{\partial B}\right) = -\frac{\partial^2 H_1}{\partial x^2}\left(\frac{\partial x}{\partial B}\right) - \frac{\partial^2 H_1}{\partial x \partial p}\left(\frac{\partial p}{\partial B}\right) - \frac{\partial^2 H_1}{\partial x \partial B}\ , \tag{2.77}$$

where the nonhomogeneous partials in (2.77) are computed through the appearance of B in the control function (2.73) from the last of (2.71). The forcing terms are zero, of course, for the unconstrained subarc, and the initial condition for (2.77) is the zero vector.

Let $\eta_{ij}(t)$ and $\zeta_{ij}(t)$, $i = 1, \ldots, 4$; $j = 1, \ldots, 5$, be the elements of the partial derivative solutions obtained from (2.26) and (2.77). Then the Newton-Raphson equations for the expanded set (2.25) and (2.76) may be written

$$\begin{bmatrix} dT \\ dp_{10} \\ dp_{20} \\ dp_{30} \\ dp_{40} \\ dB \end{bmatrix} = -\begin{bmatrix} \dot{v}(T) & \eta_{11}(T) & \eta_{12}(T) & \eta_{13}(T) & \eta_{14}(T) & \eta_{15}(T) \\ \dot{\xi}(T) & \eta_{31}(T) & \eta_{32}(T) & \eta_{33}(T) & \eta_{34}(T) & \eta_{35}(T) \\ \dot{\zeta}(T) & \eta_{41}(T) & \eta_{42}(T) & \eta_{43}(T) & \eta_{44}(T) & \eta_{45}(T) \\ \dot{p}_2(T) & \zeta_{21}(T) & \zeta_{22}(T) & \zeta_{23}(T) & \zeta_{24}(T) & \zeta_{25}(T) \\ 0 & f_1(0) & f_2(0) & f_3(0) & f_4(0) & 0 \\ 0 & 0 & 0 & 0 & 0 & 1 \end{bmatrix}^{-1} \begin{bmatrix} v(T)-X_1 \\ \xi(T)-X_2/R \\ \zeta(T)-X_3 \\ p_2(T) \\ H \\ B-B_o \end{bmatrix} \tag{2.78}$$

2. Experiences with Various Optimization Schemes

The objective of the studies was to obtain a 10-g optimal trajectory, and to evaluate various optimization schemes during the process. The starting trajectory was the unconstrained optimal trajectory with terminal range X_3 = 1000 miles, shown in Figures 2-8 through 2-13, with peak acceleration of about 20.7 g's. Existence of the 10-g trajectory was assumed from the u_1 = 16 degrees acceleration plot of Figure 2-2. The function f of Appendix B was taken as

$$f = w_1^2 \left|v(T) - X_1\right|^2 + w_2^2 \left|\xi(T) - X_2/R\right|^2 + w_3^2 \left|\zeta(T) - X_3\right|^2 + w_4^2 \left|p_2(T)\right|^2 + w_5^2 H^2 + w_6^2 \left|B - B_o\right|^2. \tag{2.79}$$

The problem, as stated, turned out to be extremely difficult, and a 10-g optimal trajectory was never found. Thus, the optimization schemes were compared under worst conditions.

The modified Newton-Raphson scheme, used first, refused to converge after several successful iterations. Marquardt's method (Appendix B) produced good initial changes in f, and gradually deteriorated in performance as B approached B_o. The difficulty appeared to be that second-order terms, neglected in the development of the scheme, became larger as the minimum was approached. When the weights in (2.79) were changed, the scheme again worked well at first, then deteriorated rapidly. It always, however, produced some improvement in f.

The parameter B was reduced to about 11.5 g's during the course of the experiments, whereas the other components in (2.79) gradually became larger. The constrained subarc exhibited a variety of behavior. It sometimes contained a corner, and other times did not, and in some trajectories it was absent.

The Fletcher-Powell method was never successfully used. The H-matrix (see Appendix B), modified after the first step, was either indefinite (it should be positive-definite), or it had a very small eigenvalue. This was on the order of computer roundoff error and caused the method to break down. No means of correcting the situation was found, although a recent note (Reference 10) may contain the answer.

The use of the identity matrix as the initial H-matrix led to the optimal gradient method, in which the gradient direction is used, and the magnitude of change is chosen to minimize f. Initial convergence was good but rapidly went to zero due to the "saw-tooth" effect. This effect, noted by many users of gradient techniques, makes level surfaces of f appear as extremely elongated ellipses, and gradient changes in general, therefore, produce little or no change in the functional to be minimized.

The use of

$$H_o = \left[\frac{\partial \phi'}{\partial x} \quad \frac{\partial \phi}{\partial x}\right]^{-1} \tag{2.80}$$

as the initial H-matrix (see Appendix B) results in the Newton-Raphson direction for the first step of the Fletcher-Powell method. This led to the optimal Newton-Raphson method, which was tried on a trajectory which satisfied $B = B_o$ but whose terminal conditions were very far from those desired. The method worked quite well, and almost produced the 10g-optimal trajectory. The singular point $u = \pm\pi$, however, caused computational difficulties, so the approach was abandoned.

The predictor scheme of Appendix A was also tried on this problem. In terms of the notation of Equation (2.78), the derivatives used in the predictor equation (2.29) are

$$\frac{d}{dB}\begin{bmatrix} T \\ p_{10} \\ p_{20} \\ p_{30} \\ p_{40} \end{bmatrix} = -\begin{bmatrix} \dot{v}(T) & \eta_{11}(T) & \eta_{12}(T) & \eta_{13}(T) & \eta_{14}(T) \\ \dot{\xi}(T) & \eta_{31}(T) & \eta_{32}(T) & \eta_{33}(T) & \eta_{34}(T) \\ \dot{\zeta}(T) & \eta_{41}(T) & \eta_{42}(T) & \eta_{43}(T) & \eta_{44}(T) \\ \dot{p}_2(T) & \zeta_{21}(T) & \zeta_{22}(T) & \zeta_{23}(T) & \zeta_{24}(T) \\ 0 & f_1(0) & f_2(0) & f_3(0) & f_4(0) \end{bmatrix}^{-1} \begin{bmatrix} \eta_{15}(T) \\ \eta_{35}(T) \\ \eta_{45}(T) \\ \zeta_{25}(T) \\ 0 \end{bmatrix}. \qquad (2.81)$$

A 17.9-g optimal trajectory was obtained using the optimal Newton-Raphson method (Equations (2.28) with C determined to minimize (2.79) with $w_6 = 0$). The initial conditions for the iterations were taken as those for the $u_1 = 55$ degrees optimal trajectory of Figures 2-1 through 2-8. A second optimal trajectory for B = 16.9 g's was similarly obtained, using the 17.9-g optimal values as starting conditions. A cubic was fit through the initial conditions and their derivatives [obtained from (2.81)] to obtain estimated initial conditions for the B = 17.7-, 17.5-, 17.3-, and 17.1-g optimal paths. The new paths were then obtained, and the predictor scheme was used [with h= 0.2 g in (2.29)] to compute optimals down to B = 14.9 g's. All of these paths had a corner point, which migrated toward the initial point of the constrained subarc as B was lowered. The predictor scheme failed to obtain the 14.7-g optimal because the corner point was too close to the initial point of the constrained subarc. This caused computational problems because of the singular point u= 0. On the other hand, the terminal range of the 16.7-g optimal trajectory was extended to 1460 miles using the predictor scheme, and the corner point migrated toward the endpoint of the constrained subarc. Once again, the singular point u= 0 prevented further range extension. Thus, two parameters were found which controlled the location of the corner point, and a 10-g optimal trajectory could have been obtained by manipulating them properly. This was not done, however, since a 10-g optimal trajectory with a continuous control function was sought. Instead, the constraint equation was modified so as to isolate the singular point u= 0 and to thus allow the corner point to move across the constrained-unconstrained subarc junction points.

3. Constraint Equation Modification

The singular point $u = \pm \pi$ has a clear physical significance: in the next instant of time the pilot's acceleration will exceed B g's, since no control function exists which will alleviate the situation. Computations are accordingly stopped at this point. (Normally, $0 < |u| < \pi$, on a constrained subarc, and $|u|$ moves, in time, toward zero or π. The subarc either terminates normally, or runs into computational difficulties as a singular point is approached.) The point $u = 0$ should define the endpoint of the constrained subarc, since no control exists, for the next instant of time, which will keep $a_p = B$ g's. It should be possible to show, mathematically, that this is so. However, the mechanization of any such solution would undoubtedly add complexity to an already complicated computer program. It was decided, instead, to modify the constraint equation so as to isolate the singular point $u = 0$. The modified equation reads

$$a_p = \frac{S\rho v^2}{2 m g_o} \sqrt{C_L^2 + C_D^2 + \frac{2K}{1-\cos u}} \quad . \tag{2.82}$$

With the constant $2K = 0.0001$, the added term normally contributes very little to the original equation; hence, there is a very small difference between the two expressions. The error maintains the "real" acceleration less than B g's. As u approaches zero, however, the adder becomes large, and effectively isolates the point $u = 0$. The equation to be solved for the control function, analogous to Equation (2.70), is

$$a \cos^2 u + 2b \cos u + c + \frac{2K}{1-\cos u} = 0 \tag{2.83}$$

with a, b and c defined by (2.71). Although this may be solved as a cubic, it was found more convenient to use Newton's method. Also, since cos u may be close to unity, the transformation

$$z = \cos u - 1 \tag{2.84}$$

was introduced for somewhat better accuracy.

The transformed version of (2.83) reads

$$z^2 + \frac{2(a+b)}{a} z + \frac{(a+2b+c)}{a} - \frac{2K}{az} = 0. \tag{2.85}$$

The constrained subarc equations in the computer program were changed for the modification. Lack of time prevented more than one or two debugging runs to be made, so the corner point was never removed from the constrained subarc.

F. EXTENSION TO THE BOUNDED STATE COORDINATE PROBLEM

1. Statement of the Problem

The theory for the problem of minimizing

$$J = \int_0^T f_o(x, u) d\tau \tag{2.86}$$

subject to differential equations

$$\dot{x} = f(x, u), \quad x(0) = x_o, \tag{2.87}$$

inequality constraints

$$G(x, u) \geq 0, \tag{2.88}$$

in which u must appear explicitly, and terminal conditions in either the form

$$x_i(T) - X_i = 0, \quad i = 1, \ldots, r \leq n \tag{2.89}$$

or

$$x_j(T) - X_j = 0, \quad j = 1, \ldots, r-1 \leq n \tag{2.90}$$

$$T - K = 0,$$

is treated in Reference 1. The objective here is to add inequality constraints of the form

$$G(x) \geq 0 \tag{2.91}$$

and to develop a method for numerically solving the resulting problem.

2. Necessary Conditions

A set of necessary conditions for this problem has been known for some time (see References 11-14). They are stated here with one control function and one inequality constraint equation (2.91) assumed for simplicity. Generalization to more control functions and more inequality constraints is readily accomplished. It is also assumed that the time derivative of (2.91),

$$\dot{G} = \frac{\partial G}{\partial x}\dot{x} = \frac{\partial G}{\partial x} f \quad , \tag{2.92}$$

contains the control function explicitly. The case where higher derivatives are required to involve the control function is treated in References 11 and 14.

The Hamiltonian for this problem is

$$H = f_o + p'f \, , \tag{2.93}$$

where f_o is the integrand of (2.86), p is an n dimensional multiplier vector, ($'$) represents transpose, and f is the right hand side of the vector differential equation (2.87). Now a constrained subarc is one over which inequality (2.91) is an equation. A necessary and sufficient condition for G to be zero over such a subarc is that $\dot{G}$ be identically zero over that arc (see Reference 13). This condition is included in a new Hamiltonian, defined by

$$H_1 = H + \mu\dot{G}, \tag{2.94}$$

where the new multiplier μ is identically zero over unconstrained subarcs ($G(x) > 0$) but may be different from zero over constrained subarcs. Equations (2.93) and (2.94) clearly have the same value, and the last term of (2.94) may be though of as a constraint on the Hamiltonian.

The usual necessary conditions now hold. The Euler-Lagrange equations are derived from the Hamiltonian (2.94), and the minimum principle requires that

$$H(x, u, p, \mu) \leq H(x, U, p, \mu), \tag{2.95}$$

where u is the extremal value and U is any admissible control (satisfying $\dot{G} \geq 0$ over constrained subarcs). The Clebsch condition must also be satisfied, and usually is if (2.95) holds. In fact, it can be shown that the Clebsch condition gives the necessary condition

$$\mu \leq 0 . \tag{2.96}$$

Boundary conditions at the initial and terminal points of the trajectory are the same as those given in Reference 1. Additional conditions may, however, be required at junction points between constrained and unconstrained subarcs. If there are only two subarcs, the condition $G = 0$ may be treated as either an initial condition or terminal condition, depending on the ordering of constrained and unconstrained subarcs, and the multipliers will be continuous over the path. If the ordering is constrained-unconstrained-constrained for a three-subarc-path, the multipliers will be continuous for the same reason. All other cases with three or more subarcs will produce discontinuous multipliers. It is well known (see Reference 12) that the discontinuities take place at one end of the constrained subarc and that the multipliers are continuous at the other end. It does not matter which end has the discontinuities (for proof see Appendix G), so the initial point t_1 is chosen here, as in Figure 2-33.

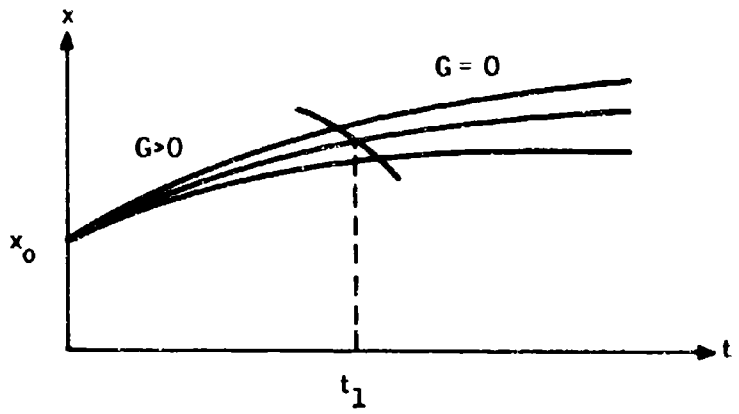

Figure 2-33. State Coordinate Geometry in the Vicinity of the Constrained Subarc Initial Point

The necessary conditions at t_1 (the analog of the Weierstrass-Erdman corner conditions) then read

$$p^+(t_1) = p^-(t_1) - \nu \frac{\partial G(t_1)}{\partial x} \tag{2.97}$$

$$H^+ = H^- \tag{2.98}*$$

$$G^-(t_1) = 0, \tag{2.99}$$

where superscripts + and - indicate limits from the right and left, respectively.

Notice that when (2.97) is substituted into the left-hand side of Equation (2.98), the coefficient of ν becomes $\dot{G}^+$ [Equation (2.92)], which is zero by definition. Equation (2.98) is thus independent of ν, and contains only p^- values of the multipliers. This equation can usually be reduced to an equivalent necessary condition.

*If G contains t explicitly, then the Hamiltonian is discontinuous by the amount $\nu \frac{\partial G}{\partial t}(t_1)$.

For example, it is used in the bounded brachistochrone problem (subsection F4) to show that the optimal control is continuous in time at the point t_1, which implies that

$$\dot{G}^- = 0. \tag{2.100}$$

This condition, rather than (2.98), is used there.

3. Basis for Computational Scheme

In the optimization problem treated in previous subsections, the extremal solutions were functions of the independent variable (call it t) and the multiplier vector p_o. The constant ν in equation (2.97) cannot be determined from the necessary conditions, and hence, becomes an additional parameter for the solutions. The extremal solutions thus have the functional forms

$$\begin{aligned} x &= x(t, p_o, \nu) \\ p &= p(t, p_o, \nu). \end{aligned} \tag{2.101}$$

Each time the multipliers are discontinuous another constant ν is introduced. Unless one has an a priori knowledge of the number of constrained subarcs, the problem could have a variable number of variables. This gives no theoretical difficulty, but the practical bookkeeping problems in a digital computer program could become unmanageable. In what follows, then, it is assumed that the optimal path consists of three subarcs, ordered unconstrained-constrained-unconstrained.

The necessary conditions at the terminal point give (n+1) equations in the (n+2) variables (T, p_o, ν). The necessary conditions (2.98) (or equivalent) and (2.99) determine the point t_1 and give an additional equation in (T, p_o, ν).

The problem is thus one of determining the solution of (n+2) equations in (n+2) unknowns and the Newton-Raphson method may be used to find the solution.

Partial derivatives of the solutions with respect to p_o are obtained as before, by integrating the accessory differential equations. An additional column in the solution matrix is reserved for partials with respect to ν. Initial conditions for this solution are obtained by differentiating Equation (2.97), and noting that $x(t_1)$ is independent of ν. The method of solving the problem is illustrated in the following example.

4 The Bounded Brachistochrone Problem

The bounded brachistochrone problem was chosen to test the theory. It is simple enough to have an analytical solution, yet nonlinear in nature. The equations of motion, as given in Reference 11, are

$$\dot{x} = v \cos \gamma \tag{2.102}$$

$$\dot{y} = v \sin \gamma \tag{2.103}$$

$$\dot{v} = -g \sin \gamma. \tag{2.104}$$

The problem is to minimize the time it takes to go from a given initial point to $x = x_f$ while satisfying the path constraint

$$G = y - ax - b \geq 0 . \tag{2.105}$$

The state vector has the components (x, y, v) and γ is the control function to be determined. Figure 2-34 shows the path constraint, terminal condition and a possible path.

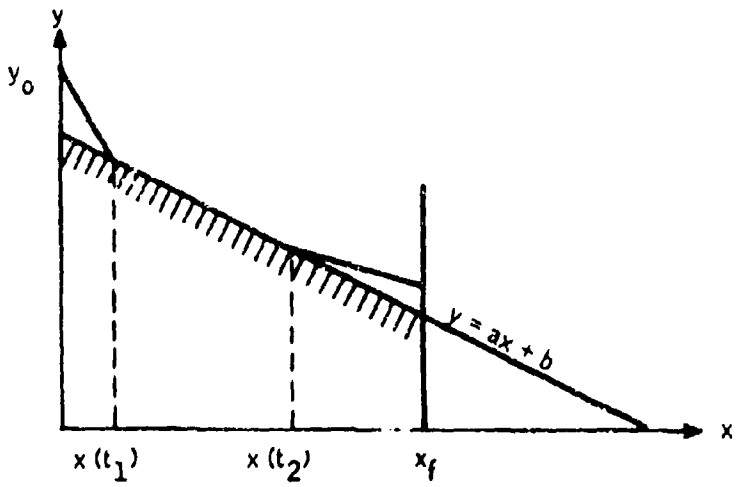

Figure 2-34. Bounded Brachistochrone Problem Geometry

The time derivative of (2.105) is

$$\dot{G} = v(\sin\gamma - a\cos\gamma) \tag{2.106}$$

so the Hamiltonian is written as

$$H_1 = 1 + p_1 v\cos\gamma + p_2 v\sin\gamma - p_3 g\sin\gamma + \mu v(\sin\gamma - a\cos\gamma) \ . \tag{2.107}$$

The Euler-Lagrange equations become

$$\dot{p}_1 = 0 \tag{2.108}$$

$$\dot{p}_2 = 0 \tag{2.109}$$

$$\dot{p}_3 = -\left[p_1\cos\gamma + p_2\sin\gamma\right] \tag{2.110}$$

$$0 = -p_1 v\sin\gamma + p_2 v\cos\gamma - p_3 g\cos\gamma + \mu v(\cos\gamma + a\sin\gamma) \ . \tag{2.111}$$

Over unconstrained subarcs the multiplier μ is zero, so (2.111) may be solved for $\gamma(v, p_1, p_2, p_3)$ as

$$\tan \gamma = \frac{p_2 v - p_3 g}{p_1 v} \tag{2.112}$$

or

$$\sin \gamma = \frac{-(p_2 v - p_3 g)}{\sqrt{(p_1 v)^2 + (p_2 v - p_3 g)^2}} \tag{2.113}$$

$$\cos \gamma = \frac{-p_1 v}{\sqrt{(p_1 v)^2 + (p_2 v - p_3 g)^2}} \, . \tag{2.114}$$

The minus signs in (2.113) and (2.114) are chosen to minimize the Hamiltonian (2.107).

On constrained subarcs, solution of $G = 0$ [Equation (2.106)] gives

$$\tan \gamma = a \, , \tag{2.115}$$

since by assumption $v \neq 0$, and Equation (2.111) gives

$$\mu = \frac{p_1 v a - (p_2 v - p_3 g)}{v(1+a^2)} \, . \tag{2.116}$$

Now let ϕ be the angle defined by (2.113) and (2.114). This is a convenient definition, since at the boundary point t_2 (see Figure 2-34) everything is continuous, so ϕ becomes γ at that point. The constrained subarc Hamiltonian may then be written

$$H = 1 - \sqrt{(p_1 v)^2 + (p_2 v - p_3 g)^2} \cos(\gamma - \phi) \, . \tag{2.117}$$

The minimizing value of γ makes the cosine positive, so it must satisfy

$$\phi - \frac{\pi}{2} < \gamma < \phi + \frac{\pi}{2} , \tag{2.118}$$

thus resolving the ambiguity of Equation (2.115).

The multiplier μ of Equation (2.116) is negative over the constrained subarc. To see this, consider the complete statement of the minimum principle for this problem. It reads

$$H(\gamma) \leq H(\Gamma) \tag{2.119}$$

for all Γ satisfying $\dot{G}(\Gamma) \geq 0$. Written out,

$$p_1 v \cos\gamma + (p_2 v - p_3 g)\sin\gamma \leq p_1 v \cos\Gamma + (p_2 v - p_3 g)\sin\Gamma , \tag{2.120}$$

or from (2.117),

$$\cos(\gamma - \phi) \geq \cos(\Gamma - \phi) . \tag{2.121}$$

Now $\Gamma = \phi$ contadicts (2.121) if $\gamma \neq \phi$, so ϕ must satisfy $\dot{G}(\phi) < 0$ except at the endpoint t_2 where $\gamma = \phi$. Thus,

$$\dot{G}(\phi) = v(\sin\phi - a\cos\phi) < 0, \quad t_1 < t < t_2. \tag{2.122}$$

Substitution of (2.113) and (2.114) then gives

$$\frac{v}{\sqrt{|p_1 v|^2 + |p_2 v - p_3 g|^2}} \left[p_1 v\, a - (p_2 v - p_3 g)\right] < 0, \quad t_1 < t < t_2. \tag{2.123}$$

The bracketed term of (2.123) is the only term which can be negative, and is the numerator of (2.116). Since the denominator of (2.116) is positive, μ must be negative over the second subarc. An interesting interpretation of the angle ϕ is that it is the extremal value of γ if the constraint is not present.

The relevant boundary conditions for this problem are the terminal and intermediate conditions

$$x(T) - x_f = 0 \tag{2.124}$$

$$y(t_1) - ax(t_1) - b = 0 \tag{2.125}$$

and the transversality conditions

$$p_2(T) = 0 \tag{2.126}$$

$$p_3(T) = 0 \tag{2.127}$$

$$p_1^+(t_1) = p_1^-(t_1) + va \tag{2.128}$$

$$p_2^+(t_1) = p_2^-(t_1) - v \tag{2.129}$$

$$p_3^+(t_1) = p_3^-(t_1) \tag{2.130}$$

$$H^+(t_1) = H^-(t_1) \tag{2.131}$$

$$H = 0 \quad (0 \le t \le T). \tag{2.132}$$

The condition (2.131) implies continuity of the control function at $t = t_1$, which in turn implies $\dot{G}^-(t_1) = 0$, or

$$v(t_1) \sin \gamma^-(t_1) - a \cos \gamma^-(t_1) = 0. \tag{2.133}$$

Continuity of γ follows from substitution of (2.128) through (2.130) into (2.131), giving

$$p_1^- v(\cos \gamma^+ - \cos \gamma^-) + (p_2^- v - p_3 g)(\sin \gamma^+ - \sin \gamma^-) + vv\left[a \cos \gamma^+ - \sin \gamma^+\right] = 0, \tag{2.134}$$

where the parameter t_1 has been suppressed and the bracketed term vanishes.

Now let ψ be the angle defined by (2.113) and (2.114) using p^- values. (2.134) then becomes

$$\cos(\gamma^+ - \psi) = \cos(\gamma^- - \psi) = 1,$$

since $\gamma^- = \psi$, so it follows that

$$\gamma^+ = \psi = \gamma^- , \quad (0 \le \gamma < 2\pi) \tag{2.135}$$

on the optimal path.

From a numerical standpoint the problem falls into two categories, determined by the number of subarcs contained in the path.

Case I: $G > 0$ Over the Entire Path (One Subarc) -- Although the optimal path is to consist of three subarcs, it is possible that some intermediate extremal will not reach the boundary. The reduced differential equations of the extremals are (2.102)-(2.104) and (2.108)-(2.110) with control γ determined from (2.113) and (2.114). The problem then becomes one of finding (T, p_o) which satisfy

$$x(T, p_o) - x_f = 0 \tag{2.136}$$

$$p_{2_o} = 0 \tag{2.137}$$

$$p_3(T, p_o) = 0 \tag{2.138}$$

$$H(p_o) = 0. \tag{2.139}$$

The modified Newton-Raphson equations are

$$-C\begin{bmatrix} 0 \\ p_{2_o} \\ p_3(T) \\ H(p_o) \end{bmatrix} = \begin{bmatrix} \dot{x}(T) & \eta_{11}(T) & \eta_{12}(T) & \eta_{13}(T) \\ 0 & 0 & 1 & 0 \\ \dot{p}_3(T) & \zeta_{31}(T) & \zeta_{32}(T) & \zeta_{33}(T) \\ 0 & f_1(0) & f_2(0) & f_3(0) \end{bmatrix} \begin{bmatrix} dT \\ dp_{1_o} \\ dp_{2_o} \\ dp_{3_o} \end{bmatrix} \tag{2.140}$$

where the η's are the elements of the first row of $\frac{\partial x(T)}{\partial p_o}$, and the ζ's are the second and third row components of $\frac{\partial p(T)}{\partial p_o}$. Since the Hamiltonian is zero over the entire path it can be evaluated at $t = 0$ where all p's are initial values, so the last row contains the partials of the Hamiltonian with respect to the p_o's at that point. Equation (2.136) is used as the stopping-condition for the integrations which accounts for the zero in the left-hand vector of (2.140). The accessory differential equations are

$$\begin{aligned}
\dot{\eta}_1 &= \left[\frac{\partial f_1}{\partial v} + \frac{\partial f_1}{\partial \gamma}\frac{\partial \gamma}{\partial v}\right]\eta_3 + \frac{\partial f_1}{\partial \gamma}\left[\frac{\partial \gamma}{\partial p_1}\zeta_1 + \frac{\partial \gamma}{\partial p_2}\zeta_2 + \frac{\partial \gamma}{\partial p_3}\zeta_3\right] \\
\dot{\eta}_2 &= \left[\frac{\partial f_2}{\partial v} + \frac{\partial f_2}{\partial \gamma}\frac{\partial \gamma}{\partial v}\right]\eta_3 + \frac{\partial f_2}{\partial \gamma}\left[\frac{\partial \gamma}{\partial p_1}\zeta_1 + \frac{\partial \gamma}{\partial p_2}\zeta_2 + \frac{\partial \gamma}{\partial p_3}\zeta_3\right] \\
\dot{\eta}_3 &= \frac{\partial f_3}{\partial \gamma}\frac{\partial \gamma}{\partial v}\eta_3 + \frac{\partial f_3}{\partial \gamma}\left[\frac{\partial \gamma}{\partial p_1}\zeta_1 + \frac{\partial \gamma}{\partial p_2}\zeta_2 + \frac{\partial \gamma}{\partial p_3}\zeta_3\right] \\
\dot{\zeta}_1 &= 0 \\
\dot{\zeta}_2 &= 0 \\
\dot{\zeta}_3 &= \frac{\partial \dot{p}_3}{\partial \gamma}\frac{\partial \gamma}{\partial v}\eta_3 + \frac{\partial \dot{p}_3}{\partial \gamma}\left[\frac{\partial \gamma}{\partial p_1}\zeta_1 + \frac{\partial \gamma}{\partial p_2}\zeta_2 + \frac{\partial \gamma}{\partial p_3}\zeta_3\right],
\end{aligned} \tag{2.141}$$

and the initial conditions are

$$\begin{bmatrix} \frac{\partial x(0)}{\partial p_o} \\ \hline \frac{\partial p(0)}{\partial p_o} \end{bmatrix} \quad \left[\begin{array}{cccc} 0 & 0 & 0 & 0 \\ 0 & 0 & 0 & 0 \\ 0 & 0 & 0 & 0 \\ \hline 1 & 0 & 0 & 0 \\ 0 & 1 & 0 & 0 \\ 0 & 0 & 1 & 0 \end{array}\right] \qquad (2.142)$$

The last column of (2.142) will, of course, give a zero vector solution of (2.141). It is included for the three-subarc-case in which case it will contain the partials of x and p with respect to ν.

Case II: Two or Three Subarcs -- The first and third (if present) subarcs satisfy the differential equations for Case I. Over the second subarc the reduced differential equations of the extremals are (2.102)-(2.104) and (2.108)-(2.110) with γ determined from (2.115) and (2.118). Since γ is a constant, the accessory equations simplify to

$$\begin{aligned} \dot{\eta}_1 &= \cos\gamma\ \eta_3 \\ \dot{\eta}_2 &= \sin\gamma\ \eta_3 \\ \dot{\eta}_3 &= 0 \\ \dot{\zeta}_1 &= 0 \\ \dot{\zeta}_2 &= 0 \\ \dot{\zeta}_3 &= -[\cos\gamma\ \zeta_1 + \sin\gamma\zeta_2]. \end{aligned} \qquad (2.143)$$

The initial conditions for (2.108)-(2.110) are given by (2.128)-(2.130), with constant ν to be determined, whereas initial conditions for (2.143) are

$$\eta_{ij}^{+} = \eta_{ij}^{-} + [\dot{x}_i^{-} - \dot{x}_i^{+}] \frac{\partial t_1}{\partial p_{o_j}}, \quad i, j = 1, 2, 3 \tag{2.144}$$

$$\eta_{i4}^{+} = 0, \quad i = 1, 2, 3 \tag{2.145}$$

$$\left.\begin{aligned} \zeta_{1j}^{+} &= \zeta_{1j}^{-} \\ \zeta_{2j}^{+} &= \zeta_{2j}^{-} \\ \zeta_{3j}^{+} &= \zeta_{3j}^{-} + (\dot{p}_3^{-} - \dot{p}_3^{+}) \frac{\partial t_1}{\partial p_{o_j}} \end{aligned}\right\} \quad j = 1, 2, 3 \tag{2.146}$$

$$\begin{aligned} \zeta_{14}^{+} &= a \\ \zeta_{24}^{+} &= -1 \\ \zeta_{34}^{+} &= 0. \end{aligned} \tag{2.147}$$

In these equations j designates the column number in the matrices $\frac{\partial x}{\partial p_o}$, $\frac{\partial p}{\partial p_o}$, and i corresponds to the numbering in (2.143).

Intermediate extremals computed during iterations will not in general satisfy the necessary conditions at the point t_1. In particular, the control function may be discontinuous, which implies $\dot{G}^{-} \neq 0$. In this case the partials of t_1 in (2.144) and (2.146) are computed from $G(t_1) = 0$, i.e.,

$$\frac{\partial t_1}{\partial p_{o_j}} = \frac{a\,\eta_{1j}^{-} - \eta_{2j}^{-}}{-a\dot{x}^{-} + \dot{y}^{-}}, \quad j = 1, 2, 3 \quad (\dot{G}^{-} \neq 0). \tag{2.148}$$

If $\dot{G}^-$ happens to be zero, the coefficients of $\frac{\partial t_1}{\partial p_{o_j}}$ disappear in (2.144) and (2.146). These partial derivative solutions are then continuous at $t = t_1$, and $\frac{\partial t_1}{\partial p_{o_j}}$ need not be computed. All variables are continuous at the junction point t_2 between the second and third subarcs (if there happens to be a third subarc).

Two additional necessary conditions are required to set up the modified Newton-Raphson equations. These are

$$G(t_1) = y(t_1, p_o) - ax(t_1, p_o) - b = 0 \tag{2.149}$$

$$\dot{G}^-(t_1) = \dot{y}^-(t_1, p_o) - a\dot{x}^-(t_1, p_o) = 0 . \tag{2.150}$$

If $\dot{G}^-(t_1) \neq 0$, then (2.149) determines $t_1(p_o)$, and (2.150) is the additional necessary condition to be satisfied. The modified Newton-Raphson equations are then

$$-C \begin{bmatrix} 0 \\ p_2(T) \\ p_3(T) \\ H(p_o) \\ G(t_1) \end{bmatrix} = \begin{bmatrix} \dot{x}(T) & \eta_{11}(T) & \eta_{12}(T) & \eta_{13}(T) & \eta_{14}(T) \\ 0 & \zeta_{21}(T) & \zeta_{22}(T) & \zeta_{23}(T) & \zeta_{24}(T) \\ \dot{p}_3(T) & \zeta_{31}(T) & \zeta_{32}(T) & \zeta_{33}(T) & \zeta_{34}(T) \\ 0 & f_1(0) & f_2(0) & f_3(0) & 0 \\ 0 & \frac{\partial \dot{G}^-(t_1)}{\partial p_{1_o}} & \frac{\partial \dot{G}^-(t_1)}{\partial p_{2_o}} & \frac{\partial \dot{G}^-(t_1)}{\partial p_{3_o}} & 0 \end{bmatrix} \begin{bmatrix} dT \\ dp_{1_o} \\ dp_{2_o} \\ dp_{3_o} \\ d\nu \end{bmatrix} \tag{2.151}$$

where

$$\frac{\partial \dot{G}^-(t_1)}{\partial p_{i_o}} = \dot{\eta}_{1i}^- - a\dot{\eta}_{2i}^- + \ddot{G}(t_1) \frac{\partial t_1}{\partial p_{o_i}} , \quad i = 1, 2, 3, \tag{2.152}$$

$$\dot{G}(t_1) = ag(\sin^2 \gamma^- - \cos^2 \gamma^-), \tag{2.153}$$

and $\dfrac{\partial t_i}{\partial p_{o_i}}$ is defined by Equation (2.148). If (2.150) is satisfied, then it determines t_1, and (2.149) becomes the additional equation which must be satisfied. In this case the last equation of (2.151) is replaced by

$$-C\, G(t_1) = \frac{\partial G(t_1)}{\partial p_{1_o}} dp_{1_o} + \frac{\partial G}{\partial p_{2_o}} dp_{2_o} + \frac{\partial G}{\partial p_{3_o}} dp_{3_o}$$

where

$$\frac{\partial G(t_1)}{\partial p_{o_i}} = r_{2i} - a r_{1i} \quad , \quad i = 1, 2, 3 \tag{2.154}$$

The First Constrained Path -- It is possible to choose the initial values $(p_{1_o}, p_{2_o}, p_{3_o})$ such that the path strikes the boundary (2.149) before the stopping-condition (2.136) is satisfied. There will then be a second subarc, and the problem is that of determining a value of ν to go with it. Since the optimal path is to consist of three subarcs, the scheme chosen is based upon leaving the constrained subarc as soon as possible.

According to Appendix G, the multiplier discontinuities may be computed at either end of a constrained subarc. Assuming they are determined at the point $t = t_2$, Equation (2.110) takes the form

$$\dot{p}_3 = -[p_1^- \cos \gamma^+ + p_2^- \sin \gamma^+]. \tag{2.155}$$

Since $p_1^- = p_{1_o}$, $p_2^- = p_{2_o}$, and γ^+ is found from (2.115) and (2.118), $p_3(t)$ is well determined. The conditions $\mu^+(t_2) = 0$,* $\dot{G}^+(t_2) > 0$ and ν continuous must be satisfied if t_2 is the endpoint of the second subarc. The first condition is solved for ν giving

$$\nu = \frac{(p_2^- v - p_3^- g) - p_1^- v a}{v(1+a^2)}, \tag{2.156}$$

* $\dot{\mu}^+(t_2) \neq 0$ is satisfied, so t_2 is well determined.

whereas the second requires that

$$\ddot{G}^{+}(t_2) = g(1-a^2)\cos^2\gamma^{+} > 0 \qquad (2.157)$$

Inequality (2.157) is always satisfied for the value of a considered. The determining factor is the continuity of γ which requires (from the minimum principle)

$$\begin{aligned} \operatorname{sgn}(p_1^{-} + \nu a) &= \operatorname{sgn}(\cos\gamma^{+}) \\ \operatorname{sgn}[(p_2^{-} - \nu)v - p_3 g] &= -\operatorname{sgn}(\sin\gamma^{+}). \end{aligned} \qquad (2.158)$$

Satisfaction of (2.158) then determines the endpoint of the second subarc. If the third subarc comes back to the boundary, the second subarc is extended to this point, and testing for the end of the second subarc is resumed. On the other hand, if the second subarc extends to the endpoint, then $\eta_{14}(T) = \zeta_{34}(T) = 0$, and $\zeta_{24}(T) = 1$. Solution of (2.151) (or its equivalent if $\dot{G}^{-} = 0$) gives iterative corrections which tend to satisfy the last three necessary conditions. The computed $d\nu$ is ignored, since the necessary condition for $p_2(T)$ on a two subarc optimal is $p_2(T) = \nu$, rather than zero. The optimal path is to have three subarcs, so the corrections are used iteratively with the first constrained path logic. A three-subarc path is eventually obtained.

Numerical Results -- The constants for the problem solved are the same as those used by Dreyfus in Reference 11. They are $x_o = 0$, $y_o = 6$, $v_o = 1$, $g = 32.172$, $a = -0.5$, $b = 5$ and $x_f = 6$. A set of initial multipliers were found which produced a three-subarc path having a terminal time of 1.25429 seconds. The optimal path of Figure 2-35 resulted after 33 iterations, and a comparison of this path with the exact solution is given in Table 2-4.

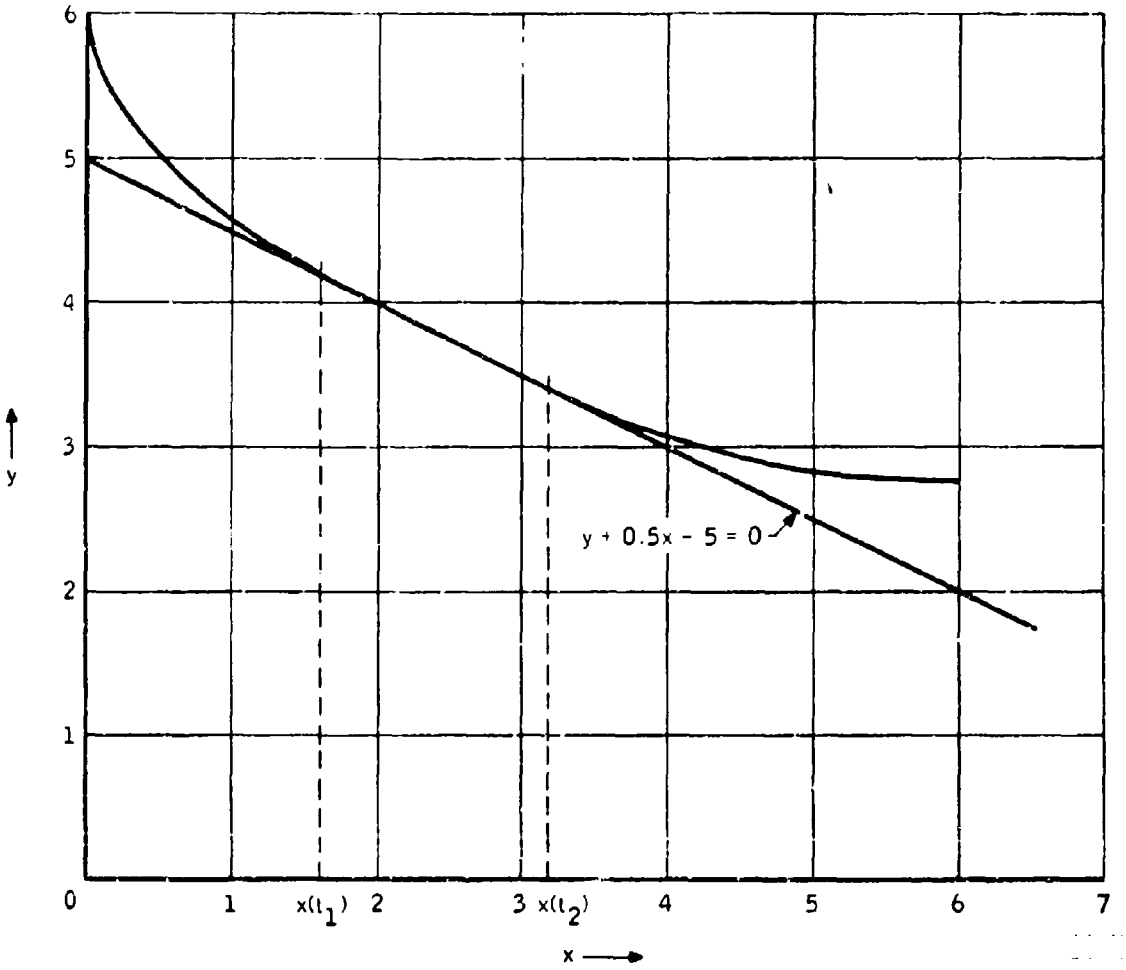

Figure 2-35. Bounded Brachistochrone Optimal Solution

Table 2-4. Comparison of Computed and Exact Optimal Paths

Quantity	Computed Value	Exact Value
γ_o (degrees)	-85.2577	-85.2578
t_1	0.385117	0.385141
$x(t_1)$	1.60687	1.60710
$y(t_1)$	4.19657	4.19645
$G(t_1)$	1×10^{-5}	0.25×10^{-9}
$\dot{G}(t_1)$	-0.7×10^{-3}	0
t_2	0.533530	0.533526
$x(t_2)$	3.18470	3.18465
$y(t_2)$	3.40766	3.40767
T	0.742246	0.742245
$x(T)$	6.00001	6
$y(T)$	2.75571	2.75571
H(0)	0.1×10^{-10}	0
$H(t_1)$	0.6×10^{-8}	0
$p_2(T)$	0.6×10^{-13}	0
$p_3(T)$	0.7×10^{-11}	0

The differences between exact and computed values resulted from rather loose interpolation procedures in the computer program. Although these could have been corrected to obtain more accurate results, it was not felt necessary since the purpose of solving the problem was to prove the method.

SECTION III
THE CONTROL FUNCTION

A. JUSTIFICAT'ON OF THE FORM OF THE CONTROL FUNCTION

The form of the nonlinear optimal feedback control function is

$$u = u(x, t), \tag{3.1}$$

where x is an n-dimensional state vector and t is the independent variable. This form is justified theoretically, and a simple example is given. The general procedure for obtaining the control is also outlined.

1. Theory

Consider a set of optimal trajectories, starting at various initial conditions, which all satisfy the same set of terminal transversality conditions. The control functions for their trajectories are clearly those required for the nonlinear optimal feedback control scheme. The fact that the control for the family of trajectories is of the form (3.1) follows from the field theory of the calculus of variations. For the control problem, a field is a region of (t, x) - space with which there is associated a set of slope functions, control functions and multipliers

$$\begin{aligned} \dot{x} &= \dot{x}(t, x) \\ u &= u(t, x) \\ p &= p(t, x), \end{aligned} \tag{3.2}$$

having continuous first partial derivatives, which satisfy the differential

equations $\dot{x} = f(x, u)$, and which make the Hilbert integral

$$I^* = \int \left[H(x, u(t, x), p(t, x))\, dt - p'(t, x)\, dx \right] \tag{3.3}$$

independent of path. A field is constructed through the use of a theorem which states that an n-parameter family of trajectories which smoothly covers a region of (t, x) - space and cuts a surface transversally exactly once defines a field. (The proof follows from Bliss' corollary 83.1 and the fact that $I^* \equiv 0$ on a transversal surface.) Smoothness is established by the non-singularity of a matrix representing $\frac{\partial x(t)}{\partial x_o}$, as in Section IIC, over each path. The transversal surface is excluded from the field since, by construction, the matrix $\frac{\partial x(t)}{\partial x_o}$ is singular at the endpoint of each trajectory.

2. Example

Consider the problem

$$J = \int_{t_o}^{T} \frac{u^2}{2}\, d\tau = \text{minimum} \tag{3.4}$$

$$\dot{x}_1 = x_2$$
$$\dot{x}_2 = u, \tag{3.5}$$

with terminal conditions

$$T - K = 0$$
$$x_2(T) - X_2 = 0. \tag{3.6}$$

The Hamiltonian is

$$H = \frac{u^2}{2} + p_1 x_2 + p_2 u, \tag{3.7}$$

so the Euler-Lagrange equations are

$$\begin{aligned} \dot{p}_1 &= 0 \\ \dot{p}_2 &= -p_1 \end{aligned} \tag{3.8}$$

and the control satisfies

$$u = -p_2. \tag{3.9}$$

The solutions after (3.9) is inserted into (3.5), are

$$\begin{aligned} x_1 &= x_{10} + x_{20}t - p_{20}\frac{t^2}{2} + p_{10}\frac{t^3}{6} \\ x_2 &= x_{20} - p_{20}t + p_{10}\frac{t^2}{2} \\ p_1 &= p_{10} \\ p_2 &= p_{20} - p_{10}t, \end{aligned} \tag{3.10}$$

where the (0) subscripts indicate conditions at t = 0. The transversality conditions (Reference 1) require

$$\begin{aligned} p_1(T) &= 0 \\ p_2(T) &= \nu_2 \\ H &= \nu_3. \end{aligned} \tag{3.11}$$

The last two of (3.11) can always be satisfied. However, the first and (3.6) require

$$p_{10} = 0$$
$$p_{20} = -\frac{(X_2 - x_{20})}{K}, \tag{3.12}$$

The set of all trajectories which cut the terminal surface (3.6) transversally are thus found to be

$$x_1 = x_{10} + x_{20}t + \frac{(X_2 - x_{20})}{K}\frac{t^2}{2} \tag{3.13}$$
$$x_2 = x_{20} + \frac{(X_2 - x_{20})}{K}t$$

$$p_1 = 0$$
$$p_2 = -\frac{(X_2 - x_{20})}{K},$$

with control function from (3.9)

$$u = \frac{(X_2 - x_{20})}{K}, \tag{3.14}$$

The matrix $\frac{\partial x}{\partial x_o}$ is found to be

$$\frac{\partial x}{\partial x_o} = \begin{bmatrix} 1 & \left(1 - \frac{t}{2K}\right)t \\ 0 & 1 - \frac{t}{K} \end{bmatrix}, \tag{3.15}$$

which is non-singular everywhere, except at t=K. The trajectories thus smoothly cover the solution space. The first two of (3.13) may be solved to obtain

$$x_{10} = x_1 - x_{20}t - (X_2 - x_{20})\frac{t^2}{2K}$$
$$x_{20} = \frac{Kx_2 - X_2 t}{K-t}. \tag{3.16}$$

Substituting into the last of (3.13) gives

$$p_1 = 0$$
$$p_2 = \frac{X_2 - x_2}{K-t}, \tag{3.17}$$

with control determined from (3.17) and (3.9).

Of course, the control may be deduced from (3.14) directly in this simple example. One simply replaces K by $(K-t_o)$ and regards the present point as the initial point.

The example illustrates the general procedure of constructing the desired field. For more complex problems, Equation (3.9) is found to have the general form

$$u = u(x, p), \tag{3.18}$$

and the solutions (3.10) are

$$x = x(t, x_o, p_o)$$
$$p = p(t, x_o, p_o). \tag{3.19}$$

The transversality conditions give the relationships

$$p_o = p_o(x_o) \tag{3.20}$$

so that (3.19) becomes

$$x = x(t, x_o)$$
$$p = p(t, x_o). \tag{3.21}$$

Note that the transversality conditions and terminal equations must constitute an n-dimensional non-singular (or normal) system to obtain the solution (3.20). Non-singularity of the matrix (3.15) allows inversion of the first of (3.21) to obtain

$$x_o = x_o(t, x), \tag{3.22}$$

which is the general form of (3.16). Substitution of (3.22) into the last of (3.21) gives

$$p = p(t, x) \tag{3.23}$$

as the general form of (3.17). The control (3.18) then assumes the desired form (3.1). Substitution of the control into the original differential equations then gives the last of the field equations (3.2).

In more complex problems, the process described above can be done only in a small region about a trajectory, as in Section II C.

B. METHODS FOR DETERMINING THE CONTROL

As shown in the example, the control may sometimes be obtained by direct solution of the optimization problem. This is generally impossible; however, one might include in the category of "direct solution, the faster than real

time solution of the optimization problem in an airborne computer. This approach is unrealistic at the present time, due to large computational requirements.

An alternate possibility is that of solving of an approximate optimization problem. The model differential equations are usually as simple as the process allows; however, most optimal trajectories are fairly insensitive to path deviations, so far as the optimal criterion is concerned. With feedback, the approximate problem solution would approach an optimal solution as the re-entry progressed so that terminal errors would be nulled as well.

Some time was spent seeking suitable simplifications to the re-entry problem, and some useful relationships were found. However, the problem was not realistically simplified to the point that analytical solutions could be obtained. Another possibility considered was that of using a Rayleigh-Ritz-Galerkin procedure to compute near-optimal trajectories in the airborne computer. This process also ran into large computer requirements, and hence, was not pursued further.

A final alternative is that of using surface fitting procedures to approximate the optimal control function. This has the advantage of moderate on-board computer requirements and may well handle large deviations from "nominal" re-entry conditions. The method also has growth potential, in that self adaptive features may be built in by increasing the dimensionality of the fit. However, several facts should be borne in mind in such an approach. There is, in general, no way of determining the best form of the approximating function. Polynomial approximations are probably best from the standpoint of evaluation in the airborne computer, so this form is assumed for the remainder of the report.

The region over which an approximation is to be valid is usually determined by the errors which can be tolerated. It is generally not true that higher-ordered fits produce more accuracy after a certain point, for computer truncation and roundoff errors destroy the benefits of the additional terms. It is better to segment the region into subregions and to use lower-ordered fits to obtain more accuracy. The segmentation is readily accomplished and mechanized for one-dimensional approximations, but may lead to serious mechanization problems in more dimensions.

The larger the dimensionality of the approximation, the harder the problem of obtaining the fit. It is best, if possible, to split the over-all approximation problem into subproblems of reduced dimension.

The polynomial approximation approach was chosen as the approach for further development of the non-linear optimal feedback control scheme.

C. DEVELOPMENT OF THE CONTROL FUNCTION

The polynomial approximations considered are of the form

$$w = \sum_{i,j,k,\ell} b_{ijk\ell} y_1^i y_2^j y_3^k z^\ell, \quad \begin{matrix} i,j,k,\ell \geq 0, \\ i+j+k \leq m, \end{matrix} \tag{3.24}$$

where w is the approximated control function u, or one of the multipliers P_1, P_2. z is range, and the variables y_1, y_2 and y_3 are related to V, γ, h through the equations

$$\begin{aligned} y_1 &= V - V_n \\ y_2 &= \gamma - \gamma_n \\ y_3 &= h - h_n . \end{aligned} \tag{3.25}$$

Nominal state variables V_n, γ_n, h_n are taken as those for trajectory 1 in Table 2.2, and the reason for the transformation is made clear below. The multiplier approximations are used in evaluating the expression

$$u = \tan^{-1} \frac{-C_{LO} P_2}{2 C_{DL} P_1 V} . \tag{3.26}$$

It is possible to split the over-all approximation (3.24) into two parts because of the method in which the data was collected (Section II C). Thus, consider the two approximations

$$a_{ijk}(z) = \sum_{\ell} b_{ijk\ell} z^{\ell} , \quad \ell \geq 0 \tag{3.27}$$

$$w = \sum_{i,j,k} a_{ijk}(z)\ y_1^{\,i}\, y_2^{\,j}\, y_3^{\,k} , \quad i,j,k \geq 0 \atop i+j+k \leq m . \tag{3.28}$$

The method of solution is to determine sets of coefficients $a_{ijk}(z_r)$,

$$z_r = 15r , \quad r = 0, 1, \ldots, 99, \tag{3.29}$$

for the three-dimensional approximation (3.28), and to use these as data for the several one-dimensional fits (3.27).

Consider, then, the problem of determining the coefficients a_{ijk} for a given value of range. It is convenient to transform the problem to the form

$$w = \sum_{ijk} c_{ijk} x_1^{\,i} x_2^{\,j} x_3^{\,k} , \quad i,j,k \geq 0 \atop i+j+k \leq m \tag{3.30}$$

in which $|x_n| \le 1$, $n = 1, 2, 3$, through the relationships

$$\begin{aligned} x_1 &= \alpha_1 y_1 + \gamma_1 \\ x_2 &= \alpha_2 y_2 + \gamma_2 \\ x_3 &= \alpha_3 y_3 + \gamma_3. \end{aligned} \tag{3.31}$$

The transformation (3.31) gives a better conditioned system of equations to be solved for the coefficients, and, moreover; makes it easy to find negligible coefficients, if there should happen to be any. The coefficients a_{ijk} are obtained by substituting (3.31) into (3.30) and rearranging the results.

When derivatives are included as data, the normal procedure is to differentiate the approximating polynomial to obtain equations. Thus, for example,

$$\frac{\partial w}{\partial x_1} = \frac{\partial w}{\partial V}\frac{\partial V}{\partial y_1}\frac{\partial y_1}{\partial x_1} = \frac{1}{\alpha_1}\frac{\partial w}{\partial V} = \sum_{ijk} c_{ijk}\, i x_1^{i-1} x_2^{j} x_3^{k}, \tag{3.32}$$

with similar expressions for $\frac{\partial w}{\partial x_2}$, $\frac{\partial w}{\partial x_3}$. The four equations

$$\begin{bmatrix} 1 & x_1 & x_2 & x_3 & x_1^2 & x_1x_2 & x_1x_3 & x_2^2 & x_2x_3 & x_3^2 & \cdots \\ 0 & 1 & 0 & 0 & 2x_1 & x_2 & x_3 & 0 & 0 & 0 & \cdots \\ 0 & 0 & 1 & 0 & 0 & x_1 & 0 & 2x_2 & x_3 & 0 & \cdots \\ 0 & 0 & 0 & 1 & 0 & 0 & x_1 & 0 & x_2 & 2x_3 & \cdots \end{bmatrix} c = \begin{bmatrix} w \\ \frac{\partial w}{\partial x_1} \\ \frac{\partial w}{\partial x_2} \\ \frac{\partial w}{\partial x_3} \end{bmatrix} \tag{3.33}$$

with vector

$$c' = \left[c_{000}, c_{100}, c_{010}, c_{001}, c_{200}, c_{110}, c_{101}, c_{020}, c_{011}, c_{002}, \cdots\right].$$

are expansions of (3.30) and its partial derivative equations, in which terms through second-order in x are shown. The matrix of (3.33) may be evaluated numerically for each of the 27 trajectories. These are collected into a matrix system of equations

$$Ac = f \tag{3.34}$$

in which A is a (108 x q) matrix, c is a q-dimensional vector of coefficients, and f is the right-hand side of (3.33) for the 27 trajectories. The dimension q is related to the order of fit m through

$$q = 1 + \frac{m}{6}(11+6m+m^2), \tag{3.35}$$

and the range on m is $0 < m \leq 6$.

1. Lagrange Fits

The approximating function is required to agree with actual function values and derivatives q times. Then q of Equations (3.34) are selected and the right-hand sides contain the relevant function values and partial derivatives determined during the data generating process. The question of which equations to use is resolved on the basis of the least singular system of equations, as determined by the process of Appendix F. Notice that the matrix of evaluated basis functions is the same, regardless of which function (u, P_1, P_2) is fit.

An exploratory program was written to obtain Lagrange fits for (u, P_1, P_2) for all values of m considered. As originally constructed, the matrix of basis functions was inverted, and three matrix multiplies produced the coefficients for the fits. Each fit was evaluated at the 27 data points, and errors were computed. Output included actual and computed function values, errors, and the mean and deviation for each fit, computed from

$$E = \sum_{i=1}^{27} \frac{\epsilon_i}{27} \tag{3.36}$$

$$\sigma = \left[\sum_{i=1}^{27} \frac{\epsilon_i^2}{27} - E^2 \right]^{1/2} \tag{3.37}$$

in which ϵ_i is the error in the function for the i^{th} trajectory. Additionally, the arc tangent relationship (3.26) was evaluated, and errors and statistics for this were included as output. Adequate precautions were taken to ensure that the inverse matrix was well conditioned. If the product of the matrix of basis functions and its inverse were not close to the identity matrix, a well-known Newton-Raphson correction was applied.* Those function errors which were supposed to be zero provided an additional accuracy check (at least one function equation must be included in the set of equations solved, to obtain the coefficient c_{000}).

The first attempts at fitting used (V, γ, h) in place of (x_1, x_2, x_3) in Equation (3.30). The matrix of basis functions turned out to be very badly conditioned, so the linear transformations

$$\begin{aligned} x_1 &= \alpha_1 V + \beta_1 \\ x_2 &= \alpha_2 \gamma + \beta_2 \\ x_3 &= \alpha_3 h + \beta_3 \end{aligned} \tag{3.38}$$

with $|x_i| \leq 1$, $i=1,2,3$, were introduced. The α's and β's, of course, are computed from maximum and minimum values of (V, γ, h) at the given value of range. The new matrix of basis functions was well conditioned, and fits for all values of m were obtained.

*See Reference 9, report No. 3, pg. 216. The NASA project reports contain a wealth of information on surface fitting techniques, as applied to a problem similar to the one considered here.

The exploratory program was run for several range points and the following conclusions were reached:

- Fits for m=5 in Equation (3.30) were best for most of the range points explored. Maximum control errors on the order of 10° were found, although the means and deviations were much less.
- The control function fit was superior (in all cases) to the fit obtained from Equation (3.26).
- The equations used in the fitting process changed from one range point to the next.
- The equations used in the fitting process changed when the accuracy of the constants in Equation (3.38) was increased from 5 to 8 significant digits (at a given range point), indicating great sensitivity.
- The constants in Equation (3.38) were dependent on range.

An attempt was made to fit the constants of Equation (3.38) as functions of range so that the approximations (3.30) could be used directly. The Chebyscheff fitting program described below was used in the attempt. In view of the behavior of the variables (see Figures 2-16 - 2 28) it is evident that the constants are only piecewise smooth as functions of range. Hence, the fits obtained were not good. Moreover, when the fitted constants were used in the transformation, the inverse basis function matrix again became ill conditioned. Hence, it became necessary to perform a "back" transformation by inserting (3.38) into (3.30) and rearranging the results. This gave polynomials in terms of (V, γ, h). The coefficients a_{ijk} so obtained were fairly large, indicating that subtraction

must take place in the evaluation of the polynomial. In a seven digit word-length computer, this could lead to severe truncation and roundoff error.

Moreover, the back transformation could not be performed at all for fits like (3.30) in which $3 \geq i, j, k \geq 0$. (The computer used had a 12-digit word-length, and the fits obtained were somewhat worse than those for m= 5 above.) When the transformation (3.31) was used, the back transformation was readily accomplished, and the coefficients a_{ijk} so obtained were well behaved. Thus the conclusion:

- The approximation (3.28) with variables (3.35) should be used for evaluation in a seven digit wordlength airborne computer.

The transformation (3.31) is obtained from (3.38) by adding and subtracting the appropriate amounts. Thus,

$$x_1 = \alpha_1 V + \beta_1 = \alpha_1 (V - V_n) + (\alpha_1 V_n + \beta_1) = \alpha_1 y_1 + \gamma_1 , \qquad (3.39)$$

with similar expressions for x_2 and x_3.

It was decided to explore least squares approximations as the next step in the development of the control function.

2. Least Squares Fits

One may readily verify that the system of equations to be solved is (see Reference 2)

$$(A'A)\, c = A'f , \qquad (3.40)$$

where the notation is that of Equation (3.34), and vector f contains function values and partial derivatives obtained during the data generating process. Unit weights are used since the derivative equations were of the same order of magnitude as the functional equations. An exploratory program similar to that for the Lagrange fits was constructed, except that a subroutine to solve simultaneous equations was used in place of matrix inversion. The accuracy of the fits so obtained was very good, as measured by the closeness to zero of the mean, Equation (3.36). One may readily verify that the first normal equation for the system (3.34) requires (3.36) to be zero. Then the deviation, Equation (3.37), may be interpreted as the functional portion of the error minimized by the least squares process.

The exploratory program was run with the following conclusions:

- The least squares fits were better than the corresponding Lagrange fits.
- Fits for m = 5 were again best for most of the range points.
- The control function fit was superior (in all cases) to the fit obtained from Equation (3.26).
- The approximation (3.28) with variables (3.25) should be used for evaluation in a seven-digit wordlength airborne computer.

It was decided to use the least squares approximations for the control function. Accordingly, fifth-order least squares fits were obtained for the range values (3.29), excluding r = 95 - 99. The order of the best fits for these range points are summarized in Table 3-1.

Table 3-1. Order of Best Fits Near Terminal Point

Range Point (r)	Order of Fit (m)
95	4
96	4
97	1
98	1
99	2

The control functions of Figure 2-28 are shown in Figures 3-1 through 3-27, together with the corresponding errors in the least squares approximations. The maximum errors occur in the vicinity of maximum change in the control function which corresponds to the bottom of the first dip into the atmosphere. The approximations are quite good before this region, and very accurate from about z = 800 to z = 1300 miles, which covers the complete skip after the first dive. The approximations become somewhat worse as the endpoint is approached.

3. Chebyscheff Fits

The final phase of the control function approximation is that of performing the 56 one-dimensional approximations (3.27). This was not done, since time did not permit both this approximation and the simulation studies of Section IV to be accomplished. It is evident, from Figure 3-28, that the one-dimensional fits must be segmented into several parts in order to obtain any degree of accuracy in the approximations so the final phase is not a trivial problem.

A Chebyscheff criterion fitting computer program was constructed for this final phase. The method is due to Professor F. Koehler of the University of Minnesota, who was a consultant during the contract period. Assume that equally-spaced data is given over the interval $[0, 1]$, and that the order of the fit to be obtained is n. A Lagrange polynomial of order n is constructed for the (n+1) tabular points closest to the Chebyscheff zeros, denoted by

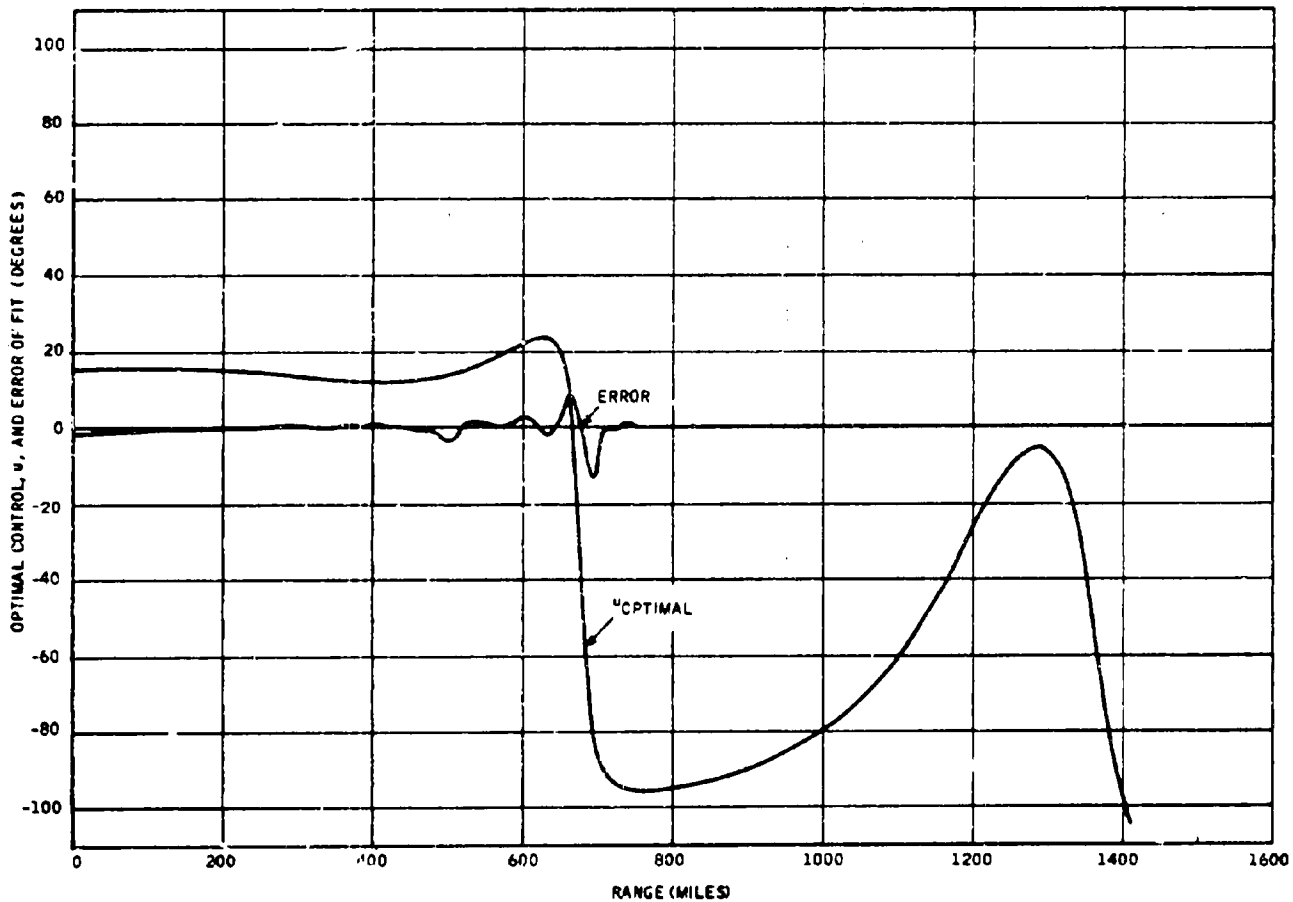

Figure 3-1. Optimal Control u and Error of Fit for Trajectory 1

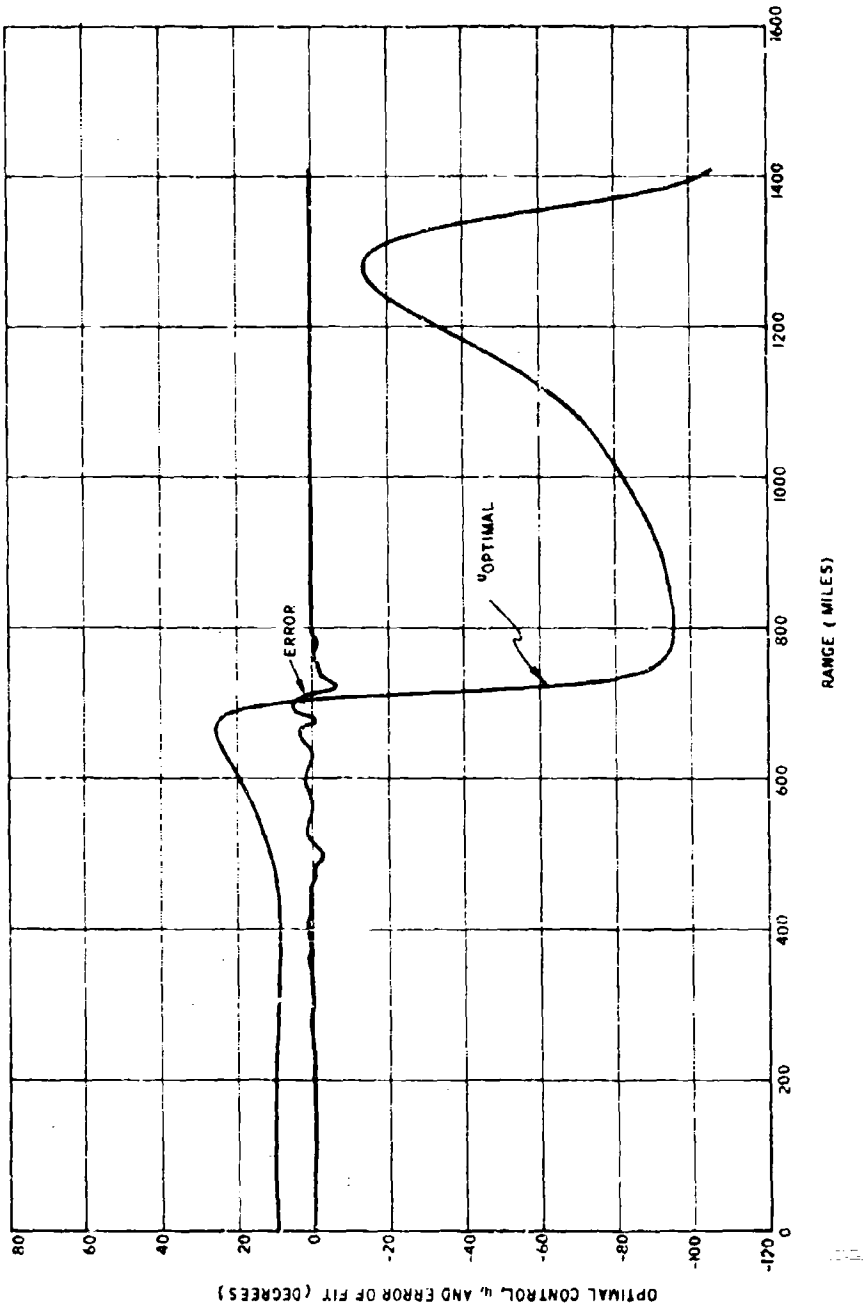

Figure 3-2. Optimal Control u and Error of Fit for Trajectory 2

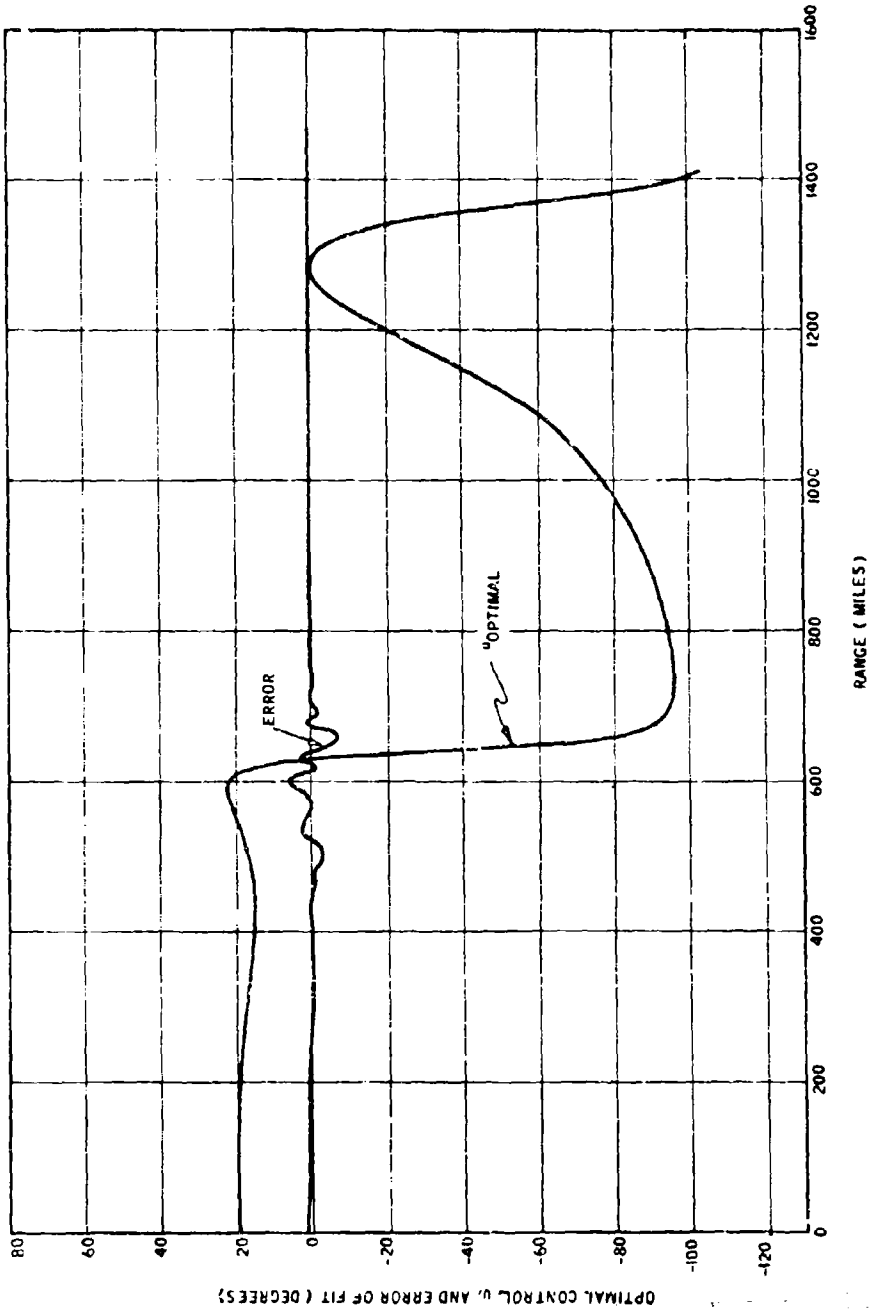

Figure 3-3. Optimal Control u and Error of Fit for Trajectory 3

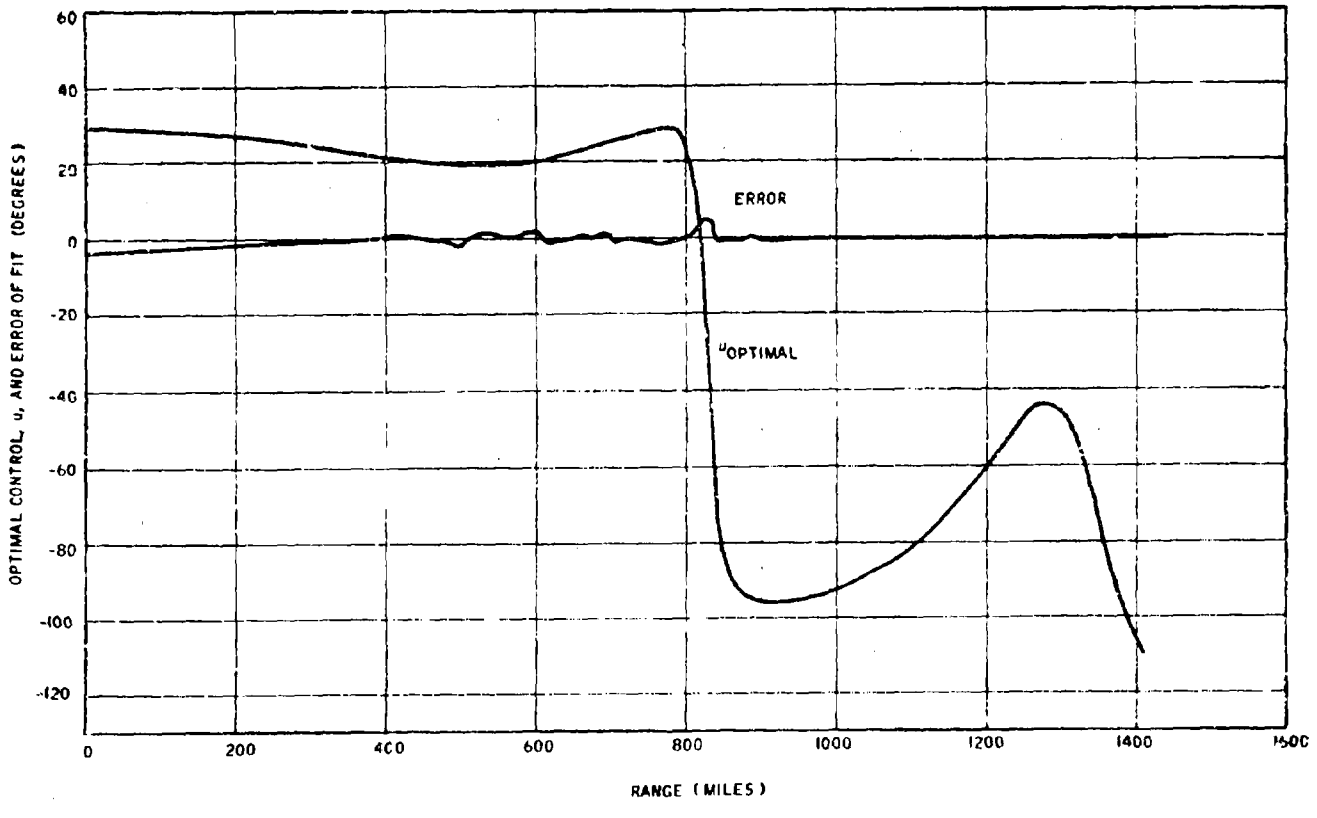

Figure 3-4. Optimal Control u and Error of Fit for Trajectory 4

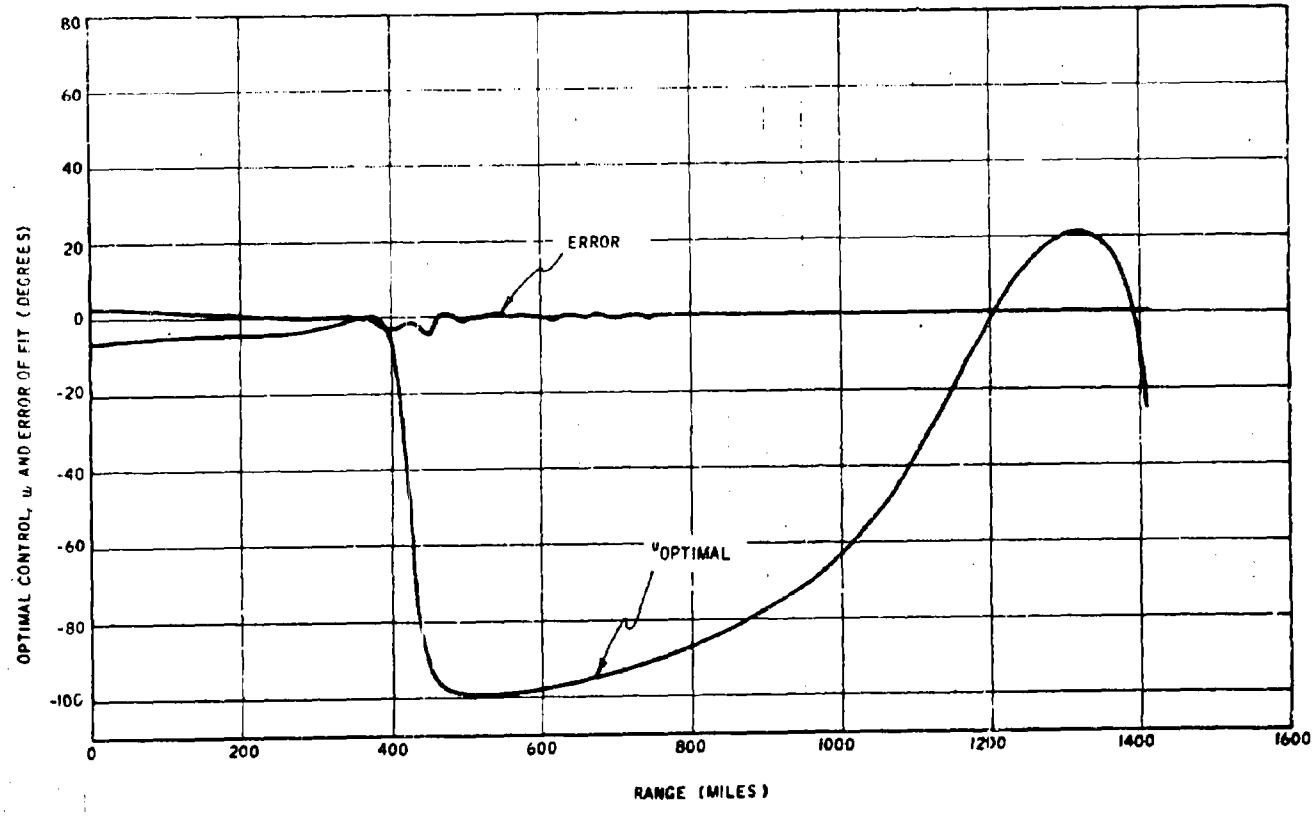

Figure 3-5. Optimal Control u and Error of Fit for Trajectory 5

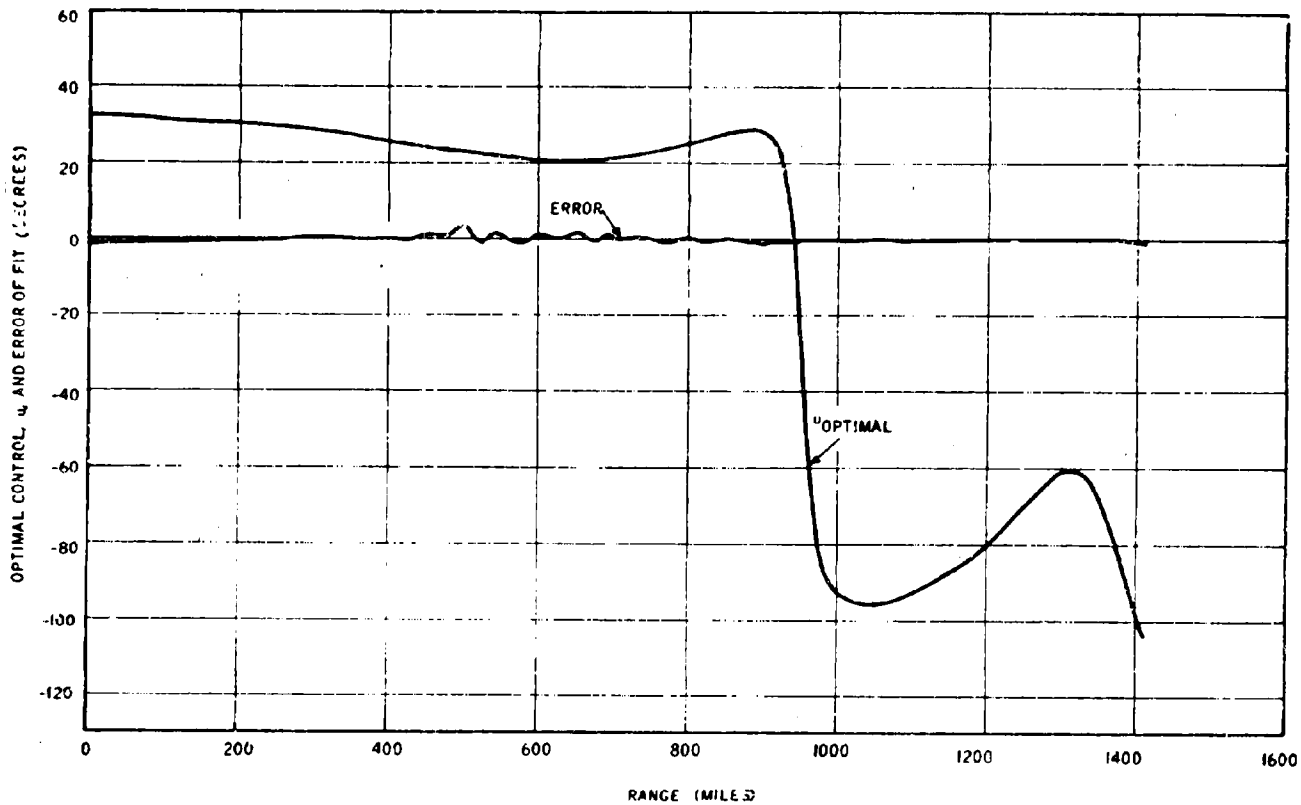

Figure 3-6. Optimal Control u and Error of Fit for Trajectory 6

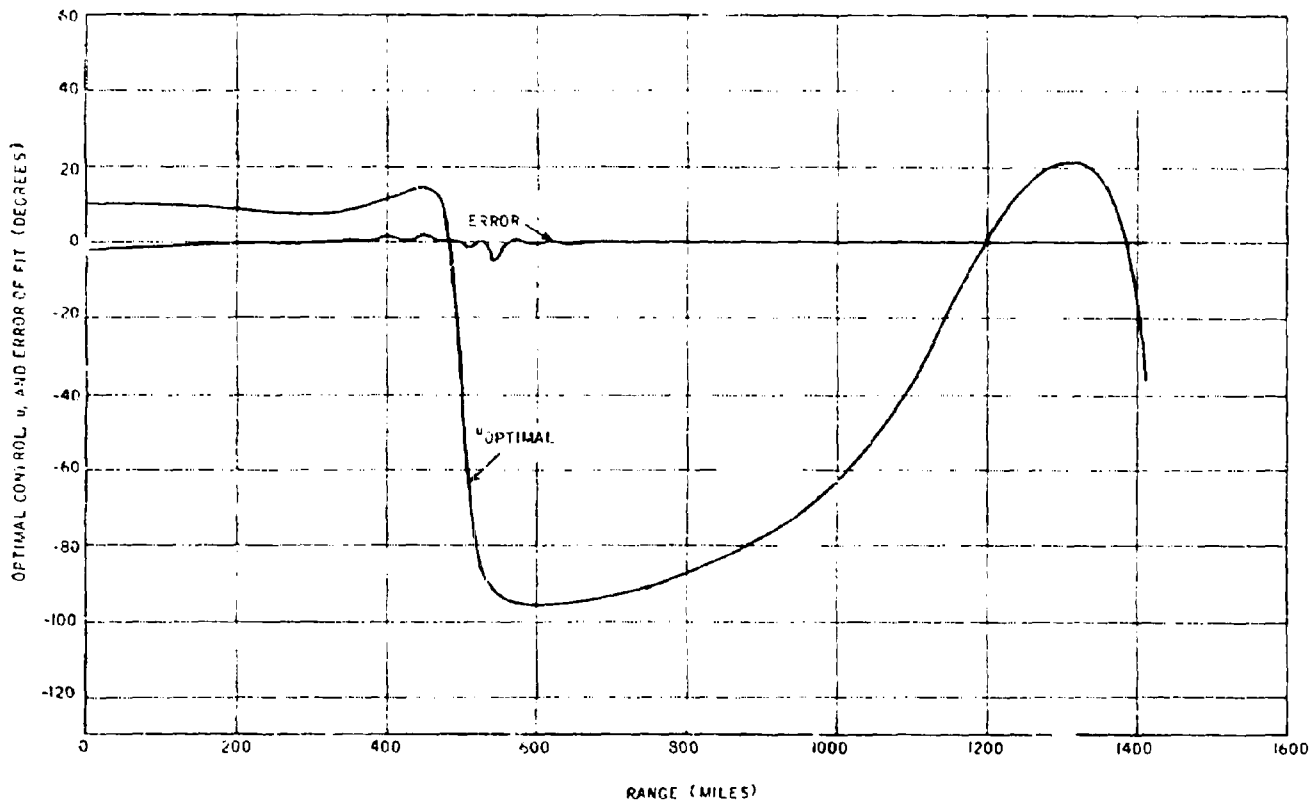

Figure 3-7. Optimal Control u and Error of Fit for Trajectory 7

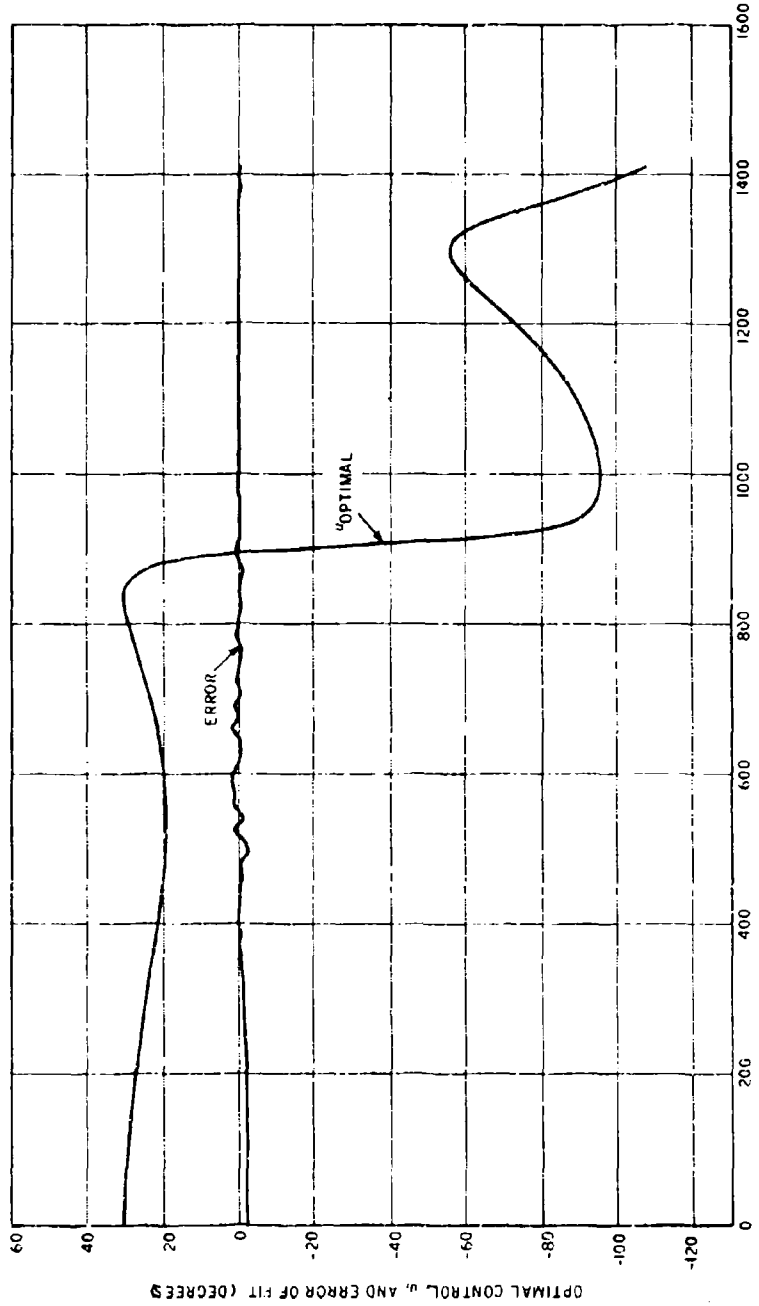

Figure 3-8. Optimal Control u_* and Error of Fit for Trajectory 8

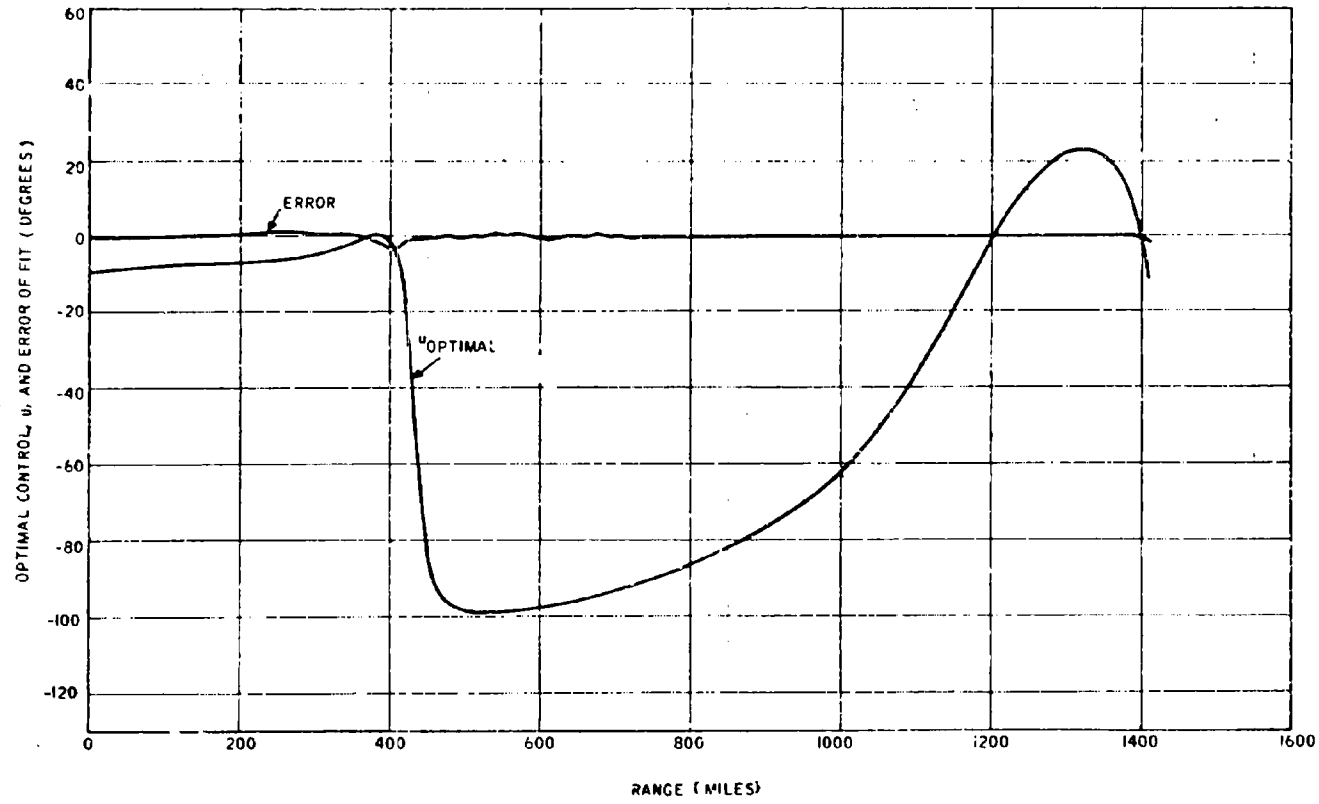

Figure 3-9. Optimal Control u and Error of Fit for Trajectory 9

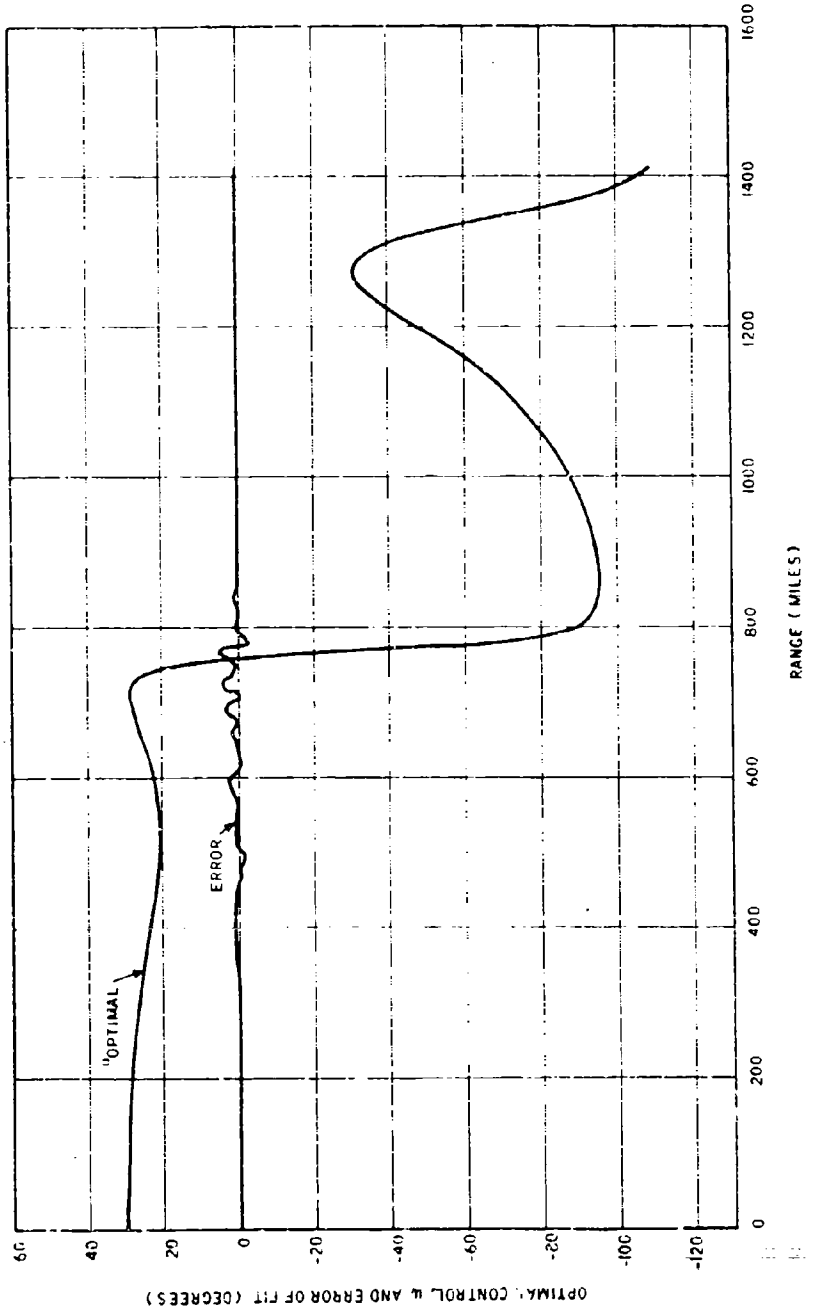

Figure 3-10. Optimal Control u and Error of Fit for Trajectory 10

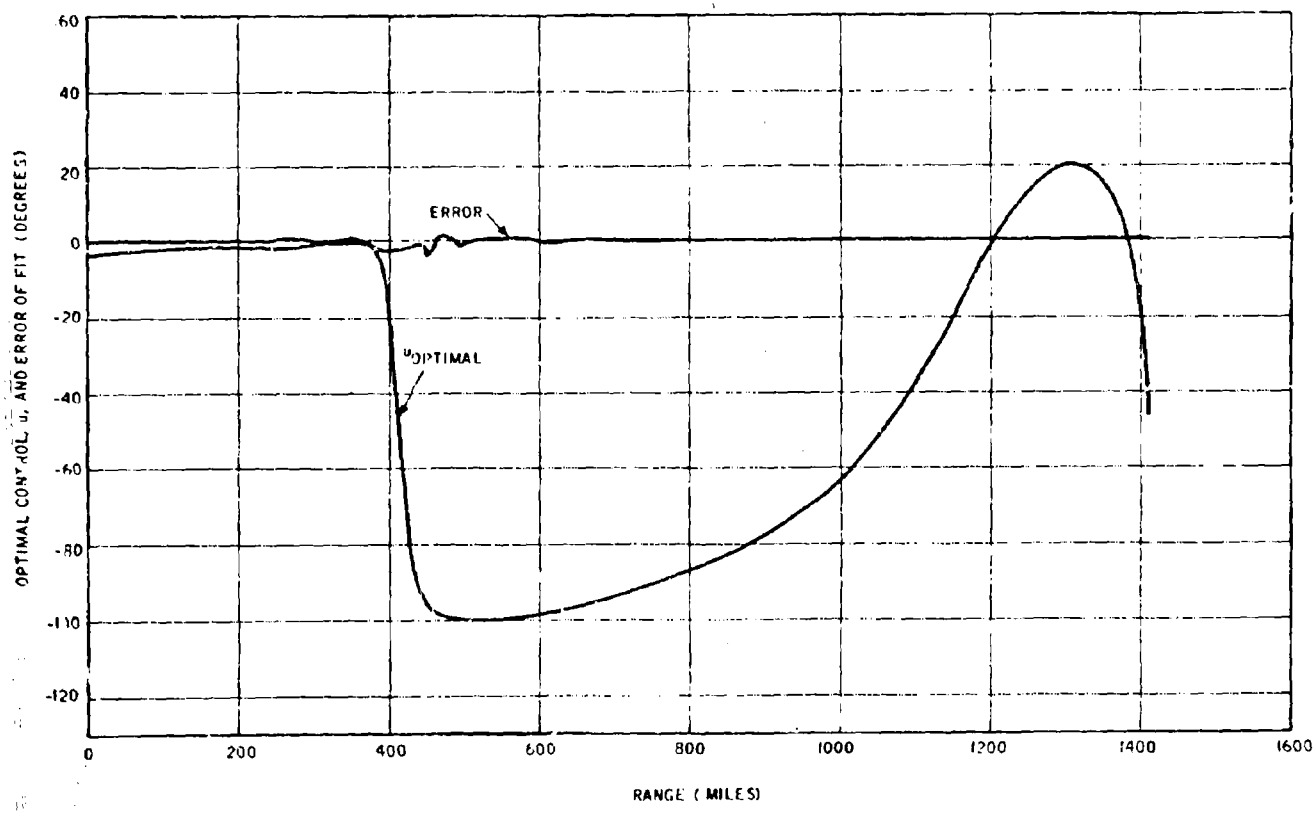

Figure 3-11. Optimal Control u and Error of Fit for Trajectory 11

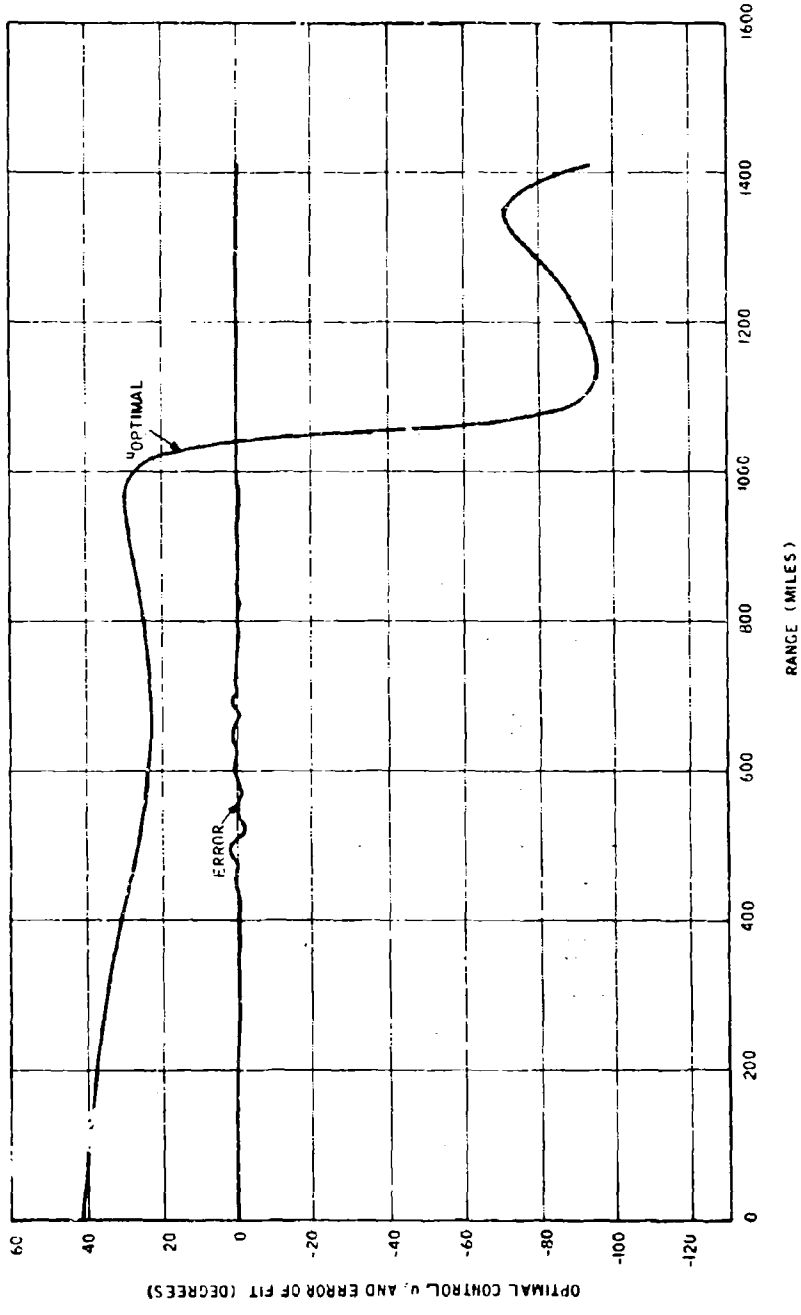

Figure 3-12. Optimal Control u and Error of Fit for Trajectory 12

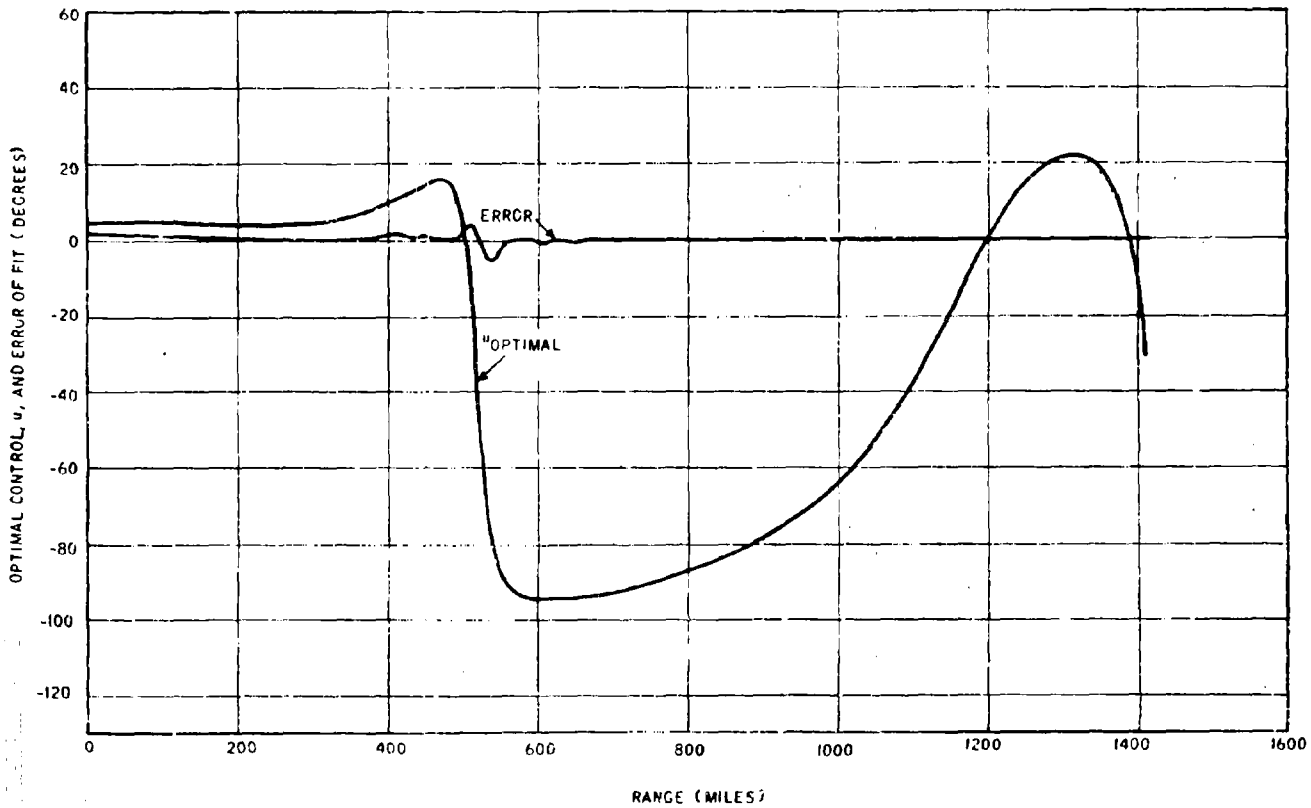

Figure 3-13. Optimal Control u and Error of Fit for Trajectory 13

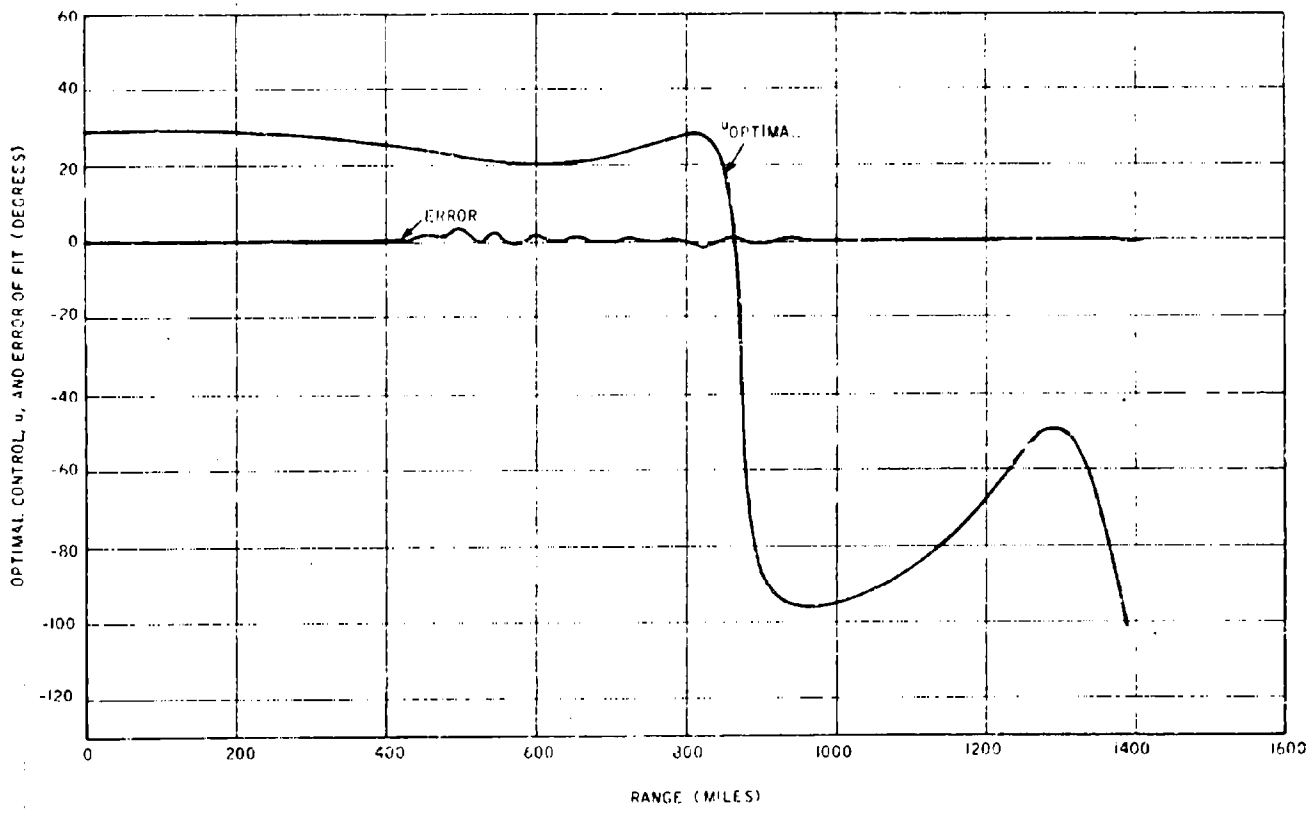

Figure 3-14. Optimal Control u and Error of Fit for Trajectory 14

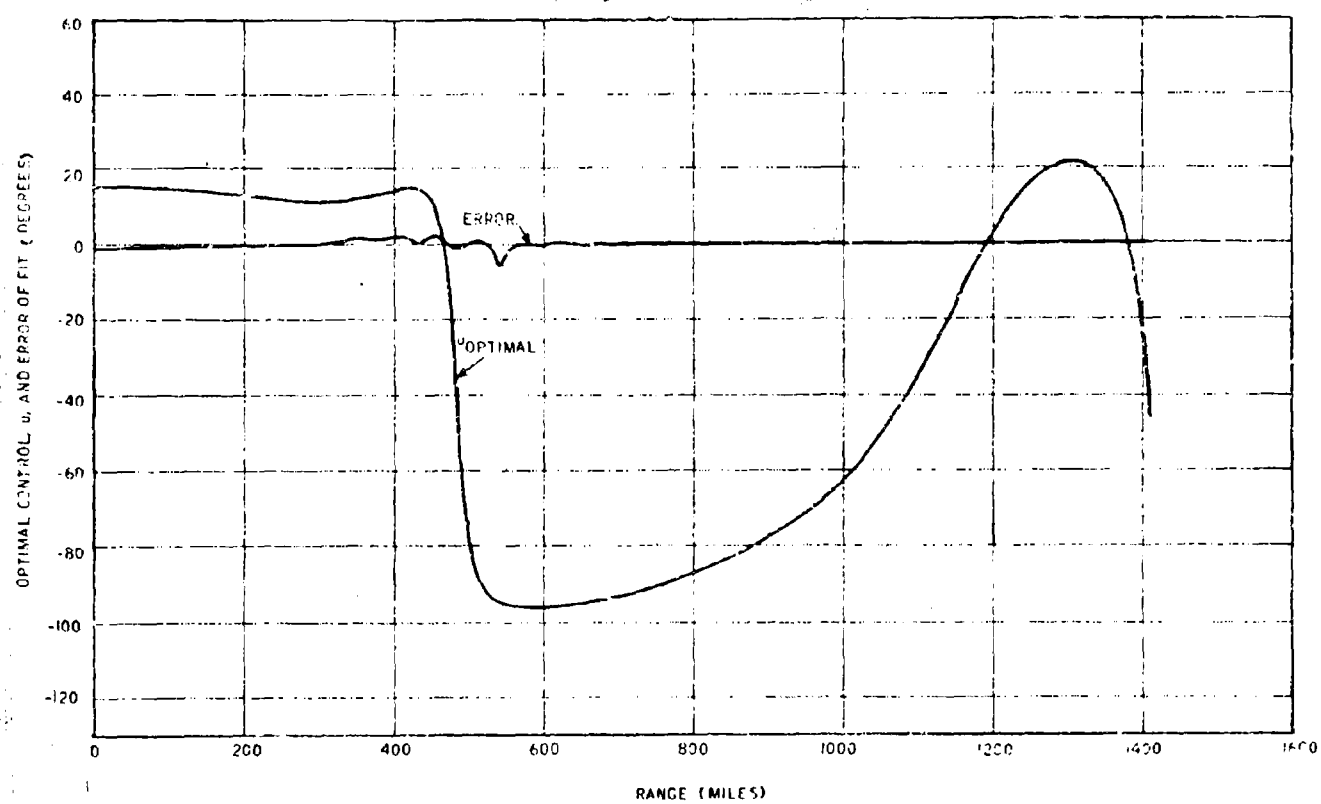

Figure 3-15. Optimal Control u and Error of Fit for Trajectory 15

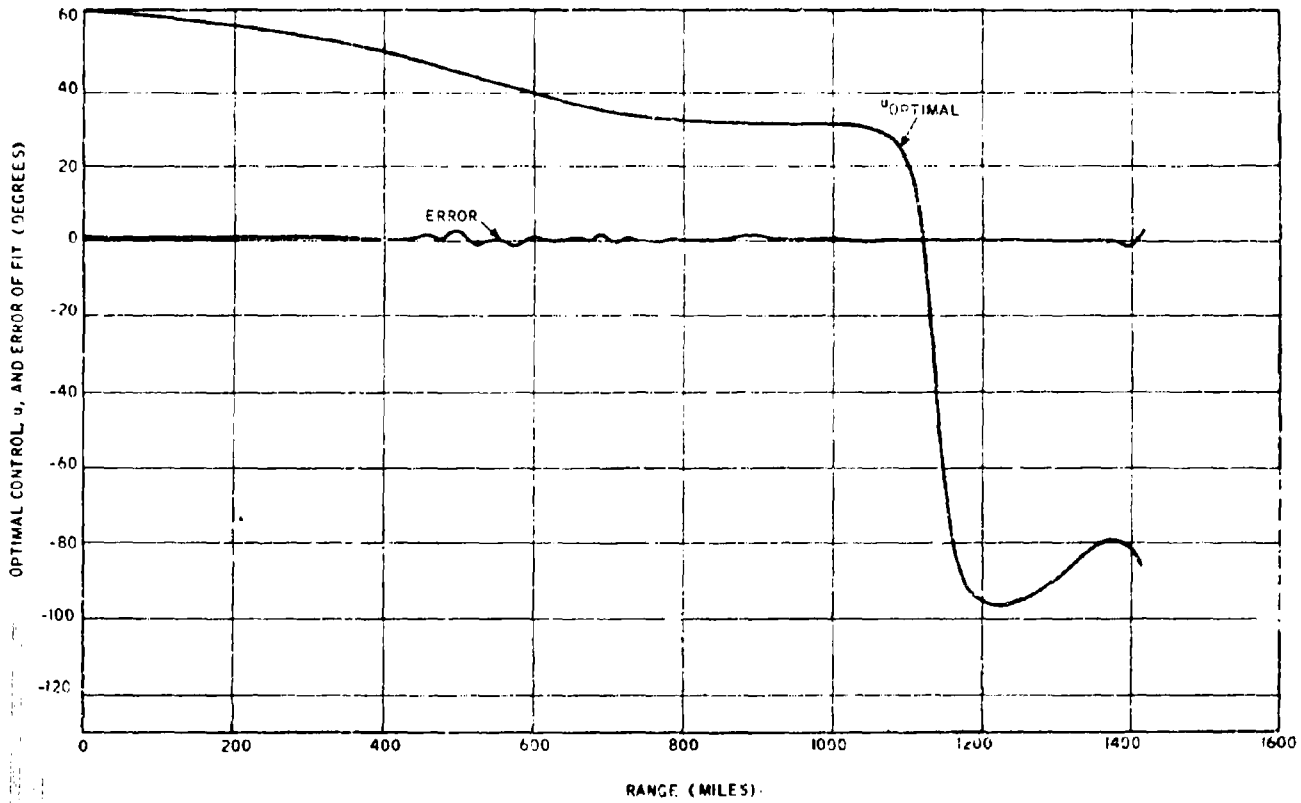

Figure 3-16. Optimal Control u and Error of Fit for Trajectory 16

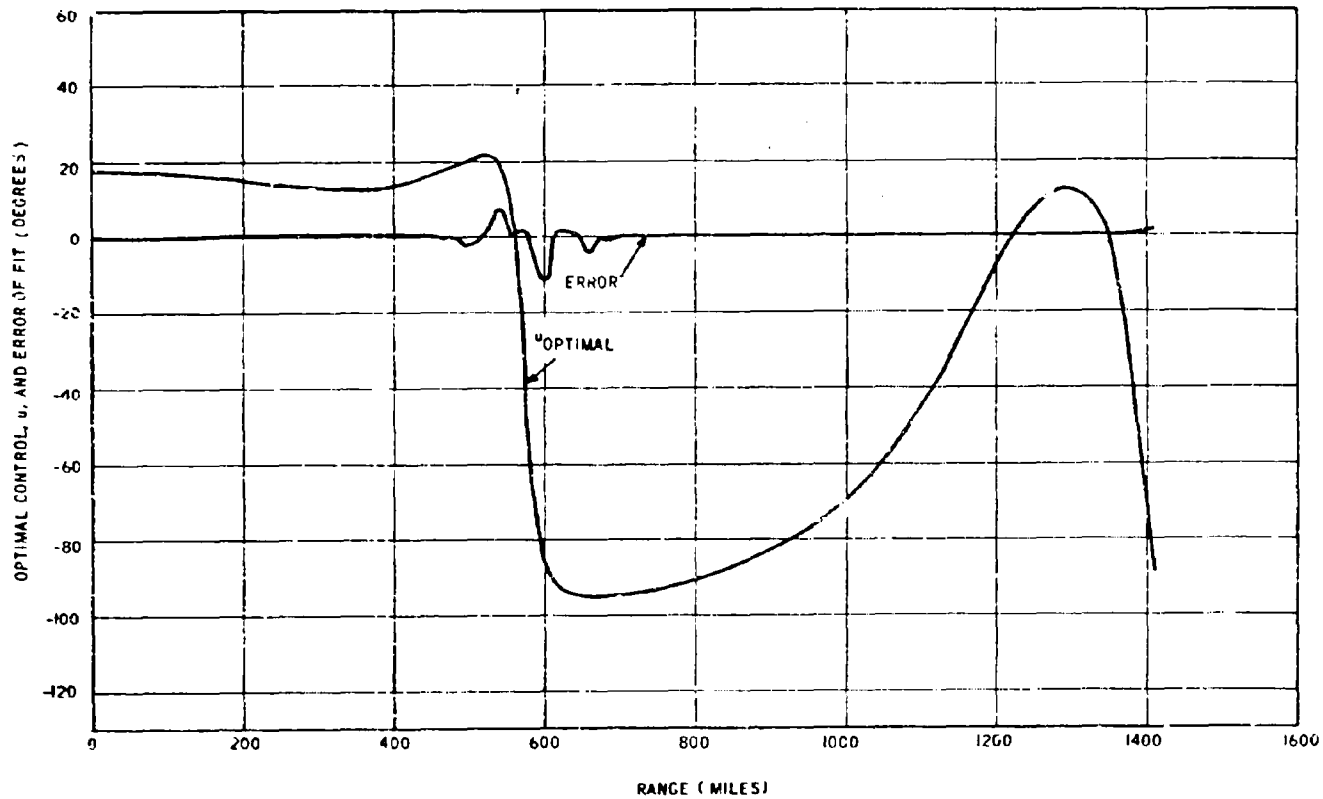

Figure 3-17. Optimal Control u and Error of Fit for Trajectory 17

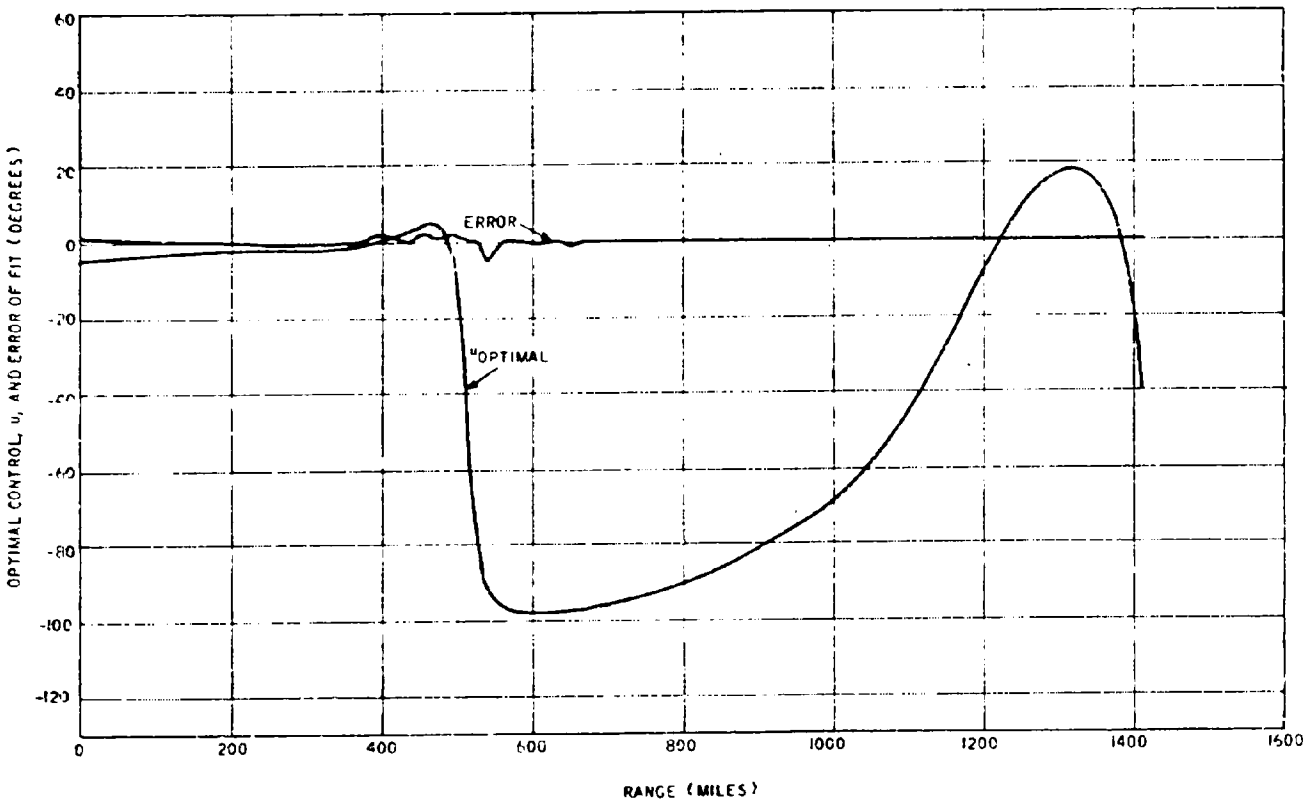

Figure 3-18. Optimal Control u and Error of Fit for Trajectory 18

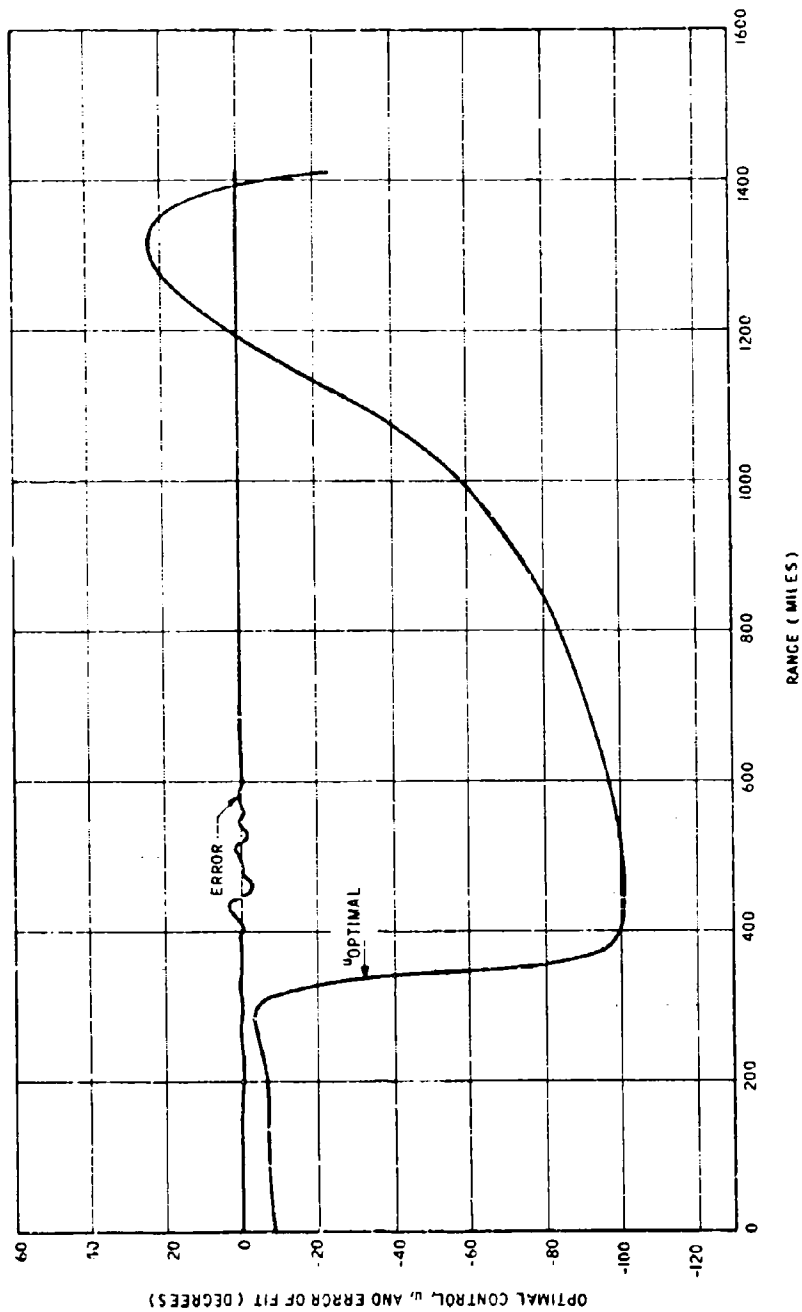

Figure 3-19. Optimal Control u and Error of Fit for Trajectory 19

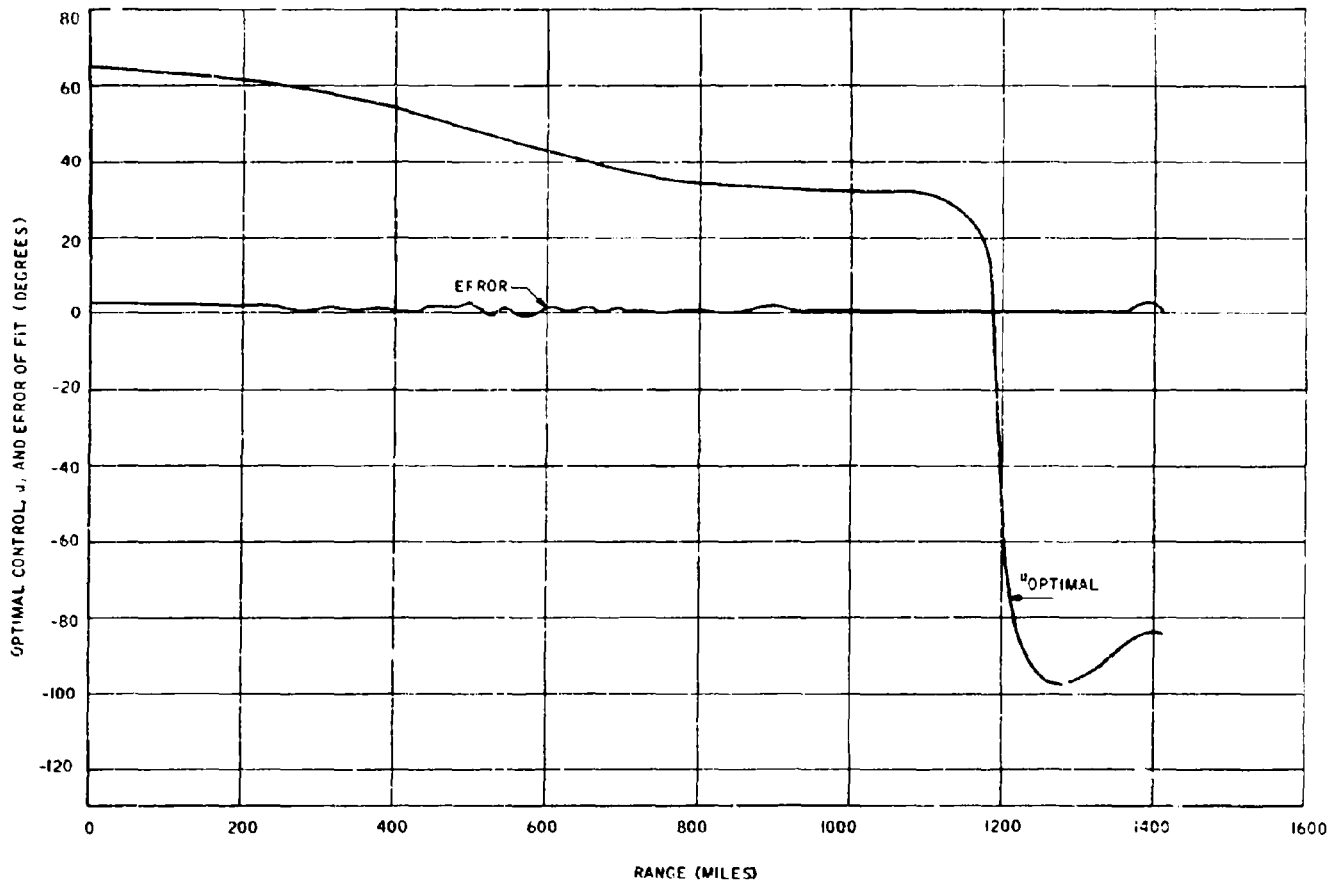

Figure 3-20. Optimal Control u and Error of Fit for Trajectory 20

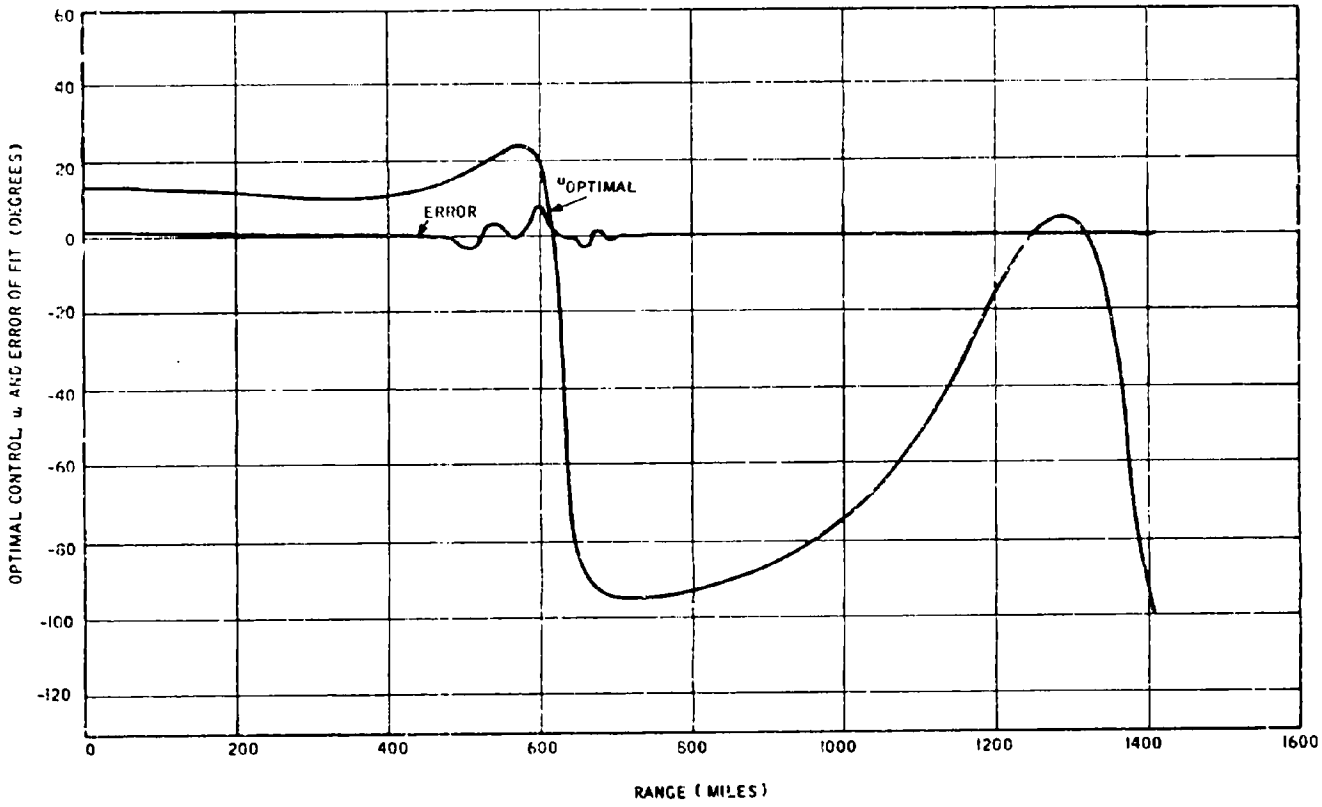

Figure 3-21. Optimal Control u and Error of Fit for Trajectory 21

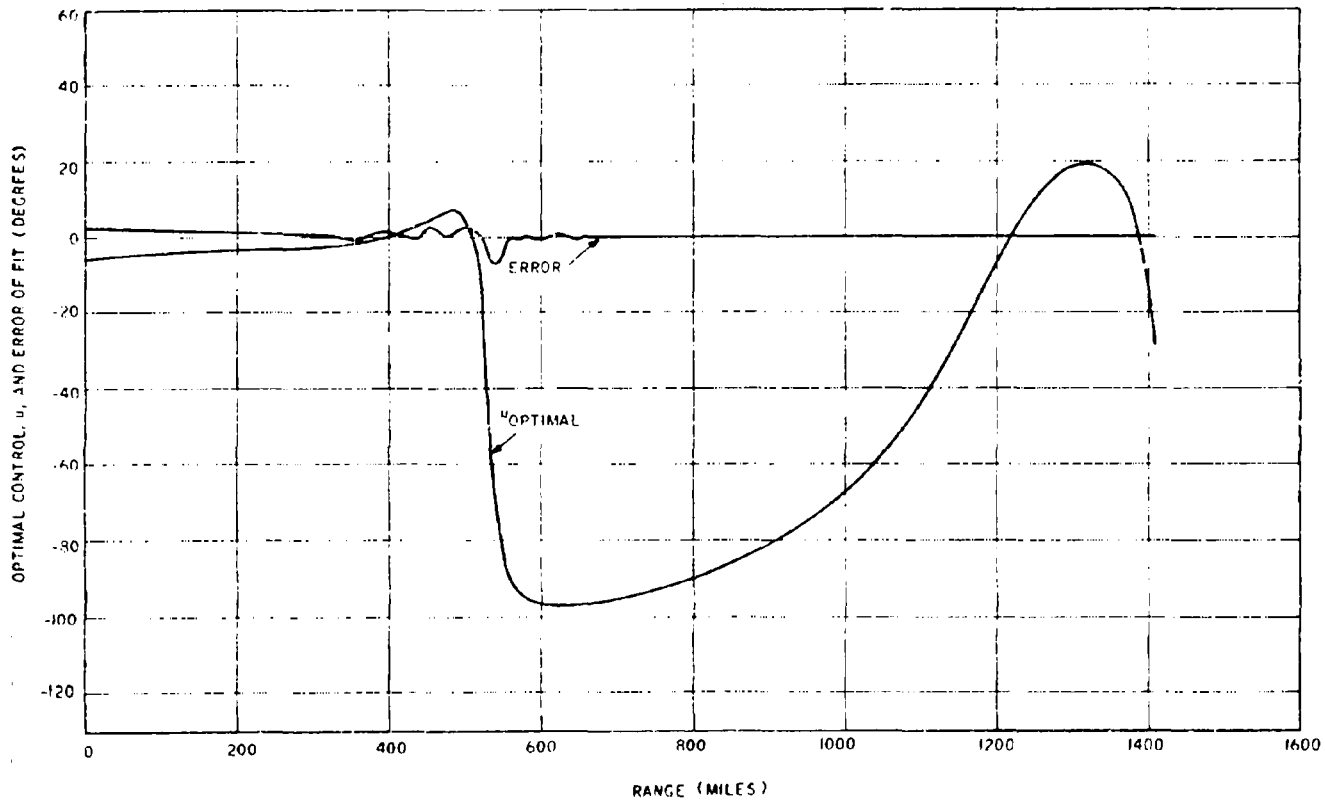

Figure 3-22. Optimal Control u and Error of Fit for Trajectory 22

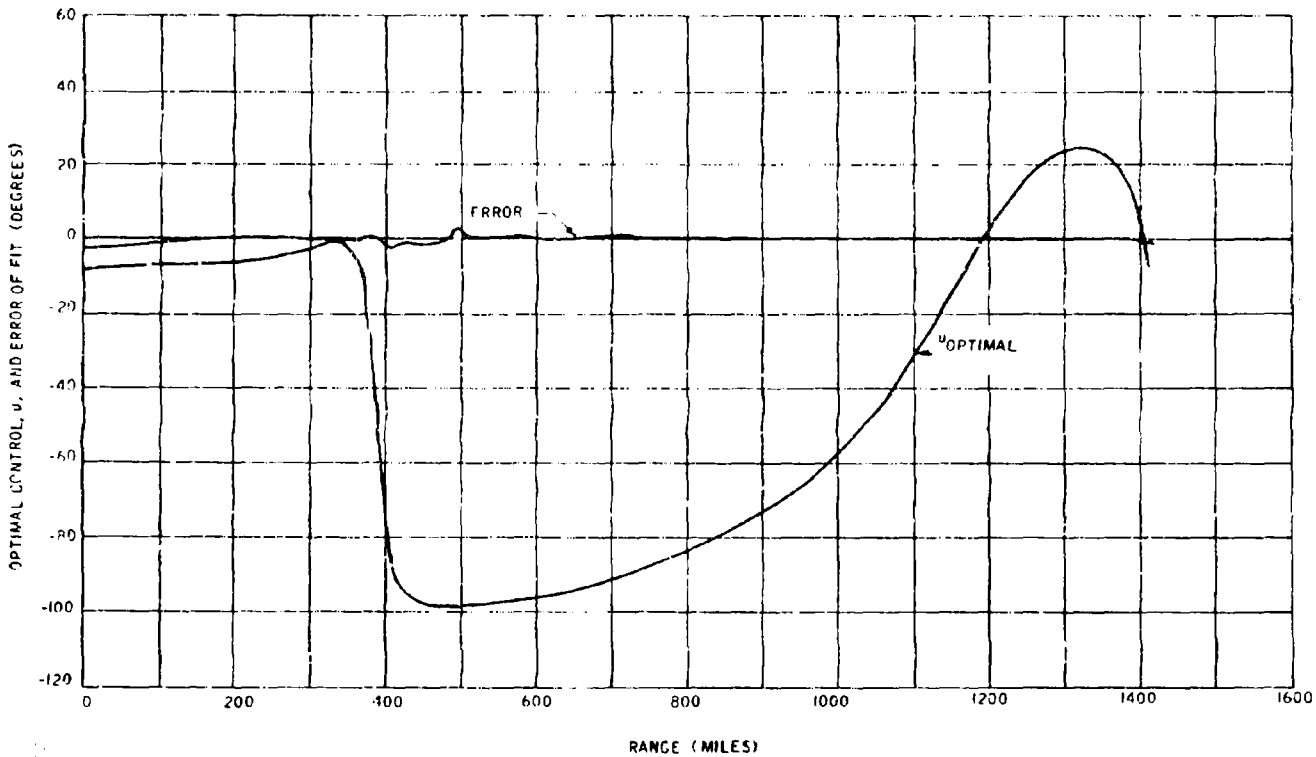

Figure 3-23. Optimal Control u and Error of Fit for Trajectory 23

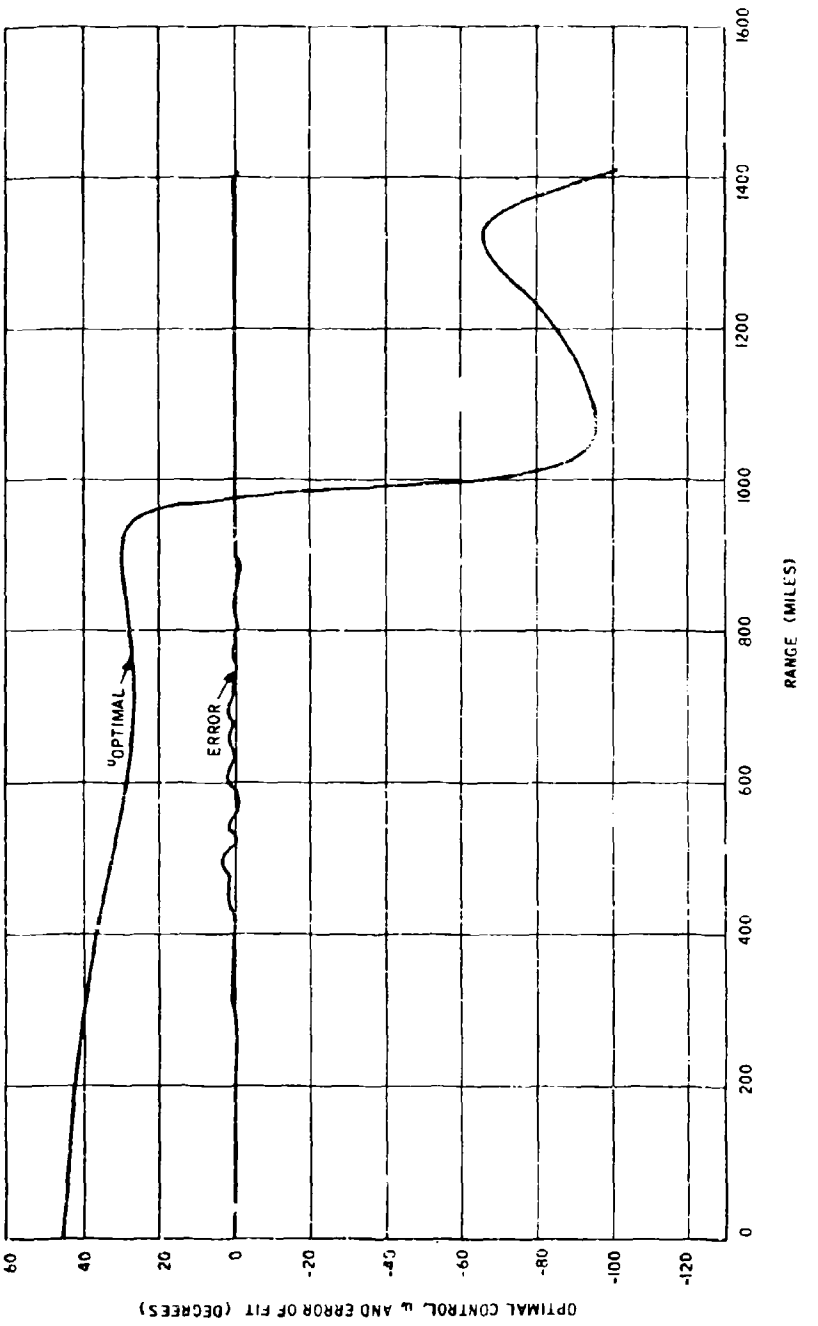

Figure 3-24. Optimal Control u and Error of Fit for Trajectory 24

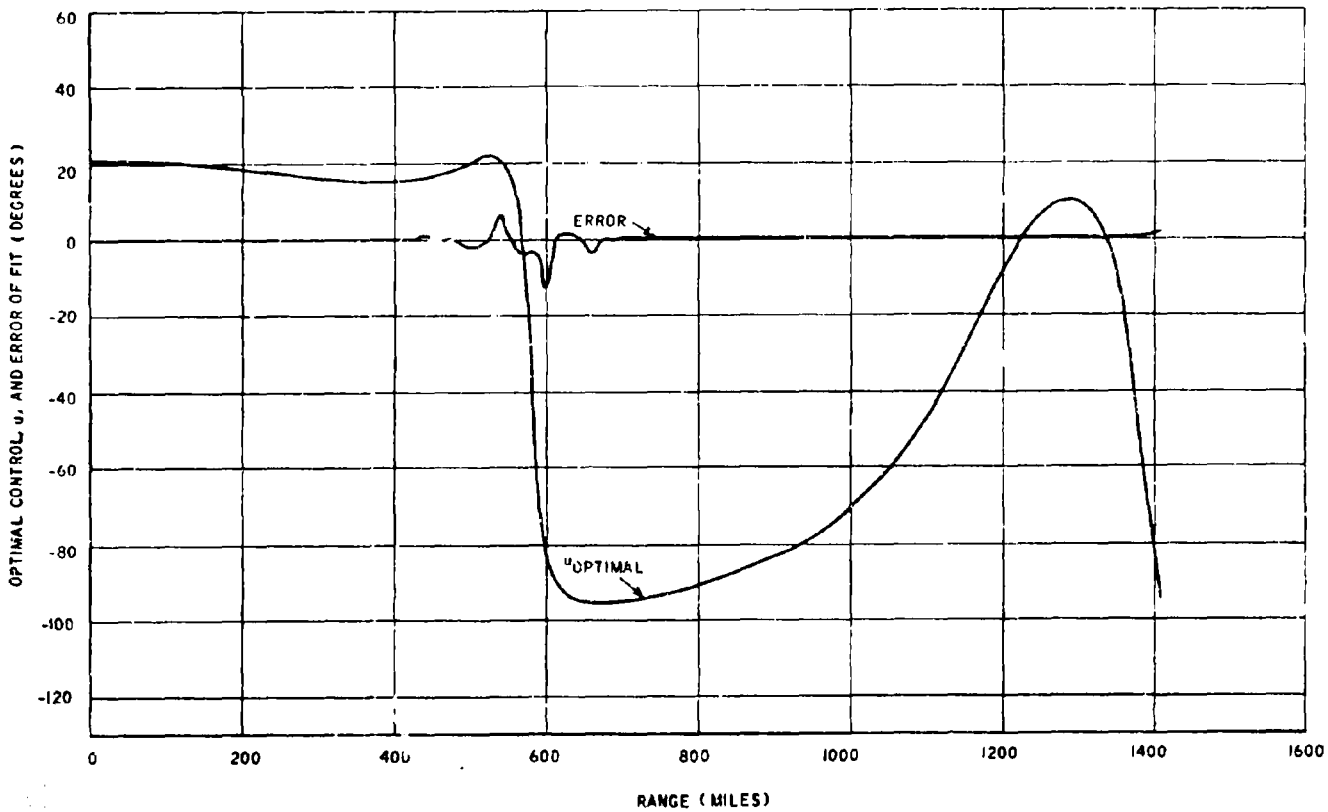

Figure 3-25. Optimal Control u and Error of Fit for Trajectory 25

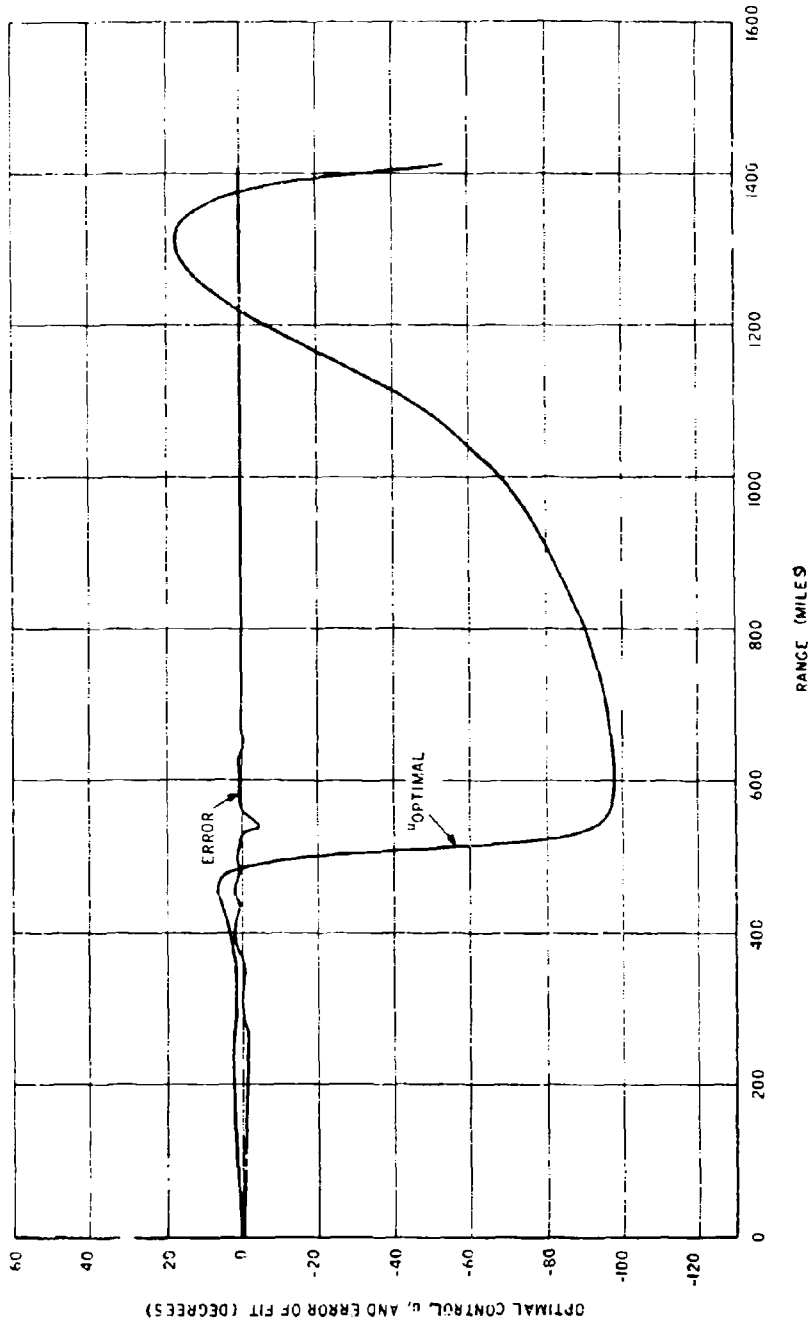

Figure 3-26. Optimal Control u and Error of Fit for Trajectory 26

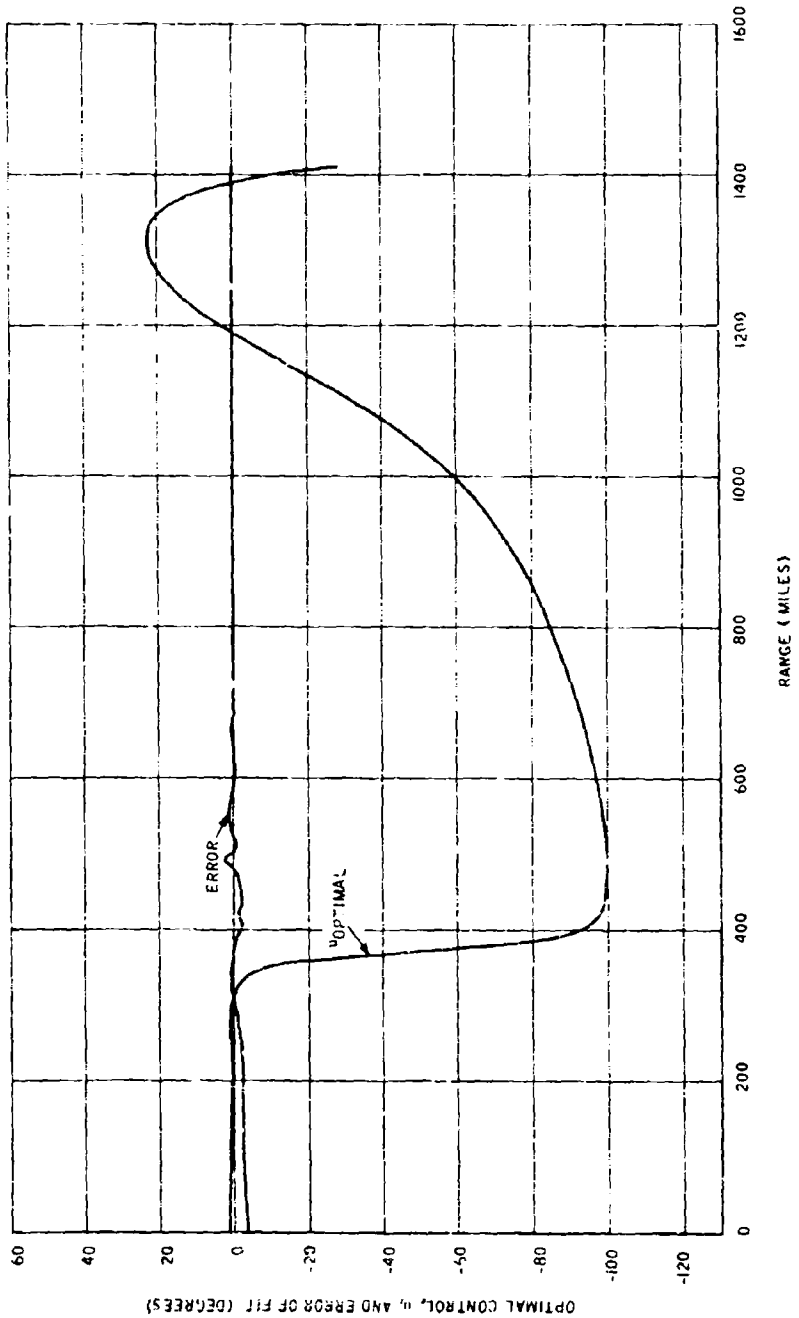

Figure 3-27. Optimal Control u and Error of Fit for Trajectory 27

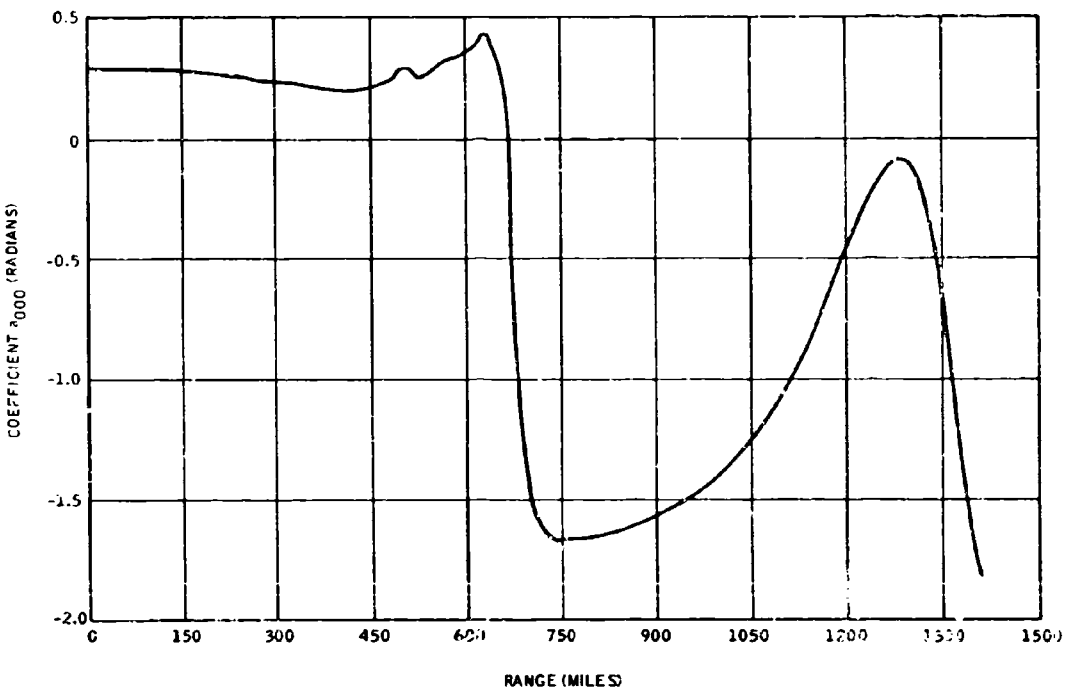

Figure 3-28. Coefficient a_{000} as a Function of Range

$$x_i^{(n+1)} = \frac{1}{2}\left[1 - \cos\left(i - \frac{1}{2}\right)\frac{\pi}{n+1}\right], \quad i = 1, \ldots, n+1 \tag{3.41}$$

Let $p_n^{(1)}(x)$ denote the Lagrange polynomial. If the function f(x) to be approximated is a polynomial of degree n+1, then $p_n^{(1)}(x)$ is the solution which satisfies the Chebyscheff criterion

$$\underset{[0 \le x \le 1]}{\text{Max}} \; | f(x) - p_n(x) | = \text{Min}. \tag{3.42}$$

In general, this is not true, so the method proceeds iteratively to the solution. Let $\epsilon(x)$ be the error

$$\epsilon(x) = f(x) - p_n(x) \tag{3.43}$$

which vanishes at n+1 points by construction. If the data is smooth enough, $\epsilon(x)$ will vanish exactly n+1 times, and there will be n+2 maximum errors (two at 0 and 1, and n relative maximum and minimums). The objective, on each iteration, is to equalize the n+2 absolute errors. Let $z_0, z_1, \ldots, z_{n+1}$ denote the points at which the maximum errors occur, and let $\eta(x)$ be a correction polynomial chosen to equalize the errors. Then

$$-\epsilon(z_0) + \eta(z_0) = \epsilon(z_1) - \eta(z_1) = \ldots = (-1)^n\left[\epsilon(z_{n+1}) - \eta(z_{n+1})\right]. \tag{3.44}$$

Let h be the common value in (3.44) so that

$$\begin{aligned}
\eta(z_0) &= h + \epsilon(z_0) \\
\eta(z_1) &= -h + \epsilon(z_1) \\
&\vdots \\
\eta(z_n) &= (-1)^n h + \epsilon(z_n) \\
\eta(z_{n+1}) &= (-1)^{n+1} h + \epsilon(z_{n+1}).
\end{aligned} \tag{3.45}$$

Equations (3.45) are n+2 equations in h and the n+1 coefficients of the n^{th} order polynomial $\eta(x)$. The approximating polynomial for the next iteration is taken as

$$p_n^{(2)}(x) = p_n^{(1)}(x) + \eta(x). \tag{3.46}$$

Iteration is required, since the location of the maximum errors, in general, shifts at each stage.

The method was found to work very well in practice. It rapidly converged to stationary points, z_i, i= 0, 1, . . . , n+1, and the selection of the same set of points z_i on two successive iterations was found to be a good stopping condition.

SECTION IV

MECHANIZATION AND SIMULATION OF THE NONLINEAR OPTIMAL FEEDBACK CONTROL SCHEME

A. SIMULATION DESCRIPTION

The mechanization of the scheme for the re-entry problem is illustrated in Figure 4-1. Detailed descriptions of each block in the diagram follow.

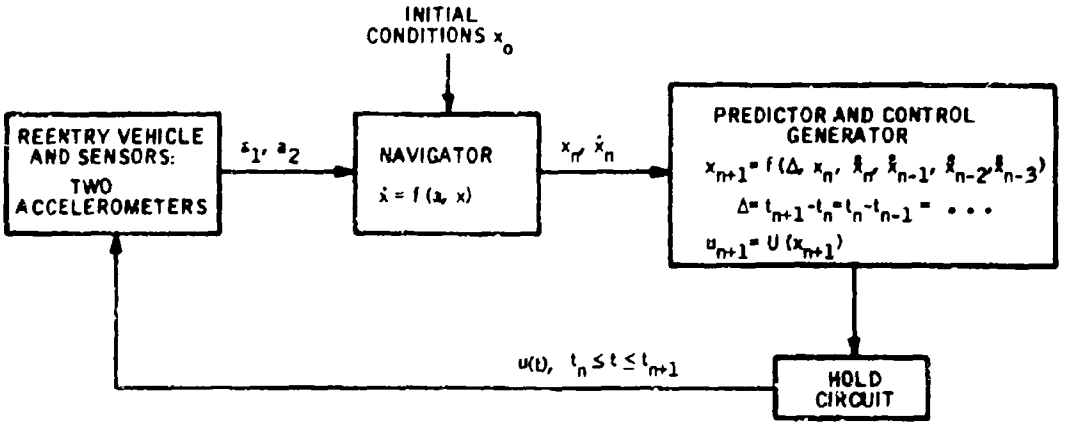

Figure 4-1. Nonlinear Optimal Feedback Control Scheme Mechanization for the Re-entry Application

1. Re-entry Vehicle and Sensors

In view of the short time of flight (15 minutes or less), accelerometers are the only sensors assumed to be aboard the vehicle. They measure the acceleration components (smoothed, if necessary) in the lift and drag directions,

$$a_1 = \frac{S\rho v^2}{2m} C_{L\alpha} \sin u$$

$$a_2 = -\frac{S\rho v^2}{2m}\left(C_{DO} + C_{DL} \cos u\right) . \qquad (4.1)$$

The constants $\frac{S}{2m}$, C_{LO}, C_{DO} and C_{DL} may be changed from their nominal values to evaluate the over-all performance of the scheme, and the density profile may assume one of several forms for the same purpose.

2. Navigator

The navigator integrates the differential equations of motion and supplies the state vector and its time derivative at discrete instants of time. In terms of accelerometer measurements, the equations of motion are

$$\begin{aligned}
\frac{dv}{dt} &= a_2 - \frac{g_o R^2 \sin\gamma}{(R+h)^2} \\
\frac{d\gamma}{dt} &= \frac{a_1}{v} + \frac{v\cos\gamma}{(R+h)} - \frac{g_o R^2 \cos\gamma}{v(R+h)^2} \\
\frac{dh}{dt} &= v\sin\gamma \\
\frac{dz}{dt} &= \frac{R\, v\cos\gamma}{c_3(R+h)} \quad .
\end{aligned} \tag{4.2}$$

The state vector components are velocity v, flight path angle γ, altitude h, and range z (measured in miles), and the state vector derivative is the right-hand side of (4.2). The total heat is also found, for scheme evaluation purposes, by integrating equation (2.2) along with system (4.2).

3. Predictor and Control Generator

The predictor equation is the Adams-Moulton equation

$$x_{n+1} = x_n + \frac{\Delta}{24}\left(55\dot{x}_n - 59\dot{x}_{n-1} + 37\dot{x}_{n-2} - 9\dot{x}_{n-3}\right) , \tag{4.3}$$

used to introduce lead into the system. Lack of time prevented experiments with other predictor equations, and Δ = 1/2 and 2 seconds were the only time increments considered.

Equation (4.3) requires three back derivatives as well as the present point, so it is not applicable for the first 6 seconds of flight. The first three back derivatives are generated from (4.2) with a constant control in Equations (4.1). The actual value of this control is unimportant since the vehicle is out of the sensible atmosphere during the first 6 seconds. However, it is taken as the control generator equation value at the initial point (which assumes $z_o = 0$) for continuity purposes. (Figure 2-28 shows that th control is almost constant during the initial phase of the flight.)

In Section III, 100 control function fits of the form

$$u = \sum_{i,j,k} a_{ijk} \left(V-V_N\right)^i \left(\gamma-\gamma_N\right)^j \left(h-h_N\right)^k \quad ; \quad \begin{matrix} i,j,k \geq 0 \\ i+j+k \leq m, \end{matrix} \qquad (4.4)$$

in which V_N, γ_N and h_N are "nominal" trajectory values, were found. The coefficients a_{ijk} were noted to be functions of range; however, they were not reduced to polynomial form due to lack of time.

The control generator interpolates linearly between fitted range points (spaced 15 miles apart) to determine the coefficients a_{ijk} at the predicted range point. Also, the nominal trajectory values are determined by the same process. The polynomial (4.4) is then evaluated with the predicted values of V, γ and h.

Of course, the control is constant for the first 6 seconds of flight. It is also evaluated differently for the last 30 miles. This is necessitated by the singular endpoint and the general compression of the state vector differences near the endpoint (see Figures 2-16 through 2-28). Hence, a linear interpolation for the control is performed with range as the variable. The two points used are the control at $z_{n+1} = 1470$, and $-\pi$ at $z = 1500$ miles. $z = 1500$ miles is the stopping condition for simulated trajectories.

4. Hold Circuit

The hold circuit supplies the constant control during the first 6 seconds, and the linear function of range during the last 30 miles of flight. In the intermediate region, it is taken as a cubic in time using the points $u_{n+1}, \ldots, u_{n-2}$ to evaluate the coefficients. The transformation

$$S = \frac{t - t_{n-2}}{\Delta} = 2 + \frac{(t - t_n)}{\Delta} \tag{4.5}$$

allows the cubic coefficients to be computed from

$$\begin{bmatrix} a_0 \\ a_1 \\ a_2 \\ a_3 \end{bmatrix} = \begin{bmatrix} 1 & 0 & 0 & 0 \\ -\frac{11}{6} & 3 & -1\frac{1}{2} & \frac{1}{3} \\ 1 & -2\frac{1}{2} & 2 & -\frac{1}{2} \\ -\frac{1}{6} & \frac{1}{2} & -\frac{1}{2} & \frac{1}{6} \end{bmatrix} \begin{bmatrix} u_{n-2} \\ u_{n-1} \\ u_n \\ u_{n+1} \end{bmatrix} . \tag{4.6}$$

B. SIMULATION RESULTS

Table 4-1 contains results of simulation runs for the 27 optimal trajectories. ΔJ is the difference between simulation and optimal trajectory total heat, and is seen to be a positive quantity; Δ is the time increment used in the Adams-Moulton predictor equation (4.3), and Δv and Δh are the terminal velocity and altitude errors from the optimal trajectory values of 1650 ft/sec and 75,000 feet respectively.

Table 4-1. Simulation Results for the 27 Optimal Trajectories of Table 2-2.

Trajectory Number	Total Heat Optimal Traj.	Total Heat Simulation	ΔJ (BTU/ft^2)	Δ (sec)	Δv (ft/sec)	Δh (ft)
1	28,872	28,898	26	2	226	- 8,655
2	31,888	31,913	25	2	59	- 8,565
3	26,252	26,270	18	2	234	- 8,537
4	29,278	29,295	17	2	218	- 8,982
5	28,666	28,721	55	2	298	- 5,804
6	29,032	29,051	19	2	227	- 8,898
7	28,757	28,810	53	2	217	-10,566
8	32,280	32,295	15	2	226	- 8,884
9	32,116	32,148	32	1/2	281	- 6,254
10	26,657	26,687	30	2	211	- 9,018
11*	25,792	25,844	52	2	- 49	-25,640
12	32,135	32,344	209	1/2	220	- 7,649
13	31,844	31,900	56	2	246	- 9,34[illegible]
14	26,362	26,382	20	2	225	- 8,952
15	26,128	26,173	45	2	244	- 9,520
16	29,963	Fail at z = 1056 miles				
17	29,017	Fail at z = 1431 miles				
18	28,510	28,562	52	2	243	- 9,603
19	28,817	Fail at z = 472 miles				
20	32,444	Fail at z = 1077 miles				
21	31,374	31,397	23	2	249	- 8,447
22	31,110	31,173	63	2	250	- 9,168
23	31,375	31,449	74	1/2	263	- 5,570
24	27,326	27,348	22	2	220	- 9,048
25	26,891	27,043	152	1/2	137	-12,201
26	26,216	26,266	50	2	253	- 8,930
27	26,368	26,417	49	1/2	- 43	-10,750

* Δz = -6 miles.

Most of the trajectories were simulated using Δ = 2 seconds. The advantage of making Δ as large as possible is that the onboard computer can be used for other tasks (such as computing display information) during the idle time. It was found that several trajectories failed with this increment (trajectories 9, 12, 16, 17, 19, 20, 23, 25 and 27), and a failure was recorded if the control for a given trajectory exceeded ±500 degrees. This was an adequate test, since if the control for a given trajectory exceeded ±180 degrees, it also exceeded ±500 degrees. Computations were also stopped if the altitude fell below 50,000 feet. This happened with trajectory 11, which stopped with a range error Δz = -6 miles, as shown in Table 4-1.

With Δ = 1/2 sec., only trajectories 16, 17, 19 and 20 failed. This time trajectory 11 stopped with a range error Δz = -0.1 mile, as indicated in Table 4-2. Trajectory 1 was also run and only small improvement in terminal conditions resulted (Table 4-2).

A simulation program with no prediction (Δ = 0) was constructed to test the ultimate capabilities of the control function polynomial approximation. (The polynomial is evaluated at each integration step, and the system is assumed to react instantaneously.) This was run for trajectories 1, 9 and 11 with the results shown in Table 4-2. There was no change in terminal conditions for trajectory 1 (compared with the Δ = 1/2 second case), and only slight changes for trajectory 9. Path 11 reached the stopping condition (z = 1500 miles) even through the final altitude was less than 50,000 feet. Trajectories 16, 17, 19 and 20 failed again when run with this program.

Table 4-2. Additional Simulation Results

Trajectory Number	Total Heat Optimal Traj.	Total Heat Simulation	ΔJ (BTU/ft^2)	Δ (sec)	Δv (ft/sec)	Δh (ft)
1	28,872	28,897	25	1/2	226	- 8,655
:	28,872	28,897	25	0	226	- 8,655
9	32,116	32,147	31	0	281	- 6,279
11*	25,792	25,842	50	1/2	-171	-25,107
11	25,792	25,842	50	0	-170	-25,043
28	29,589	Fail at z = 1044 miles				
29	29,011	29,048	37	2	223	- 8,579
30	28,496	28,551	55	2	253	- 9,026
31	28,687	28,720	33	1/2	263	- 8,081

* Δz = -0.1 mile

Four additional trajectories, numbered 28-31 in Table 4-2, were run to test the nonlinear optimal feedback control scheme for off-design trajectories. The initial conditions for these are given in Table 4-3, and they correspond to the initial conditions of trajectories 20-27 with $\Delta x_{10} = 0$. Trajectories 29 and 30 ran with $\Delta = 2$ seconds, whereas $\Delta = 1/2$ second was required for path 31. Trajectory 28 fails, even with $\Delta = 0$.

Table 4-3. Initial Conditions for Trajectories 28-31

Trajectory Number	Initial Velocity (ft/sec)	Initial Flight Path Angle (degrees)	Initial Altitude (ft)	Sign of Change From Trajectory		
				Δx_{10}	Δx_{20}	Δx_{30}
28	35,000	-5.40	430,000	0	+	+
29	35,000	-5.40	370,000	0	+	-
30	35,000	-7.35	430,000	0	-	+
31	35,000	-7.35	370,000	0	-	-

Path 28 may be compared with paths 20 and 24 to see the effects of initial velocity changes, since Δx_{20} and Δx_{30} are the same. Numbers 20 ($+\Delta x_{10}$) and 28 ($\Delta x_{10} = 0$) fail, whereas path 24 ($-\Delta x_{10}$) is successful with $\Delta = 2$ seconds. Similar comparisons are shown in Table 4-4.

Table 4-4. Effects of Initial Velocity Change on Δ

Trajectory Number	Sign of			Δ
	Δx_{10}	Δx_{20}	Δx_{30}	
21	+	+	-	2
29	0	+	-	2
25	-	+	-	1/2
22	+	-	+	2
30	0	-	+	2
26	-	-	+	2
23	+	-	-	1/2
31	0	-	-	1/2
27	-	-	-	1/2

The characteristics of the successful flights are illustrated in Figures 4-2 through 4-5. Only those for trajectory 1 are displayed, since most of the flights are fairly similar. The first dip into the atmosphere is quite critical, and the inaccuracies in the control function (Figure 3-1) drastically affect the remainder of the path. The vehicle emerges into the skip region (where the control function fit is very accurate) following a new optimal path. This is pursued through the second dip to a point (about 1410 miles) where the control fit again becomes somewhat inaccurate. Inaccuracies from this point onward do not affect total heat very much, but do contribute to terminal velocity and altitude errors. Another sources of these errors is the linear fit of the control in the last 30 miles of flight. The control is still rising at 1470 miles (Figure 2-28) and the additional lift available to the optimal trajectory is neglected in the simulation. This causes the vehicle to dive more steeply and (in general) to lose less velocity as the endpoint is approached. The terminal errors should be reduced by starting the linear interpolation closer to the endpoint; however, no experiments of this nature were performed.

It is understandable that trajectory 16 failed. This path was difficult to obtain during the mapping process, indicating that it was near the edge of the corridor, and consequently, that the control fit is near the edge of the region of applicability. Control function inaccuracies could easily move the vehicle into a region where the control function fit is no longer applicable. A comparison of optimal and simulated trajectories shows that the vehicle is quite far from the optimal at the point of failure (Δv = -450 ft/sec, Δh = 7,000 feet).

The large inaccuracies in the control function of trajectory 17 (Figure 3-17) occur in the vicinity of the first dip into the atmosphere (the bottom is at z = 600 miles). They cause the skip to be quite different from that of the optimal trajectory. The effect, however, is not noticed until near the end of the trajectory, since the accurate control fit produces a reasonable control for the intermediate portion of the flight. The vehicle eventually leaves the region of applicability for the control function polynomial.

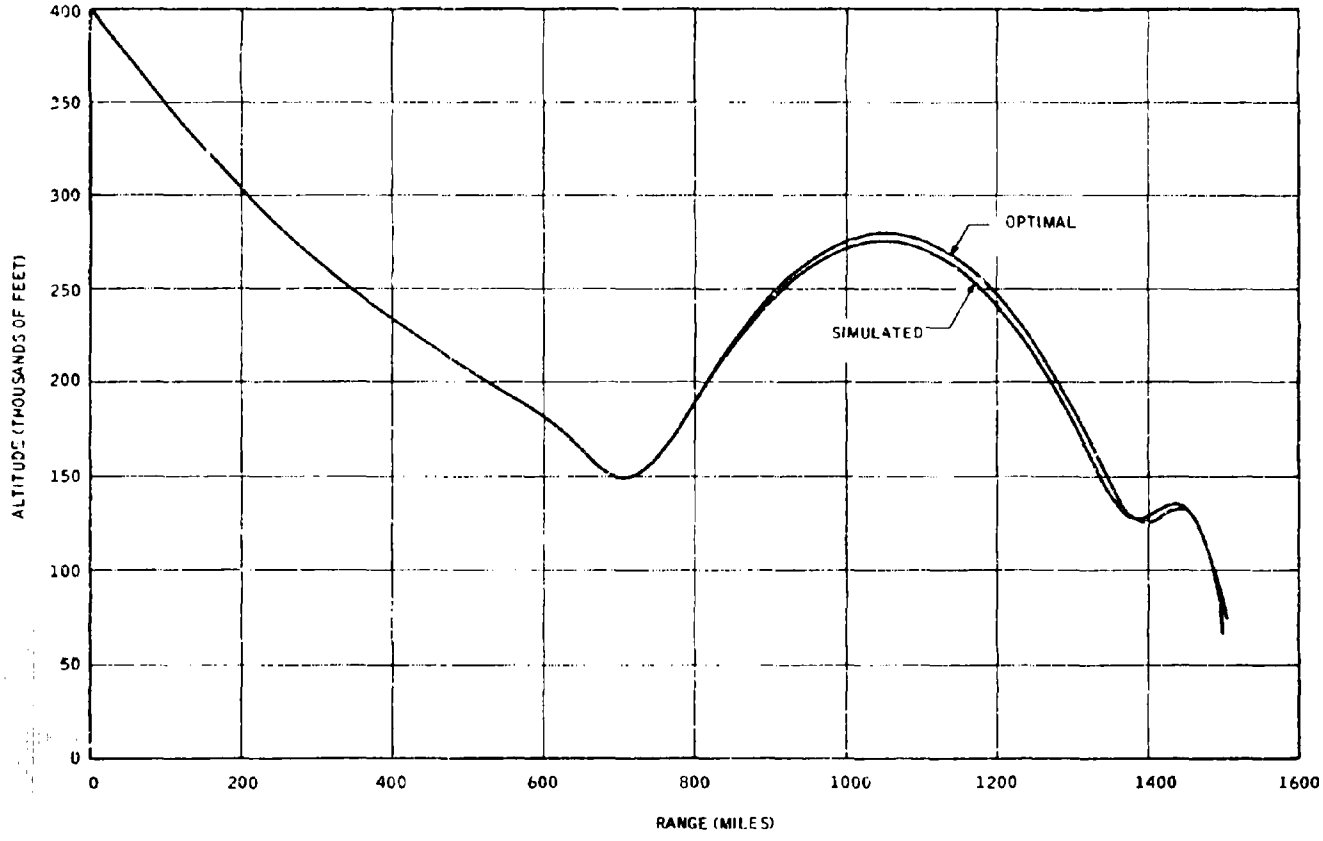

Figure 4-2. Simulation Results for Trajectory 1 - Altitude Versus Range

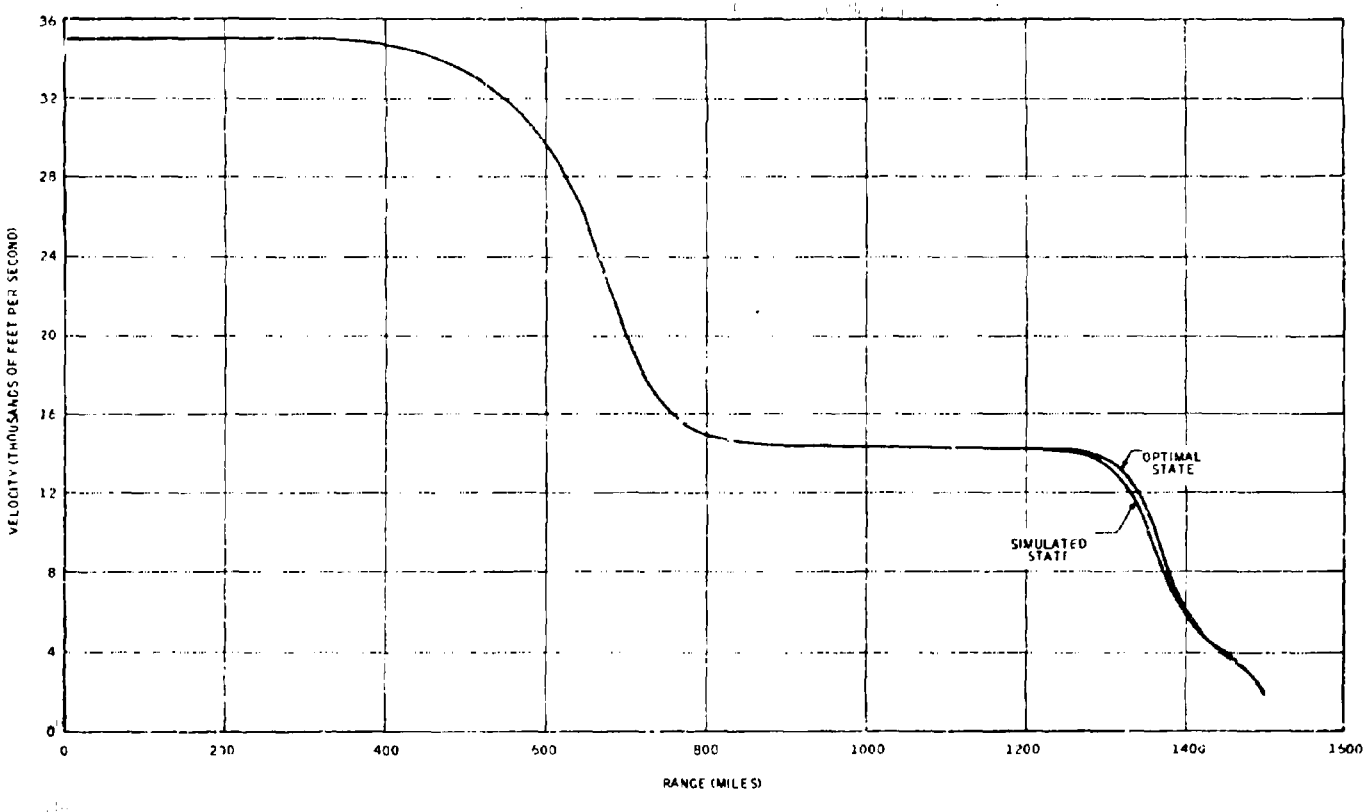

Figure 4-3. Simulation Results for Trajectory 1 - Velocity Versus Range

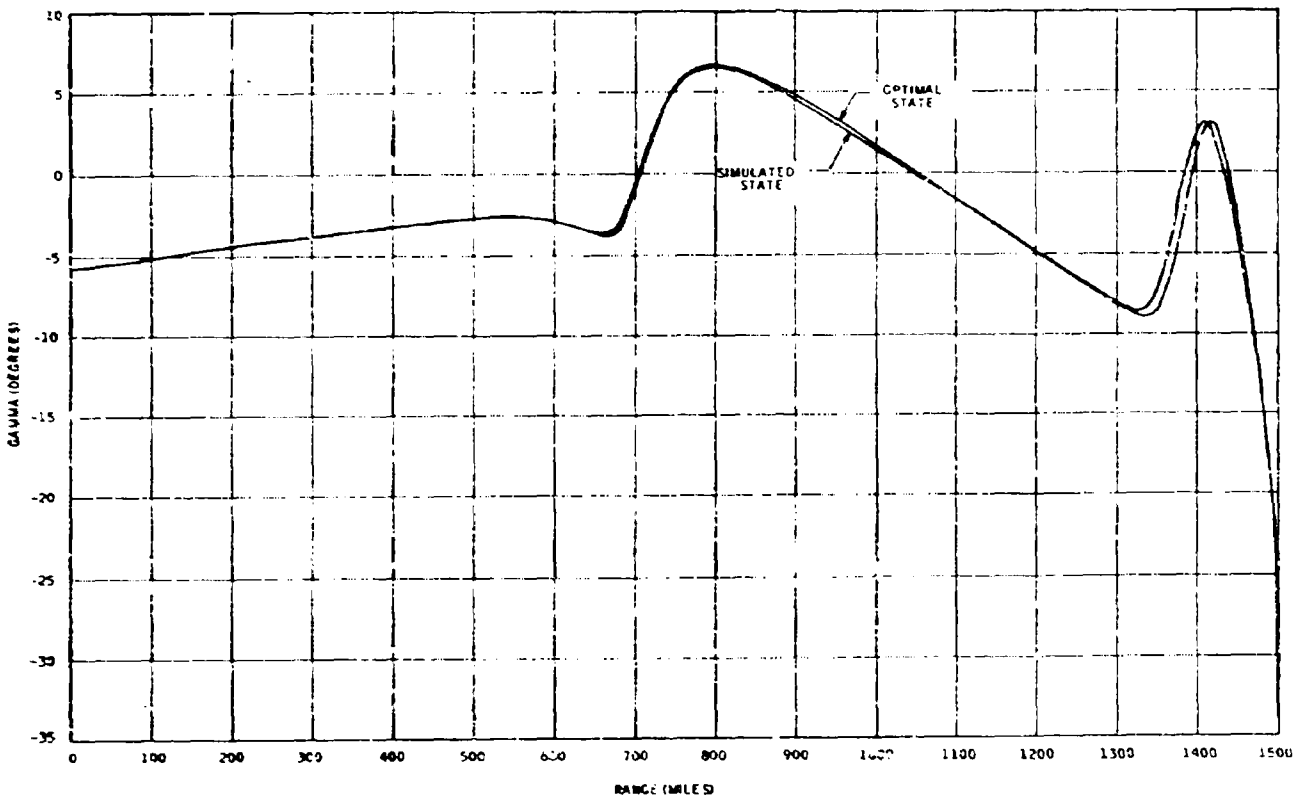

Figure 4-4. Simulation Results for Trajectory 1 - Flight Path Angle Versus Range

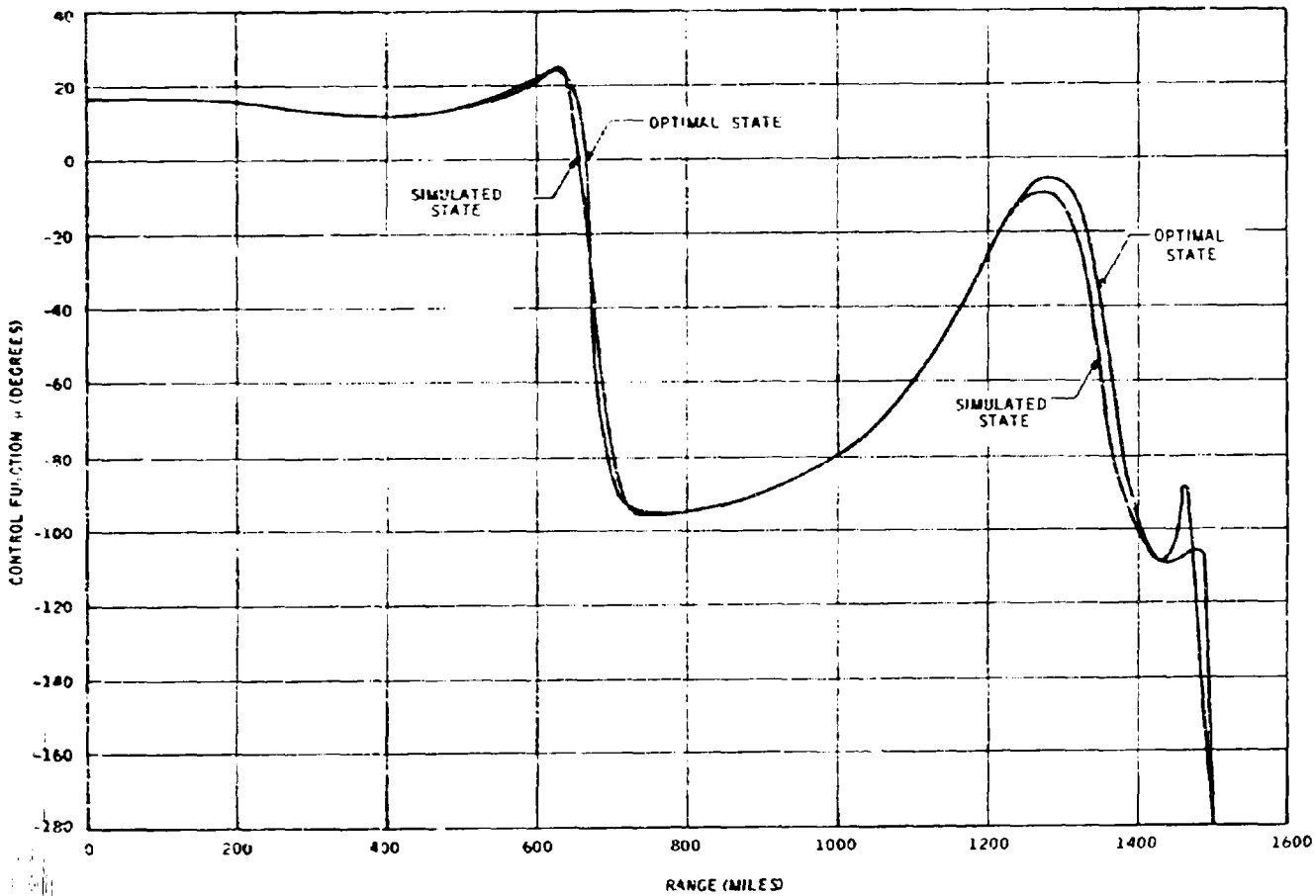

Figure 4-5. Simulation Results for Trajectory 1 - Control Versus Range

The initial conditions for trajectory 19 cause the vehicle to dive deeper into the atmosphere which in turn produces greater lift and drag forces. The vehicle follows the optimal path through the bottom of the dip (at z = 375 miles). However, the control inaccuracy bulge in the region z = 400 miles to z = 450 miles (Figure 3-19) causes the vehicle to be captured by the atmosphere, instead of following the skip of the optimal path. This shows the sensitivity of the paths to the control function errors near the bottom of the first dip.

The flights of trajectories 20 and 28 are similar to that of path 16, and they show that simultaneous positive perturbations in initial flight path angle and altitude are not tolerated by the control function fit.

The conclusions drawn from the simulation results are:

- In its present form, the nonlinear optimal feedback control scheme produces reasonable re-entry trajectories with modest increases in total heat from the optimal values, for a suitably restricted region of initial conditions.
- The inaccuracy of the control function fit over the first dip into the atmosphere drastically affects the remainder of the flight. The accuracy of the fit should be made better here to eliminate the failures, and to consequently decrease the total heat.
- It is believed that the terminal point errors can be reduced by starting the linear interpolation for the control as a function of range closer to the endpoint.
- The time interval Δ, used in the predictor equation, was found to be a function of the simulated trajectory; Δ should be made a variable quantity, dependent upon the state of the vehicle.

SECTION V
CONCLUSIONS AND RECOMMENDATIONS

A. ACCOMPLISHMENTS

A re-entry optimization problem is presented and solved through the methods developed in Reference 1. These produce an accurate solution to the optimization problem. A powerful predictor scheme was developed, which supplements the work of Reference 1 and which allows the optimal solutions to be changed as a function of a parameter. This was used to extend the range of the original optimal trajectory, and to perform an "absolute minimum" test. The latter showed that the optimal path is a minimizing path, at least over a large region of solution space. Sufficiency tests for a relative minimum were also developed. It was shown that the trajectories considered are relative minimums.

The predictor scheme was used to map the re-entry corridor, and 27 optimal trajectories spanning the corridor were obtained. The control functions for these trajectories, and partials of the control with respect to the state vector, were used to obtain a polynomial approximation for the control function over the optimal re-entry corridor. The approximation was used in the mechanization of a nonlinear optimal feedback control scheme. Simulation results showed that modest increases in total heat over optimal values were experienced, and that large (although tolerable) terminal errors resulted. It is believed that the terminal condition errors can be greatly reduced, if necessary. A few of the trajectories failed, which, in effect, limits the region of applicable initial re-entry conditions to some extent.

Another re-entry optimization problem, in which the sensed acceleration is constrained to be less than or equal to a given number of g's, was posed, and several optimization methods were used in an attempt to obtain a 10-g optimal path. The methods all failed, although the predictor scheme emerged as the

most powerful of the group. A singular point on the constrained subarc prevents convergence to the solution. A means of circumventing this problem was found but remains to be tested.

The optimization methods were also extended to include the bounded-state coordinate problem.

B. RECOMMENDATIONS

The nonlinear optimal feedback control scheme in its present form produces near optimal re-entry trajectories if the space of initial conditions is suitably restricted. The scheme is technically sound but fails in some instances only because of control function errors.

The polynomial approximation is based upon control values for several optimal trajectories, and the paths are readily generated through use of the predictor scheme. It is possible to generate many more paths than were used in the study, and consequently, to fill out the optimal re-entry corridor with optimal values of the control function. The increased number of data points should enable better control function approximations to be made.

The data processing task is that of reducing the data points to a form readily implemented in the control scheme. Polynomial approximations are probably best for this purpose; however, there are many ways of approaching the fitting problem. It may be that surface fits of the partial derivatives are well behaved over a large region of the corridor, so that fits of these, followed by an integration, may produce more accurate control function approximations. On the other hand, it may be necessary to segment the corridor into several pieces, and to perform surface fits for each of these to obtain the required accuracy. Also, it may be possible to split the over-all fit into several low-dimensional subfits, so that each stage of the fitting process may be carefully controlled.

The data processing task is seen to be in an incomplete state at the present time. Since many practical optimal feedback control problems could be implemented if this task were accomplished in a practical way, it is recommended that:

- Practical methods should be sought for performing the data processing task.

The control function polynomial approximation is presently based upon unconstrained optimal trajectories. However, many real optimization problems necessarily contain constraints upon the control and state vectors. It is recommended that:

- Mechanization problems associated with inequality constraints should be examined.

In view of the rising importance of adaptive control capabilities, the methods should be extended to this case. Theoretically there is no problem, although practically, the dimensionality of the surface fit is increased. Thus:

- Problems associated with extending the methods to include adaptive control capabilities should be examined.

Finally, most feedback control schemes which operate over a finite time interval contain a singular point at the endpoint. This is true for the problem studied in the report. The singular point causes difficulties in the vicinity of the endpoint, and usually results in terminal point errors. Thus:

- The singular terminal point problem should be examined theoretically to determine if the endpoint errors can be minimized.

MATERIALS SECTION (TABLE LXXV)

No work of the nature described in Section 2 of Table LXXV was performed under Contract AF33(615)-1858, BPS Number 4(6399-62405364-822501).

APPENDIX A
A PREDICTOR SCHEME

Suppose that one has an n-dimensional system of equations of the form

$$\psi(x, b) = 0 \tag{A. 1}$$

in which x is an n-dimensional vector and b is a single parameter. Assume further that the matrix $\frac{\partial \psi}{\partial x}$ exists and is non-singular over the range of b considered, and that the vector $\frac{\partial \psi}{\partial b}$ also exists. Then by the implicit function theorem it follows that

$$x = x(b), \tag{A. 2}$$

and

$$\frac{dx}{db} = - \left|\frac{\partial \psi}{\partial x}\right|^{-1} \frac{\partial \psi}{\partial b} \tag{A. 3}$$

If m solutions (A. 2) to the system (A. 1) are known for equally spaced values of the parameter b, and if the corresponding derivatives are computed from (A. 3) (call the complete system $x_1, \ldots, x_m$, and $x_1', \ldots, x_m'$ respectively), the problem is that of predicting the next member of the family of solutions, x_{m+1}.

Open type integration formulas are well suited for this task, and many such formulas are given in Chapter 6 of Reference 2. In particular, a formula truncated after third differences (the Adams-Moulton predictor equation) is

$$x_{m+1} = x_m + \frac{h}{24} (55\, x_m' - 59\, x_{m-1}' + 37\, x_{m-2}' - 9 x_{m-3}'), \tag{A. 4}$$

where h is the spacing between parameter values. Notice that the present point and derivative, and three previous derivatives are required for this equation. Other formulas using less back information are easily derived from the results given in Reference 2. The simplest such equation, using only the present point and derivative, is the Newton-Raphson equation,

$$x_{m+1} = x_m + hx'_m. \tag{A.5}$$

As an example of the use of the predictor scheme, consider the range extension problem of Section IIB. The equations corresponding to (A.1) are

$$\begin{aligned} &V(T, P_o) - X_1 = 0 \\ &\xi(T, P_o) - X_2/R = 0 \\ &\zeta(T, P_o) - X_3 = 0 \\ &P_2(T, P_o) = 0 \\ &H(P_o) = 0 . \end{aligned} \tag{A.6}$$

The parameter b is identified with the terminal range X_3, so Equations (A.3) become

$$\begin{bmatrix} T' \\ P'_{10} \\ P'_{20} \\ P'_{30} \\ P'_{40} \end{bmatrix} = \begin{bmatrix} \dot{V}(T) & \eta_{11}(T) & \eta_{12}(T) & \eta_{13}(T) & \eta_{14}(T) \\ \dot{\xi}(T) & \eta_{31}(T) & \eta_{32}(T) & \eta_{33}(T) & \eta_{34}(T) \\ \dot{\zeta}(T) & \eta_{41}(T) & \eta_{42}(T) & \eta_{43}(T) & \eta_{44}(T) \\ \dot{P}_2(T) & \zeta_{21}(T) & \zeta_{22}(T) & \zeta_{23}(T) & \zeta_{24}(T) \\ 0 & f_1(0) & f_2(0) & f_3(0) & f_4(0) \end{bmatrix}^{-1} \begin{bmatrix} 0 \\ 0 \\ 1 \\ 0 \\ 0 \end{bmatrix}. \tag{A.7}$$

It is seen that the third column of the inverse Newton-Raphson matrix contains the derivatives for the predictor equation when the solutions (T, P_o) satisfy system (A. 6) (for a given value of the parameter X_3).

APPENDIX B
THREE OPTIMIZATION TECHNIQUES

In addition to the modified Newton-Raphson method and the predictor scheme, three other optimization techniques were considered during the period devoted to optimal trajectory computations. They include the optimal Newton-Raphson scheme, the Fletcher-Powell method (Reference 3) and Marquardt's scheme (Reference 4).

As a common basis for discussion, let the system of equations to be solved by the optimization schemes be

$$\psi(x) = 0, \tag{B. 1}$$

where both ψ and x are n-dimensional vectors. Multiply this system by a diagonal weighting matrix W to obtain

$$\phi(x) = W\psi(x) = 0. \tag{B. 2}$$

W clearly does not change the solution, but does aid in the numerical computations. Define a function

$$f(x) = \phi'(x)\phi(x), \tag{B. 3}$$

whose absolute minimum value (zero) corresponds to the solution of (B. 1) or (B. 2), and let g(x) be the gradient vector,

$$g(x) = 2 \left[\frac{\partial \phi(x)}{\partial x}\right]' \phi(x). \tag{B. 4}$$

Both the optimal Newton-Raphson and Fletcher-Powell methods require that a minimum value for f be found in a direction s. Let

$$x = x_o + \lambda s \tag{B.5}$$

where x_o is the present point and λ is a parameter, and determine a point

$$x_1 = x_o + K\eta s, \quad 0 < K \leq 1, \tag{B.6}$$

where

$$\eta = \text{minimum of} \left\{ 1, \frac{-2f(x_o)}{g'(x_o)s} \right\} . \tag{B.7}$$

Equation (B.7) was found in the appendix of Reference 3, where W.C. Davidon (Reference 5) is given credit for its origin. The factor K in Equation (B.6) was found necessary for the re-entry problem since Equation (B.7), in some instances, produced too large an estimate for η. If $f(x_o)$ $g(x_o)$, $f(x_1)$ and $g(x_1)$, are known numerically, then the function f(x) may be approximated by the cubic equation

$$f(x_o + \lambda s) = a_o + a_1 \lambda + a_2\lambda^2 + a_3\lambda^3. \tag{B.8}$$

Values for the coefficients are found to be

$$\begin{aligned} a_o &= f(x_o) \\ a_1 &= g'(x_o)s \\ a_2 &= -\frac{1}{K\eta}[Z+g'(x_o)s] \\ a_3 &= \frac{1}{3(K\eta)^2}[2Z + g'(x_o)s+g'(x_1)s] \\ Z &= \frac{3}{K\eta}\left[f(x_o) - f(x_1)\right]+ g'(x_o)s+g'(x_1)s \end{aligned} \tag{B.9}$$

When Equation (B. 8) is differentiated and evaluated for the minimizing value $\lambda = \alpha$, it is found that

$$\alpha = \frac{1}{3a_3} \left[-a_2 + \sqrt{a_2^2 - 3a_1 a_3} \right], \tag{B. 10}$$

so the approximate minimum value of f in the direction s is given by $f(x_o + \alpha s)$.

The direction s in the optimal Newton-Raphson method is given by the Newton-Raphson change

$$S_N = -\left[\frac{\partial \phi(x_o)}{\partial x}\right]^{-1} \phi(x_o). \tag{B. 11}$$

When K and η are both unity in (B. 6) and (B. 7), x_1 is the Newton-Raphson predicted point, so the method becomes straight Newton-Raphson as the solution is approached.

The Fletcher-Powell direction is

$$S_F = -H(x_o)\, g(x_o), \tag{B. 12}$$

where $H(x_o)$ is a positive-definite matrix to be updated after each step (Reference 3 suggests the identity matrix as a suitable initial choice). When α,

$$x_2 = x_o + \alpha S_F, \tag{B. 13}$$

$f(x_2)$ and $g(x_2)$ have been evaluated, the updating equations for the next step are

$$H(x_2) = H(x_o) + A + B$$

$$A = \frac{\sigma\sigma'}{\sigma' y}$$

$$B = - \frac{(H(x_o)y)(H(x_o)y)'}{y' H(x_o)y} \qquad \text{(B. 14)}$$

$$\sigma = \alpha S_F$$

$$y = g(x_2) - g(x_o).$$

In Marquardt's scheme it is assumed that a linearized expansion adequately describes the surface behavior in a suitably small sphere of radius δ_o about x_o. Thus, Equation (B. 2) may be written

$$\phi(x_o + \delta) = \phi(x_o) + \frac{\partial\phi(x_o)}{\partial x}\delta, \qquad \text{(B. 15)}$$

where the change δ is to satisfy the constraint

$$\delta'\delta - \delta_o^2 = 0. \qquad \text{(B. 16)}$$

The function (B. 3), using approximation (B. 15), is minimized subject to the constraint (B. 16) by setting the partials of

$$F(\delta, \lambda) = f(x_o + \delta) + \lambda(\delta'\delta - \delta_o^2) \qquad \text{(B. 17)}$$

to zero. Upon performing the operations it turns out that

$$\left[\left(\frac{\partial\phi(x_o)}{\partial x}\right)'\left(\frac{\partial\phi(x_o)}{\partial x}\right) + \lambda I\right]\delta = \frac{-g(x_o)}{2}. \qquad \text{(B. 18)}$$

In practice, $\lambda \geq 0$ is a parameter. When $\lambda = 0$, it follows from (B. 4) and (B. 11) that δ is the Newton-Raphson change. On the other hand, if λ is large, δ approaches a gradient change. The policy is to make λ as small as possible during iterations.

APPENDIX C
THE TRANSFORMED OPTIMIZATION PROBLEM

The system of differential equations for the re-entry problem are

$$\dot{q} = \frac{c}{\sqrt{N}} \rho^{1/2} v^3 + 7.5 N \left(\frac{\rho}{\rho_o} \right)^{3/2} \left(\frac{v}{10,000} \right)^{12.5} \tag{C.1}$$

$$\dot{v} = \frac{-S}{2m} \rho v^2 C_D(u) - \frac{g_o \sin \gamma}{(1+\xi)^2}$$

$$\dot{\gamma} = \frac{S}{2m} \rho v C_L(u) + \frac{v \cos \gamma}{R(1+\xi)} - \frac{g_o \cos \gamma}{v(1+\xi)^2} \tag{C.2}$$

$$\dot{\xi} = \frac{v}{R} \sin \gamma$$

$$\frac{d\zeta}{dt} = \frac{v}{(1+\xi)} \cos \gamma \, .$$

The transformation

$$z = \frac{\zeta}{c_3}, \quad c_3 = 5,280 \, , \tag{C.3}$$

changes the units of range from feet to miles, and transforms the last of (C.2) to

$$\frac{dz}{dt} = \frac{1}{c_3} \frac{d\zeta}{dt} = \frac{v}{c_3(1+\xi)} \cos \gamma \tag{C.4}$$

Now z is a monotonic increasing function of t, so z may be used as independent variable in place of t. Using the transformation

$$\frac{d}{dz} = \frac{dt}{dz}\frac{d}{dt} \tag{C.5}$$

and (C. 4) on (C. 1) and the first three of (C. 2), one finds

$$\frac{dq}{dz} = \frac{c_3 c}{\sqrt{N}} \frac{(1+\xi)\rho^{1/2} v^2}{\cos\gamma} + 7.5 \times 10^{-4} N \frac{(1+\xi)}{\cos\gamma}\left(\frac{\rho}{\rho_o}\right)^{3/2}\left(\frac{v}{10,000}\right)^{11.5}$$

$$\frac{dv}{dz} = -\frac{c_3 S}{2m} \frac{(1+\xi)\rho v C_D(\omega)}{\cos\gamma} - \frac{c_3 g_o \tan\gamma}{v(1+\xi)} \tag{C.6}$$

$$\frac{d\gamma}{dz} = \frac{c_3 S}{2m} \frac{(1+\xi)\rho}{\cos\gamma} C_L(\omega) + \frac{c_3}{R} - \frac{c_3 g_o}{v^2(1+\xi)}$$

$$\frac{d\xi}{dz} = \frac{c_3}{R}(1+\xi)\tan\gamma .$$

Now let

$$V = v^2 \tag{C.7}$$

and note that

$$\frac{dV}{dz} = 2v\frac{dv}{dt} \qquad \text{(C. 8)}$$

Also, transform altitude to units of feet through

$$h = R\xi \qquad \text{(C. 9)}$$

Then Equations (C. 6) become

$$\frac{dq}{dz} = \frac{c_3 c}{R\sqrt{N}} \frac{(R+h)\rho^{1/2}V}{\cos\gamma} + \frac{7.5 \times 10^{-4} c_3 N}{R} \frac{(R+h)}{\cos\gamma} \left(\frac{\rho}{\rho_o}\right)^{3/2} \left(\frac{V}{10^8}\right)^{23/4}$$

$$\frac{dV}{dz} = \frac{-c_3 S}{mR} \frac{(R+h)\rho V}{\cos\gamma} C_D(u) - 2c_3 g_o R \frac{\tan\gamma}{(R+h)} \qquad \text{(C. 10)}$$

$$\frac{d\gamma}{dz} = \frac{c_3 S}{2mR} \frac{(R+h)\rho}{\cos\gamma} C_L(u) + \frac{c_3}{R} - \frac{c_3 g_o R}{V(R+h)}$$

$$\frac{dh}{dz} = \frac{c_3}{R}(R+h)\tan\gamma$$

$$\frac{dt}{dz} = \frac{c_3}{R} \frac{(R+h)}{V^{1/2}\cos\gamma} .$$

The Hamiltonians for the system (C. 1) and (C. 2), and the system (C. 10) are, respectively,

$$H = f_o + p'f \tag{C.11}$$

and

$$H_2 = g_o + P'g. \tag{C.12}$$

Each Hamiltonian represents a canonical system of equations, so a canonical transformation may be used, in part, to transform one system into the other. A second transformation is required for the change of independent variable.

The generating function F_2 (q, P, t) of Reference 6, page 240, represents a canonical transformation between old and new state vectors (q, Q) and multipliers (p, P). The transformed equations satisfy

$$p = \frac{\partial F_2}{\partial q} \tag{C.13}$$

$$Q = \frac{\partial F_2}{\partial P}$$

$$K = H + \frac{\partial F_2}{\partial t}.$$

Let

$$F_2 = \lambda_1 v^2 + \lambda_2 \gamma + \lambda_3 R\xi + \lambda_4 \frac{\zeta}{c_3}. \tag{C14}$$

Then in the transformed system,

$$\begin{aligned} V &= v^2 \\ \gamma &= \gamma \\ h &= R\xi \\ z &= \frac{\zeta}{c_3} \end{aligned} \qquad \text{(C. 15)}$$

and

$$\begin{aligned} \lambda_1 &= \frac{p_1}{2v} \\ \lambda_2 &= p_2 \\ \lambda_3 &= \frac{p_3}{R} \\ \lambda_4 &= c_3 p_4 \, . \end{aligned} \qquad \text{(C. 16)}$$

The first, third and fourth of (C. 15) are respectively, the transformations (C. 7), (C. 9) and (C. 3), and the second represents the identity transformation on γ. The corresponding multipliers are given by (C. 16), and the new Hamiltonian K (the same form as the old) is evaluated in terms of the new variables.

The transformation for the change of independent variable is based upon the proof of Bliss' theorem 74. 2, page 205 of Reference 7. Let f_o, f be the right-hand sides of the differential equations in the variables (V, γ, h, z) = x and u. The generalized Lagrangian associated with this system is

$$F = f_o + \lambda' (f - \dot{x}) \qquad \text{(C. 17)}$$

where λ is the multiplier vector (C. 16), and the first variation of the function

$$J = \int_0^T F \, dt \tag{C. 18}$$

is to be taken. Let the independent variable of (C. 18) be changed from t to $x_4 = z$. This may be done since range is an increasing function of time. Then (C. 18) becomes

$$J = \int_0^{z_f} F \left(\lambda, x, \frac{\frac{dx}{dz}}{\frac{dt}{dz}}, \quad u = \frac{\frac{dx_5}{dz}}{\frac{dt}{dz}} \right) \frac{dt}{dz} \, dz \tag{C. 19}$$

where u is taken as the time derivative of a fifth state coordinate. The generalized Lagrangian for (C. 19) is

$$F^1 = \left[f_o + \sum_{i=1}^{3} \lambda_i \left(f_i - \frac{\frac{dx_i}{dz}}{\frac{dt}{dz}} \right) + \lambda_4 \left(f_4 - \frac{1}{\frac{dt}{dz}} \right) \right] \frac{dt}{dz} . \tag{C. 20}$$

In the following, the derivative subscripts represent partials with respect to the derivatives. One may readily verify the relationships

$$F_{\dot{x}_i} = F^1_{\frac{dx_i}{dz}} = -\lambda_i, \quad i = 1, 2, 3 \tag{C. 21}$$

$$F_u = F^1_{\frac{dx_5}{dz}} \tag{C. 22}$$

$$F^1_{\frac{dt}{dz}} = F + \sum_{i=1}^{4} \lambda_i \dot{x}_i - u F_u = H_1 \tag{C. 23}$$

In (C. 23), the definition for the Hamiltonian

$$H = F - \sum_i y_i' F_{y_i'} \tag{C. 24}$$

has been used, where the derivatives y_i' include the control function as well as the derivatives of the state components with respect to the independent variable. In the present case, F_u of (C. 22) is zero (from the transversality conditions) so that (C. 23) is recognized as the usual control problem Hamiltonian. When the Hamiltonian for F^1 is formed, according to (C. 24), and (C. 21), (C. 22), and the center expression of (C. 23) are inserted, one finds

$$H' = -\lambda_4 , \tag{C. 25}$$

On the other hand, when H_1 is used for (C. 23) one finds

$$H' = \frac{f_o}{f_4} + \sum_{i=1}^{3} \lambda_i \frac{f_i}{f_4} - H_1 \frac{dt}{dz} - \frac{dx_5}{dz} F_u + \lambda_4 f_4 \left(\frac{dt}{dz} - \frac{1}{f_4} \right) \tag{C. 26}$$

The last expression is zero, so with F_u taken as zero, this is the same as the Hamiltonian (C. 12), for by the transformation (C. 5) (taken as the last transformation),

$$g_i = \frac{f_i}{f_4} , \quad i = 0, 1, 2, 3. \tag{C. 27}$$

Thus,

$$P_1 = \lambda_1 = \frac{p_1}{2v}$$

$$P_2 = \lambda_2 = p_2$$

$$P_3 = \lambda_3 = \frac{p_3}{R} \qquad \text{(C. 28)}$$

$$P_4 = -H_1 = -H$$

$$H_2 = H' = -\lambda_4 = -c_3 p_4.$$

APPENDIX D
A NON-HOMOGENEOUS RICATTI EQUATION FOR FIELD PARTIAL DERIVATIVES

The fundamental system of solutions for the system of equations

$$\frac{d}{dt}\begin{bmatrix} \eta \\ \zeta \end{bmatrix} = \begin{bmatrix} \frac{\partial^2 H}{\partial p \partial x} & \frac{\partial^2 H}{\partial p^2} \\ -\frac{\partial^2 H}{\partial x^2} & -\frac{\partial^2 H}{\partial x \partial p} \end{bmatrix}\begin{bmatrix} \eta \\ \zeta \end{bmatrix} \tag{D.1}$$

is

$$\pi(t) = \begin{bmatrix} \frac{\partial x(t)}{\partial x_o} & \frac{\partial x(t)}{\partial p_o} \\ \frac{\partial p(t)}{\partial x_o} & \frac{\partial p(t)}{\partial p_o} \end{bmatrix}, \quad \pi(0) = I. \tag{D.2}$$

A field of extremals is constructed by obtaining solutions to the linearized boundary conditions for the optimization problem such that

$$\frac{\partial p_o}{\partial x_o} = K \tag{D.3}$$

as, (for example) in Section IIC, and then determining the partial derivatives

$$\frac{\partial p}{\partial x} = \left[\frac{\partial p}{\partial x_o} + \frac{\partial p}{\partial p_o} K\right]\left[\frac{\partial x}{\partial x_o} + \frac{\partial x}{\partial p_o} K\right]^{-1}. \tag{D.4}$$

This field cannot be constructed if the inverse matrix fails to exist at any point along the extremal (excluding the end point).

Let

$$U = \frac{\partial x}{\partial x_o} + \frac{\partial x}{\partial p_o} K$$

$$V = \frac{\partial p}{\partial x_o} + \frac{\partial p}{\partial p_o} K. \tag{D.5}$$

Then from differentiation of

$$U U^{-1} = I \tag{D.6}$$

it follows that

$$\dot{U}^{-1} = -U^{-1} \dot{U} U^{-1}. \tag{D.7}$$

Substituting from (D.1), and premultiplying by V, one finds

$$V \dot{U}^{-1} = -\left[VU^{-1} \frac{\partial^2 H}{\partial p \partial x} + VU^{-1} \frac{\partial^2 H}{\partial p^2} VU^{-1} \right]. \tag{D.8}$$

Also from (D.1), by post-multiplying the expression for $\dot{V}$ by U^{-1},

$$\dot{V} U^{-1} = -\left[\frac{\partial^2 H}{\partial x^2} + \frac{\partial^2 H}{\partial x \partial p} VU^{-1} \right]. \tag{D.9}$$

When (D.8) and (D.9) are added, the left-hand side is found to be a perfect differential, so that

$$\frac{d}{dt}(VU^{-1}) = -\left[\frac{\partial^2 H}{\partial x^2} + \frac{\partial^2 H}{\partial x \partial p} VU^{-1} + VU^{-1} \frac{\partial^2 H}{\partial p \partial x} + VU^{-1} \frac{\partial^2 H}{\partial p^2} VU^{-1} \right]. \tag{D.10}$$

From (D.5), (D.4) and (D.3) it is found that

$$VU^{-1} = \frac{\partial p}{\partial x}, \quad \frac{\partial p(0)}{\partial x} = K, \tag{D.11}$$

where $\frac{\partial p}{\partial x}$ is known to be a symmetric matrix. Other fields may be generated by changing the initial conditions to other symmetric matrices, such as the matrix considered in the sufficiency test, Section IIB.

APPENDIX E
RELATIONSHIPS FOR SUFFICIENCY CONDITIONS

NON-SINGULAR NEWTON - RAPHSON MATRIX AND NORMALITY

According to Reference 7 (pages 230 and 231), the accessory minimum problem has order of abnormality q if there exist q linearly-independent sets of constants and solutions of the canonical accessory equations

$$\dot{\eta} = \frac{\partial^2 H}{\partial p \partial x}\,\eta + \frac{\partial^2 H}{\partial p^2}\,\zeta$$

$$\dot{\zeta} = -\frac{\partial^2 H}{\partial x^2}\,\eta - \frac{\partial^2 H}{\partial x \partial p}\,\zeta \qquad \text{(E. 1)}$$

of the form $\tau \equiv 0$, $\zeta(t)$, ϵ_μ for each of which

$$\left(\zeta_i + \epsilon_\mu \frac{\partial \psi_\mu}{\partial x_i}\right) \Bigg|_0^T = 0 \qquad \text{(E. 2)}$$

$$\epsilon_\mu \left(\frac{\partial \psi_\mu}{\partial t} + \frac{\partial \psi_\mu}{\partial x_j}\,\dot{x}_i\right) \Bigg|_0^T = 0\,. \qquad \text{(E. 3)}$$

The functions

$$\psi_\mu\left[0, x(0), T, x(T)\right] = 0 \qquad \text{(E. 4)}$$

are end conditions satisfied by the extremal path, and repeated subscripts in (E. 2) and (E. 3) denote sums. If the order of abnormality q is zero, the path is normal.

In the optimization problem the initial conditions are all specified, which implies

$$\eta_i(0) = 0 \qquad i = 1, \ldots, n$$

$$\zeta_i(0) = -\epsilon_i \tag{E.5}$$

$$\epsilon_{n+1} + \epsilon_i \dot{x}_i(0) = 0 .$$

Thus the solutions to be considered are linear combinations of the solutions

$$\begin{bmatrix} \frac{\partial x(t)}{\partial p_o} \\ \frac{\partial p(t)}{\partial p_o} \end{bmatrix} = \begin{bmatrix} \pi_{12}(t) & \pi_{12}(0) \\ \pi_{22}(t) & \pi_{22}(0) \end{bmatrix} = \begin{bmatrix} 0 \\ I \end{bmatrix} \tag{E.6}$$

with

$$\eta(t) = -\pi_{12}(t)\,\epsilon$$

$$\zeta(t) = -\pi_{22}(t)\,\epsilon \quad . \tag{E.7}$$

By hypothesis, the first of (E.7) are all zero. It is shown that if the Newton-Raphson matrix is non-singular, the constants ϵ are all zero, so from (E.7) there are no non-zero solutions $\eta_i = 0$, $\zeta(t)$, ϵ. Thus, $\varsigma_i = 0$, and the problem is normal by lemma 81.1 of Reference 7.

The terminal conditions (E.4) are assumed to be

$$x_K(T) - X_k = 0, \quad k = 1, \ldots, r \leq n \tag{E.8}$$

$$T - K = 0 , \tag{E.9}$$

where (E. 9) is omitted if the terminal value of the independent variable is not specified. The terminal equations (E. 2) and (E. 3) are then

$$\zeta_k(T) = -\epsilon_{n+1+k}, \quad k = 1, \ldots, r \tag{E. 10}$$

$$\zeta_j(T) = 0, \qquad j = r+1, \ldots, n$$

$$\epsilon_{(n+1)+k}\dot{x}_k(T) = -\epsilon_{n+r+2}. \tag{E. 11}$$

Assume first that (E. 9) is included. Then the first r and the last (n-r) of (E. 7) at t = T = K give

$$B\,\epsilon = 0\,, \tag{E. 12}$$

where B is the Newton-Raphson matrix (as in Section IIC). If B is non-singular, $\epsilon = 0$, and the result follows. If (E. 9) is omitted, then (E. 11) must be included, since with $\epsilon_{n+r+2} = 0$, it is an additional constraint equation. However,

$$\epsilon_{(n+1)+k}\dot{x}_k(T) = -\zeta_i(T)\dot{x}_i(T) + \dot{p}_i(T)\eta_i(T) = -\zeta_i(0)\dot{x}_i(0) = \epsilon_i\dot{x}_i(0) = 0 \tag{E. 13}$$

since the expression is constant in t. This may be shown by using the canonical equations

$$\dot{x} = \frac{\partial H}{\partial p}$$

$$\dot{p} = -\frac{\partial H}{\partial x} \tag{E. 14}$$

and (E. 1) when differentiating the second of (E. 13) with respect to t to obtain zero. The Newton-Raphson matrix is formed with the total differentials

$$0 = dx_k(T) = \dot{x}_k(T)\, dT + \eta_k(T) \qquad k = 1, \ldots, r$$

$$0 = dp_j = \dot{p}_j(T)\, dT + \zeta_j(T) \qquad j = r+1, \ldots, n \tag{E.15}$$

and the last of (E.14), as in Section IIA. Then if B is non-singular the set $(\epsilon, \epsilon_{n+1})$ in (E.5) is zero, and the result again follows.

RELATIONSHIP BETWEEN MAXIMUM PRINCIPLE AND MINIMUM PRINCIPLE ACCESSORY SOLUTIONS

The difference in maximum and minimum principle formulations of the optimization problem is the signs of the multipliers, including the unit multiplier for the integrand f_o of J, the function to be minimized. Thus, the Hamiltonian for the maximum principle is the negative of the Hamiltonian for the minimum principle. Let the functional form of the solutions for the maximum principle formulation be

$$x = x(t, x_o, z_o)$$

$$z = z(t, x_o, z_o) \tag{E.16}$$

and the corresponding forms for the minimum principle formulation be

$$x = x(t, x_o, p_o)$$

$$p = p(t, x_o, p_o) \tag{E.17}$$

It follows that

$$x(t, x_o, p_o) = x(t, x_o, z_o) \tag{E.18}$$

if the multipliers for the two systems satisfy

$$p(t, x_o, p_o) = -z(t, x_o, z_o). \tag{E.19}$$

The accessory solutions are the partial derivatives of (E. 18) and (E. 19) with respect to x_o, p_o and z_o. Upon differentiating, the correspondance between systems of solutions is found to be

$$\frac{\partial x}{\partial x_o}(t, x_o, p_o) = \frac{\partial x}{\partial x_o}(t, x_o, z_o)$$

$$-\frac{\partial x}{\partial p_o}(t, x_o, p_o) = \frac{\partial x}{\partial z_o}(t, x_o, z_o)\frac{\partial z_o}{\partial p_o} = -\frac{\partial x}{\partial z_o}(t, x_o, z_o) \qquad \text{(E. 20)}$$

$$\frac{\partial p}{\partial x_o}(t, x_o, p_o) = -\frac{\partial z}{\partial x_o}(t, x_o, z_o)$$

$$\frac{\partial p}{\partial p_o}(t, x_o, p_o) = -\frac{\partial z}{\partial z_o}(t, x_o, z_o)\frac{\partial z_o}{\partial p_o} = \frac{\partial z}{\partial z_o}(t, x_o, z_o)$$

In constructing a field of extremals for the sufficiency test, Bliss uses the maximum principle formulation of the problem. A suitable choice for the conjugate system of solutions is

$$U = \frac{\partial x}{\partial x_o}(t, x_o, z_o) + \frac{\partial x}{\partial z_o}(t, x_o, z_o)\left[\frac{\partial z_o}{\partial x_o} + I\right]$$

$$V = \frac{\partial z}{\partial x_o}(t, x_o, z_o) + \frac{\partial z}{\partial z_o}(t, x_o, z_o)\left[\frac{\partial z_o}{\partial x_o} + I\right]. \qquad \text{(E. 21)}$$

Upon substitution from (E. 20), these become, for the minimum principle,

$$U = \frac{\partial x}{\partial x_o}(t, x_o, p_o) + \frac{\partial x}{\partial p_o}(t, x_o, p_o)\left[\frac{\partial p_o}{\partial x_o} - I\right]$$

$$-V = \frac{\partial p}{\partial x_o}(t, x_o, p_o) + \frac{\partial p}{\partial p_o}(t, x_o, p_o)\left[\frac{\partial p_o}{\partial x_o} - I\right]. \qquad \text{(E. 22)}$$

REDUCTION OF FIELD FROM (n+2) DIMENSIONS TO (n+1) DIMENSIONS

Consider the system of equations

$$\begin{aligned}
\dot{x} &= \frac{\partial H}{\partial z}(x, z, z_{n+1}) \\
\dot{x}_{n+1} &= u(x, z, z_{n+1}) \\
-\dot{z} &= \frac{\partial H}{\partial x}(x, z, z_{n+1}) \\
\dot{z}_{n+1} &= 0
\end{aligned} \tag{E. 23}$$

which arises from the maximum principle formulation of the optimization problem when x_{n+1} (the integral of u) is considered as an additional state coordinate. It is tacitly assumed that x_{n+1} does not appear in the right-hand side of system (E. 23) and that it does not appear in the boundary conditions. Hence, as a necessary condition,

$$z_{n+1} = 0, \tag{E. 24}$$

and the first and third of (E. 23) are the system of equations to be solved for the optimal trajectory. It is not immediately obvious that the field of extremals used in the sufficiency test can be correspondingly reduced from (n+2) dimensions to (n+1) dimensions. This, however, can be shown as follows. The accessory equations corresponding to (E. 23) are

$$\frac{d}{dt}\left[\begin{array}{c} \eta \\ \eta_{n+1} \\ \hline \zeta \\ \zeta_{n+1} \end{array}\right] = \left[\begin{array}{cc|cc} \frac{\partial^2 H}{\partial z \partial x} & 0 & \frac{\partial^2 H}{\partial z^2} & \frac{\partial^2 H}{\partial z \partial z_{n+1}} \\ \frac{\partial u'}{\partial x} & 0 & \frac{\partial u'}{\partial z} & \frac{\partial u}{\partial z_{n+1}} \\ \hline -\frac{\partial^2 H}{\partial x^2} & 0 & -\frac{\partial^2 H}{\partial x \partial z} & -\frac{\partial u}{\partial x} \\ 0 & 0 & 0 & 0 \end{array}\right] \left[\begin{array}{c} \eta \\ \eta_{n+1} \\ \hline \zeta \\ \zeta_{n+1} \end{array}\right] \tag{E. 25}$$

and the fundamental solution matrix may be written

$$\pi(t) = \left[\begin{array}{cc:cc} \pi_{11}(t) & 0 & \pi_{12}(t) & b(t) \\ a'(t) & 1 & c'(t) & d(t) \\ \hdashline \pi_{21}(t) & 0 & \pi_{22}(t) & e(t) \\ 0 & 0 & 0 & 1 \end{array}\right] \qquad \pi(0) = I, \tag{E.26}$$

where a, b, c and e are n dimensional vectors and d is a scalar. A conjugate system of solutions is determined by its initial matrices, now taken as

$$\begin{bmatrix} U(0) \\ V(0) \end{bmatrix} = \left[\begin{array}{cc} I & 0 \\ 0 & 1 \\ \hdashline I & 0 \\ 0 & 0 \end{array}\right] \tag{E.27}$$

for when the initial conditions satisfy

$$U'V = V'U \tag{E.28}$$

then so do the solutions

$$\begin{bmatrix} U \\ V \end{bmatrix} = \pi(t) \left[\begin{array}{c:c} U_o & \\ \hdashline & V_o \end{array}\right] = \begin{bmatrix} \left[\pi_{11}(t) + \pi_{12}(t)\right] & 0 \\ \left[a(t) + c(t)\right]' & 1 \\ \left[\pi_{21}(t) + \pi_{22}(t)\right] & 0 \\ 0 & 0 \end{bmatrix}. \tag{E.29}$$

Then the determinant of U is

$$\det U = \det \begin{bmatrix} \left[\pi_{11}(t) + \pi_{12}(t)\right] & 0 \\ \left[a(t) + c(t)\right]' & 1 \end{bmatrix} = \det \left[\pi_{11}(t) + \pi_{12}(t)\right] \tag{E.30}$$

so that if $\pi_{11}(t) + \pi_{12}(t)$ is non-singular, then so is U. The reduced system

$$\begin{bmatrix} U_R \\ V_R \end{bmatrix} = \begin{bmatrix} \pi_{11}(t) & \pi_{12}(t) \\ \pi_{12}(t) & \pi_{22}(t) \end{bmatrix} \begin{bmatrix} U_R(0) \\ V_R(0) \end{bmatrix} \quad \begin{bmatrix} U_R(0) \\ V_R(0) \end{bmatrix} = \begin{bmatrix} I \\ I \end{bmatrix} \tag{E.31}$$

is a conjugate system of solutions which forms a field for the reduced problem if $\left[\pi_{11}(t) + \pi_{12}(t)\right]$ is non-singular. Thus, the field in (n+1)-space implies the existence of the field in (n+2)-space.

The system (E.21) results when V(0) is taken as

$$V(0) = \begin{bmatrix} \left[\frac{\partial z_o}{\partial x_o} + I\right] & 0 \\ 0 & 0 \end{bmatrix}. \tag{E.32}$$

APPENDIX F
THE LEAST SINGULAR SQUARE MATRIX OF AN nxq MATRIX

Let n be greater than q, and let each row vector V_i of the matrix be normalized to 1,

$$(V_i, V_i) = \sum_{j=1}^{q} V_{ij}^2 = 1, \quad i = 1, \ldots, n. \tag{F.1}$$

The method proceeds by construction, so let

$$W_K = a_1 V_1 + \ldots + a_K V_K \tag{F.2}$$

be a unit vector made up of the first K most orthogonal vectors, and find the maximum projection (V_m, W_K) of W_K on a row vector V_m, $m > K$. The projection is the cosine of the angle between V_m and W_K, which, when maximized, gives the smallest angle between V_m and the K-dimensional Euclidian space determined by the K vectors in (F. 2). Thus, the problem is that of finding the minimum of the maximum projections of the remaining (n-m) row vectors, and using this to form W_{K+1}.

Consider the maximization problem represented by

$$f_m(a) = (V_m, W_K) = \text{maximum}, \quad m > K, \tag{F.3}$$

subject to the constraint

$$(W_K, W_K) = 1. \tag{F.4}$$

Introduce a Lagrange multiplier λ and form the expression

$$F(a, \lambda) = (V_m, W_K) + \lambda \left[1 - (W_K, W_K)\right]. \tag{F.5}$$

The derivatives of F with respect to $a_j, j = 1, \ldots, K$, must vanish at a maximum, so

$$\frac{\partial F}{\partial a_j} = 0 = (V_m, V_j) - 2\lambda(V_j, W_K), \quad j = 1, \ldots, K. \tag{F.6}$$

Multiplying by a_j, summing over j and using (F.4) results in

$$(W_K, V_m) = 2\lambda = f_m(a). \tag{F.7}$$

On the other hand, the system (F.6) maybe written in the matrix form

$$\begin{bmatrix} (V_1, V_m) \\ (V_2, V_m) \\ \vdots \\ (V_K, V_m) \end{bmatrix} = \begin{bmatrix} (V_1, V_1) & (V_1, V_2) & \cdots & (V_1, V_K) \\ (V_2, V_1) & (V_2, V_2) & \cdots & (V_2, V_K) \\ \vdots & \vdots & & \vdots \\ (V_K, V_1) & (V_K, V_2) & \cdots & (V_K, V_K) \end{bmatrix} \begin{bmatrix} 2\lambda\, a_1 \\ 2\lambda\, a_2 \\ \vdots \\ 2\lambda\, a_K \end{bmatrix}, \tag{F.8}$$

or more simply

$$b_m = \phi_K (2\lambda\, a), \tag{F.9}$$

from which

$$2\lambda\, a = \left[\phi_K\right]^{-1} b_m. \tag{F.10}$$

Now b_m is the left-hand side of (F.8), which, when multiplied by a, gives f_m, so in view of (F.7),

$$2\lambda(b_m' a) = f_m^2 = b_m' \left[\phi_K^{-1}\right] b_m. \tag{F.11}$$

Equation (F.11) shows that the maximum and minimum projections have opposite signs and allows the squared value of the projection to be evaluated in terms of known quantities. This is good enough for the computer mechanization of the scheme, which almost suggests itself.

Consider the (n x n) matrix

$$\begin{bmatrix} (V_1, V_1) & \cdots & (V_1, V_n) \\ \vdots & & \vdots \\ (V_n, V_1) & \cdots & (V_n, V_n) \end{bmatrix} \tag{F.12}$$

which is symmetric and has ones down the main diagonal. At the K^{th} stage, this may be partitioned into four submatrices

$$\begin{bmatrix} \phi_K & B \\ B' & C \end{bmatrix}, \tag{F.13}$$

so consider the product

$$\begin{bmatrix} \phi_K & B \\ B' & C \end{bmatrix} \begin{bmatrix} \phi_K^{-1} & 0 \\ 0 & I \end{bmatrix} = \begin{bmatrix} I & B \\ B'\phi_K^{-1} & C \end{bmatrix} \tag{F.14}$$

The $(m-K)^{th}$ row of the lower left submatrix times the $(m-K)^{th}$ column of B gives the square of the projection (F.11). This is easily computed for each of the remaining vectors, and the minimum of these identifies the most orthogonal vector to the K-dimensional subspace.

Now suppose that rows and columns are interchanged in the last matrix of (F.14) to bring the minimizing row and column next to the identity matrix. This retains the symmetry of C. Then elementary column operations may be used to obtain the (K+1) x (K+1) identity matrix for the next step.

APPENDIX G

PROOF THAT DISCONTINUITIES IN THE MULTIPLIERS CAN BE DETERMINED AT EITHER END OF A CONSTRAINED SUBARC

The geometry is shown in Figure G-1. It is to be shown that the value p_2 is obtained by following either path A or path B. Path A assumes that the multipliers are continuous at the initial point t_1 and discontinuous at the endpoint t_2. Path B assumes the discontinuities are at the initial point.

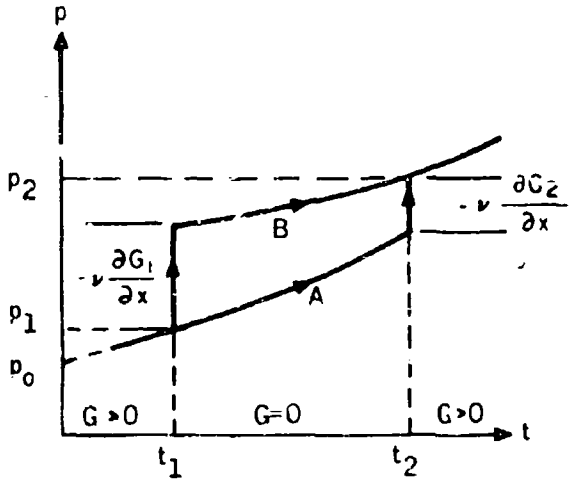

Figure G1.
Geometry of the Problem

The necessary conditions for the constrained subarc are

$$\dot{x} = f(x, u) \tag{G.1}$$

$$-\dot{p} = \left[\frac{\partial f_o}{\partial x}\right]' + \left[\frac{\partial f}{\partial x}\right]' p + \mu\left[\frac{\partial \dot{G}}{\partial x}\right]' \tag{G.2}$$

$$0 = p' \frac{\partial f}{\partial u} + \frac{\partial f_o}{\partial u} + \mu \frac{\partial \dot{G}}{\partial u} = \frac{\partial H}{\partial u}(x, u, p, \mu) \tag{G.3}$$

$$0 = \dot{G}(x, u) . \tag{G.4}$$

The last two equations are "solved" to obtain

$$u = u(x) \tag{G.5}$$

$$\mu = \mu(x, p) = -\frac{1}{\left(\frac{\partial G}{\partial u}\right)}\left(p' \frac{\partial f}{\partial u} + \frac{\partial f_o}{\partial u}\right). \tag{G.6}$$

Substitution of (G.5) and (G.6) into (G.1) and (G.2) gives the reduced differential equations for the constrained subarc:

$$\dot{x} = f(x, u(x)) \tag{G.7}$$

$$-\dot{p} = p_o\left[\frac{\partial f_o}{\partial x} - \frac{\frac{\partial f_o}{\partial u}}{\frac{\partial G}{\partial u}}\left(\frac{\partial G}{\partial x}\right)\right]' + \left[\frac{\partial f}{\partial x} - \frac{\frac{\partial f}{\partial u}}{\frac{\partial G}{\partial u}}\left(\frac{\partial G}{\partial x}\right)\right]' p \tag{G.8}$$

$$\dot{p}_o = 0, \tag{G.9}$$

Equation (G.9) has been added for convenience.

Now (G.7) and (G.8) are "uncoupled" since p does not appear in (G.7). Since $x = x(t)$ and the coefficients of p in (G.8) contain x alone, (G.8) and (G.9) form a linear first-order homogeneous system of differential equations with time varying coefficients,

$$\dot{\psi} = A(t)\psi, \tag{G.10}$$

where ψ is the n+1 dimensional vector

$$\psi = \begin{bmatrix} p \\ p_o \end{bmatrix}. \tag{G.11}$$

Let ϕ be the fundamental solution matrix of (G. 10) with $\phi(t_1) = I$, the (n+1) x (n+1) identity matrix. Then the value of p_2 computed along path A is

$$\begin{bmatrix} p_{2_A} \\ p_o \end{bmatrix} = \phi(t_2) \begin{bmatrix} p_{1_A} \\ 1 \end{bmatrix} - \nu \begin{bmatrix} \left(\frac{\partial G_2}{\partial x}\right)' \\ 0 \end{bmatrix} \tag{G. 12}$$

Along path B,

$$\begin{bmatrix} p_{2_B} \\ p_o \end{bmatrix} = \phi(t_2) \begin{bmatrix} p_{1_A} - \nu\left(\frac{\partial G_1}{\partial x}\right)' \\ 1 \end{bmatrix}. \tag{G. 13}$$

If (G. 12) and (G. 13) give the same value for p_2 it follows that

$$\begin{bmatrix} \left(\frac{\partial G_2}{\partial x}\right)' \\ 0 \end{bmatrix} = \phi(t_2) \begin{bmatrix} \left(\frac{\partial G_1}{\partial x}\right)' \\ 0 \end{bmatrix}, \tag{G. 14}$$

and hence that $\frac{\partial G(t)}{\partial x}$ is a solution of (G. 8) with $p_o = 0$. To show this, consider the vector identity

$$\frac{\partial \dot{G}}{\partial x}(x, u(x)) = \frac{\partial \dot{G}}{\partial x} + \frac{\partial \dot{G}}{\partial u}\frac{\partial u}{\partial x} = 0 \tag{G. 15}$$

since

$$\frac{\partial u}{\partial x} = -\frac{1}{\left(\frac{\partial G}{\partial u}\right)} \frac{\partial \dot{G}}{\partial x} \tag{G. 16}$$

results from equations (G. 4) and (G. 5). On the other hand,

$$\left(\frac{\partial \dot{G}}{\partial x}\right)' = \frac{\partial}{\partial x}\left(f' \frac{\partial G}{\partial x}\right) - \frac{\partial^2 G}{\partial x^2} f + \left[\frac{\partial f'}{\partial x} + \frac{\partial u'}{\partial x}\left(\frac{\partial f}{\partial u}\right)'\right] \frac{\partial G}{\partial x}' . \tag{G. 17}$$

Additionally,

$$\frac{d}{dt}\left(\frac{\partial G'}{\partial x}\right) = \frac{\partial^2 G}{\partial x^2} f . \tag{G. 18}$$

Combining (G. 15) - (G. 18), one finds

$$-\frac{d}{dt}\left(\frac{\partial G'}{\partial x}\right) = \left[\frac{\partial f}{\partial x} - \frac{1}{\left(\frac{\partial G}{\partial u}\right)} \frac{\partial f}{\partial u} \frac{\partial \dot{G}}{\partial x}\right]' \frac{\partial G}{\partial x}' , \tag{G. 19}$$

which is the same as (G. 8) with $p_o = 0$ and $p = \frac{\partial G}{\partial x}'$. Thus $\frac{\partial G}{\partial x}$ is a solution of (G. 8) with $p_o = 0$, and the values of p_2 computed along paths A and B are the same.

REFERENCES

1. Scharmack, D. K., Swanlund, G. D., Johnson, R. G., Ward, M. D., and Rang, E. R.: "Feasibility Study of New Techniques for Control of Re-Entry Vehicles, Volume I, Calculation of Optimal Trajectories and Synthesis of Control Functions", TDR Report No. FDL-TDR-64-13, March 1964. Final report to Flight Dynamics Laboratory, RTD, Wright-Patterson Air Force Base, Ohio.

2. Hildebrand, F. B.: "Introduction to Numerical Analysis". McGraw-Hill Book Company, Inc., New York (1946).

3. Fletcher, R. and Powell, M. J. D. "A Rapidly Convergent Descent Method for Minimization", Computer J., pp 163-168, July, 1963.

4. Marquardt, D. W.: "An Algorithm for Least-Squares Estimation of Nonlinear Parameters", J. Soc. Indust. Appl. Math., Vol. II, No. 2 June, 1963.

5. Davidon, W. C.: "Variable Metric Method for Minimization", A.E.C. Research and Development Report ANL-5990 (Rev.)(1959).

6. Goldstein, H.: "Classical Mechanics". Addison-Wesley Publishing Company, Inc. Cambridge, Mass. (1950).

7. Bliss, G. A.: "Lectures on the Calculus of Variations". The University of Chicago Press, Chicago, 1946.

8. Breakwell, J. V., Speyer, J. L., and Bryson, A. E.: "Optimization and Control of Nonlinear Systems Using the Second Variation". SIAM Journal on Control, Vol. 1, No. 2, June 1963.

9. George C. Marshall Space Flight Center Progress Reports 1-5 on Studies in the Fields of Space Flight and Guidance Theory.

10. Volz, Richard A.: "The Minimization of a Function by Weighted Gradients", Proc. of the IEEE, Vol. 53, No. 6, June, 1965.

11. Dreyfus, S.: "The Numerical Solution of Variational Problems", Jour. of Math. Anal. and Appl., Vol. 5, No. 1, August 1962.

12. Gamkrelidge, R. V.: "Optimal Processes with Bounded Phase Coordinates", Izv. Akad. Nauk. SSSR, Ser. Mat., Vol. 24, 1960, pp 315-356.

13. Troitskii, V. A.: "Variational Problems on the Optimization of Control Processes in Systems with Bounded Coordinates". Prikladnay a Matematika I. Mekhanika, Vol. 26, No. 3, pp. 431-443, May-June 1962. Available as Minneapolis-Honeywell translation No. 585.

14. Bryson, A. E. and Denham, W. F.: "The Solution of Optimal Programming Problems with Inequality Constraints", IAS Paper No. 63-78, presented at the IAS 31st Annual Meeting, January 1963.

15. Wingrove, Rodney C.: "Survey of Re-Entry Guidance and Control Methods", AIAA Journal, Volume 1, No. 9, September 1963.

Unclassified

Security Classification

DOCUMENT CONTROL DATA - R&D

(Security classification of title, body of abstract and indexing annotation must be entered when the overall report is classified)

1 ORIGINATING ACTIVITY (Corporate author)

Honeywell, Inc.
Minneapolis, Minnesota

2a REPORT SECURITY CLASSIFICATION

Unclassified

2b GROUP

N/A

3 REPORT TITLE

RE-ENTRY VEHICLE CONTROL SYSTEM DESIGN AND MECHANIZATION

4 DESCRIPTIVE NOTES (Type of report and inclusive dates)

Final Report

5 AUTHOR(S) (Last name, first name, initial)

Scharmack, D. K.
Ward, M. D.

6 REPORT DATE	7a TOTAL NO. OF PAGES	7b NO. OF REFS
April 1966	198	15

8a CONTRACT OR GRANT NO.	9a ORIGINATOR'S REPORT NUMBER(S)
AF33(615)-1858	AFFDL-TR-66-3
b PROJECT NO. 8225	
c	9b OTHER REPORT NO(S) (Any other numbers that may be assigned this report)
d	

10 AVAILABILITY/LIMITATION NOTICES

This document is subject to special export controls & each transmittal to foreign governments or foreign nationals may be made only with prior approval of the Flight Control Div. (FDC), AF Flight Dynamics Lab., W-PAFB, Ohio 45433.

11 SUPPLEMENTARY NOTES	12 SPONSORING MILITARY ACTIVITY
N/A	AFFDL (FDCL) Wright-Patterson AFB, Ohio

13 ABSTRACT

A nonlinear optimal feedback control scheme for controlling a vehicle re-entering the earth's atmosphere from lunar return initial conditions is reported.

The optimal feedback control law used in the scheme is obtained from a multi-dimensional surface fit of the control function for several optimal trajectories. Partials of the control with respect to the state vector are included in the fitting procedure. The functional minimized by the trajectories is the total (convective plus radiative) stagnation point heat.

The feedback control scheme is developed, and several re-entry trajectories are simulated. Modest increases in total heat from optimal values are observed, and large (although tolerable) terminal point errors occur. It is believed that the terminal errors can be greatly reduced, if necessary.

A powerful predictor scheme is developed which allows optimal trajectories to be changed as a function of a parameter. This is used to extend the range of an optimal trajectory, to perform an "absolute minimum" test, and to map the optimal re-entry corridor.

Sufficiency tests for a relative minimum are mechanized, and it is shown that the trajectories considered are minimizing paths. The optimization method is extended to include the bounded state-coordinate problem.

DD FORM 1473

Unclassified

Security Classification

Unclassified

Security Classification

14 KEY WORDS	LINK A		LINK B		LINK C	
	ROLE	WT	ROLE	WT	ROLE	WT
Re-entry						
Optimization						
Control						

INSTRUCTIONS

1. ORIGINATING ACTIVITY: Enter the name and address of the contractor, subcontractor, grantee, Department of Defense activity or other organization *(corporate author)* issuing the report.

2a. REPORT SECURITY CLASSIFICATION: Enter the overall security classification of the report. Indicate whether "Restricted Data" is included. Marking is to be in accordance with appropriate security regulations.

2b. GROUP: Automatic downgrading is specified in DoD Directive 5200.10 and Armed Forces Industrial Manual. Enter the group number. Also, when applicable, show that optional markings have been used for Group 3 and Group 4 as authorized.

3. REPORT TITLE: Enter the complete report title in all capital letters. Titles in all cases should be unclassified. If a meaningful title cannot be selected without classification, show title classification in all capitals in parenthesis immediately following the title.

4. DESCRIPTIVE NOTES: If appropriate, enter the type of report, e.g., interim, progress, summary, annual, or final. Give the inclusive dates when a specific reporting period is covered.

5. AUTHOR(S): Enter the name(s) of author(s) as shown on or in the report. Enter last name, first name, middle initial. If military, show rank and branch of service. The name of the principal author is an absolute minimum requirement.

6. REPORT DATE: Enter the date of the report as day, month, year, or month, year. If more than one date appears on the report, use date of publication.

7a. TOTAL NUMBER OF PAGES: The total page count should follow normal pagination procedures, i.e., enter the number of pages containing information.

7b. NUMBER OF REFERENCES: Enter the total number of references cited in the report.

8a. CONTRACT OR GRANT NUMBER: If appropriate, enter the applicable number of the contract or grant under which the report was written.

8b, 8c, & 8d. PROJECT NUMBER: Enter the appropriate military department identification, such as project number, subproject number, system numbers, task number, etc.

9a. ORIGINATOR'S REPORT NUMBER(S): Enter the official report number by which the document will be identified and controlled by the originating activity. This number must be unique to this report.

9b. OTHER REPORT NUMBER(S): If the report has been assigned any other report numbers *(either by the originator or by the sponsor)*, also enter this number(s).

10. AVAILABILITY/LIMITATION NOTICES: Enter any limitations on further dissemination of the report, other than those imposed by security classification, using standard statements such as:

(1) "Qualified requesters may obtain copies of this report from DDC."

(2) "Foreign announcement and dissemination of this report by DDC is not authorized."

(3) "U. S. Government agencies may obtain copies of this report directly from DDC. Other qualified DDC users shall request through _____."

(4) "U. S. military agencies may obtain copies of this report directly from DDC. Other qualified users shall request through _____."

(5) "All distribution of this report is controlled. Qualified DDC users shall request through _____."

If the report has been furnished to the Office of Technical Services, Department of Commerce, for sale to the public, indicate this fact and enter the price, if known.

11. SUPPLEMENTARY NOTES: Use for additional explanatory notes.

12. SPONSORING MILITARY ACTIVITY: Enter the name of the departmental project office or laboratory sponsoring *(paying for)* the research and development. Include address.

13. ABSTRACT: Enter an abstract giving a brief and factual summary of the document indicative of the report, even though it may also appear elsewhere in the body of the technical report. If additional space is required, a continuation sheet shall be attached.

It is highly desirable that the abstract of classified reports be unclassified. Each paragraph of the abstract shall end with an indication of the military security classification of the information in the paragraph, represented as *(TS)*, *(S)*, *(C)*, or *(U)*.

There is no limitation on the length of the abstract. However, the suggested length is from 150 to 225 words.

14. KEY WORDS: Key words are technically meaningful terms or short phrases that characterize a report and may be used as index entries for cataloging the report. Key words must be selected so that no security classification is required. Identifiers, such as equipment model designation, trade name, military project code name, geographic location, may be used as key words but will be followed by an indication of technical context. The assignment of links, roles, and weights is optional.

Unclassified

Security Classification